Nano Studies

5

2012

Nano Studies

5

2012

Nano Studies, 2012, 5

UDG [53 + 54 + 620.22] (051.2)
N – 21

Nano Studies is a biannual scientific journal published in Georgia.

Nano Studies' topics of interest include Nanoscience and related problems of Physics, Chemistry and Materials Science.

Nano Studies publish following categories of scientific articles: research papers, communications, reviews and discussions.

Nano Studies publish scientific articles in English and also in Georgian and in Russian.

Summaries of all the articles of **Nano Studies** are referred in **Georgian Abstracts Journal** and are accessible in **Tech Inform** (Georgia's Central Institute for Scientific and Technical Information) database: **http://www.tech.caucasus.net**

Full-texts of articles published in **Nano Studies** are free-accessible in **Nano Archive** database: **http://www.nanoarchive.org**

Editor-Founder: **Levan Chkhartishvili**
Editorial Assistant: **Tamar Berberashvili**

Address of Editorial Office: **Department of Physics**
Georgian Technical University
Campus 4, Room 307
77 Merab Kostava Avenue
Tbilisi, 0175, Georgia
www.NanoStudies.org

E-mail: **chkharti2003@yahoo.com**
Phone: **995 322 37 19 42**
Mobile: **995 599 34 07 36**

Publishing House **Nekeri**

ISSN 1987 – 8826

CONTENTS

Research Papers

Contents.

Science History Pages

Nano Forums

Books and Media News

ეძღვნება გ. გორდაძის ხსოვნას და დაბადებიდან 75 წლისთავს

დასავლეთ საქართველოს ნიადაგებში მიკროელემენტების კონცენტრაციის განსაზღვრა და მათი შედარებითი ანალიზი

გ. გორდაძე, ა. გორდაძე, პ. იმნაძე,
ც. კვირიკაშვილი, გ. კიკნაძე, ნ. ლობჟანიძე

ი. ჯავახიშვილის სახ. თბილისის სახელმწიფო უნივერსიტეტი
ე. ანდრონიკაშვილის ფიზიკის ინსტიტუტი
თბილისი, საქართველო
Platon.Imnadze@gmail.com

მიღებულია 2012 წლის 9 იანვარს

ი. ჯავახიშვილის სახ. თბილისის სახელმწიფო უნივერსიტეტის ე. ანდრონიკაშვილის ფიზიკის ინსტიტუტის ნეიტრონულ-აქტივაციური ანალიზისა და რადიოლოგიური კვლევების ლაბორატორიაში, რეაქტორის ბაზაზე, ჩატარებულია მრავალი სამუშაო სხვადასხვა სახის ნიმუშებში ელემენტშემცველობის დასადგენად. სამუშაოები წლების განმავლობაში ტარდებოდა სხვადასხვა ორგანიზაციებთან ერთად, რომელთაგან ზოგიერთი დღეს აღარ ფუნქციონირებს ანდა განიცადა გარკვეული მოდერნიზაცია და დამატებით ახალი ფუნქციები შეიძინა, კერძოდ, ი. ჯავახიშვილის სახელობის სახელმწიფო უნივერსიტეტის ნიადაგმცოდნეობის კათედრასთან, სანიტარიისა და ჰიგიენის სამეცნიერო-კვლევით ინსტიტუტთან, ბუნების დაცვის სახელმწიფო კომიტეტის რესპუბლიკურ ლაბორატორიასთან, სახელმწიფო აგრომრეწველობის ჩაისა და სუბტროპიკული კულტურების სამეცნიერო გართიანებასთან და სხვ. შედეგები სხვადასხვა სამეცნიერო ჟურნალშია გამოქვეყნებული [1 – 3].

სახელმწიფო აგრომრეწველობის ჩაისა და სუბტროპიკული კულტურების სამეცნიერო გაერთიანების მიერ მოწოდებული ნიადაგების ნიმუშების ანალიზი ტარდებოდა ბირთვული რეაქტორის ბაზაზე, ინსტრუმენტული ნეიტრონულ-აქტივაციური ანალიზის მეთოდის გამოყენებით. მიუხედავად იმისა, რომ სამუშაოები ჩატარებული იქნა გასული საუკუნის 90-იან წლებში, ექსპერიმენტების შედეგები არ გამოქვეყნებულა აღნიშნულ პერიოდში საქართველოში მიმდინარე პროცესების გამო. მაგრამ მიღებულ შედეგებს არ დაუკარგავთ აქტუალობა, უფრო მეტიც, შეიძლება ითქვას, რომ მათი მნიშვნელობა გიზარდა კიდეც. მართლაც, ნაშრომში წარმოდგენილი მასალა საშუალებას იძლევა, კვლევების გაგრძელების შემთხვევაში, აღნიშნული პრობლემა დინამიკაში იქნეს დანახული და შესწავლილი, რასაც დიდი მნიშვნელობა აქვს ეკოლოგიური პრობლემების გადაწყვეტის საქმეში.

ადამიანის ჯანმრთელობა დიდად არის დამოკიდებული იმ პროდუქტების სისუფთავესა და სიჯანსაღეზე, რომლითაც იგი იკვებება. ამ მხრივ განსაკუთრებით მნიშვნელოვანია საკვებ პროდუქტებში სათანადო მიკროელემენტების არსებობა და მათი კონცენტრაციების შესაბამისობა ზღვრულად დასაშვებ ნორმებთან. მცენარეული საფარი ძირითადად სწორედ ნიადაგიდან ითვისებს სხვადასხვა ელემენტებს, რომლებიც შემდგომ მათი საშუალებით ხვდებიან ცხოველურ საკვებში. ამრიგად, შეგვიძლია ვთქვათ, რომ როგორც მცენარეული, ისე ცხოველური საკვების ელემენტშემცველობა დიდადაა განპირობებული ნიადაგის ელემენტშემადგენლობით [4]. აქედან გამომდინარე, სხვადასხვა ნიადაგებში ელემენტების კონცენტრაციების განსაზღვრა ყოველთვის იყო და დარჩება მნიშვნელოვან ანალიტიკურ ამოცანად ეკოლოგიური პრობლემების გადაწყვეტის საქმეში.

შესრულებული სამუშაო საკმაოდ კარგ წარმოდგენას იძლევა იმის შესახებ, თუ როგორია დასავლეთ საქართველოს სხვადასხვა რეგიონის ნიადაგების ელემენტშემადგენლობა. აღნიშნული პრობლემის მნიშვნელობიდან გამომდინარე, დღის წესრიგში დგას ნიადაგების პერიოდული მონიტორინგის ჩატარება და, ამ თვალსაზრისით, წარმოდგენილი შედეგები მნიშვნელოვან მონაცემებს შეიცავს შედარებისა და შესაბამისი დასკვნების გაკეთებისათვის.

დღეისათვის ყველა არსებულ საკვლევ მეთოდთან შედარებით ყველაზე ზუსტი და სწრაფია ინსტრუმენტული ნეიტრონულ–აქტივაციური ანალიზი (ინაა). ეს მეთოდი არ მოითხოვს ნიმუშის სპეციალურ მომზადებას და მისი მეშვეობით შესაძლებელია ელემენტების მცირე შემცველობების აღმოჩენა. ჩვენს ლაბორატორიაში შემუშავებულია ნეიტრონულ-აქტივაციური ანალიზის ოპტიმიზაციისა და მრავალელემენტიანი ანალიზის მეთოდიკები, რომელსაც ვიყენებთ ექსპერიმენტების დროს [5 – 8].

ნიადაგების ნიმუშები იდენტურ ფენოლფორმალდეჰიდის ფისზე დამზადებულ სტანდარტთან ერთად სხივდებოდა ბირთვული რეაქტორის სველ არხში ВЭК–1 ნაკადით $2.6 \cdot 10^{12}$ ნეიტრონი / სმ^2 · წმ. პოლიეთილენში შეფუთული ნიმუში და სტანდარტი თავსდებოდა ალუმინის კონტეინერში (კონტეინერის მასალაა АЭ1 № 06106). განსაკუთრებული ყურადღება ექცეოდა იმ გარემოებას, რომ დასხივებულ ნიმუშში საძიებო ელემენტის განსაზღვრისას მნიშვნელოვანია ოპტიმალური მასისა და დროითი რეჟიმის შერჩევა, რათა სპექტრიდან მაქსიმალური ინფორმაციის მოპოვება შევძლოთ.

დასხივებული ნიმუშების გამოკვლევა ხდებოდა ანალიზატორით АИ–4096А–90 და გერმანიუმის დიფუზურ-დრეიფული დეტექტორით ДГДК 50 А1–3. დეტექტორის მოცულობაა 50 სმ^3 და გარჩევითობა – 3 კევ (Co^{60}-ის 1333 კევ ენერგიის γ-ხაზისათვის). გაზომვის შედეგად მიღებული სპექტრიდან ყველა საინტერესო იზოტოპის შესახებ მეტნაკლები ინფორმაციის მატარებელი ხაზის მონაცემებით და ფარდობითი მეთოდის გამოყენებით იზომებოდა ნიმუშში შესაბამისი მიკროელემენტების შემცველობა (აღმოჩენის ზღვარი შეადგენდა $10^{-8} – 10^{-9}$ გ / გ).

შრომაში შესწავლილი გვაქვს სხვადასხვა სახის ნიადაგები და შედარებული გვაქვს ერთმანეთთან ელემენტების რაოდენობრივი და თვისობრივი ცვლილებები სიღრმეების მიხედვით.

გაზომვების შედეგები მოცემულია ცხრილებში, სადაც ელემენტები დალაგებულია საანალიზო გამა-ხაზების ენერგიების ზრდის მიხედვით.

ცხრილი 1. წვერმაღალას ნიადაგების ელემენტშემცველობები (გ / გ).

№	ელემენტი	(0 – 5)სმ		(5 – 10) სმ		(10 – 20) სმ		(20 – 30) სმ	
		ნაკვეთი № 1	ნაკვეთი № 2	ნაკვეთი № 1	ნაკვეთი № 2	ნაკვეთი № 1	ნაკვეთი № 2	ნაკვეთი № 1	ნაკვეთი № 2
1	Mo	–	–	–	$(3.5\pm2.4)\cdot10^{-6}$	–	–	–	$(4.4\pm1.2)\cdot10^{-6}$
2	Cr	$(5.3\pm1.3)\cdot10^{-5}$	$(6.9\pm1.6)\cdot10^{-5}$	$(8.7\pm1.6)\cdot10^{-5}$	$(2.4\pm1.2)\cdot10^{-5}$	$(3.9\pm1.4)\cdot10^{-5}$	$(5.4\pm1.2)\cdot10^{-5}$	$(6.9\pm1.6)\cdot10^{-5}$	$(3.7\pm1.1)\cdot10^{-5}$
3	Cd	–	–	$(4.1\pm1.6)\cdot10^{-7}$	–	–	–	$(9.1\pm3.0)\cdot10^{-7}$	$(9.4\pm9.0)\cdot10^{-7}$
4	As	–	–	–	–	$(6.9\pm2.5)\cdot10^{-6}$	–	–	–
5	Ag	–	–	$(4.2\pm1.8)\cdot10^{-6}$	–	$(3.3\pm2.0)\cdot10^{-6}$	$(2.3\pm1.5)\cdot10^{-6}$	–	–
6	Zr	–	–	–	$(2.9\pm0.8)\cdot10^{-4}$	$(7.5\pm5.6)\cdot10^{-4}$	–	–	–
7	Cs	$(4.2\pm3.0)\cdot10^{-6}$	–	$(2.8\pm0.8)\cdot10^{-6}$	–	$(8.8\pm6.0)\cdot10^{-6}$	–	–	–
8	Sc	$(1.0\pm0.08)\cdot10^{-5}$	$(2.6\pm0.2)\cdot10^{-5}$	$(1.7\pm0.17)\cdot10^{-5}$	$(8.0\pm0.5)\cdot10^{-6}$	$(2.9\pm0.2)\cdot10^{-5}$	$(1.3\pm0.13)\cdot10^{-5}$	$(1.9\pm0.13)\cdot10^{-5}$	$(1.8\pm0.1)\cdot10^{-5}$
9	Rb	–	–	$(1.7\pm1.2)\cdot10^{-5}$	$(3.5\pm1.3)\cdot10^{-5}$	$(1.6\pm1.4)\cdot10^{-5}$	$(2.1\pm1.2)\cdot10^{-5}$	–	$(2.8\pm1.1)\cdot10^{-5}$
10	Zn	$(6.6\pm1.0)\ 10^{-5}$	–	–	$(8.2\pm1.0)\cdot10^{-5}$	$(4.1\pm1.2)\cdot10^{-5}$	$(2.0\pm0.26)\cdot10^{-4}$	–	–
11	Ta	–	$(2.3\pm1.2)\cdot10^{-7}$	$(4.0\pm0.5)\cdot10^{-7}$	$(1.2\pm0.85)\cdot10^{-7}$	$(3.9\pm1.6)\cdot10^{-7}$	–	–	–
12	Fe	$(7.3\pm0.95)\cdot10^{-2}$	$(4.0\pm0.5)\cdot10^{-2}$	$(1.8\pm0.25)\cdot10^{-2}$	$(2.1\pm0.27)\cdot10^{-2}$	$(3.8\pm0.5)\cdot10^{-2}$	$(2.9\pm0.38)\cdot10^{-2}$	$(2.2\pm0.3)\cdot10^{-2}$	$(2.6\pm0.34)\cdot10^{-2}$
13	Co	$(6.3\pm1.4)\cdot10^{-6}$	$(1.8\pm0.3)\cdot10^{-5}$	$(9.7\pm0.24)\cdot10^{-6}$	$(5.4\pm1.0)\cdot10^{-6}$	$(4.8\pm0.9)\cdot10^{-6}$	$(1.2\pm0.3)\cdot10^{-5}$	$(1.2\pm0.25)\cdot10^{-5}$	$(1.4\pm0.3)\cdot10^{-5}$
14	Na	$(6.0\pm2.8)\cdot10^{-4}$	$(1.2\pm0.3)\cdot10^{-3}$	$(5.6\pm2.8)\cdot10^{-4}$	$(1.21\pm0.6)\cdot10^{-4}$	$(6.2\pm2.6)\cdot10^{-4}$	$(2.1\pm0.8)\cdot10^{-4}$	$(5.4\pm3.2)\cdot10^{-4}$	$(7.2\pm1.8)\cdot10^{-4}$
15	Sb	–	$(8.0\pm2.5)\cdot10^{-7}$	–	–	–	–	$(8.0\pm2.8)\cdot10^{-7}$	–
16	La	$(3.6\pm0.3)\cdot10^{-5}$	$(4.9\pm0.8)\cdot10^{-5}$	$(2.3\pm0.5)\cdot10^{-5}$	$(5.2\pm1.0)\cdot10^{-5}$	$(6.3\pm0.9)\cdot10^{-5}$	$(2.8\pm0.5)\cdot10^{-5}$	$(3.2\pm0.5)\cdot10^{-5}$	$(4.8\pm0.7)\cdot10^{-5}$

ცხრილი 2. მამათისა და ფოთის ნიადაგების ელემენტშემცველობები (გ / გ).

№	ელემენტი	იზოტოპი	$T_{1/2}$	ენერგია E_γ, მევ ($T_{1/23}$)	(5 – 10) სმ		(10 – 20) სმ		(20 – 30) სმ	
					მამათი	ფოთი	მამათი	ფოთი	მამათი	ფოთი
1	Mo	Mo^{99}	67 სთ	142 (85)	–	$(7.2\pm1.6)\cdot10^{-5}$	–	$(1.3\pm0.65)\cdot10^{-5}$	$(4.4\pm2.9)\cdot10^{-6}$	–
2	Cr	Cr^{51}	27.8 დღ	320 (10)	$(2.2\pm0.3)\cdot10^{-4}$	$(1.2\pm0.2\cdot10^{-4}$	$(8.4\pm1.5)\cdot10^{-5}$	$(2.1\pm0.8)\cdot10^{-5}$	$(7.8\pm1.5)\cdot10^{-5}$	$(5.4\pm1.2)\cdot10^{-5}$
3	Cd	Cd^{115}	2.3 დღ	527.7 (33)	$(1.5\pm1.0)\cdot10^{-6}$	$(8.3\pm7.0)\cdot10^{-7}$	$(8.2\pm7.0)\cdot10^{-7}$	$(4.5\pm1.2)\cdot10^{-7}$	–	$(2.5\pm1.2)\cdot10^{-6}$
4	As	As^{100}	26.8 სთ	559 (44.7)	–	$(3.6\pm1.5)\cdot10^{-6}$	–	$(2.1\pm0.5)\cdot10^{-5}$	–	–
5	Ag	Ag^{110}	253 დღ	657.7 (96)	–	$(3.4\pm1.2)\cdot10^{-6}$	$(1.6\pm1.4)\cdot10^{-6}$	–	–	–
6	Zr	Zr^{95}	64.5 დღ	757 (55)	–	$(6.8\pm3.5)\cdot10^{-4}$	–	–	–	$(8.0\pm4.4)\cdot10^{-4}$
7	Cs	Cs^{134}	2.3 წლ	796 (85.4)	$(9.9\pm4.3)\cdot10^{-6}$	–	–	$(1.3\pm0.9)\cdot10^{-5}$	–	–
8	Sc	Sc^{46}	83.9 დღ	889 (99.8)	$(1.4\pm0.1)\cdot10^{-5}$	$(1.3\pm0.1)\cdot10^{-5}$	$(1.4\pm0.1)\cdot10^{-5}$	$(1.40\pm0.04)\cdot10^{-5}$	$(9.0\pm0.6)\cdot10^{-6}$	$(1.0\pm0.08)\cdot10^{-5}$
9	Rb	Rb^{86}	18.66 დღ	1076.6 (8.78)	–	$(1.4\pm1.0)\cdot10^{-5}$	$(1.4\pm1.0)\cdot10^{-5}$	–	$(2.4\pm1.1)\cdot10^{-5}$	–
10	Zn	Zn^{65}	244 დღ	1115.5 (5.7)	$(1.4\pm0.18)\cdot10^{-4}$	$(1.4\pm1.0)\cdot10^{-5}$	$(4.6\pm0.5)\cdot10^{-5}$	–	$(7.2\pm0.9)\cdot10^{-5}$	–
11	Fe	Fe^{59}	46.5 დღ	1291.5(43.20)	$(2.7\pm0.27)\cdot10^{-2}$	$(1.4\pm0.22)\cdot10^{-2}$	$(2.5\pm0.3)\cdot10^{-2}$	$(1.2\pm0.2)\cdot10^{-2}$	$(3.4\pm1.1)\cdot10^{-2}$	$(1.0\pm0.18)\cdot10^{-2}$
12	Co	Co^{60}	5.26 წლ	1332 (99.98)	$(1.2\pm0.26)\cdot10^{-5}$	$(1.2\pm0.26)\cdot10^{-5}$	$(7.1\pm2.0)\cdot10^{-6}$	$(8.90\pm2.67)\cdot10^{-6}$	$(2.1\pm0.5)\cdot10^{-6}$	$(1.0\pm0.24)\cdot10^{-5}$
13	Na	Na^{24}	15.05 სთ	1368 (100)	$(3.2\pm2.2)\cdot10^{-4}$	$(1.3\pm0.38)\cdot10^{-3}$	$(1.1\pm0.3)\cdot10^{-3}$	$(110\pm0.35)\cdot10^{-3}$	$(5.4\pm0.14)\cdot10^{-4}$	$(9.4\pm3.5)\cdot10^{-4}$
14	Sb	Sb^{124}	60.1 დღ	1496 (48.7)	–	$(4.1\pm2.0)\cdot10^{-7}$	–	$(6.2\pm2.5)\cdot10^{-7}$	–	–
15	La	La^{140}	40.27 სთ	1596.5 (95.2)	$(2.5\pm0.5)\cdot10^{-5}$	$(2.2\pm0.4)\cdot10^{-5}$	$(2.5\pm0.4)\cdot10^{-5}$	$(2.3\pm0.4)\cdot10^{-5}$	$(2.5\pm1.0)\cdot10^{-5}$	$(5.4\pm0.7)\cdot10^{-5}$

ცხრილში 1 მოცემულია წვერმაღალას № 1 და № 2 ნაკვეთების ნიადაგების ანალიზი-შედარება. ცხრილიდან ჩანს, რომ ორივე ნაკვეთში Cr, Se, Fe, Co, Na და La ცდომილების ფარგლებში ერთნაირი რაოდენობითაა განლაგებული სიღრმეების მიხედვით. Mo მხოლოდ № 2 ნაკვეთშია (5 – 10) და (20 – 30) სმ სიღრმეზე. As განისაზღვრა № 1 ნაკვეთში (10 – 20) სმ სიღრმეზე. Sb იზომება № 1 ნაკვეთში (20 – 30) სმ სიღრმეზე, ხოლო № 2 ნაკვეთში – (0 – 5) სმ სიღრმეზე. შემცველობები განისაზღვრა 65 %-იანი საიმედობის ალბათობით.

ცხრილში 2 განხილულია მამათის და ფოთის ნიადაგები. ცხრილიდან ჩანს, რომ Cr და Co შედარებით მეტი რაოდენობითაა მამათის ნიადაგში (10 – 20) და (20 – 30) სმ სიღრმეზე, Sb – ფოთის ნიადაგში (5 – 10) და (10 – 20) სმ სიღრმეზე. Ta არ განისაზღვრება არც ერთ ნაკვეთზე. Ag, Rb და Cs იზომება მამათის ნაკვეთზე. Cd მამათის ნიადაგში ცოტათი მეტია.

ცხრილში 3 განსაზღვრულია 29 ელემენტი (5 – 10), (10 – 20) და (20 – 30) სმ სიღრმეზე ურეკის და პირველი მაისის ნიადაგებში ჩაის პლანტაციის ქვეშ. Ce განისაზღვრა (5 – 10) სმ სიღრმეზე მხოლოდ მდ. რიონის სანაპირო ნიადაგში და დასაშვებ ნორმაზე ნაკლებია. Ag – მხოლოდ ჩაის ქვეშ ნიადაგში (20 – 30) სმ სიღრმეზე.

ცხრილი 3. ურეკისა და პირველი მაისის ნიადაგების ელემენტშემცველობები (გ / გ).

№	ელემენტი	(5 – 10) სმ		(10 – 20) სმ		(20 – 30) სმ	
		ურეკი	პირველი მაისი	ურეკი	პირველი მაისი	ურეკი	პირველი მაისი
1	Sm	$(2.21\pm0.19)\cdot10^{-7}$	$(2.3\pm0.27)\cdot10^{-7}$	$(6.70\pm0.33)\cdot10^{-7}$	$(3.56\pm0.32)\cdot10^{-7}$	$(3.04\pm0.24)\cdot10^{-7}$	$(2.15\pm0.28)\cdot10^{-7}$
2	Mo	$(2.89\pm1.18)\cdot10^{-5}$	$(1.37\pm1.12)\cdot10^{-5}$	$(8.0\pm2.16)\cdot10^{-5}$	$(2.04\pm1.26)\cdot10^{-5}$	$(2.20\pm1.08)\cdot10^{-5}$	$(1.49\pm1.28)\cdot10^{-5}$
3	Lu	–	$(1,18\pm0.67)\cdot10^{-7}$	$(1.96\pm0.98)\cdot10^{-7}$	$(1.10\pm0.88)\cdot10^{-7}$	$(1.20\pm1.03)\cdot10^{-7}$	$(1.12\pm0.75)\cdot10^{-7}$
4	Ce	$(8.5\pm6.9)\cdot10^{-5}$	–	–	–	–	–
5	Ir	–	$(3.4\pm2.07)\cdot10^{-8}$	$(1.18\pm0.34)\cdot10^{-7}$	$(1.47\pm0.84)\cdot10^{-7}$	$(4.99\pm2.34)\cdot10^{-8}$	$(2.02\pm1.49)\cdot10^{-8}$
6	Cr	$(5.92\pm1.42)\cdot10^{-5}$	$(2.17\pm1.21)\cdot10^{-5}$	$(6.5\pm1.56)\cdot10^{-5}$	$(8.92\pm1.78)\cdot10^{-5}$	$(1.0\pm0.17)\cdot10^{-4}$	$(2.17\pm1.32)\cdot10^{-5}$
7	Au	$(1.07\pm0.6)\cdot10^{-8}$	$(2.03\pm0.63)\cdot10^{-8}$	–	$(1.47\pm0.59)\cdot10^{-8}$	$(1.70\pm0.58)\cdot10^{-8}$	$(2.05\pm0.63)\cdot10^{-8}$
8	Ba	$(2.3\pm2.07)\cdot10^{-4}$	$(4.03\pm2.13)\cdot10^{-4}$	–	$(1.69\pm1.52)\cdot10^{-4}$	$(2.63\pm1.89)\cdot10^{-4}$	$(6.5\pm2.6)\cdot10^{-4}$
9	Cd	$(2.57\pm2.2)\cdot10^{-6}$	$(3.36\pm2.02)\cdot10^{-6}$	–	$(1.15\pm1.03)\cdot10^{-6}$	$(1.80\pm1.62)\cdot10^{-6}$	$(1.26\pm1.13)\cdot10^{-6}$
10	Nd	$(1.13\pm1.01)\cdot10^{-5}$	$(1.13\pm1.0)\cdot10^{-5}$	$(3.1\pm1.98)\cdot10^{-5}$	$(1.28\pm1.02)\cdot10^{-5}$	–	$(1.23\pm0.98)\cdot10^{-5}$
11	As	–	–	–	–	–	$(1.20\pm0.38)\cdot10^{-5}$
12	Pr	–	–	$(6.26\pm3.31)\cdot10^{-6}$	$(5.06\pm2.68)\cdot10^{-6}$	$(4.45\pm2.44)\cdot10^{-6}$	$(3.08\pm1.78)\cdot10^{-6}$
13	Ag	$(4.86\pm2.47)\cdot10^{-6}$	$(4.86\pm2.67)\cdot10^{-6}$	–	–	–	$(2.63\pm1.81)\cdot10^{-6}$
14	W	$(5.5\pm3.85)\cdot10^{-5}$	$(3.47\pm2.77)\cdot10^{-5}$	$(8.3\pm4.98)\cdot10^{-5}$	$(8.51\pm3.74)\cdot10^{-5}$	$(7.8\pm4.1)\cdot10^{-5}$	$(8.98\pm4.13)\cdot10^{-5}$
15	Zr	$(1.12\pm0.68)\cdot10^{-3}$	$(3.85\pm0.88\cdot10^{-3}$	$(1.81\pm0.83)\cdot10^{-3}$	–	–	$(5.27\pm4.74)\cdot10^{-4}$
16	Br	$(4.2\pm1.34)\cdot10^{-5}$	$(4.76\pm1.23)\cdot10^{-5}$	$(2.8\pm1.12)\cdot10^{-5}$	$(1.08\pm0.90)\cdot10^{-5}$	$(2.80\pm1.12)\cdot10^{-5}$	–
17	Cs	$(5.03\pm4.93)\cdot10^{-6}$	$(4.44\pm3.6)\cdot10^{-6}$	$(1.04\pm0.57)\cdot10^{-6}$	$(1.95\pm0.65)\cdot10^{-6}$	$(1.45\pm0.72)\cdot10^{-5}$	–
18	Sc	$(3.94\pm0.43)\cdot10^{-5}$	$(2.86\pm0.31)\cdot10^{-5}$	$(4.2\pm0.46)\cdot10^{-5}$	$(2.65\pm0.28)\cdot10^{-5}$	$(4.32\pm0.47)\cdot10^{-5}$	$(1.53\pm0.16)\cdot10^{-5}$
19	Th	$(3.03\pm2.09)\cdot10^{-7}$	$(8.55\pm2.99)\cdot10^{-7}$	$(6.77\pm3.18)\cdot10^{-7}$	$(8.55\pm3.25)\cdot10^{-7}$	$(4.45\pm3.11)\cdot10^{-7}$	–
20	Rb	–	$(1.36\pm0.72)\cdot10^{-5}$	$(1.09\pm0.69)\cdot10^{-5}$	$(1.05\pm0.49)\cdot10^{-5}$	$(1.05\pm0.53)\cdot10^{-5}$	–
21	Zn	–	$(1.09\pm0.19)\cdot10^{-4}$	–	$(3.74\pm0.71)\cdot10^{-5}$	–	$(3.16\pm0.60)\cdot10^{-4}$
22	Ta	$(3.86\pm1.5)\cdot10^{-7}$	$(2.97\pm1.42)\cdot10^{-7}$	$(4.76\pm1.8)\cdot10^{-7}$	$(2.67\pm1.73)\cdot10^{-7}$	$(3.56\pm2.06)\cdot10^{-7}$	$(2.08\pm1.78)\cdot10^{-7}$
23	Fe	$(2.2\pm0.24)\cdot10^{-2}$	$(2.79\pm0.3)\cdot10^{-2}$	$(1.45\pm0.2)\cdot10^{-2}$	$(2.30\pm0.25)\cdot10^{-2}$	$(2.35\pm0.25)\cdot10^{-2}$	$(2.68\pm0.29)\cdot10^{-2}$
24	Co	$(3.04\pm1.5)\cdot10^{-6}$	$(1.18\pm0.18)\cdot10^{-5}$	$(5.07\pm2.0)\cdot10^{-6}$	$(1.32\pm0.29)\cdot10^{-5}$	$(8.40\pm1.76)\cdot10^{-6}$	$(1.09\pm0.19)\cdot10^{-5}$
25	Na	$(4.2\pm0.84)\cdot10^{-3}$	$(1.19\pm0.28)\cdot10^{-3}$	$(3.4\pm0.78)\cdot10^{-3}$	–	$(3.40\pm0.78)\cdot10^{-3}$	$(1.6\pm0.4)\cdot10^{-3}$
26	Ho	$(7.3\pm4.82)\cdot10^{-8}$	$(6.09\pm2.49)\cdot10^{-8}$	$(4.87\pm6.08)\cdot10^{-8}$	–	$(1.46\pm0.40)\cdot10^{-7}$	$(7.32\pm3.88)\cdot10^{-8}$
27	K	$(1.06\pm0.43)\cdot10^{-3}$	$(5.81\pm3.02)\cdot10^{-4}$	$(7.7\pm4.93)\cdot10^{-4}$	$(1.35\pm0.60)\cdot10^{-3}$	$(1.06\pm0.44)\cdot10^{-3}$	$(1.06\pm0.43)\cdot10^{-3}$
28	La	$(1.3\pm0.18)\cdot10^{-5}$	$(2.24\pm0.22)\cdot10^{-5}$	$(4.46\pm0.40)\cdot10^{-5}$	$(3.35\pm0.33)\cdot10^{-5}$	$(1.50\pm0.24)\cdot10^{-5}$	$(2.09\pm0.25)\cdot10^{-5}$
29	Sb	–	–	$(9.83\pm3.93)\cdot10^{-6}$	$(3.78\pm1.66)\cdot10^{-6}$	$(4.53\pm3.53)\cdot10^{-6}$	$(5.29\pm2.06)\cdot10^{-6}$

ცხრილში 4 მოცემულია ნიადაგებში ელემენტების შემცველობები (0 – 5), (5 – 10), (10 – 20) და (20 – 30) სმ სიღრმეზე გვანაში კომშის ქვეშ და ხულოში მუხის ქვეშ. სულ განსაზღვრულია 27 ელემენტი. Lu, Ce, Cr, Au, Ba, Cd, Nd, As, Pr, Ag და Zn (0 – 5) სმ სიღრმეზე მუხის ქვეშ ნიადაგში არ იზომება, მაშინ როცა კომშის ქვეშ იმავე სიღრმეზე ეს ელემენტები იზომება. Ce გაიზომა კომშის ქვეშ ნიადაგში (10 – 20) სმ სიღრმეზე.

ცხრილში 5 მოცემულია ფოთის საცდელი სადგურის ნიადაგში ფორთოხლის ქვეშ და ლანჩხუთის რაიონში ჩაის ქვეშ ელემენტების შემცველობები. გაიზომა 25 ელემენტი (5 – 10), (10 – 20) და (20 – 30) სმ სიღრმეზე. აღმოჩნდა რომ Sm, Cr, Se, Fe, Co, Na და La ორივე ნიადაგში ერთნაირად იცვლება სიღრმის მიხედვით. Mo ფორთოხლის ქვეშ იზომება (5 – 10) და (10 – 20) სმ სიღრმის ნიადაგში, ხოლო ჩაის ქვეშ – (20 – 30) სმ სიღრმეზე. Au – მხოლოდ ფორთოხლის ქვეშ (20 – 30) სმ სიღრმეზე იზომება. ჩაის ქვეშ (20 – 30) სმ სიღრმეზე არ იზომება Au, Ba, Cd, Nd, As, Br, Cs და Ag.

ცხრილი 4. ხულოსა და გვანას ნიადაგების ელემენტშემცველობები (გ / გ).

№	ელემენტი	(0 – 5) სმ		(5 – 10) სმ		(10 – 20) სმ		(20 – 30) სმ	
		გვანა (კომშის ქვეშ)	ხულო (მუხის ქვეშ)	გვანა (კომშის ქვეშ)	ხულო (მუხის ქვეშ)	გვანა (კომშის ქვეშ)	ხულო (მუხის ქვეშ)	გვანა (კომშის ქვეშ)	ხულო (მუხის ქვეშ)
1	Sm	$(5.82\pm0.23)\cdot10^{-7}$	$(2.85\pm0.31)\cdot10^{-6}$	$(1.79\pm0.2)\cdot10^{-7}$	$(1.29\pm0.2)\cdot10^{-7}$	$(1.88\pm0.2)\cdot10^{-7}$	$(3.78\pm0.3)\cdot10^{-7}$	$(1.95\pm0.2)\cdot10^{-6}$	$(1.91\pm0.2)\cdot10^{-7}$
2	Mo	$(4.24\pm1.57)\cdot10^{-5}$	$(4.59\pm1.23)\cdot10^{-4}$	$(1.55\pm1.0)\cdot10^{-5}$	$(9.79\pm2.3)\cdot10^{-5}$	–	$(8.36\pm2.1)\cdot10^{-5}$	$(2.37\pm1.4)\cdot10^{-5}$	$(5.05\pm1.3)\cdot10^{-5}$
3	Lu	$(1.85\pm0.99)\cdot10^{-7}$	$(1.18\pm0.67)\cdot10^{-7}$	$(4.9\pm1.2)\cdot10^{-7}$	$(9.67\pm9.3)\cdot10^{-8}$	–	$(1.04\pm0.7)\cdot10^{-7}$	$(8.69\pm7.7)\cdot10^{-7}$	$(1.23\pm0.7)\cdot10^{-7}$
4	Ce	–	–	–	–	$(1.55\pm1.1)\cdot10^{-6}$	–	–	–
5	Ir	–	$(2.46\pm1.6)\cdot10^{-8}$	$(4.34\pm2.2)\cdot10^{-8}$	–	–	$(4.34\pm1.9)\cdot10^{-8}$	–	$(4.56\pm2.0)\cdot10^{-8}$
6	Cr	$(1.81\pm1.07)\cdot10^{-5}$	–	$(3.67\pm1.6)\cdot10^{-5}$	$(4.14\pm1.1)\cdot10^{-5}$	$(1.54\pm0.8)\cdot10^{-5}$	$(3.94\pm1.4)\cdot10^{-5}$	–	$(3.78\pm1.2)\cdot10^{-5}$
7	Au	–	–	–	–	–	$(2.1\pm0.7)\cdot10^{-8}$	$(5.84\pm5.2)\cdot10^{-9}$	–
8	Ba	–	–	$(2.72\pm2.3)\cdot10^{-4}$	$(4.94\pm2.1)\cdot10^{-4}$	–	$(2.47\pm2.0)\cdot10^{-4}$	–	$(9.62\pm2.5)\cdot10^{-4}$
9	Cd	$(1.94\pm1.55)\cdot10^{-6}$	–	$(1.26\pm1.1)\cdot10^{-6}$	$(1.2\pm1.1)\cdot10^{-6}$	$(1.89\pm1.2)\cdot10^{-6}$	$(1.47\pm1.3)\cdot10^{-6}$	–	$(6.26\pm5.0)\cdot10^{-6}$
10	Nd	$(5.19\pm2.6)\cdot10^{-5}$	–	$(2.36\pm1.5)\cdot10^{-5}$	$(1.44\pm1.2)\cdot10^{-5}$	$(1.59\pm1.4)\cdot10^{-5}$	$(2.26\pm1.6)\cdot10^{-5}$	$(1.85\pm1.7)\cdot10^{-5}$	–
11	Pr	$(8.24\pm2.88)\cdot10^{-6}$	–	–	$(3.24\pm2.1)\cdot10^{-6}$	$(6.45\pm3.9)\cdot10^{-6}$	–	$(7.74\pm3.4)\cdot10^{-6}$	–
12	Ag	$(2.63\pm2.36)\cdot10^{-6}$	–	$(4.45\pm3.36)\cdot10^{-6}$	$(3.24\pm2.13)\cdot10^{-6}$	–	–	$(3.84\pm2.91)\cdot10^{-6}$	–
13	W	–	$(7.09\pm3.97)\cdot10^{-5}$	$(8.35\pm4.92)\cdot10^{-5}$	$(4.25\pm3.82)\cdot10^{-5}$	$(1.43\pm0.45)\cdot10^{-4}$	$(5.04\pm4.53)\cdot10^{-5}$	$(6.3\pm4.53)\cdot10^{-5}$	$(1.43\pm0.26)\cdot10^{-4}$
14	Zr	$(2.9\pm0.78)\cdot10^{-3}$	$(2.8\pm0.75)\cdot10^{-3}$	–	$(1.12\pm0.73)\cdot10^{-3}$	$(2.34\pm0.86)\cdot10^{-3}$	$(1.32\pm0.7)\cdot10^{-4}$	$(1.28\pm0.78)\cdot10^{-3}$	$(8.57\pm6.08)\cdot10^{-4}$
15	Br	$(2.53\pm1.26)\cdot10^{-5}$	$(2.53\pm1.08)\cdot10^{-5}$	$(2.74\pm1.37)\cdot10^{-5}$	$(1.55\pm1.84)\cdot10^{-5}$	$(4.34\pm1.73)\cdot10^{-5}$	$(1.19\pm1.07)\cdot10^{-5}$	$(2.69\pm1.42)\cdot10^{-5}$	$(1.03\pm0.9)\cdot10^{-5}$
16	Cs	–	$(5.04\pm0.45)\cdot10^{-6}$	$(1.07\pm0.69)\cdot10^{-6}$	$(1.51\pm0.62)\cdot10^{-6}$	–	$(1.12\pm0.63)\cdot10^{-6}$	$(1.8\pm0.66)\cdot10^{-5}$	$(8.59\pm5.24)\cdot10^{-6}$
17	Sc	$(4.23\pm0.46)\cdot10^{-5}$	$(3.36\pm0.36)\cdot10^{-5}$	$(6.77\pm0.74)\cdot10^{-5}$	$(3.72\pm0.4)\cdot10^{-5}$	$(6.38\pm0.7)\cdot10^{-5}$	$(4.02\pm0.44)\cdot10^{-5}$	$(5.64\pm0.61)\cdot10^{-5}$	$(3.42\pm0.37)\cdot10^{-5}$
18	Th	$(4.81\pm3.41)\cdot10^{-7}$	$(2.67\pm1.89)\cdot10^{-7}$	$(9.62\pm4.1)\cdot10^{-7}$	$(3.32\pm2.4)\cdot10^{-7}$	–	–	$(3.56\pm3.2)\cdot10^{-7}$	–
19	Rb	$(5.25\pm4.2)\cdot10^{-2}$	$(1.46\pm0.59)\cdot10^{-5}$	$(1.05\pm0.6)\cdot10^{-5}$	–	$(1.4\pm0.5)\cdot10^{-5}$	$(8.78\pm0.5)\cdot10^{-6}$	$(3.03\pm0.9)\cdot10^{-5}$	$(1.32\pm0.5)\cdot10^{-5}$
20	Ta	$(3.26\pm1.49)\cdot10^{-7}$	$(6.24\pm1.74)\cdot10^{-7}$	$(1.28\pm0.3)\cdot10^{-6}$	–	$(1.78\pm1.6)\cdot10^{-7}$	$(9.8\pm3.3)\cdot10^{-7}$	$(5.64\pm2.5)\cdot10^{-7}$	$(8.91\pm1.9)\cdot10^{-7}$
21	Fe	$(3.46\pm0.37)\cdot10^{-2}$	$(1.07\pm0.11)\cdot10^{-2}$	$(2.9\pm0.3)\cdot10^{-2}$	$(2.36\pm0.2)\cdot10^{-2}$	$(3.35\pm0.4)\cdot10^{-2}$	$(1.38\pm0.2)\cdot10^{-2}$	$(2.76\pm0.3)\cdot10^{-2}$	$(1.99\pm0.2)\cdot10^{-2}$
22	Co	$(2.75\pm0.3)\cdot10^{-5}$	$(9.47\pm0.19)\cdot10^{-6}$	$(1.8\pm0.2)\cdot10^{-5}$	$(7.94\pm2.1)\cdot10^{-6}$	$(1.7\pm0.3)\cdot10^{-5}$	$(1.25\pm0.2)\cdot10^{-5}$	$(1.52\pm0.2)\cdot10^{-5}$	$(4.22\pm1.6)\cdot10^{-6}$
23	Na	$(2.42\pm0.58)\cdot10^{-3}$	$(5.74\pm3.3)\cdot10^{-4}$	$(1.66\pm0.4)\cdot10^{-3}$	$(1.66\pm0.4)\cdot10^{-3}$	$(2.11\pm0.5)\cdot10^{-3}$	$(1.18\pm0.4)\cdot10^{-3}$	$(5.74\pm3.1)\cdot10^{-4}$	$(1.18\pm0.4)\cdot10^{-3}$
24	Ho	$(3.65\pm2.29)\cdot10^{-8}$	$(3.65\pm2.9)\cdot10^{-8}$	$(4.87\pm2.5)\cdot10^{-8}$	–	$(1.4\pm0.5)\cdot10^{-7}$	$(8.48\pm4.2)\cdot10^{-8}$	–	$(1.09\pm0.4)\cdot10^{-7}$
25	K	–	$(7.74\pm4.3)\cdot10^{-4}$	$(1.35\pm0.5)\cdot10^{-3}$	–	$(8.71\pm5.1)\cdot10^{-4}$	$(8.71\pm5.6)\cdot10^{-4}$	$(6.77\pm3.3)\cdot10^{-4}$	–
26	La	$(7.26\pm1.59)\cdot10^{-6}$	$(1.6\pm0.2)\cdot10^{-5}$	$(8.3\pm2.1)\cdot10^{-6}$	$(2.24\pm0.2)\cdot10^{-5}$	$(2.2\pm1.3)\cdot10^{-6}$	$(2.4\pm0.3)\cdot10^{-5}$	$(7.78\pm1.5)\cdot10^{-6}$	$(1.03\pm0.2)\cdot10^{-5}$
27	Sb	$(4.53\pm3.85)\cdot10^{-6}$	$(5.29\pm2.1)\cdot10^{-6}$	$(9.07\pm2.8)\cdot10^{-6}$	$(1.05\pm0.3)\cdot10^{-5}$	$(7.56\pm3.1)\cdot10^{-6}$	$(1.05\pm0.3)\cdot10^{-5}$	$(7.94\pm2.7)\cdot10^{-6}$	$(3.78\pm1.3)\cdot10^{-8}$

ცხრილი 5. ღანჩხუთისა და ფოთის ნიადაგების შედარება (გ / გ).

N	ელემენტი	(5 – 10) სმ		(10 – 20) სმ		(20 – 30) სმ	
		ფოთის საცდელი სადგური (ფორთოხლის ქვეშ)	ღანჩხუთის რაიონი, მამათი (ჩაის ქვეშ)	ფოთის საცდელი სადგური (ფორთოხლის ქვეშ)	ღანჩხუთის რაიონი, მამათი (ჩაის ქვეშ)	ფოთის საცდელი სადგური (ფორთოხლის ქვეშ)	ღანჩხუთის რაიონი, მამათი (ჩაის ქვეშ)
1	Sm	$(2.9\pm1.9)\cdot10^{-7}$	$(1.70\pm0.18)\cdot10^{-7}$	$(1.2\pm0.1)\cdot10^{-7}$	$(1.37\pm0.17)\cdot10^{-7}$	$(2.8\pm0.2)\cdot10^{-7}$	$(1.7\pm0.2)\cdot10^{-7}$
2	Mo	$(7.2\pm1.6)\cdot10^{-5}$	–	$(1.30\pm0.65)\cdot10^{-5}$	–	$(1.40\pm0.47)\cdot10^{-7}$	$(4.4\pm2.9)\cdot10^{-6}$
3	Lu	$(1.4\pm0.5)\cdot10^{-7}$	$(5.8\pm1.0)\cdot10^{-7}$	–	$(5.5\pm4.0)\cdot10^{-8}$	$(1.40\pm0.47)\cdot10^{-7}$	$(6.5\pm6.0)\cdot10^{-8}$
4	Ir	$(4.9\pm1.4)\cdot10^{-8}$	$(5.3\pm1.6)\cdot10^{-8}$	–	$(8.5\pm1.8)\cdot10^{-8}$	$(7.4\pm1.7)\cdot10^{-8}$	$(3.4\pm1.7)\cdot10^{-8}$
5	Cr	$(1.2\pm0.2)\cdot10^{-7}$	$(2.2\pm0.3)\cdot10^{-4}$	$(2.1\pm0.8)\cdot10^{-5}$	$(8.4\pm1.5)\cdot10^{-5}$	$(5.4\pm1.2)\cdot10^{-5}$	$(7.8\pm1.5)\cdot10^{-5}$
6	Au	–	–	–	–	$(5.9\pm2.6)\cdot10^{-9}$	–
7	Ba	–	$(9.0\pm8.0\cdot10^{-4}$	–	–	$(1.0\pm0.15)\cdot10^{-3}$	–
8	Cd	$(8.3\pm7.0)\cdot10^{-7}$	$(1.5\pm1.0)\cdot10^{-6}$	$4.5\pm1.2)\cdot10^{-7}$	$(8.2\pm7.0)\cdot10^{-7}$	$(2.5\pm1.2)\cdot10^{-6}$	–
9	Nd	–	–	$(1.5\pm0.9)\cdot10^{-5}$	$(1.6\pm1.0)\cdot10^{-5}$	$(1.2\pm0.9)\cdot10^{-5}$	–
10	As	$(3.6\pm1.5)\cdot10^{-6}$	–	$(2.1\pm0.5)\cdot10^{-6}$	–	–	–
11	Br	–	–	$(1.5\pm0.8)\cdot10^{-5}$	–	$(1.0\pm0.67)\cdot10^{-5}$	–
12	Cs	–	$(9.9\pm4.3)\cdot10^{-6}$	$(1.3\pm0.9)\cdot10^{-5}$	–	–	–
13	Sc	$(1.3\pm0.1)\cdot10^{-5}$	$(1.4\pm0.1)\cdot10^{-5}$	$(1.40\pm0.04)\cdot10^{-5}$	$(1.4\pm0.1)\cdot10^{-5}$	$(1.00\pm0.08)\cdot10^{-5}$	$(9.0\pm0.6)\cdot10^{-6}$
14	Ag	$(3.4\pm1.2)\cdot10^{-6}$	–	–	$(1.6\pm1.4)\cdot10^{-6}$	–	–
15	Th	–	–	–	–	$(1.9\pm1.5)\cdot10^{-7}$	$(1.6\pm0.4)\cdot10^{-7}$
16	Rb	$(1.4\pm1.0)\cdot10^{-5}$	–	–	$(1.4\pm1.0)\cdot10^{-5}$	–	$(2.4\pm1.1)\cdot10^{-5}$
17	Zn	–	$(1.40\pm0.18)\cdot10^{-4}$	–	$(4.6\pm0.6)\cdot10^{-5}$	–	$(7.2\pm0.9)\cdot10^{-5}$
18	Fe	$(1.40\pm0.22)\cdot10^{-2}$	$(2.70\pm0.27)\cdot10^{-2}$	$(1.2\pm0.2)\cdot10^{-2}$	$(2.5\pm0.3)\cdot10^{-2}$	$(1.0\pm0.18)\cdot10^{-2}$	$(3.4\pm1.1)\cdot10^{-2}$
19	Co	$(1.20\pm0.26)\cdot10^{-5}$	$(1.20\pm0.26)\cdot10^{-5}$	$(8.90\pm2.67)\cdot10^{-6}$	$(7.1\pm2.0)\cdot10^{-6}$	$(1.0\pm0.24)\cdot10^{-5}$	$(2.1\pm0.5)\cdot10^{-6}$
20	Na	$(1.30\pm0.38)\cdot10^{-3}$	$(3.8\pm2.2)\cdot10^{-4}$	$(1.10\pm0.35)\cdot10^{-3}$	$(1.1\pm0.3)\cdot10^{-3}$	$(9.4\pm3.5)\cdot10^{-4}$	$(5.40\pm0.14)\cdot10^{-4}$
21	La	$(2.2\pm0.4)\cdot10^{-5}$	$(2.5\pm0.5)\cdot10^{-5}$	$(2.3\pm0.4)\cdot10^{-5}$	$(2.5\pm0.4)\cdot10^{-5}$	$(5.4\pm0.7)\cdot10^{-5}$	$(5.2\pm1.0)\cdot10^{-5}$
22	Sb	$(4.1\pm2.0)\cdot10^{-4}$	–	$(6.2\pm2.5)\cdot10^{-7}$	–	–	–
23	Zr	$(6.8\pm3.5)\cdot10^{-4}$	–	–	–	$(8.0\pm4.4)\cdot10^{-4}$	–
24	Pr	$(7.6\pm4.5)\cdot10^{-6}$	$(7.6\pm6.0)\cdot10^{-6}$	$(4.5\pm3.0)\cdot10^{-6}$	$(4.4\pm3.5)\cdot10^{-6}$	$(1.6\pm0.6)\cdot10^{-6}$	–
25	W	$(7.3\pm2.8)\cdot10^{-5}$	–	$(5.6\pm2.5)\cdot10^{-5}$	–	$(2.5\pm2.0)\cdot10^{-5}$	$(4.8\pm0.8)\cdot10^{-5}$

ნიადაგი არასტაბილური და არაინერტული მასაა. ხდება ელემენტების კანონზომიერი მიგრაცია სისტემაში ნიადაგი – მცენარეები – ნიადაგი და რადგან ადამიანი ნიადაგიდან იღებს თითქმის ყველაფერს, ამიტომ მისი ჯანმრთელობის

მდგომარეობა დიდად არის დამოკიდებული ნიადაგის და მასზე მოსული პროდუქტების ელემენტშემცველობაზე. დღევანდელი ცხოვრების პირობების გამო, როდესაც ხშირად შეუძლებელია დაავადების გამომწვევი მიზეზების დადგენა, აუცილებელია ჩვენს ხელთ არსებული ყველანაირი საშუალება გამოვიყენოთ ეკოლოგიურად სუფთა საცხოვრებელი გარემოს შესაქმნელად [8, 9]. ამ საქმეში ჩვენს ლაბორატორიასაც შეუძლია თავისი სიტყვა თქვას. აღნიშნული მიმართულებით განხორციელებული კვლევები უნდა გაგრძელდეს და გაფართოვდეს. უნდა მოხდეს სასოფლო-სამეურნეო რაიონებში ნიადაგებისა და მცენარეული საფარის ელემენტშემადგენლობის შესწავლა საქართველოს მთელი ტერიტორიის მასშტაბით. გარდა აღნიშნული კვლევებისა, აუცილებელია ჩატარდეს რადიოლოგიური კვლევები ნიადაგებში ბუნებრივი და ტექნოგენური წარმოშობის რადიოიზოტოპების კონცენტრაციების განსაზღვრის მიზნით. მიღებული შედეგების საფუძველზე შესაძლებელი იქნება შედგეს საქართველოს ნიადაგების ელემენტშემადგენლობისა და რადიოიზოტოპების გავრცელების მაჩვენებელი რუკა. ამჟამად ჩვენს ლაბორატორიაში გვაქვს ნეიტრონული გამამრავლებელი ПС–1, რომელიც წარმოადგენს სითბური ნეიტრონების წყაროს. ნეიტრონების ნაკადის სიდიდეა $2.5 \cdot 10^6$ ნეიტრონი / სმ^2 · წმ. ლაბორატორია აღჭურვილია თანამედროვე გამა-სპექტრომეტრული კომპლექსით, კერძოდ, მაღალი სისუფთავის HpGe-ის დეტექტორით, მრავალარხიანი ანალიზატორით InSpector 2000 და პროგრამული უზრუნველყოფით Genie–2000. არსებული ტექნიკური ბაზა და ჩვენს მიერ შემუშავებულ "ოპტიმიზაციისა" და "პოლიკომპარატორის" (გ. გორდაძე) მეთოდები საშუალებას იძლევა მიკროელემენტების კონცენტრაციები, მაღალი სიზუსტით გაიზომოს როგორც ბიოლოგიურ, ისე – გეოლოგიურ ნიმუშებში.

მითითებები

1. Г. П. Гордадзе, А. А. Гоголи, Г. Г. Сванидзе, В. В. Лежава, А. Г. Надибаидзе, Ц. И. Квирикашвили, В. Я. Кинцурашвили, Л. Г. Мачавариани. Результаты массового нейтронного активационного анализа почв, вод и перспективы дальнейших исследований. Нейтронно-активационный анализ и его применение в народном хозяйстве, III, 1989, Тбилиси: Мецниереба, 34-62.
2. Г. П. Гордадзе, А. А. Гоголи, В. В. Лежава, О. Т. Кения, А. Г. Надибаидзе. Разработка методик нейтронного активационного анализа сельскохозяиственных и экологических объектов и возможность их использования для повышения продуктивности, охраны и оздоровления окружающей среды Грузии. Нейтронно-активационный анализ и его применение в народном хозяйстве, II, 1987, Тбилиси: Мецниереба, 57-88.
3. Г. П. Гордадзе, В. В. Лежава, М. Г. Шеварднадзе, Г. Э. Самаргуляни, Ц. И. Пипиа, Г. Г. Мачавариани, А. Г. Надибаидзе. Определение содержаниа и распроделения элементов в железо–марганцевых конкрециях почв влажных субтропиков Западной Грузии с использованием НАА. Тез. докл. V Всесоюз. сов. по активац. анализу и другим радиоаналит. методом, II, 1987, Ташкент, 372.
4. А. А. Кист. Феноменология биогеохимии и бионеорганической химии. 1987, Ташкент: Фан.
5. Г. Гордадзе. Оптимизация активационного анализа. 1985, Москва: Энергоатомиздат.
6. А. Г. Надибаидзе, Г. П. Гордадзе, Ц. И. Квирикашвили, В. Я. Кинцурашвили, А. А. Гоголи, Н. И. Джагоднишвили. Выбор оптимальных нейтронно-активационных методик определения содержания микроэлементов в биологических объектах и природных водах. Тр. II Всесоюз. совещ. «Ядерно-физические методы анализа в контроле окружающей среды», 1985, Ленинград: Гидрометеоиздат, 84-87.
7. Г. Гордадзе. Поликомпараторный метод нейтронного активационного анализа с использованием нейтронов ядерного реактора. Нейтронно-активационный анализ и его применение в народном хозяйстве, III, 1989, Тбилиси: Мецниереба, 28-36.
8. P. Imnadze, Ts. Kvirikashvili K. Megrelishvili, G. Ghotvadze, T.Getsadze, V. Kintsurashvili. Determination of element of "Sabe" Earth using a neutron multiplier. Science and Technologies (J. Georg. Acad. Sci.), 2004, 1-3, 18-22.
9. პ. იმნაძე, ც. კვირიკაშვილი, ა. გორდაძე, ნ. ლობჟანიძე. ბუნებრივი რადიონუკლიდების კონცენტრაციების განსაზღვრა საშენ მასალებში რადიომეტრული და გამა-სპექტრომეტრული ანალიზის გამოყენებით. თეზ. კრ. საერთ. სამეც. კონფ. "გამოყენებითი ფიზიკის აქტუალური საკითხები", 2011, თბილისი: ტექნიკური უნივერსიტეტი, 40-41.

APPLYING SOCIAL SCIENCE RESEARCH METHODS FOR TECHNOLOGY ASSESSMENT OF NANOTECHNOLOGIES

T. Chachibaia [1], E. R. Raupp [2]

[1] Responsible Nanotechnology Center of Georgia
Tbilisi, Georgia
nanogeorgia@gmail.com
[2] The Georgia Forecast
Tbilisi, Georgia

Accepted March 3, 2012

Introduction

Research into nanotechnology's impact on any societal implication, as ethical, environmental, economic, legal aspects, must try to keep pace with the technological progress that has been made. Otherwise, the technological progress will slow down [1]. This will be one of the first times in history that social scientists have such a participatory role in nanotechnology's development. Research methods in the economic, social, and behavior science will allow social sciences to evaluate nanotechnology developments, as well as government funding for research provides input toward the improvement of potential applications. To have such a role, social scientists need to proceed beyond the data in econometric studies in order to get inside the research and development processes as they occur. The techniques of interpretive social research (e.g. interviews and focus groups), as well as original data collection with surveys will enhance our ability to understand societal and economic effects much more than archival data [2].

Technology and society evolve together. Nuclear weapons joined with U.S. and Soviet hegemonies to constitute a prime determinant of geopolitical evolution after World War II. Cars, television, air conditioning, and birth control likewise arose in particular social contexts and contributed to the remaking of everyday life [3].

No one can fully understand the long-term implications of such advances, emerging under the heading of nanotechnology – "the art and science of building complex, practical devices with atomic precision", with components measured in nanometers, billionths of a meter. The essence of the nanotechnology story is the continuation of a fifty-year trend of machine miniaturization culminating in the rise of design control at the molecular level. Nanotechnology is not confined to a single area of innovation; "smallness" is its unifying attribute. Researchers in a number of technical fields are keenly interested in manipulation of matter at the nanoscale, and funding is assured because many of the research forefronts hold promise for business and military applications [3].

In an ideal world, scientists would communicate scientific knowledge clearly and effectively to laypersons, who would then understand the knowledge and use it to make sound judgments about science policy. After Hiroshima and Nagasaki, scientists made a great effort to

explain the atom to the public, thereby preparing the public to accept nuclear plants to generate electricity. During the 1950s and 60s, NASA and the media presented the basics of space science in a friendly way which enabled millions to understand it, at least at a rudimentary level. Currently the Human Genome Project devotes at least 3 % of its budget to ethical, legal and social issues, including public understanding. In these three examples, scientists and science teachers have aspired to an ideal model of communication and understanding. In many other cases, however, the world is far from ideal. Certain cultural values, including strong hopes and deep fears, are likely to shape public understanding of nanotechnology. To paraphrase Rosenberg, nanotechnology will be appreciated or feared, not because of its scientific merits, but because of pre-existing extrascientific values. Nanophilic hopes and nanophobic fears will not wait until after scientific work is completed, assessed and disseminated. According to Toumey (2004), the tangible results of nanotech will be selectively appreciated and interpreted in accordance with those hopes and fears.

Nanotechnology must be developed in a safe and responsible manner. Ethical principles must be adhered to and potential health, safety or environmental risks scientifically studied, also in order to prepare for possible regulation. Societal impacts need to be examined and taken into account. Dialogue with the public is essential to focus attention on issues of real concern rather than "science fiction" scenarios [4].

Exploring importance of technology assessment

Scientific and technological innovation continually remakes society. *Technology Assessment* (TA) can significantly enhance the societal value of research-based innovation.

A half-century ago, philosopher and skeptics critic of technology, Jacques Ellul (1967) argued that the rise of technology leads to the decline of traditional spirituality, as man transfers "his sense of the sacred … to technique itself". We develop a "worship of technique", Ellul said, and we associate our technology with a "feeling of the sacred".

According to skeptics point of view Jacques Ellul (1967, 1980), technology perhaps is the most pervasive and potentially dehumanizing product of modern life.

Selected questions adapted from the Jacques Ellul Society's Seventy-Six Reasonable Questions to Ask About Any Technology (International Center for Technology Assessment, 2002) were used specifically to stimulate debate and analysis in the ethics seminars. The following questions were used:

Ecological: Does it preserve or reduce ecosystem integrity? How much, and what kind of waste, does it generate? Does it incorporate the principles of ecological design?

Social: How does it affect our way of seeing and experiencing the world? Does it serve to commodify knowledge or relationships? To what extent does it redefine reality?

Moral: What values does its use foster? What is gained by its use? What are its effects on the least advantaged in society?

Ethical: What does it allow us to ignore? Can we assume personal or communal responsibility for its effects? Can its effects be directly apprehended? What behavior might it make possible in the future? What other technologies might it make possible?

Political: Does it concentrate or equalize power? Does it require or institute a knowledge elite? Does it require military defense? Does it enhance or serve military purposes? How does it

affect warfare? Is it consistent with the creation of a global economy? Does it empower transnational corporations? What kind of capital does it require?

According to Ellul, technology ultimately acts to isolate people from each other and from the natural environment, and despite the (usual) benignity of its intended consequences, there always are unforeseen negative consequences. Most provokingly, Ellul (1980) also suggested that technological development will soon reach a point at which direct human control will no longer be necessary or possible [5]. Eric Drexler's the author of "Machines of Creation" and who was awarded an interdisciplinary degree, the world's first doctorate in nanotechnology, noted that nanotechnology is perfectly suited to arouse religious enthusiasm, it involves incredible, invisible powers.

Richard Smalley (1995), Nobel Prize winner, claims in the introductory part of a public speech about his very specific work on the use of carbon nanotubes for energy storage, that, the list of things you could do with such a technology, i.e. nanotechnology, reads like much of the Christmas Wish List of our civilization.

The starting points with the development of nanotechnology needs to develop approaches and methodologies that can address doubly "fictional" character of *technology assessment* of nanotechnology. Many of the envisaged uses of nanotechnology are still science fiction, and the study of possible impacts is therefore social science fiction [6].

Headlines about, e.g. self-replicating nano-robots (according to M. Crichton, Prey), that are well beyond our present capability but are often presented as an immediate risk, demonstrate that there is an urgent need to provide information about present-day nanotechnology research and its possible applications [4].

"Real time" TA has been proposed [7] by Sarewitz and Guston (now at Arizona State University). Further development of such approaches and methods is important, including ways of 'public engagement' as it is now called in the UK (see: Report of the Royal Society – 2004). However, methods development should be embedded in understanding of innovation dynamics and the embedding of technology in society [6].

Public reactions to nanotechnology in the U.S. are more difficult to envision this way because there has been practically no history of public awareness. In lieu of such information, we need to turn to past episodes of the arrival of new forms of science and technology, and public reactions to them: atomic energy, space science, cold fusion, stem cell research, remediation of environmental disasters, genetically modified foods, and so on. American society has had many experiences with the arrival of new technologies, and perhaps comparisons and analogies with some of them will help us anticipate public reactions to nanotechnology. According to Toumey (2004), the following general statements describe numerous episodes of the arrival of new technologies presented here as the these and anti-these.

New technologies perceptions by scoity	
these	**anti-these**
1A. When a new technology arrives, it will be so expensive that only the very wealthy can afford it, thereby exaggerating class differences. (Think of the initial days of cell phones, hand-held calculators, and air bags in cars, for example.)	1B. Shortly after a new technology arrives, mass production will great reduce the cost, thereby democratizing its availability. (Think of the second phase of cell phones, hand-held calculators, and air bags in cars.)

2A. If a new technology involves profound changes in health or medicine, some people will object that scientists and doctors are playing god. (Here one might recall organ transplants, tissue transplants and technology-assisted reproduction.)	2B. If a new technology involves profound changes in health or medicine, some people (including patients, their doctors, and their families, plus administrators, investors and manufacturers) will fervently advocate for its use, on the grounds that patients should not suffer or die needlessly. (Here one might recall organ transplants, tissue transplants and technology-assisted reproduction.)
3A. The best way to nurture an expensive new technology is to consign it to processes of proprietary capitalism, centered on patents and copyrights, because no one else besides proprietors and their investors will have the will or the resources to develop it, and because this will protect it from political interference. (Currently this argument is made on behalf of pharmaceutical research.)	3B. The best way to nurture an expensive new technology is through public funding and government regulation, so that potential dangers can be closely monitored, and the benefits of the new technology will become available to the largest possible number of people. (Here a good example is the Human Genome Project.)
4A. As Dorothy Nelkin (1987) pointed out, the media usually embrace a new technology enthusiastically and emphasize its promises and supposed advantages. (Perhaps you can recall the initial accounts of cold fusion from 1988.)	4B. As Dorothy Nelkin (1987) pointed out, the media often denounce a new technology when it is seen to be imperfect, that is, when it fails to fulfill utopian expectations, even though the exact same media may have previously exaggerated its promises and supposed advantages. (No doubt you can recall the later accounts of cold fusion.)

Survey reveals public attitudes to NanoS&T

Jan / Feb 2005 survey on Europeans' experience and perception of science and technology includes some questions regarding nanotechnology:

– Ca. 20 % not at all interested in general S&T (U.S. – ca. 10 %);
– Among those interested, NT receives by far the lowest rate of interest;
– Developments in medicine are by far the field in which respondents are the most interested in (W 73 %, M 50 %), and the second most mentioned item is the environment.

High interest in medicine and environment can be explained: both areas are linked to health issues – public health issues S&T area with highest interest (also in the U.S.). Positive effect on our way of life in the next 20 years are especially expected from new medical and energy technologies, though people are not interested in NT so far (lowest numbers 8 % and high 'no-response' rate) [8].

Scientific literacy for nanotechnology is practically nonexistent and general scientific literacy in this country is very poor. Trends seem to be similar in U.S. and Europe.

General public does not know very much about nanotechnology:

– GB 2004: 29 % have heard about NT, 19 % can give some kind of definition;
– D 2004: 30 % have heard about NT, 15 % can link it to specific developments;

- USA 2004: > 80 % had heard "little" or "nothing" about NT, most could not correctly answer factual questions about it;
- Majority (~ 90 %) is not interested in NT (or does not care);
- Nanotechnology is perceived as a 'fuzzy' concept;
- Positive expectations prevail over negative;
- The higher the (subjective) level of information and the level of education, the lower the 'fear of risk'.

To summarize attained results of this survey that reveals 'no attitudes'. Since qualitative judgments about NT mainly similar to general attitudes to S&T.

Conceptual focus of technology assessment

Technology assessment (TA) developed as a scientific and societal reaction to the problem of how to deal with complex side effects and uncertainties in science and technology [8]. The main questions defined to be answered by TA:

- whether and how knowledge of side-effects can already be integrated into decision-making processe;
- the problem of dealing with the inevitable uncertainties of knowledge;
- the unintended side-effects of science, technology and technological advance can be experienced in modern age.

The respective concepts offered by TA to society and politics are strongly dependent on the context – and require continued modernization if these contexts are subject to rapid changes in a dynamically developing global society [9].

Technology assessment is dedicated to help business, government and the public anticipate and manage possible health and environmental implications of nanotechnology [10].

It is therefore important that, in parallel with technological development, appropriate R&D is undertaken to provide quantitative data on toxicology and ecotoxicology (including human and environmental dose response and exposure data) to perform risk assessments and, where necessary, to enable risk assessment procedures to be adjusted. Scientific investigation and assessment of possible health or environmental risks associated with nanotechnology need to accompany the R&D and technological progress. Addressing the potential risks of nanotechnologies to public health, the environment and consumers will require evaluating the possible re-use of existing data and generating new, nanotechnology-specific data on toxicology and ecotoxicology (including dose response and exposure data). This also calls for examining and, if required, adjusting risk assessment methods. In practice, addressing the potential risks associated with nanotechnologies necessitates that risk assessment be integrated into every step of the life cycle of nanotechnology-based products [4].

Nanotechnologies present new challenges also for the assessment and the management of risks. We need formal risk analysis because risk is one of the most important ethical and social issues we could imagine [11].

Public uncertainty of NT benefits vs. risks perceptions on health and environment

Nanotechnology could ultimately turn out to be risky, but the prudent way to assess the risks is not the abandonment of the field. Society needs formal risk analysis because risk is one

of the most important ethical and social issues. Just as fear of cloning could slow efforts in biomedicine and fear of genetically modified foods could contribute to hunger, fear of futuristic nanobots running amok could delay the benefits offered by nanotechnology. When discourse is founded on emotional prejudices, its unreasonableness discredits the legitimate need to identify and assess risks [11].

Health risks of nanoparticles may link NT to areas of greater public attention. Proven health risks, or uncertainties, may link NT debates with historical technology debates (hazardous chemicals, GMO) [12].

Science & Engineering typically assume probabilities and consequences of adverse events, and hence the "risks", as to be objectively quantified by *risk assessment*. Social Science analysis rejects this notion. It focuses instead on the effects that risky outcome distributions have on the people who experience them. By Paul Slovic and Elke Weber, risk is seen as inherently subjective.

Two aspects of risk

Characterisation of risk has both quantitative and qualitative components:

a) Risk can be technically defined, e.g.:
   Risk = Hazard × Exposure (health risk);
   Risk = Damage × Probability of Occurrence (insurance);

b) Risk can be culturally defined:
   "A thread to that which we value";
   "The probability of loss of that which we value" risk;
   "Perceptions of risk play a prominent role in the decisions people make, in the sense that differences in risk perception lie at the heart of disagreements about the best course of action" (Slovic);
   "It is not the things themselves that disturb us but our views of them" (Epiktet).

The risk debate

According to [13], there are different types of risks:
Risks of visions: Visions show real consequences regardless of their seriousness;
Risks of unknown material properties at the nanoscale;
Risks of (failed) communication and of public engagement.

TA could include a 'vision assessment' that aims to achieve transparent, knowledge-based discussion about imaginations of the future. Vision assessment within a TA process could prevent 'fear of fears' and help to avoid damages for the development of S&T and for the culture of democratic decisions.

Visions (positive and negative) are an important topic in the public communication of NT ('Bill Joy – Debate', visualizations in magazines, popular culture: 'Prey', 'Matrix', …). Visions may shape acceptance and further development of this field. Visions are ambivalent: high potentials often include high risks.

Challenging issues that may arise associated with the risks of new material properties:

New (surprising and partially still unknown) properties of materials at the nanoscale. (e.g. behaviour of nanoparticles in the human body and the environment needs extensive research, though already on the market);

NanoToxicology – first results, knowledge still insufficient, challenges for conventional methods of toxicological research;

"New forms of known chemicals" or "new chemicals because of different chemistry"?

Recommendations for policymakers for public involvement in dialogue and risk evaluation: to incorporate views from the general public in decision-making; improve the knowledge base and quality of decisions establish trust and legitimacy; identify issues, mediate and resolve conflicts, reduce risk of rejection; educate and inform.

TA provides procedural knowledge on risk communication and experiences from public and political debates about other 'risk technologies' (nuclear, genetic, …). TA as a process contributes to societal opinion forming, addresses public concerns, supports public understanding of science and technology. TA provides knowledge and methods to avoid mistakes, to reduce uncertainties and support diffusion of NT [13].

In light of this perception of potential danger, the Foresight Institute (nonprofit educational organization established to help society prepare for advanced technologies) has drafted a set of guidelines for the ethical development of nanotechnology. These include the banning of free-foraging self-replicating pseudoorganisms on the Earth's surface, at least, and possibly in other places.

A fear exists that nanomechanical robots, if achieved, and if designed to self-replicate using naturally occurring materials (a difficult task), could consume the entire planet in their hunger for raw materials, or simply crowd out natural life, out-competing it for energy. Some commentators have referred to this situation as the "grey goo" or "ecophagy" scenario. K. Eric Drexler considers an accidental "grey goo" scenario extremely unlikely and says so in later editions of Engines of Creation. The "grey goo" scenario begs the Tree Sap Answer: what chances exist that one's car could spontaneously mutate into a wild car, run off road and live in the forest off tree sap?

Enforsement visions of nanotechnology – Strength in science, sound ethics

"The best defense against nanotech misuse is good nanotechnology" (Reynolds).

"Any powerful technology can be abused" (Carroll) [14].

It would be difficult to deny the potential benefits of nanotechnology and stop development of research related to it since it has already begun to penetrate many different fields of research. However, nanotechnology can be developed using guidelines to insure that the technology does not become too potentially harmful. *Technology assessment* recognizes the fact that scientists normally are not trained ethicists themselves and accordingly ought to be very careful when passing ethical judgment on their own, or their colleagues', new findings, projects, or work in progress.

As with any new technology, it is impossible to stop every well funded organization who may seek to develop the technology for harmful purposes. However, if the researchers in this field put together an ethical set of guidelines (e.g. Molecular Nanotechnology Guidelines, Foresight Institute – 2000) and follow them, then we should be able to develop nanotechnology safely while still gathering its promised benefits. Recent technical proposals for Molecular

Nanotechnology (MNT) nanofactories do not include self-replicating nanobots, and recent ethical guidelines prohibit self-replication. MNT nanofacturing is popularly linked with the idea of swarms of coordinated nanoscale robots working together, as proposed by Drexler in his 1986 popular discussions of the subject in the "Engines of Creation". It is proposed that sufficiently capable nanobots could construct more nanobots.

New scientific discoveries and the ensuing technologies are often accompanied or followed by utopian or dystopian visions about the future of humankind under their new dominance. These visions can be found in science communication, literature ('high' and 'low' level), in popular science, in newspaper articles, books, cinema and TV series, Internet and also in more or less arcane religious sects. This especially holds for current themes around nanotechnology. What effects do such visions have on society and back on the further development of nanoscience? (see [15]).

What are the chances and what are the risks of the fictionalisation of nanotechnology? Nanoscience and nanotechnology are among today's most promising fields of research. As NT quickly develops, the ethical evaluation of such a development has yet to begin. If their full potential is to be realized, we need to attend along the way to key ethical issues. But ethics should not be grounded in exaggerations, either positive or negative; hyperbole just obscures important issues [15].

To what extent does this already influence the interpretation of facts and the visions of future development? "The need for special ethical principles in a scientific society is the same as the need for ethical principles in society as a whole. They are mutually beneficial. We must become competent in dealing with moral concerns related to all new technologies. And remember that a code of ethics will not solve all ethical problems". "We must remember that good laws, if they are not obeyed, do not constitute good government. Hence there are two parts of good government; one is the actual obedience of citizens to the laws, the other part is the goodness of the laws which they obey ..." (Aristotle, Politics).

In 1980s, when nanotech pioneer and Foresight Institute's founder and Chairman up to 2003, K. Eric Drexler considered keeping his thoughts quiet, rather than risk opening a Pandora's box of new technology with threats that could include a range of microscopic terrors. But in the end Drexler and his colleagues reached a simple conclusion: "If you don't discuss it, someone else would come along and develop it. And their intentions might not be as good" [14].

K. Eric Drexler, author of Engines of Creation, has begun to develop guidelines for the use of NT, particularly concerning self-replication, but also issues such as wealth distribution and environmental protection [1] (see: Foresight Guidelines for Responsible Nanotechnology Development) .

The ethical issues associated with NT fall into a variety of categories including:

1) Equity: NT does not stand to help developed countries only, but also (and perhaps mainly) developing countries. For example, third world countries suffer most from things that can be improved upon from advancements made in NT. For instance, providing cleaner water, developing cheaper energy, and also the enormous health benefits to be reaped from NT are all aspects of NT that could have a dramatic impact on third world countries. A global opinion-leaders network for social and ethical implications ought to be established so that third world countries may be involved.
2) Privacy and security: While NT could dramatically improve surveillance systems and would undoubtedly have numerous military applications, some are left wondering how

personal privacy would be affected. Questions concerning the regulation of this new technology are arising without many answers being offered. As nanotechnology begins to deliver new and improved weapons, secrecy will eventually mask important research work.

The first round of nanotech-inspired materials, for example, is likely to find an active suitor within the U.S. defense industry – particularly for radar-resistant, lighter and much more durable materials. And as the first weapons to use nanotechnology go into development, secrecy is likely to follow.

For now nanotechnology doesn't have any applications in the war on terrorism because it's still too young. Nanotechnology lurks between five and ten years into the future.

3) Environment: The effects of NT materials on the environment. The funding have to increased to study the effects of NT on the environment.

4) Human or machine? How far are humans willing to go with replacement of human parts with replacement robot parts? Some avenues of research in NT include the incorporation of artificial materials or machines into human systems, as is beginning to happen with implanted computer chips. The modification of living systems is met with great skepticism by much of society. How acceptable will technologies such as implantable cells and sensors be for the general population? What are its implications and what are our limits? (see [1]).

Role of technology assessement for responsible development of NT

Ethical principles must be respected and, where appropriate, enforced through regulation. These principles are embodied in the European Charter of Fundamental Rights [16] and other European and other international documents [17]. The opinion of the European Group of Ethics (EGE) [18], who are examining the ethical aspects of medical applications related to nanotechnologies, should also be taken into account [4].

If it is difficult to predict the future direction of nanoscience and nanotechnologies and the timescale over which particular developments will occur, it is even harder to predict what will trigger social and ethical concerns. In the short to medium term concerns are expected to focus on two basic questions: 'Who controls uses of nanotechnologies?' and 'Who benefits from uses of nanotechnologies?' These questions are not unique to nanotechnologies but past experience with other technologies demonstrates that they will need to be addressed (Report of the Royal Society).

Apart from denying society the possible benefits, it may lead to the constitution of "technological paradises", i.e. where research is carried out in zones without regulatory frameworks and is open to possible misuse. Our consequent inability to follow developments and intervene under such circumstances could lead to even worse consequences. The Precautionary Principle, as used up to now, could be applied in the event that realistic and serious risks are identified (Commission of the European Communities, "Communication from the Commission on the Precautionary Principle", COM (2000) 1).

Given the huge uncertainties about the future social impacts of nanotechnology, we ought to think of the unfolding revolution as a grand experiment – a clinical trial – that technologists are conducting on society. From this perspective, we can reflect upon the robust societal consensus that demands prior informed consent as a basis for participation in scientific

experiments. This consensus is formally codified in the World Medical Association's Helsinki Declaration, strengthened most recently in 2000, and reinforced in the public consciousness by the memory of, for example, the Tuskegee experiments, where African American males with syphilis were left untreated as part of a "control group", despite the existence of treatments known to be efficacious. In the United States, every publicly funded research project involving human subjects is monitored by an institutional review board (IRB) that must approve the research before it can be conducted. Every university, independent laboratory, and private-sector lab receiving federal funding for human subjects research has an IRB; there are thousands of boards operating in the United States, nearly 800 in California alone. These boards demonstrate that comprehensive governance is a reasonable goal, and while IRBs certainly impose a cost in terms of the efficiency of conducting research, they are an accepted element of a scientific infrastructure that respects human dignity. Similar commitments of the entire research enterprise to larger democratic strictures occur in experiments with animals and in compliance with environmental health and safety regulations. Comprehensiveness, in other words, is possible, when the stakes are high and societal intent is clear [3].

Some of the basic ethical values include: the principle of respect for dignity; the principle of individual autonomy; the principle of justice and of beneficence; the principle of freedom of research; and the principle of proportionality. The relevance of such principles towards human and non-human applications of nanotechnology should be understood. In addition, certain applications, e.g. miniaturised sensors, may have specific implications for the protection of privacy and personal data [4].

Analyses of technology assessment

Since NanoTA deals with emerging enabling technologies, novel methodical approaches are needed as a tool to link R&D activities with visions for applications and as a 'support layer' for the technological interpretation of (political) scenarios including future technology options.

Science & Technology Roadmapping methodology can be adapted for TA for emerging enabling technologies. When integrated into a TA process, roadmapping may serve as a powerful tool to provide empirical and structural knowledge and to produce consensus on strategies. Traditionally used to gather, structure and communicate information about technologies and products, and to link them to options for the future in companies and industries. According to de Laat, more recently used as decision aids to design public policies related to research and development. For NT, a number of roadmaps exists - produced by small groups of experts with a "technology push" perspective – most remain unnoticed or ignored in R&D policies.

Hypothesis used for the acceptance and the relevance of a roadmap, process aspects (design, participants, modes of communication) are as important as the technical product (the roadmap) itself. Variety of technology forecasts, foresight reports, market studies – general or sectoral are available [12].

Forecasting, scenario-building and other futures research tools

Forecasting, scenario-building and other futures research tools will help tease out the possible landscapes of the world to come.

Research need to talk directly to and listen to business leaders, nanotechnology researchers and nano-product development personnel. With respect to studying the possible impacts of disruptive technologies on public perceptions, new research methodologies are needed (such as "preview" represent communities) that can provide prospective information on social impacts prior to the mass deployment of the new technology. Most NSF (national science Foundation) supported work on the public understanding of sciences focuses on attitudes toward science and knowledge about science rather than the ends to which science could or should be put. Several modes of identifying social needs on which to base justifications for advances in S&T have been outlined. These include Foresight and Delphi techniques, Charettes in city planning, as well as public discussion models from the philosophy of science. The identification of technology goals could also process from social science research on human needs, e.g. Maslow's hierarchy of goals. Foresight studies attempt to depict an image of a possible future using a variety of techniques. An important foresight method is the Delphi survey. A Delphi survey basically is a tool to create consensus and detect areas of conflicting expert opinions. In a first round, experts are confronted with a number of topics they have to evaluate with respect to time of realization, implication on wealth creation, quality of life, and similar issues. In another round the results of the previous round are introduced to the experts who then have a chance to re-evaluate the topic [19].

Future social scenarios

Bainbridge and Kasperson (2003) performed future social scenario analysis, which, can help identify issues and hypotheses, and thus is a useful tool of theoretical analysis. This panel puts forth two very different scenarios for the coming 10 to 20 years, in order to help clarify both the issues related to nanotechnology that policy makers will face, and the knowledge that needs to be gained through research. In one scenario, the transition will he smooth and benign, whereas in the other scenario the transition will be rough and marked by many different kinds of harm and conflicts with social values and institutions.

Smooth transition: In this optimistic scenario nanotechnology produces clear, demonstrable benefits and solutions for real-world problems, and management strategies for threats. For example, it will enable low-cost energy production with minimal impact on the environment, as well as achieving greater efficiency in energy use. It will help prevent and cure disease, and will provide many rewarding jobs. It will contribute to applications that strengthen the nation's defense capabilities without unduly burdening the privacy of citizens, while also reducing the incidence of terrorist activity and strengthening the cause of peace worldwide. In this scenario, early applications stress positive effects on publicly valued areas, such as health, energy and food development, pollution abatement, and environmental protection.

Importantly, the smooth transition scenario assumes that nanotechnology development will benefit from strong public involvement.

Rough Transition : This scenario could lead eventually to a happy situation like that described in the smooth scenario, hut only after a longer period of delay and with very substantial human costs. Clearly unmanaged or unanticipated risks become evident with this scenario. At the extreme, it could lead to the near-permanent abandonment of some forms of nanotechnology and thus to a failure to take advantage of their benefits.

Societal institutions and the general public would not he effectively involved in the policy-setting process. Perhaps nanotechnology-enabled weaponry would be used in such a way as to increase rather than decrease fatalities, ultimately leading to reduced security. The public would perceive that industry and scientists are concerned only with their own profits and careers, causing widespread apprehension and mistrust. There could be irrational fads leading to government regulation that was either too rigid or too lax, and a tremendous loss of investment coupled with tragic failures to realize the greatest benefits of nanotechnology.

There are parallels in previous technology revolutions or evolutions that can inform us about the future of nanotechnology. Genetically modified organisms, stem cells, and nuclear power exemplify the rough transition scenario. Indeed, one of the more disturbing possibilities is that policy makers and leaders of social movements may respond to nanotechnology not as it actually is, but in terms of false analogies.

Research and evaluation methodologies

Scenario analysis, as mentioned earlier, can help identify issues and hypotheses, and thus is a useful tool of theoretical analysis. A worthwhile variant of scenario analysis is backcasting, the mirror image of forecasting, which specifies an outcome and tries to identify the steps that might lead to it. Scenarios are an art form, akin to brainstorming, but there are ways to render them more rigorous. For example, acknowledged experts can be asked to write the scenarios, and their output can he harmonized with known facts (such as demographic data or statistics on availability of natural resources). Even when they are not fully rigorous, scenarios can help policy makers and ordinary citizens alike to imagine possible futures, both to prepare responses to anticipated problems and to set goals for positive accomplishments. Ideas generated through scenarios can become the focus of more rigorous methods of empirical research.

Multi-agent modeling is akin to scenarios, but is carried out through computer simulation. An agent is a dynamic computer representation of an individual person, organization (such as a corporation), sector of the economy, or other social unit. Among the most intellectually influential examples is a study by political scientist Robert Axelrod (1984), in which a computer modeled the interaction of a number of individual people, who followed various strategies in their economic dealings with each other. The point of the study was to see if these agents could learn to cooperate, despite the fact that each was programmed to seek his or her own best selfish interests, and indeed they could. The relevance to real people was that the study showed that cooperation between humans was logically possible even without shared social values, religion, or any of the other sophisticated cultural factors that are often assumed to help humans he reliable partners. For 30 years, agent-based and other computer simulations have contributed to a greater understanding of issues, such as the ways a society may affect the natural environment and the ways social movements may organize around a variety of issues by Bainbridge (1987), Forrester (1971) and Meadows et al. (1974).

Axelrod's simulations employed game theory; it is also possible to use pure mathematical methods in this way of conceptualizing human relations in terms of strategic interactions for personal gain.

The case study method is an important qualitative research approach that can be practiced somewhat rigorously, either with historical or ethnographic data. Given that nanotechnology is quite recent, historical studies will have to rely upon carefully drawn

analogies with earlier technologies. For example, an extensive literature (see Bunker et al. (1977), Howell (1995), etc.) already exists on the often-rocky adoption of new medical technologies, as some excellent therapies and diagnostic tools are ignored while others spread rapidly throughout the medical community despite lack of evidence for their value. The challenge is how to identify close analogies between past cases and particular nanotechnology applications. The ethnographic approach avoids this problem through direct observation of a specific emerging nanotechnology in the laboratory or in the wider organization of which it is a part. Ethnography is not well suited for prognostication, however, because it focuses on the present and very recent past. Potentially, the combination of history (to get the time perspective that reveals outcomes) and ethnography (to determine the nature of an innovation to support appropriate analogies) could he more powerful than either alone.

New technologies do not merely have an *impact upon* society. Rather, they *interact with* society and their impact is a result of technical facts with social factors. Thus, public opinion surveys and methods like market testing are important ways to chart the changing meaning of nanotechnology. Focus groups can provide insights in to how to intervene and how to get information across. The research method must be tailored to the particular population under study. For example, young people may not respond well to formalized questionnaires, so it may he best to conduct listening tours in high schools to examine youth culture and understanding. Content analysis (obtained by looking at media, popular culture, and Hollywood) could be integrated with surveys of audiences for analysis of the social values that nanotechnology may affect.

Finally, it will be important to collect solid facts about the institutions and individuals that are most involved in the development and application of nanotechnology. An inventory should be undertaken of existing institutions and assessment of how they cope with change and uncertainty. Also valuable would he research to develop a future nanotechnology-skills inventory for identifying best-of-breed competencies that will enable jobs, career development and competitiveness.

The responsible development of nanotechnologies

While the phrase ‘responsible innovation’ occurred occasionally, it is now becoming more common, especially in nanotechnology. Examples are the USA Centre for Responsible Nanotechnology (with links to the Drexlerian “social world”), and the International Dialogue on Responsible Research and Development of Nanotechnology, recently started up by Mihael Roco (US National Nanotechnology Initiative), include attempts at interactive TA from CSPO at Columbia University [6].

If still unformed, however, there is reason to believe that public debate about nanotech is about to take off – with two just founded new nanotech organizations. The Center for Responsible Nanotechnology, run by a social activist and a nanosystems theorist, Chris Phoenix, one of the Center’s founders says, “What we want, is to see molecular nanotechnology policy developed and implemented with a care appropriate to its powerful and probably transformative nature”. And two Washingtonians – a futurist, Eric Drexler and an antitrust lawyer, Chris Phoenix – are in the process of launching the Nanotechnology Policy Forum to improve the quality of public discourse about nanotech. They intend to host events every few

months, and to stay scrupulously evenhanded: the advisory panel planned for the organization will include both friends and foes of nanotech – as well as present and former congressmen.

Technology assessment – The Parliament, European Technology Assessment Group (ETAG)

Since October 2005 a group of five European scientific institutes - with the Institute of Technology Assessment and Systems Analysis (ITAS), Research Centre Karlsruhe, Germany as the leading partner - has been providing scientific services for the European Parliament on social, environmental and economic aspects of new technological developments [20].

Initially for a period of three years, the European Technology Assessment Group (ETAG; www.itas.fzk.de/etag) will carry out TA studies on behalf of the STOA Panel. Apart from being leading institutions in the field of Technology Assessment (TA) in their home countries all members of the group have long-term experience in policy consulting for parliamentary bodies. The group is made up of the following organizations:

Institute of Technology Assessment and Systems Analysis (www.itas.fzk.de), which operates the Office of Technology Assessment at the German Parliament;

Danish Board of Technology, which provides consultancy services for the national parliament (www.tekno.dk);

Flemish Institute for Science and Technology Assessment (viwTA), the TA-institution of the Flemish parliament (www.viwta.be);

Parliamentary Office of Science and Technology (POST) of the British Parliament (www.parliament.uk/post/home.htm);

Rathenau Institute, the central TA institution in the Netherlands working for the Dutch parliament (www.rathenau.nl).

The ongoing work programme funded from the 2005 STOA budget consists of a set of 10 projects dealing with a broad range of subjects from various sectors of policy making, such as R&D, ICT, environment, health and energy.

Questions with the regard to the ethical, environmental, economic, legal and social imlications of NT

Main task of nanotechnology assessment (TA) is to foster principles of ethical governance, maintenance balance of fundamental human rights and responsibilities of government regarding to emerging enabling nanotechnology.

What are linked with the new opportunities of NT; possible technological, ethical, environmental, societal, economic and health risks? What are the actual barriers to be overcome these risks in the corresponding sectors? To what uncertainties may lead illiteracy of public in NT?

The main purpose is not only defining opportunities or threats, but perform sound comparisons balancing supposed benefits and risks of NT. If ‘threats’ and ‘risks’ overwhelm the ‘strengths’ and ‘opportunities, societal attitude obviously may be rejection.

Investigate and study environmental, health and socio-economic impact of NT; Where do nanomaterials go when they enter the environment and what are their effects? There are

always possibilities for environmental or health harms. Address forecasting and roadmapping for future implications and determining the role of NT in economical development.

Create code of ethics concerning NT utilization in our country. Design principles to discourage unethical or accidental uses of nanotechnology, versus, encourage and advocate friendly 'green' NT; As the science of NT leaps ahead, so the ethics lags behind; Either the ethics of NT will catch up, or the science will slow down. NT may have devastating consequences, including public fear and rejection of NT without adequate study of its ethical and social implications.

Public engagement, involvement of NGO and promote decision making activities at governmental and international levels. Mass media need to be involved in the early stages of NT since they have an important influence on public perceptions.

Increase awareness and ferry appropriate overview information (chemo / bio – nano threats and defense) to concerning authorities about national security issues. Risk seems more prominent, as surrounding countries, e.g. Russia and Iran (?) are developing NT and already attained substantial success. NT is capable of dramatically improving surveillance devices, and producing new weapons. Will these new technologies increase security or add to the arsenal of bio- and techno- or even nano-terrorism? Who will regulate the direction of research in defensive and offensive military NT? How much transparency will be necessary in government and non-governmental NT initiatives to avoid misuses?

Promote NT education in secondary schools and universities. To emphasize that this multidisciplinary subject is gaining priority. Schools and universities could discuss the issue in depth: as well, could include exhibits on NT.

Conclusions

The aim of Technology Assessment is to measure benefit to risk ratio. The purpose of TA is to study ethical controversies in societal prism. Technology Assessment determines public perception. TA establishes visionary attitude.

Technology assessment alleviates:

- to highlight creativity of field (Nobel Prize winners, different awards and grants);
- to define unequivocal ethical and legislative statements;
- to find out readiness for investments by venture capitalists (VC);
- to recognize stakeholders willingness to benefit from technology;
- to involve equally all layers of society: government-academy-society-industry;
- to maintain balance between benefits & risks of technology;
- to match convergence with simultaneously emerging enabling technologies (cogno-nano-info-bio).

References

1. A. Mnyusiwalla, A. S. Daar, P. A. Singer. 'Mind the gap': Science and ethics in nanotechnology. J. Nanotechnology, 2003, 14, 9-13.
2. M. Roco, M. Thursby. Ten research and policy themes. Rep. NNI Workshop "Nanotechnology – Societal Implications – Maximizing Benefits for Humanity" (Eds. M. C. Roco, W. S. Bainbridge), 2003.

3. D. Sarewitz, E. Woodhouse. Small is powerful. J. Nanotechnology, 2003, 14, 63-83 – Living with the Genie: Essays on Technology and the Quest for Human Mastery (Eds. A. Lightman, D. Sarewitz, C. Desser), 2003, Washingtom: Island Press.
4. Commission of the European Communities. Communacation from the Commission: Towards a European Strategy for Nanotechnology, Brussels, 2004.
5. A. E. Sweeney, S. Seal. The promises and perils of nanoscience and nanotechnology: Exploring emerging social and ethical issues. Nanosci. Nanotechnol.: Bull. Sci. Technol. Soc., 2003, 8, 236-245.
6. A. Rip. Technology assessment as part of the co-evolution of nanotechnology and society: The thrust of the TA program in NanoNed. Conf. Nanotechnol. Sci. Econ. Soc., Marburg, 2005.
7. D. H. Guston, D. Sarewitz. Real-time technology assessment. J. Technol. Soc., 2003, 23, 4.
8. Data: Special Eurobarometer 224 & 225 / Wave 63.1 2005. NSF Sci. Eng. Indicators, 2004.
9. A. Grunwald, G. Bechmann, K. Böhle, M. Decker, U. Fiedeler, T. Fleischer, F. Gloede, B. J. Kring. Project: Future Prospects of Technology Assessment Institute of Technology Assessment and Systems Analysis (ITAS), Karlsruhe, 2004 – 2006.
10. D. Rejeski. Promoting Economic Development Opportunities Through Nano Commercialization. U.S. Senate Committee on Commerce, Science and Transportation, 2006.
11. R. H. Smith. Social, ethical, and legal implications of nanotechnology. NSET Workshop Report: Societal Implications of Nanoscience and Nanotechnology (Eds. M. C. Roco, W. S. Bainbridge), 2001, Ch. 6, 203-211.
12. T. Fleischer. Perceptions of nanotechnologies. Some Observations and Conclusions. NanoVision III, ITAS, 2005.
13. T. Fleischer, P. Hocke, A. Grunwald. Nanotechnology Assessment, Exploring Potentials of Nanotechnologies, Avoiding Pitfalls of Ignored Risk Perception. Institute for Technology Assessment and Systems Analysis (ITAS), 2005.
14. J. Carroll. Nanotech's Dark Side Debated in the Aftershock of Sept. by John Carroll Small Times, 2, 2001. http://www.smalltimes.com/document_display.cfm?document_id=2485
15. L. Stefan, M. A. Gammel. Ten research and policy themes: Visions of nanotechnology – Origins of utopian visions and their impact on society. Report of NNI Workshop Nanotechnology – Societal Implications – Maximizing Benefits for Humanity (Eds. M. C. Roco, W. S. Bainbridge), Interdepartmental Centre for Ethics in the Sciences and Humanities, 2005.
16. http://www.europarl.eu.int/charter/default_en.htm
17. http://europa.eu.int/comm/research/science-society/ethics/legislation_en.html
18. http://europa.eu.int/comm/european_group_ethics/index_en.htm
19. H. Etzkowitz. Nano-science and Society: Finding a Social Basis for Science Policy. NSET Workshop Report: "Societal Implications of Nanoscience and Nanotechnology" (Eds. M. C. Roco, W. S. Bainbridge), 2001, Ch. 6, 97-103.
20. J. Chatzimarkakis. Newsletter – European Parliament Scientific Technology Options Assessment (STOA), 2006.

PHYSICOCHEMICAL PROPERTIES OF THE $FeFe_2O_4$ & Ag^0 NANOCOMPOSITES FORMED ON THE STEEL SURFACE CONTACTING WITH $AgNO_3$ WATER SOLUTIONS IN OPEN-AIR SYSTEM

O. M. Lavrynenko

National Academy of Sciences of Ukraine
F. D. Ovcharenko Institute of Bio-Colloid Chemistry
Kyiv, Ukraine
alena-lavry@yandex.ru

Accepted April 10, 2012

Introduction

The nanosized core & shell composites that include a ferrimagnetic core such as iron oxides (magnetite or maghemite) and a precious metal shell (aurum, argentum, platinum, and palladium) are widely used for medical-biological application due to their unique optical properties, bioavailability, and selectivity in relation to the range of biological objects [1]. The similar composites are good for catalysis, analytical chemistry, separation technology, environmental protection et al. [2, 3].

The main methods of forming core & shell composite particles are co-precipitation ferric and ferrous iron salts in low-alkaline media in the presence of precious metal cations with their following reduction [4]; the method of reversive micelles [5]; the separate precipitation of iron oxide particles and precious metal seeds and making-up of the composites in organic liquids [6]. As alternative method of obtaining the ferromagnetic core & shell composites we can propose their formation on the steel surface contacting with water solution in open-air conditions [7, 8]. The red-ox reaction on the steel surface, access of oxygen and carbon dioxide to the steel surface – water dispersion medium – air oxygen interface area, presence of different species in the water solution lead to appearance of favorable conditions for the Fe(II)–Fe(III) LDH (Green Rust) formation on the steel surface [9]. Due to high reducing properties of Green Rust phase it can reduce the electropositive species from the dispersion medium to metal state and it oxidized to the iron oxide and / or hydroxide phases. At the dispersion precipitation usually two separate phases (iron oxide and precious metal particles) are obtained in the solution [10] but under specific physicochemical conditions of the process carrying out the precious metal shell is formed on the iron oxide surface [8]. In such case as a product of the process of the phase formation the composite particles are formed that include an iron oxide core and metal shell.

The core & shell composite nanoparticles differ by quantity of core particles (one [11] or more [12]), the phase composition of core (magnetite [13] or maghemite [14]) and shell (aurum [13], argentum [15], platinum [16], palladium [17]), presence [18] or absence [15] of the additional SiO_2 layer between core and shell phases, the degree of the filling of core surface with precious metal (full [19] or partial [20]), the general quantity of composite layers (two or more [21]) and other. The complicated (multiple) composite which, for example, contain two

precious metals in their shell [6] or a few alternate layers containing organic and precious metal particles [22] are considered as a separate group.

The ferrimagnetic particles including iron oxide core and argentum shell belong to a simple core & shell composite that due to partial shell filling corresponds to small galvanic couples that consist of iron oxide anodic areas and silver cathode areas. The particles of such nature not only preserve the ferrimagnetic properties of iron oxide core and optical properties of silver shell but will acquire the new unique colloidal-chemical and physicochemical behavior and perspectives for their practical usage as a functional material for different medical-biological purposes [23].

The present work is aimed at the investigation of the physicochemical peculiarities of the nanosized core & shell composites composed of the magnetite core and silver shell and formed on the steel surface contacting with water $AgNO_3$ solution in open-air system.

Materials and methods

For carrying out the process of the phase formation the disk electrode made from finished steel (St3) was used, that contains, %: C – 0.14 ÷ 0.22; Si – 0.05 ÷ 0.15; Mn – 0.4 ÷ 0.65; Cr – 0.3; Ni – 0.3; P – 0.04; S – 0.05; N – 0.01. Before every experiment the steel surface was cleaned from oxidized layer with aqueous solution of sulfuric acid. The process of phase formation usually continues until the system comes to a stationary state, when chemical composition of the dispersion medium, its pH value and quantity of the disperse phase on the steel surface are stabilized. The process of the phase formation was controlled by the chemical analysis of the dispersion medium (pH values and the species concentrations) and the mass of disperse phase obtained from the steel surface.

As dispersion medium the $AgNO_3$ water solutions with Ag^+ concentrations from 0.5 to 10.0 mg / dm^3 were chosen. The pH values of dispersion medium were set in the range of 2.5 to 12.0. As the main methods of investigation X-ray diffraction (XRD), X-ray fluorescence analysis (XRFA) and chemical analysis were used. XRD measurement was taken on computer-aided equipment (DRON 3) with filtered emission of cobalt anode. The velocity of plotting was 1 °/ min; the critical Woolf-Bragg angle was 80 °C. The XRF analysis was carried out on the ELVAX spectrometer with the titanic anode. As additional visualization technique of the derived samples the scanning electron microscopy (SEM) and transmission electron microscopy (TEM) were suggested. The images were obtained on “Selmi” equipment. The chemical analysis of the dispersion medium was carried out by the standard photocalorimetric methods [24]; for the measuring FEC – 56M was used. “Solver PRO – M” equipment and “Nova” software were used for carrying out the atom-force (AFM) and magnetic-force (MFM) microscopy and data interpretation. The scanning regime was half-contact or magnetic with the NSG 01 / Co probe; the distance to the particle surfaces was 80 nm. The induction of the magnetic field was 160 mT. PPMS – 9 equipment was used for the measuring of the magnetization and magnetic susceptibility. The investigation was carried out at 300 K.

Results

The choice of the concentration range from 0.5 to 10.0 mg / dm^3 is defined by argentum properties to be reduced on iron (steel) surface by its high content in the dispersion medium.

The values of the standard electrode potential (– 0.440 V for Fe^0 / Fe^{2+} and + 0,337 V for Ag^0 / Ag^+) direct the process according to a simple red-ox reaction (to the reduction of Ag^+ and oxidation of Fe^0) but such process is limited by argentum concentration [25].

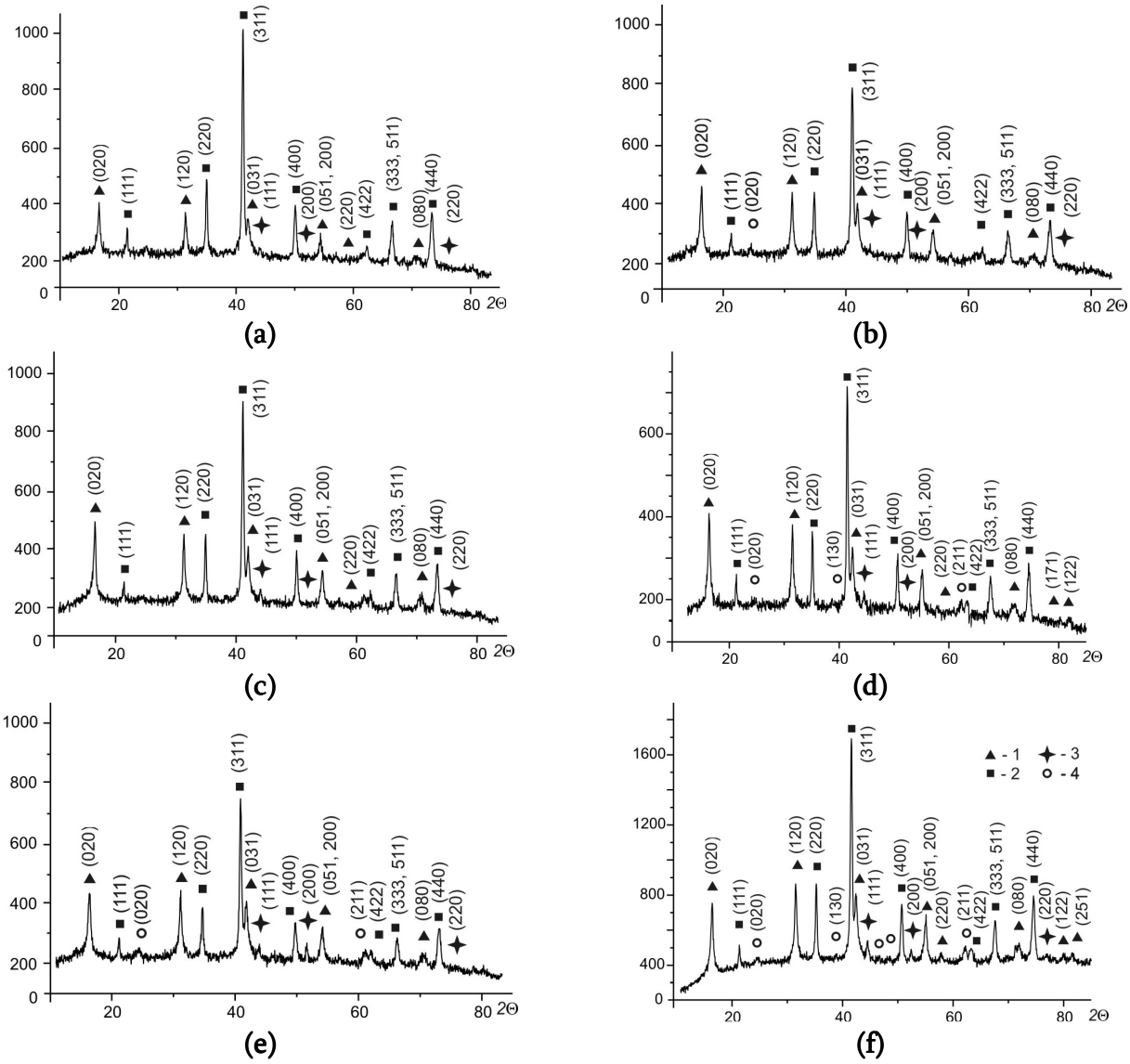

Figure 1. The XRD-patterns of the composite structures formed on the steel Surface contacting with air oxygen and argentum nitrate solutions after 24 h of carrying out the phase formation at $C_{Ag(I)}$, mg / dm³ : a – 0.5; b – 1.0; c – 2.0; d – 3.0; e – 5.0; f – 10.0. Numbers correspond to the phases: 1 – lepidocrocite γ-FeOOH; 2 – magnetite $FeFe_2O_4$, 3 – silver Ag^0; 4 – goethite α-FeOOH.

The phase composition of the surface structures was studied by X-ray diffraction. **Fig. 1** shows the XRD-patterns of the composite structures that were formed by contacting steel surface with $AgNO_3$ water solution at the wide range of argentum concentrations (from 0.5 to 10.0 mg / dm³). At all chosen $C_{Ag(I)}$ the reflexes of the magnetite $FeFe_2O_4$, lepidocrocite γ-FeOOH and metal silver are present on the XRD-patterns. As the addition phase goethite α-FeOOH appears that is identified according to some peaks (020), (130), (211). The significant peculiarity of the system is the simultaneous presence of the two iron-oxygen phases (lepidocrocite and magnetite) in the bulk of the surface sediments. At the low amounts of

argentum (0.5 mg / dm^3) the intensity of the (120) lepidocrocite peak is smaller than the intensity of the (220) magnetite peak, but at the bigger argentum concentration (1.0 – 10.0 mg / gm^3) their altitudes are practically equal to each other. At the range of $C_{Ag(I)}$ from 0.5 to 5.0 mg / dm^3 the intensity of the (311) magnetite reflex insignificantly decreases but at $C_{Ag(I)}$ = 10.0 mg / dm^3 it increases in 1.5 – 2 times and reaches its maximum. The (111), (200) and (220) silver reflexes are growing by increasing the argentum concentration in all experimental conditions. The particles size was calculated by Scherer's formula by (311) magnetite reflex. The result shows that in the range of $C_{Ag(I)}$ from 1.0 to 10.0 mg / dm^3 the particles size gradually increased from 19.5 ± 0.1 to 25.0 ± 0.1 nm.

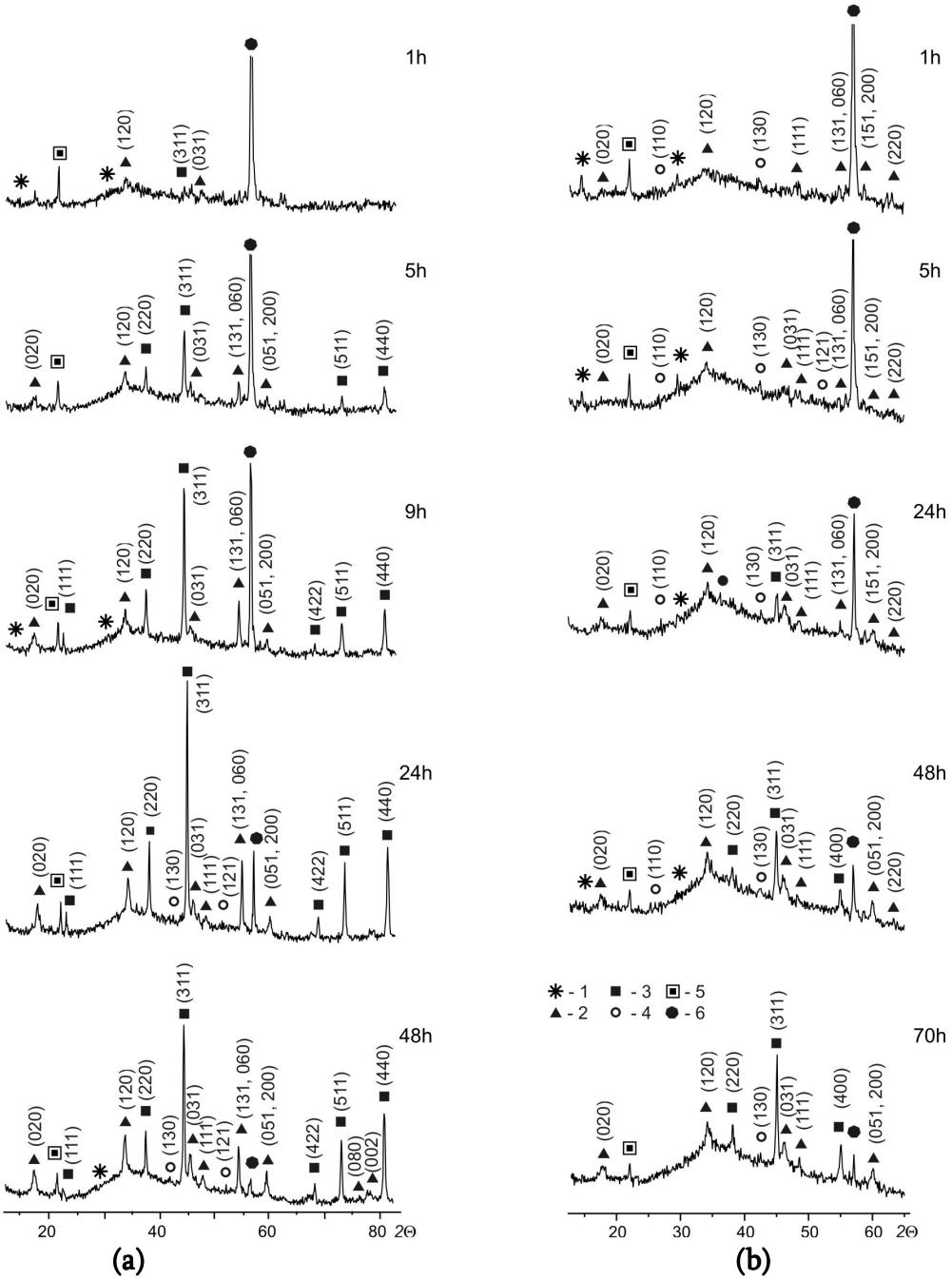

Figure 2. The XRD-patterns of the composite structures formed on the steel surface contacting with air oxygen and argentum nitrate solutions at $C_{Ag(I)}$ = 1.0 mg / dm^3 and pH values: a – 6.5; b – 11.0. Numbers correspond to the phases: 1 – Green Rust (I); 2 – lepidocrocite γ-FeOOH; 3 – magnetite $FeFe_2O_4$, 4 – goethite α-FeOOH; 5 – material of fluoroplastic holder; 6 – iron Fe^0.

The influence of initial pH values of the dispersion medium on the phase composition of the surface structures and the kinetic regularities of the phase formation were studied by X-ray diffraction *in situ*. The experiment was carried out during 48 and 70 hours at pH values 6.5 and 11.0, respectively when argentum was present in solution as ions and hydroxide species. The results are presented on **Fig. 2**. At pH value 6.5 the first magnetite reflexes are shown on the pattern after 1 h of steel contacting with air oxygen and water solution. Lepidocrocite was formed on the steel surface as a second phase. The intensity of the both type reflexes was growing during 24 hours and during the next 24 hours the partial oxidation of magnetite and appearance of a small amount of goethite α-FeOOH along with γ-FeOOH took place in the system. The other phase present on the steel surface was Green Rust (I) in a rather small quantity due to its consumption for the formation of magnetite and lepidocrocite particles. The average particles size of magnetite particles according to Scherer's formula was ~ 22.05 nm. At initial pH value 11.0 the most typical structures formed on the steel surface were oxyhydroxides such as lepidocrocite and goethite. The magnetite reflexes appeared on the pattern only after 24 hours of process. The average particles size of magnetite particles formed in the alkaline media was bigger than in the neutral medium and made up ~ 37.8 nm.

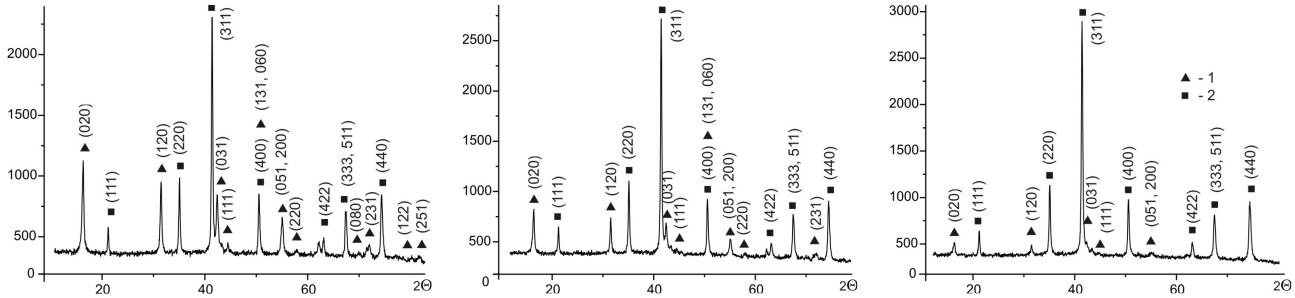

Figure 3. The XRD-patterns of the composite structures formed on the steel surface contacting with air oxygen and argentum nitrate solutions at $C_{Ag(I)}$ = 1.0 mg / dm³ and pH value 2.5: a – outer layer; b – middle layer; c – inner layer. Numbers correspond to the phases: 1 – lepidocrocite γ-FeOOH; 2 – magnetite $FeFe_2O_4$.

The role of oxidant in the phase composition and cores size were studied on the example of particles obtained in the system at $C_{Ag(I)}$ = 1.0 mg / dm³ and pH = 2.5. Three layers of the iron–oxygen structures were separated from the steel surface: the outer one (I) (**Fig. 3a**) contacting with air and water solution, the inner one (III) (**Fig. 3 c**) contacting with the steel surface and the middle one (II) (**Fig. 3b**) situated between the first and the third layers. The both magnetite and lepidocrocite reflexes were present on the XRD-patterns but at decreasing the access of oxygen the amount of lepidocrocite peaks decreased and the amount of magnetite peaks, on the contrary, increased. The particles size gradually decreased from 24.1 ± 0.1 in the first layer to 21.6 ± 0.1 in the second and 19.2 ± 0.1 nm in the third. Probably the difference of the particles size in the layer was connected with oxidizing of magnetite and forming of lepidocrocite shells on its surface [26].

The distribution of iron and silver atoms on the particle surfaces depending on initial concentration of argentum in the solution and pH values was studied by X-ray fluorescence analysis (look the **Tab. 1**) in the outer (I) and the middle (II) layers. Separately the solution precipitates was studied. Two experimental runs of the samples were investigated by such

method under different conditions: at the pH value 6.5 and $C_{Ag(I)}$ range from 0.5 to 10.0 mg / dm³ and at the $C_{Ag(I)}$ = 1.0 mg / dm³ and different pH values (the range from 2.5 to 12.0). The $FeFe_2O_4$ & Pt composite was chosen to compare systems. As XRF data showed (the run 1), the ratio of Ag to Fe were growing from (0 – 0.028) : (100.0 – 99.97) to (0.46 : 99.54) at the increasing the argentum concentration in the solutions from 0.5 to 10.0 mg / dm³. At platinum concentration 10.0 mg / dm³ its content on the magnetite surface reached only 0.14 %. On the contrary, the percentage of silver in the solution precipitations was bigger and reached ~ 39.8 % at $C_{Ag(I)}$ = 0.5 mg / dm³ and ~ 63.8 at $C_{Ag(I)}$ = 5.0 mg / dm³, but platinum did not collect as individual particles in the solution sediments even at $C_{Pt(IV)}$ = 10.0 mg / dm³.

Table 1. The distribution of iron and silver atoms on the particle surfaces according to X-ray fluorescence data.

Initial concentrations of argentum, mg / dm³ in water solution	Localization of phase formation	Initial pH values	Distributions of surface atoms, %		Association of silver with phases
			Fe	Ag or Pt*	
The run 1					
0.5	Steel surface	6.5	100	0	–
0.5	Steel surface	6.5	99.97	0.028	magnetite
0.5	Solution	6.5	60.32	39.68	silver particles
1.0	Steel surface	6.5	99.94	0.06	magnetite
2.0	Steel surface	6.5	99.90	0.10	magnetite
5.0	Steel surface	6.5	99.78	0.22	magnetite
5.0	Steel surface (I)	6.5	99.72	0.28	magnetite
5.0	Steel surface (II)	6.5	99.82	0.18	magnetite
5.0	Solution	6.5	36.26	63.74	silver particles
10.0	Steel surface	6.5	99.54	0.46	magnetite
10.0*	Steel surface (I)	6.5	100	–	–
10.0*	Steel surface (I)	6.5	99.86	0.14	magnetite
10.0*	Solution	6.5	100	–	–
The run 2					
1.0	Steel surface (I)	2.5	100	0	–
1.0	Steel surface (II)	2.5	100	0	–
1.0	Steel surface (I)	5.6	99.94	0.06	magnetite
1.0	Steel surface (II)	5.6	99.96	0.04	magnetite
1.0	Steel surface (I)	6.5	99.96	0.06	magnetite
1.0	Steel surface (II)	6.5	99.88	0.12	magnetite
1.0	Steel surface (I)	9.5	99.95	0.05	magnetite
1.0	Steel surface (II)	9.5	99.96	0.04	magnetite
1.0	Steel surface (I)	12.0	100	0	–
1.0	Steel surface (II)	12.0	100	0	–

The analysis of the run 2 showed that silver associated with surface structures in the range of pH values from 5.6 to 9.5 where magnetite was usually formed. The ratio of argentum to iron reached from (0.04 : 99.96) to (0.06 : 99.94). At lower and higher pH only phases of the oxyhydroxides such as lepidocrocite and / or goethite were obtained.

The analysis of dispersion medium was carried out after the centrifugation of the solutions at 8*g* during 10 min and separation of the disperse phases. The result showed the decrease of ferrous iron in the solution at the increasing initial concentration of argentum. It changed from 1.3 – 0.8 mg / dm^3 at $C_{Ag(I)}$ = 0.5 mg / dm^3; to 0.04 mg / dm^3 at $C_{Ag(I)}$ = 3.0 mg / dm^3 and then to the full disappearance of ferrous iron in the solution at $C_{Ag(I)} \geq 5.0$ mg / dm^3.

Fig. 4 shows SEM images of the steel surface when it contacts with argentum nitrate solutions ($C_{Ag(I)}$ = 1.0 mg / dm^3, pH values 11.0) at the beginning of the process (**Fig. 4a**), the nanoparticles formed in the steel surface pores (**Fig. 4b**), Green Rust I forming the thin layer on the steel surface (**Fig. 4c**), the spinel ferrite particles (magnetite) formed on the steel surface after 24 hours of the process (**Fig. 4d**).

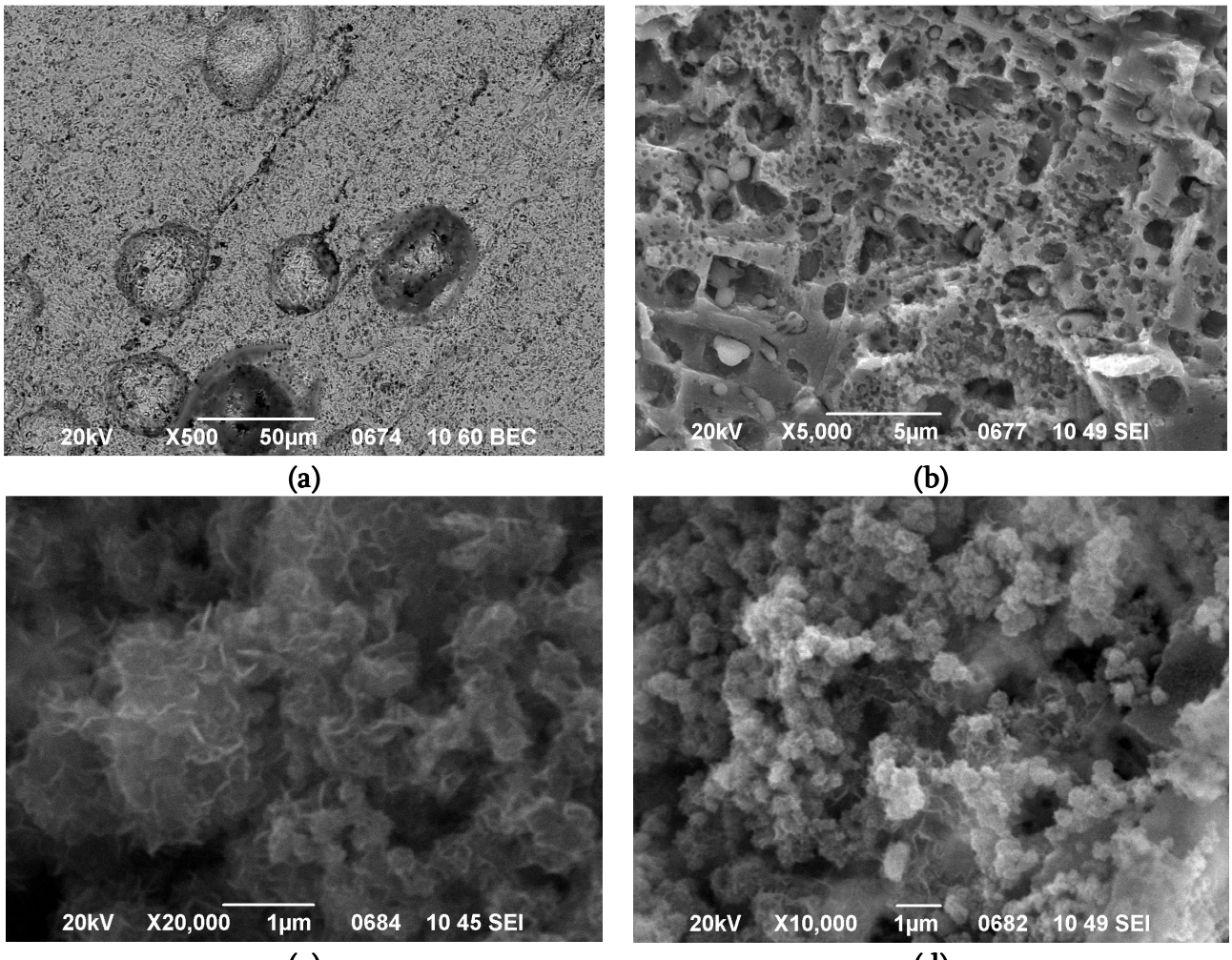

Figure 4. The SEM images of the steel surface contacting with $AgNO_3$ solution in open-air system: a – the steel surface, b – the particles in the surface pores, c – Green Rust I, d – magnetite.

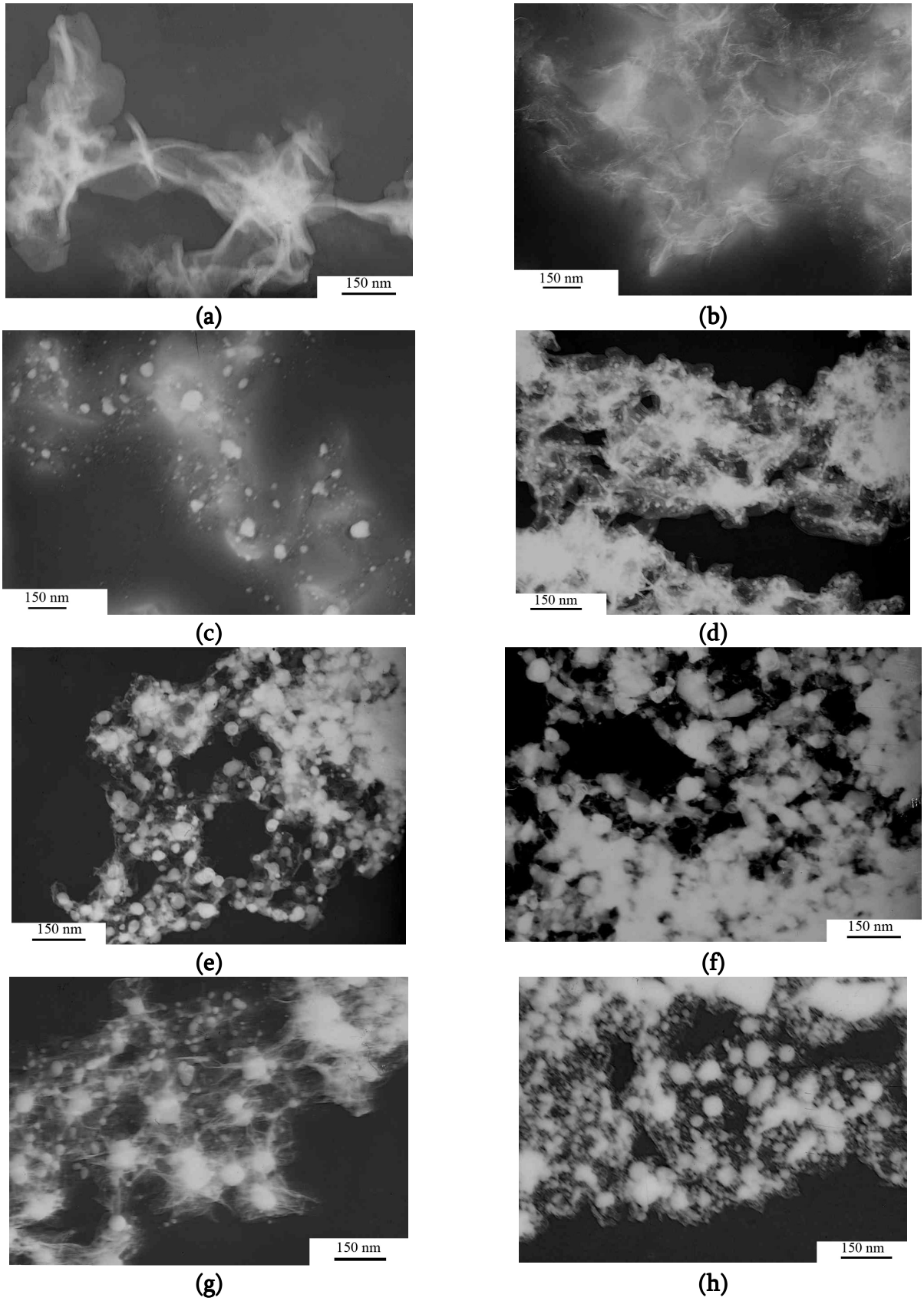

Figure 5. The TEM images of the surface structures formed when the steel contacts with $AgNO_3$ solution in open-air system: a – lepidocrocite ($C_{Ag(I)}$ = 0.5 mg / dm^3); b – lepidocrocite ($C_{Ag(I)}$ = 5.0 mg / dm^3); magnetite ($C_{Ag(I)}$ = 1.0 mg / dm^3); d – f the processes of the $FeFe_2O_4$ & Ag nanoparticle formation and their aggregation ($C_{Ag(I)}$ = 2.0 mg / dm^3); g – $FeFe_2O_4$ & Ag nanoparticles ($C_{Ag(I)}$ = 3.0 mg / dm^3); h – $FeFe_2O_4$ & Ag nanoparticles ($C_{Ag(I)}$ = 5.0 mg / dm^3).

Fig. 5 shows the TEM images of surface structures formed on the steel surface at the concentration range of argentum from 0.5 to 10.0 mg / dm³. Lepidocrocite are usually present in the outer layer of iron-oxygen phases formed on the steel surface, but its particle size and morphology depend on many factors especially on the chemical composition of the dispersion medium and its pH value. For example, the lepidocrocite needles formed at $C_{Ag(I)}$ = 0.5 mg / dm³ are shown on **Fig. 5a** and such kind of particles formed at $C_{Ag(I)}$ = 5.0 mg / dm³ are shown on **Fig. 5b**. **Fig. 5c** shows the magnetite particles ($C_{Ag(I)}$ = 1.0 mg / dm³). The formation process of the $FeFe_2O_4$ & Ag seed structures (**Fig. 5d**), their aggregation (**Fig. 5e**) and coagulation (**Fig. 5f**) are fixed for the structures obtained at $C_{Ag(I)}$ = 2.0 mg / dm³. **Fig. 5g** and **Fig. 5h** show the $FeFe_2O_4$ & Ag^0 aggregates formed at $C_{Ag(I)}$ = 3.0 mg / dm³ and $C_{Ag(I)}$ = 5.0 mg / dm³, respectively. Both lepidocrocite and core & shell composite phases are obtained in the range of the argentum concentration from 2.0 to 5.0 mg / dm³. That is very important for the interpretation of the phase formation mechanisms realized in the steel – water solution – air system.

The most important properties of the nanoparticles for their application in biology and medicine are aggregative and sedimentative stability as well as superparamagnetism. In our previous work [7] we studied the aggregative stability of γ-Fe_2O_3 & Ag nanocomposites in $AgNO_3$ water solution containing $C_{Ag(I)}$ = 1.0 mg / dm³. The sols were keeping their structure during three months. The investigation of the sols at $C_{Ag(I)}$ from 0.5 to 5.0 mg / dm³ shows the sol aggregative stability at $C_{Ag(I)}$ = 0.5; 1.0 and 5.0 mg/dm³, but at $C_{Ag(I)}$ = 2.0 and 3.0 mg / dm³ the particles form aggregates as it was shown on **Figs. 5d – f**.

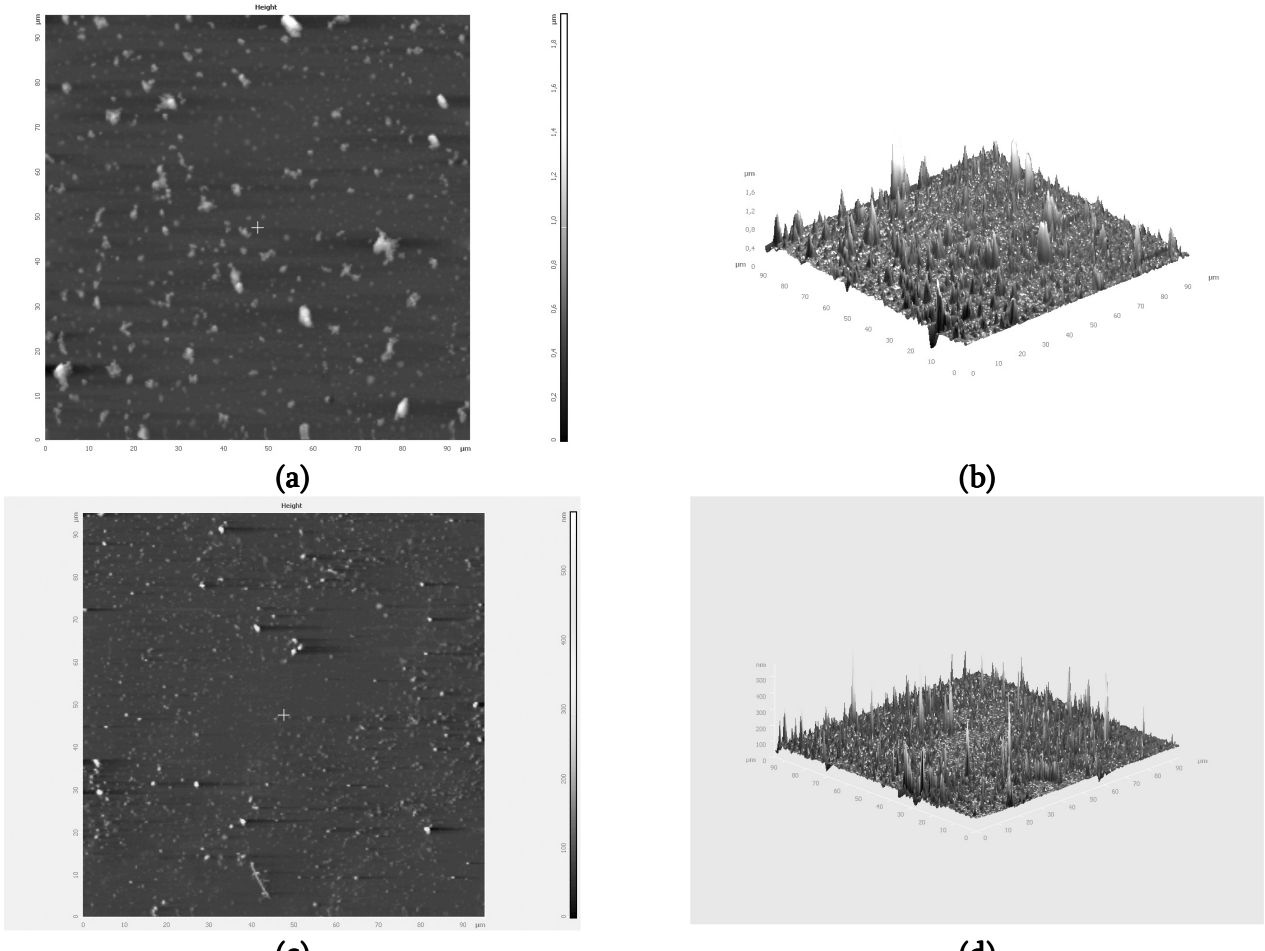

(a) **(b)** **(c)** **(d)**

Figure 6. AFM images of the particles obtained at $C_{Ag(I)}$ = 0.5 mg / dm³: a – 2D-structures; b – 3D-structures and at $C_{Ag(I)}$ = 5.0 mg / dm³: c – 2D-structures; d – 3D-structures.

The results of AFM-microscopy (2D and 3D-structures) are shown on **Fig. 6**. The nanoparticles form bigger aggregates at low argentum concentration than at higher concentration.

The MFM-microscopy is used for the studying of the magnetic properties of the $FeFe_2O_4$ & Ag^0 composites (**Fig. 7**). Probably, the magneto-sensitive structures are associated with magnetite cores of the nanocomposites.

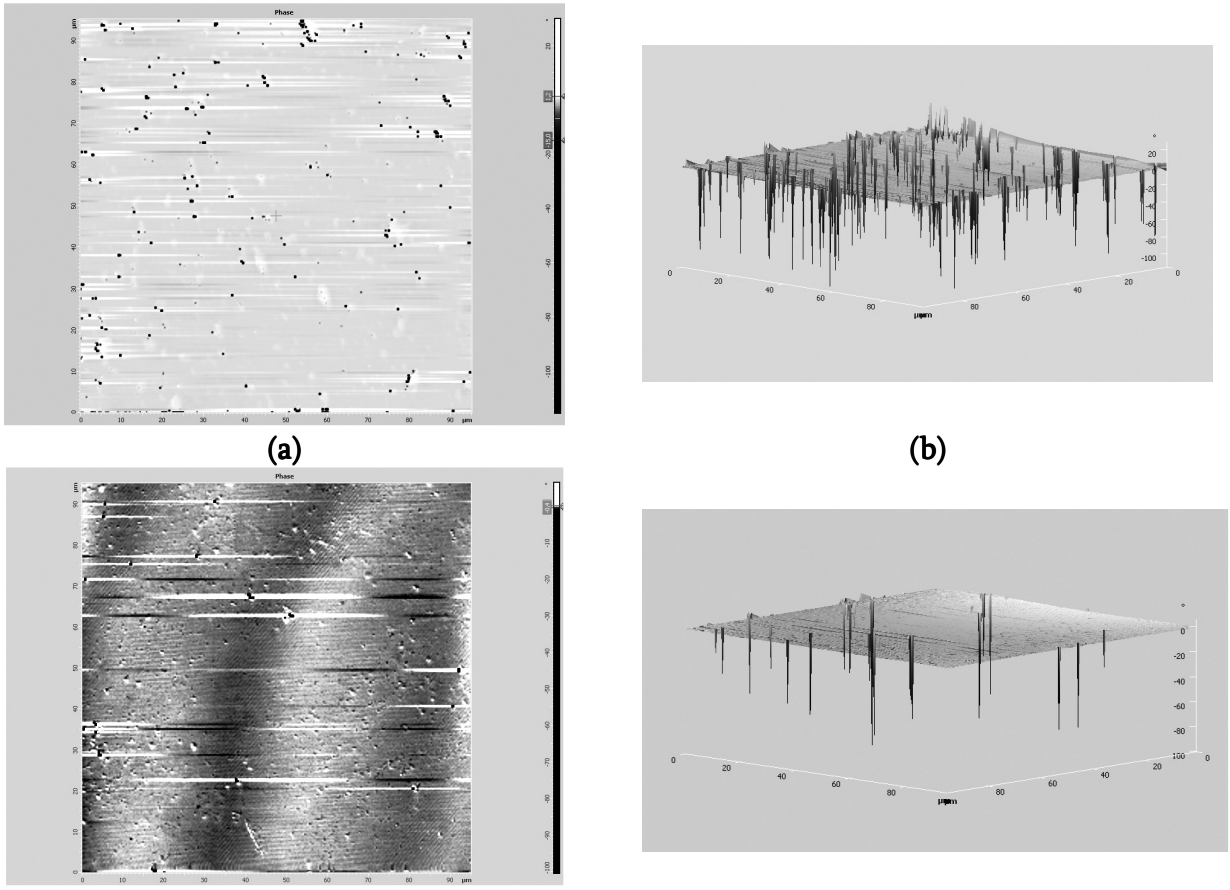

Figure 7. MFM images of the particles obtained at $C_{Ag(I)}$ = 0.5 mg / dm³: a – 2D-structures; b – 3D-structures and at $C_{Ag(I)}$ = 5.0 mg / dm³: c – 2D-structures; d – 3D-structures.

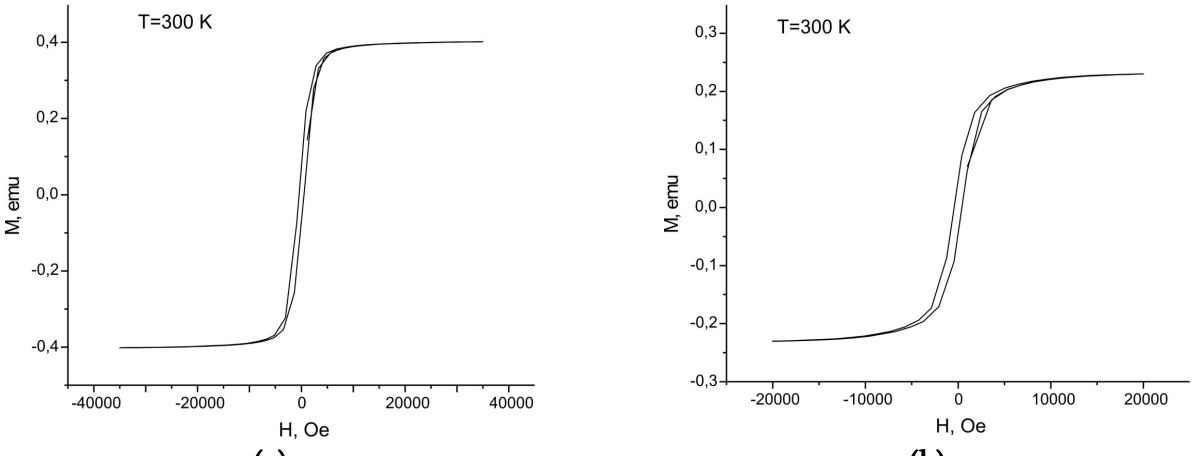

Figure 8. The dependences of the magnetization of the $FeFe_2O_4$ & Ag^0 nanocomposites obtained at $C_{Ag(I)}$ = 0.5 mg / dm³ (a) and $C_{Ag(I)}$ = 5.0 mg / dm³ (b) from the magnetic field.

The magnetization curves of the $FeFe_2O_4$ & Ag^0 nanocomposites are present on **Fig. 8**. The absence of the hysteresis loops points to the superparamagnetic properties of such structures at room temperature. The saturation magnetization decreases from 0.4 emu / g at $C_{Ag(I)}$ = 0.5 mg / dm^3 to 0.25 emu / g at $C_{Ag(I)}$ = 5.0 mg / dm^3, probably because of the influence of the silver shell. The composites obtained in whole $C_{Ag(I)}$ range belong to the soft magnetic materials, their coercitivity equals ~ 500 Oe. The values of the remnant magnetization are very small and make up ~ 0.03 emu / g for both composites formed at $C_{Ag(I)}$ = 0.5 mg / dm^3 and at $C_{Ag(I)}$ = 5.0 mg / dm^3.

Discussion

The formation of iron-oxide and iron hydroxide structures and simple core & shell composites on the steel surface contacting with water dispersion medium and air oxygen is determined by the electrochemical red-ox reaction that takes place on the steel surface and the specific physicochemical conditions created in the interface area: steel – water – air. As it was shown in our previous works [27], the products of the red-ox reaction, i.e. ferric and ferrous cations and complexes, protons, hydroxyl, carbonates, oxygen can interact with each other and form weak crystalline phases such as the Fe(II)–Fe(III) layered double hydroxides (Green Rust). Depending on the anion composition of the dispersion medium, Fe(II)–Fe(III) LDH phases may coordinate themselves as hydroxicarbonate, hydroxichloride, hydroxisulphate Green Rust of the first or the second types, respectively [28]. When several anion species are present in the dispersion medium they compete with each other in the Green Rust lattice. The anion species form the row according to the preference of the coordination of the Green Rust structure (SO_4^{2-} > CO_3^{2-} > Cl^- [29]). In our system GR(SO_4^{2-}) can form only when the remains of H_2SO_4 are present on the steel surface after its activation, but more probable way of the Green Rust formation is the interaction between Fe(II), Fe(III), OH^-, O_2 and carbonate species. The specificity of the system keeps the stable pH value (7-8) at the wide range of the initial pH (from 2.5 to 11.5). So, in such condition ferric species can be only as hydroxide $Fe(OH)_3$, but ferrous species can be as ions Fe^{2+}, complexes $FeOH^+$ as well as hydroxide $Fe(OH)_2$. Carbonates are present in the soluble forms as CO_3^{2-} or HCO_3^-. According to [30] the interaction of HCO_3^- or CO_3^{2-} species and Fe^0 by means of adsorption; the formation of the ferrous complexes and their oxidation with appearance of the particles and aggregates containing only ferric ions; the interaction of such structures and ferrous complexes leads to the formation of GR(CO_3^{2-}) on the iron surface. The extended formula of the hydroxycarbonate Green Rust usually writes as $Fe^{II}_4Fe^{III}_2(OH)_{12}CO_3 \cdot 3H_2O$ [31] but in other work [32] the water quantity was less.

In such case the formation of GR(CO_3^{2-}) on the steel surface can be described according to the reactions (1) ΔG^0_{298} = – 392 kJ · mole^{-1} or (2) ΔG^0_{298} = – 333 kJ · mole^{-1}:

$$2Fe(OH)_3 + 4Fe^{2+} + 6OH^- + CO_3^{2-} + 3H_2O \rightarrow Fe^{II}_4Fe^{III}_2(OH)_{12}CO_3 \cdot 3H_2O, \quad (1)$$

$$2Fe(OH)_3 + 4Fe^{2+} + 6OH^- + HCO_3^- + 3H_2O \rightarrow Fe^{II}_4Fe^{III}_2(OH)_{12}CO_3 \cdot 3H_2O + H^+. \quad (2)$$

The following complete oxidation of GR(CO_3^{2-}) led to the lepidocrocite formation and took place in the outer layer on the steel surface, the reaction (3) (ΔG^0_{298} = – 405 kJ · mole^{-1}) describes this process:

$$Fe^{II}_4Fe^{III}_2(OH)_{12}CO_3 \cdot 3H_2O + O_2 \rightarrow 6\gamma\text{-}FeOOH + H_2CO_3 + 5H_2O. \quad (3)$$

On the one hand, in the inner (III) layer of the surface structures the access of the oxidant is limited and on the other hand, this layer is saturated with hydroxyl and ferrous

species. In such condition two phases, videlicet magnetite and lepidocrocite are formed simultaneously according to the following reaction (4), $\Delta G^0_{298} = -202$ kJ · mole^{-1}:

$$Fe^{II}_4Fe^{III}_2(OH)_{12}CO_3{\cdot}3H_2O + 3OH^- \rightarrow Fe^{II}Fe^{III}_2O_4 + 3\gamma\text{-}Fe^{III}OOH + H_2CO_3 + 8H_2O. \quad (4)$$

As a catalyst of the Fe(II)–Fe(III) LDH transformation ferrous species were shown [33]. When the H_2CO_3 (CO_3^{2-} or HCO_3^-) are present among the products of the reactions, they will probably interact with Fe^0 and can take part in the formation of the next GR(CO_3^{2-}) amount and in our system they act as the catalyst as well. Moreover, the process of iron oxide and hydroxide phase transformation is accompanied by electron transfer that is necessary for the process continuity, as it was explained in [33].

Usually Green Rust transforms to the different disperse iron oxide and oxyhydroxide phases such as lepidocrocite and magnetite. Besides ferrous species in the Green Rust lattice give GR the strong reducing properties. So, when argentum species are present in the dispersion medium, the process of phase formation will be different and except the ferrous ions oxidized in the Green Rust lattice, argentum species will be reduced to the metal state (silver) on the products of phase transformation. Depending on the oxidizing conditions two phases: core&shell composite and lepidocrocite (4) can be formed in the system as well as the single composite phase (5), but the reaction (4) is more likely to take place in practice.

$$Fe^{II}_4Fe^{III}_2(OH)_{12}CO_3 \cdot 3H_2O + 3OH^- + Ag^+ + 1e^- \rightarrow$$
$$\rightarrow Fe^{II}Fe^{III}_2O_4\&Ag^0 + 3\gamma\text{-}Fe^{III}OOH + H_2CO_3 + 8H_2O, \quad (4)$$
$$Fe^{II}_4Fe^{III}_2(OH)_{12}CO_3 \cdot 3H_2O + Ag^+ + 1e^- \rightarrow 2Fe^{II}Fe^{III}_2O_4\&Ag^0 + H_2CO_3 + 7H_2O + 2H^+. \quad (5)$$

The $FeFe_2O_4$ & Ag^0 nanocomposites were tested for medical-biological investigations [34]. Such kind of particles, on the one hand, significantly decreased the intensity of luminol-enhanced luminescence due to silver antioxidant activity. On other hand, the influence of transition-metal ions upon lipoperoxide compounds that could be consumed by Fenton's type reaction is well-known. The highest concentration of nanoparticles with thin silver shell even enhanced chemiluminescence and more compact silver shell provided antioxidant activity of composite nanoparticles due to the ferrous iron presence in dispersion medium. So, the results showed ability of $FeFe_2O_4$ & Ag^0 nanocomposites in the wide range of initial argentum concentration as perspective therapeutic agent for target delivery and cellular oxidative damage.

Conclusions

1. The simple core & shell composites containing magnetite core and silver shell can be obtained on the steel surface contacting with water $AgNO_3$ solution in the open-air system. The mechanism of such process is realized due to initial electrochemical red-ox reaction leading to collecting ferric and ferrous species, hydroxyl, oxygen and carbonates in the steel – water – air interface. Due to the interaction of the listed compounds the Fe(II)–Fe(III) layered double hydroxide – hydroxycarbonate Green Rust is formed on the steel surface. Because of the ferrous species presence in the Green Rust structure it has a strong reductive properties and ability to reduce electropositive cations such as argentum. As a result of the phase formation process the $FeFe_2O_4$ & Ag^0 nanocomposites are formed in the system. In the most cases lepidocrocite is formed as a second phase.
2. The chemical composition of the $FeFe_2O_4$ & Ag^0 structures, their particle sizes, morphology and physicochemical properties depend on several factors, especially on the argentum concentration in the solutions and pH value. In our system the quantity of the

argentum atoms on the magnetite surface is not big (> 0.5 %) and the filling of core surface with Ag^0 is partial, but the particles obtained at $C_{Ag(I)}$ = 0.5, 1.0 and 5.0 mg / dm^3 were keeping sol stability during three months. The particles size varied ~ 19 – 38 nm, but in the most cases the average size equals ~ 22 nm. The $FeFe_2O_4$ & Ag^0 nanocomposites have superparamagnetic properties at room temperature and they belong to the soft magnetic materials. Their saturation magnetization decreases from 0.4 to 0.25 emu / g when the initial $C_{Ag(I)}$ in the dispersion medium increases, probably due to the influence of the silver shells on the magnetite cores.

3. The preliminary investigation of the core & shell composites showed their availability for medical-biological purposes – target delivery and cellular oxidative damage due to their antioxidant activity, magnetic and optical properties.

References

1. Q. A. Pankhurst, J. Connolly, S. K. Jones, J. Dobson. J. Phys. D, 2003, 36, R167.
2. K. S. Shin, Y. K. Cho, J.-Y. Choi, K. Kim. Catal. Lett., 2009, 133, 1.
3. J. Dua, Ch. Jing. J. Col. Interf. Sci., 2011, 358 (1), 54.
4. J. L. Lyon, D. A. Fleming, M. B. Stone, P. Schiffer, M. E. Williams. Nano Lett., 2004, 4 (4), 719.
5. D. K. Kim, M. Mikhailova, M. Toprak, Y. Zhang, B. Bjelke, J. Kehr, M. Muhammed. Mater. Res. Soc. Symp. Proc., 2002, 704, W6.28.1.
6. Z. Xu, Y. Hou, S. Sun. J. Am. Chem. Soc., 2007, 129 (28), 8698.
7. O. M. Lavrynenko, S. V. Netreba. Mater. Sci. Nanostr., 2009, 2, 9.
8. O. M. Lavrynenko. Mater. Sci. Nanostr., 2010, 3, 3.
9. O. M. Lavrynenko, Ya. D. Korol, S. V. Netreba, V. A. Prokopenko. Chem. Phys. Technol. Surf., 2010, 1 (3), 338.
10. Eds. J. o'Loughlin, S. D. Kelly, K. M. Kemner, R. Csencsits, R. E. Cook. Chemosphere, 2003, 53, 437.
11. H. Deng, X. L. Li, Q. Peng, X. Wang, J. P. Chen, Y. D. Li. Ang. Chem. Intern. Ed., 2005, 44 (18), 2782.
12. I. Y. Goon, L. M. H. Lai, M. Lim, P. Munroe, J. J. Gooding, R. Amal. Chem. Mater., 2009, 21 (4), 673.
13. U. Tamer, Yu. Gündogdu, I. H. Boyaci, K. Pekmez. J. Nanopart. Res., 2010, **12 (**4), 1187.
14. Y. Sun, B. Yang, Y. Tian, G. Guo, W. Cai, M. He, Y. Liu. Micro & Nano Lett. IET, 2011, 6 (2), 82.
15. E. Iglesias–Silva, J. Rivas, L. M. L. Isidro, M. A. Lopez–Quintela. J. Non-Crystal. Solids, 2007, 353 (8-10), 829.
16. Q. G. He, Z. H. Wu, R. Hu. Adv. Mater. Res., 2011, 183-185, 1989.
17. Z. Wang, B. Shen, Z. Aihua, N. He. Chem. Eng. J., 2005, 113 (1), 27.
18. L. M. Liz–Marzan, M. Giersig, P. Mulvaney. Langmuir, 1996, **12 (**18), 4329.
19. M. Mandal, S. Kundu, S. K. Ghosh, S. Panigrahi, T. K. Sau, S. M. Yusuf, T. Pal. J. Col. Interf. Sci., 2005, 286 (1), 187.
20. J. Bao, W. Chen, T. Liu, Y. Zhu, P. Jin, L. Wang, J. Liu, Y. Wei, Y. Li. ACS Nano, 2007, 1 (4), 293.

21. D. V. Leff, L. Brandt, J. R. Heath. Langmuir, 1996, 12, 4723.
22. M. Spasova, V. Salgueiriño–Maceira, A. Schlachter, M. Hilgendorff, M. Giersig, L. M. Liz–Marzán, M. Farle. J. Mater. Chem., 2005, 15, 2095.
23. O. M. Lavrynenko, G. A. Dolynskyi. Mater. Sci. Nanostr., 2011, 3, 3.
24. Ю. Ю. Лурье. Аналитическая химия промышленных сточных вод. 1984, Москва: Химия.
25. Л. И. Быстрых. Химическая активность металлов. 1976, Омск: Зап. Сиб. кн. изд.
26. У. А. Дир, Р. А. Хауи, Дж. Зусман. Породообразующие минералы. 5. Несиликатные минералы. 1966, Москва: Мир.
27. O. M. Lavrynenko. Nano Studies, 2011, 3, 5.
28. J.-M. R. Genin, M. Abdelmoula, Ph. Refait, L. Simon. Hyperfine Interact. C, 1998, 3, 313.
29. J.-M. R. Génin, Ch. Ruby, Ch. Upadhyay. Solid State Sci., 2006, 8, 1330.
30. L. Legrand, S. Savoye, A. Chausse, R. Messina. Electrochem. Acta, 2000, 46, 111.
31. R. Aissa, M. Francois, C. Ruby, F. Fauth, G. Medjahdi, M. Abdelmoula, J.-M. R. Genin. J. Phys. Chem. Solids, 2006, 67, 1016.
32. B. C. Christiansen, T. Balic–Zunic, K. Dideriksen, S. L. S. Stipp. Proc. 19th Goldschmidt Conf. 2009, Davos, 223.
33. H. Liu, Yu. Wei, Yu. Sun. J. Mol. Catal. A, 2005, 226, 135.
34. G. A. Dolynskyi, O. M. Lavrynenko. Interactions between Biogenic and Abiogenic Components in Natural and Anthropogenic Systems. 2011, St Petersburg: VVM Publ.

MAGNETIZATION DURING FINITE RADIO-FREQUENCY IMPULSES IN MAGNETIC-RESONANCE IMAGING

K. V. Kotetishvili, K. G. Kapanadze, G. G. Chikhladze

Georgian Technical University
Tbilisi, Georgia
Ketinooo@hotmail.com
guramchikhladze@gmail.com

Accepted April 12, 2012

Taking into account the field effect, $M(t)$ magnetization may be repeated by the series of the dipole field. The portions experiencing action of n dipole fields, may have the amplitude approximately proportional to g^n, where

$$g = A\mu_0\gamma M_0\delta, \tag{1}$$

δ being duration of the pulse. At the first approach of the dipole field, i.e. at the first degree of g, the local error of $M(t)$ is of g^2 order. At the growth of duration of the impulse it grows as well, but even when δ grows up to 10 m / s, for B = 9.4 T magnetic field the local error is just 1%. At lower static field δ may become greater and does not provoke great errors. Therefore solution of the equation of the magnetization evolution [1]

$$\frac{d}{dt}M_{\pm}(t) \mp i\gamma C e^{\pm i\varphi}M_z(t) + \frac{1}{T_2}M_{\pm}(t) = \mp iA\gamma\mu_0 M_z(t)M_{\pm}(t)$$

at the approach of linear dipole field is carried out within the time of typical MRI experiment. In the case of the dipole field of the first order the magnetization gives

$$\left.\begin{aligned} M_{\pm}(t) &\simeq M_{\pm}^{(0)}(t) + M_{\pm}^{(1)}(t), \\ M_z(t) &\simeq M_z^{(0)}(t) + M_z^{(1)}(t), \end{aligned}\right\}, \tag{2}$$

$\vec{M}^{(0)}$ and $\vec{M}^{(1)}$ being solutions of the zero and the first order, respectively.

Now consider the problem for the situation, when it is possible to ignore the distant dipole field (DDF), and receive the following equations:

$$\frac{d}{dt}M_{\pm}^{(0)}(t) = \pm i\gamma C e^{\pm i\varphi}M_z^{(0)}(t) - \frac{1}{T_2}M_{\pm}^{(0)}(t), \tag{3′}$$

$$\frac{d}{dt}M_z^{(0)}(t) = \frac{i}{2}\gamma C\left[e^{-i\varphi}M_+^{(0)}(t) - e^{i\varphi}M_-^{(0)}(t)\right]. \tag{3″}$$

Take into account that, if duration of the radio-frequency impulse is much less, than T_2, the transversal relaxation may be ignored, and magnetizations given by equations (3) before and after the radio-frequency impulses will be related to each other as follows [2]:

$$\left(M_x, M_y, M_z\right)_{next} = R(\theta,\varphi)\left(M_x, M_y, M_z\right)_{previous}, \tag{4}$$

$$R(\theta,\varphi) = \begin{bmatrix} cos^2\frac{\theta}{2} + sin^2\frac{\theta}{2}cos2\varphi & sin^2\frac{\theta}{2}sin2\varphi & -sin\theta sin\varphi \\ sin^2\frac{\theta}{2}sin2\varphi & cos^2\frac{\theta}{2} - sin^2\frac{\theta}{2}cos2\varphi & sin\theta cos\varphi \\ sin\theta sin\varphi & -sin\theta cos\varphi & cos\theta \end{bmatrix}. \tag{5}$$

In this case, the radio-frequency impulse turns the magnetization by $\theta = \gamma Ct$ angle in $\hat{e}\varphi = cos\varphi\hat{x} + sin\varphi\hat{y}$ direction. When $\theta = \pi$, then the magnetization after the radio-frequency impulse is given as follows:

$$\left.\begin{aligned} M_z &= -M_{z,previous} \\ M_\pm &= e^{\pm 2i\varphi}M_{\mp,previous} \end{aligned}\right\}. \tag{6}$$

Equations (3′) and (3″) may be transformed into linear differential equations of the second order relative to $M_\pm^{(0)}(t)$, and may be solved by the diagonalization method. The initial value of the magnetization before the impulse is given in the form of

$$\left.\begin{aligned} M_\pm^{(0)}(0) &= M_{\pm 0} \\ M_z^{(0)}(0) &= M_{z0} \end{aligned}\right\} \tag{7}$$

and the transversal magnetization of the zero order becomes

$$M_\pm^{(0)}(t) = C_1(t)M_{\pm 0} + C_2(t)e^{\pm 2i\varphi}M_{\mp 0} \pm C_3(t)e^{\pm i\varphi}M_{z0}. \tag{8}$$

Linear magnetization of the zero order may be found placing (8) into the solution of (3″)

$$M_z^{(0)}(t) = \frac{C_3(t)}{2}\left[e^{-i\varphi}M_{+0} - e^{i\varphi}M_{-0}\right] + C_4(t)M_{z0}. \tag{9}$$

$C_1(t), C_2(t), C_3(t)$ and $C_4(t)$ coefficients are given as follows:

$$C_1(t) = \frac{1}{2}e^{-t/2T_2}\left[e^{-t/2T_2} + cosh\frac{a_0 t}{2T_2} - \frac{1}{a_0}sinh\frac{a_0 t}{2T_2}\right], \tag{10}$$

$$C_2(t) = \frac{1}{2}e^{-t/2T_2}\left[e^{-t/2T_2} - cosh\frac{a_0 t}{2T_2} + \frac{1}{a_0}sinh\frac{a_0 t}{2T_2}\right], \tag{11}$$

$$C_3(t) = \frac{2i}{a_0}\gamma CT_2 e^{-t/2T_2}sinh\frac{a_0 t}{2T_2}, \tag{12}$$

$$C_4(t) = e^{-t/2T_2}\left[cosh\frac{a_0 t}{2T_2} + \frac{1}{a_0}sinh\frac{a_0 t}{2T_2}\right], \tag{13}$$

$$a_0 = \sqrt{1 - (2\gamma C T_2)^2}. \quad (14)$$

In most cases

$$2\gamma C T_2 \gg 1. \quad (15)$$

Inserting

$$\gamma C \delta = \pi \quad (16)$$

in a_0 for π pulses of δ duration and ignoring $0(\delta/T_2)^2$ terms of the second order, yields:

$$a_0 \approx 2i\gamma C T_2. \quad (17)$$

Then, canceling δ/T_2 terms of the first order, finally π pulses give:

$$C_1(\delta) \approx -\frac{\delta}{4T_2}, \quad (18)$$

$$C_2(\delta) \approx 1 - \frac{3\delta}{4T_2}, \quad (19)$$

$$C_3(\delta) \approx 0, \quad (20)$$

$$C_4(\delta) \approx -\left(1 - \frac{\delta}{2T_2}\right). \quad (21)$$

Equations (8) and (9) show that it is changing of $M_{\pm}$ and M_z in the same time by varying $C_3(\delta)$ amplitude during one pulse. For δ/T_2 $C_3(t) \approx 0$. It means that change of $M_{\pm}$ and M_z disappears at the end of π pulse. $C_2(t)$ coefficient is associated with turning (change of orientation) of $M_{\pm}$ to M_z, while $C_1(t)$ – with residual amplitude of $M_{\pm}$. As to $C_4(t)$ coefficient, it is related to transformation of M_z into $-M_z$. It should be noted as well that for the samples with great T_2 (water) [3, 4]

$$C_1(\delta) \sim \left(\frac{\delta}{T_2}\right) C_2(\delta) \quad (22)$$

and it is much less, than $C_2(\delta)$

$$C_1(\delta) \ll C_2(\delta). \quad (23)$$

Thus, when there is no T_2 relaxation during the impulse, $M_{\pm}$ transforms into $M_{\mp}$, while M_z – into $-M_z$. In this case

$$\left.\begin{array}{c} C_1(\delta) = C_3(\delta) = 0, \\ C_2(\delta) = 1, \\ C_4(\delta) = -1. \end{array}\right\}. \quad (24)$$

When T_2 relaxation takes place, due to Bloch's equations

$$\frac{d\vec{M}}{dt} = \gamma \vec{M} x \vec{B} - \frac{\vec{M}_x + \vec{M}_y}{T_2}. \quad (25)$$

Effective frequency of precession at the re-orientation of impulses decreases. As a result, $M_{\pm}$ and M_z do not transform into $M_{\mp}$ and $-M_z$ completely and transversal relaxation is incompletely oriented from $M_{\pm}$ into M_z as it is given in the equations (8) and (9).

References

1. K. G. Kapanadze. Influence of finite radio-frequency impulses at evolution of magnetization in nuclear-magnetic resonance. Georg. Eng. News, 2012, 1, 5-10.
2. E. Hahn. Spin echoes. Phys. Rev., 1950, 80, 580-594.
3. W. Richter et al. Imaging with Intermolecular multiple-quantum coherences in Solution NMR. Science, 1995, 654-657.
4. L. S. Bouchard, R. R. Rizi, W. S. Warren Magnetization structure contrast based on intermolecular multiple-quantum coherences. Magn. Reson. Med., 2002, 48, 973-976.

INFLUENCE OF RADIO-FREQUENCY IMPULSES AT TRANSVERSAL AND LONGITUDINAL MAGNETIZATION CAUSED BY FAR DIPOLE FIELD

K. V. Kotetisvili, K. G. Kapanadze

Georgian Technical University
Tbilisi, Georgia
Ketinooo@hotmail.com

Accepted April 12, 2012

Due to influence of the dipole field $M(t)$ the magnetization should be written down as follows [1]:

$$\frac{d}{dt}M_{\pm}(t) \mp i\gamma C e^{\pm i\varphi}M_z(t) + \frac{1}{T_2}M_{\pm}(t) = \mp iA\gamma\mu_0 M_z(t)M_{\pm}(t), \quad (1)$$

$$\frac{d}{dt}M_z(t) - \frac{i}{2}\gamma C\left[e^{-i\varphi}M_+(t) - e^{i\varphi}M_-(t)\right] = 0, \quad (2)$$

$$M_{\pm}(t) = M_x \pm iM_y. \quad (3)$$

Due to these expressions during the radio-frequency impulses the magnetization for multi-spin-echo series at the first approach of the dipole field will be given in the form of

$$\frac{d}{dt}M_{\pm}^{(1)}(t) = \pm i\gamma C e^{\pm i\varphi}M_z^{(1)}(t) \mp iA\gamma\mu_0 M_z^{(1)}(t) - \frac{1}{T_2}M_{\pm}^{(1)}(t), \quad (4)$$

$$\frac{d}{dt}M_z^{(1)}(t) = \frac{i}{2}\gamma C\left[e^{-i\varphi}M_+^{(1)}(t) - e^{i\varphi}M_-^{(1)}(t)\right]. \quad (5)$$

Just as it was at the zero approach [2], the expressions (4) and (5) may be transformed into linear differential equations of the second order relative to $M_{\pm}^{(1)}(t)$, and they should be solved by the diagonalization method. At that time the initial value of magnetization before the radio-frequency impulses (before they start) is zero $M_{\pm}^{(1)}(0) = 0$ and $M_z^{(1)}(0) = 0$, that's why we get:

$$M_{\pm}^{(1)}(t) = A\gamma\mu_0 T_2[\pm d_1(t)M_{z0}M_{\pm 0} \pm d_2(t)e^{\pm 2i\varphi}M_{z0}M_{\mp 0} + d_3(t)e^{\mp i\varphi}M_{\pm 0}^2 + d_4(t)e^{\pm 3i\varphi}M_{\mp 0}^2 + d_5(t)e^{\pm i\varphi}M_{+0}M_{-0} + d_6(t)e^{\pm i\varphi}M_{z0}^2]. \quad (6)$$

Inserting $M_{\pm}^{(1)}(t)$ into (5), yields:

$$M_{\pm}^{(1)}(t) = A\gamma\mu_0 T_2\{d_7(t)M_{z0}\left[e^{-i\varphi}M_{+0} + e^{-i\varphi}M_{-0}\right] + d_8(t)\left[e^{-2i\varphi}M_{+0}^2 - e^{2i\varphi}M_{-0}^2\right]\}, \quad (7)$$

here d_i coefficients ($i = 1 \div 8$) are given as follows:

$$d_1(t) = -\frac{i}{2a_0}e^{-t/T_2}\left[\left(1 - \frac{1}{a_0^2}\right)sinh\frac{a_0 t}{T_2} + \frac{(a_0-1)(a_0+3)}{2(a_0+1)}sinh\frac{(a_0+1)t}{2T_2} - \frac{(a_0+1)(a_0-3)}{2(a_0-1)}sinh\frac{(a_0-1)t}{2T_2} + \frac{t}{a_0 T_2}\right], \quad (8.1)$$

$$d_2(t) = -\frac{i}{2a_0}e^{-t/T_2}\left[-\left(1 - \frac{1}{a_0^2}\right)sinh\frac{a_0 t}{T_2} + \frac{(a_0-1)(a_0+3)}{2(a_0+1)}sinh\frac{(a_0+1)t}{2T_2} - \frac{(a_0+1)(a_0-3)}{2(a_0-1)}sinh\frac{(a_0-1)t}{2T_2} - \frac{t}{a_0 T_2}\right], \quad (8.2)$$

$$d_3(t) = \frac{\gamma C T_2}{4a_0^2}e^{-t/T_2}\left[-\left(1 - \frac{t}{T_2}\right) + cosh\frac{a_0 t}{T_2} - \frac{1}{a_0}sinh\frac{a_0 t}{T_2} - a_0 cosh\frac{(a_0-1)t}{2T_2} + \frac{2a_0}{a_0-1}sinh\frac{(a_0-1)t}{2T_2} + a_0 cosh\frac{(a_0+1)t}{2T_2} - \frac{2a_0}{a_0+1}sinh\frac{(a_0+1)t}{2T_2}\right], \quad (8.3)$$

$$d_4(t) = \frac{\gamma C T_2}{4a_0^2}e^{-t/T_2}\left[-\left(1 - \frac{t}{T_2}\right) + cosh\frac{a_0 t}{T_2} - \frac{1}{a_0}sinh\frac{a_0 t}{T_2} + a_0 cosh\frac{(a_0-1)t}{2T_2} - \frac{2a_0}{a_0-1}sinh\frac{(a_0-1)t}{2T_2} - a_0 cosh\frac{(a_0+1)t}{2T_2} + \frac{2a_0}{a_0+1}sinh\frac{(a_0+1)t}{2T_2}\right], \quad (8.4)$$

$$d_5(t) = -\frac{\gamma C T_2}{2a_0^2} e^{-t/T_2}\left[-\left(1-\frac{t}{T_2}\right) + cosh\frac{a_0 t}{T_2} - \frac{1}{a_0} sinh\frac{a_0 t}{T_2}\right], \quad (8.5)$$

$$d_6(t) = \frac{\gamma C T_2}{a_0^2} e^{-t/T_2}\left[-\left(1+\frac{t}{T_2}\right) + cosh\frac{a_0 t}{T_2} + \frac{1}{a_0} sinh\frac{a_0 t}{T_2}\right], \quad (8.6)$$

$$d_7(t) = \frac{\gamma C T_2}{2a_0} e^{-t/T_2}\left[cosh\frac{(a_0+1)t}{2T_2} + \frac{2}{a_0+1} sinh\frac{(a_0+1)t}{2T_2} - cosh\frac{(a_0-1)t}{2T_2} - \right.$$
$$\left. - \frac{2}{a_0-1} sinh\frac{(a_0-1)t}{2T_2}\right], \quad (8.7)$$

$$d_8(t) = -\frac{i}{8} e^{-t/T_2}\left[\left(1-\frac{1}{a_0}\right) sinh\frac{(a_0+1)t}{2T_2} - \left(1+\frac{1}{a_0}\right) sinh\frac{(a_0-1)t}{2T_2}\right]. \quad (8.8)$$

Ignoring the terms $0(\delta/T_2)^2$ of the second order, when $t = \delta$, yields:

$$\left.\begin{array}{c} d_1(S) \approx d_2(S) \approx 2d_8(S) \approx \frac{i}{4}\frac{\delta}{T_2} \\ d_3(S) \approx d_4(S) \approx d_5(S) \approx d_6(S) \approx d_7(S) = 0 \end{array}\right\}. \quad (9)$$

Due to the action of transversal relaxation, the radio-frequency impulses cause the difference between transversal and longitudinal magnetizations [3]. In any moment of the action of the impulses, longitudinal component of magnetization affects at development (evolution) of transversal component by means of the action of the dipole field. Transversal magnetization of the first approach (6) points at influence of the dipole fields of two different sources.

Under the action of the dipole field the first source is created by direct interaction between M_{z0} and $M_{\pm 0}$, and this interaction is given in (6) by $d_1(t)$ and $d_2(t)$.

Another source of influence is received by the private interaction between M_{z0} and $M_{\pm 0}$. In this case M_{z0} rotates in transversal plane and this part is developed at the varying, caused by the changing amplitude in the longitudinal direction of the dipole field.

Thus, the part of $M_{\pm 0}$ rotates in longitudinal direction, which influences at its residual amplitude from the transversal plane, being under the action of the dipole field. Interaction of M_{z0} and $M_{\pm 0}$ in (6) is defined by $d_3(t)$, $d_4(t)$, $d_5(t)$ and $d_6(t)$ conditions. From the other hand, the dipole field does not act directly at M_z, but its action is revealed at the change of M_z up to $M_{\pm 0}$ resulting from the rotation of the radio-frequency impulse (see the formula (4)).

Therefore, consider $d_7(t)$ as the direct action on $M_z^{(1)}$, while $d_8(t)$ – as the private one. Note as well that $M_z^{(1)}$ is independent on M_{+0}, M_{-0} and $M_{z0}^{(2)}$, due to their ignoring in (5).

So, resulting solutions of the zero order are given by formulae (8 – 13) of [2], while of the first order – by (6) and (7), where (8) is taken into account. As it is seen from signed solutions, transversal and longitudinal magnetizations mix after the end of the radio-frequency impulse. This mix causes as the transversal relaxation $\left(C_1(t)\right)$, as the effect of the dipole field $\left(d_i(t)\right)$. If the effect of the dipole field $d_i(t) = 0$ for all i, and relaxation time T_2 exists within the indefinite time of the impulse, then no mix of transversal and longitudinal magnetizations occur after the end of π impulses just in the same way, as it was shown in the formula (6) of [2].

References

1. K. G. Kapanadze. Influence of finite radio-frequency impulses at evolution of magnetization in nuclear-magnetic resonance. Georg. Eng. News, 2012, 1, 5-10.
2. K. V. Kotetishvili, K. G. Kapanadze, G. G. Chikhladze. Magnetization during finite radio-frequency impulses in magnetic resonance imaging. Nano Studies, 2012, 5, 41-44.
3. L. S. Bouchard, R. R. Rizi, W. S. Warren. Magnetization structure contrast based on intermolecular multiple-quantum coherences. Magn. Reson. Med., 2002, 48, 973-976.

ИЗОХРОННЫЙ ОТЖИГ ОБРАЗЦОВ n-Si, ОБЛУЧЕННЫХ ПРОТОНАМИ С ЭНЕРГИЕЙ 25 МэВ

Т. А. Пагава, М. Г. Беридзе, Н. И. Майсурадзе

Грузинский технический университет
Тбилиси, Грузия
tpagava@gtu.ge
nmaisuradze@gtu.ge

Принята 26 апреля 2012 года

1. Введение

Известно, что в кристаллах кремния, облученных частицами с энергией $E \leq 10$ МэВ в зависимости от примесного состава преимущественно возникает большое разнообразие точечных радиационных дефектов (РД). Доминирующими из них являются вакансия + донор (атом фосфора) VP, вакансия + акцептор (атом бора) VB, вакансия + фоновые примеси (кислород и углерод) VO и VC, дивакансия V_2, а также мультикомлексные точечные РД типа V_mO_n (m, n = 1, 2, 3, …) и т.д., которые до 600 °C определяют физические свойства облученных кристаллов [1 – 3].

При облучении кристаллов кремния частицами высоких энергий ($E > 10$ МэВ) возникают сложные структурные повреждения, т.н. разупорядоченные области (РО), которые согласно модели Госика [4], являются непрозрачными для основных носителей тока (диэлектрические включения). В этих кристаллах в области фононного рассеяния наблюдается уменьшение эффективного значения подвижности основных носителей тока μ_{eff} за счет уменьшения фактического объема образца [5]. Локальные РО отжигаются в интервале 200 – 260 °C. При больших дозах облучения, когда в кристалле образуются аморфные слой, структура кремния восстанавливается при 570 °C [6].

В образцах n-Si, облученных протонами с энергией 25 МэВ, в области фононного рассеяния наблюдается резкое увеличение значения μ_{eff} электронов [7, 8]. Такие высокие значения подвижности получаемые в холловских экспериментах, является признаком образования в образце относительно высокопроводящих (металлических) включений с омическим переходом на границе раздела с матрицей полупроводника [9]. По-видимому, такими включениями являются скопления межузельных атомов, которые образуются в кристаллах кремния при облучении легкими ионами и термообработках [10, 11].

В работе [7] в кристаллах n-Si, облученных протонами с энергией 25 МэВ после отжига при 90 °C и естественного старения при 300 K в течение 30 суток, наблюдается резкое уменьшение μ_{eff}. По мнению автора [7], это связано экранированием скоплений межузельных атомов отрицательно заряженными вторичными РД, которые образуются вокруг этих включении в процессе старения облученного кристалла.

Целью данной работы является с использованием методов Холла и изохронного отжига (ИО) выяснить: 1) какие дефекты являются источником неравновесных вакансий в

процессе ИО; 2) какого типа РД образуются при вступлений этих вакансий в квазихимическую реакцию с примесными атомами вокруг металлических включений; 3) какие из РД ответственны за экранирование металлических включении и соответственно за уменьшением μ_{eff}; 4) зависимость радиуса металлических включении от температуры ИО и определить температуру полного отжига этих включений.

2. Эксперимент

Были исследованы изменения характера температурных зависимостей концентраций N_H и холловской подвижности μ_H электронов в облученных кристаллах кремния, подвергшихся процессу ИО при различных температурах T_{ann}. Исследуемые образцы с размерами $1 \times 3 \times 10$ мм, представляли собой монокристаллы n-Si, легированные фосфором Р до концентрации $N_P \approx 6 \cdot 10^{13}$ см$^{-3}$. Их облучали протонами с энергией 25 МэВ при 300 К. Доза облучения – $8 \cdot 10^{12}$ см$^{-2}$. Облученные кристаллы подвергались ИО в интервале 80 – 600 °С шагом 10 °С. Время выдержки при фиксированной температуре – 10 мин. После каждого цикла ИО температурные зависимости холловской подвижности μ_H и концентраций N_H электронов были сняты от точки кипения азота вплоть до комнатной температуры. Омические контакты для измерения создавались путем втирания алюминия в поверхность исследуемого образца. Энергии ионизации уровней дефектов E_i определялись по наклону зависимостей $N_H = f(1000 / T)$ Концентрации различных РД после каждого цикла ИО вычислялись с помощью ступенчатых зависимостей $N_H = f(1000 / T)$ и $N = f(1000 / T_{ann})$ в интервал 77 – 300 К и 80 – 600 °С, соответственно. Температура образца в интервале температур 77 – 300 К контролировалась медь–константановой термопарой, а в интервале 80 – 600 °С – хромель–алюмелевой. Погрешность измерения этих величин не превышала 10 %.

3. Результаты исследований и их обсуждение

На **рис. 1** представлены зависимости $N_H = f(1000 / T)$ в исходном кристалле (кривая 1), после облучения протонами с энергией 25 МэВ интегральным потоком $8 \cdot 10^{12}$ см$^{-2}$ (кривая 2), а также после отжигов в интервале T_{ann} = 80 – 600 °С (кривые 3 – 11). Кривые 2 – 4 на **рис. 1** соответствуют истощенных акцепторных центров с энергией деионизаций E_C – 0.38 эВ, т.е. дивакансиям. Это означает, что все свободные электроны захвачены Е-центрами, дивакансиями и неизвестными дефектами с уровнями E_C – 0.54 и E_C – 0.57 эВ, а А-центры находятся в нейтральном состоянии и определить концентрацию этих центров N_A по кривым $N_H = f(1000 / T)$ невозможно. После отжига определенной части Е-центров ($T_{ann} \geq 100$ °С) А-центры заряжаются и появляется возможность проследить за изменением их концентрацией в процессе ИО.

Как видно из **рис. 2**, сразу после облучения в исследуемых кристаллах наблюдается увеличение подвижности электронов (кривая 2). После отжига при 80 °С холловская подвижность электронов незначительно уменьшается (рис. 2, кривая 3) и опять растет после отжига при 90 °С (**рис. 2**, кривая 4). Отжиг же при 110 °С приводит к появлению на кривой $\mu_H(T)$ минимума, в котором значение μ_H снижено почти на порядок по сравнению исходного значения μ_H (**рис. 2**, кривая 5).

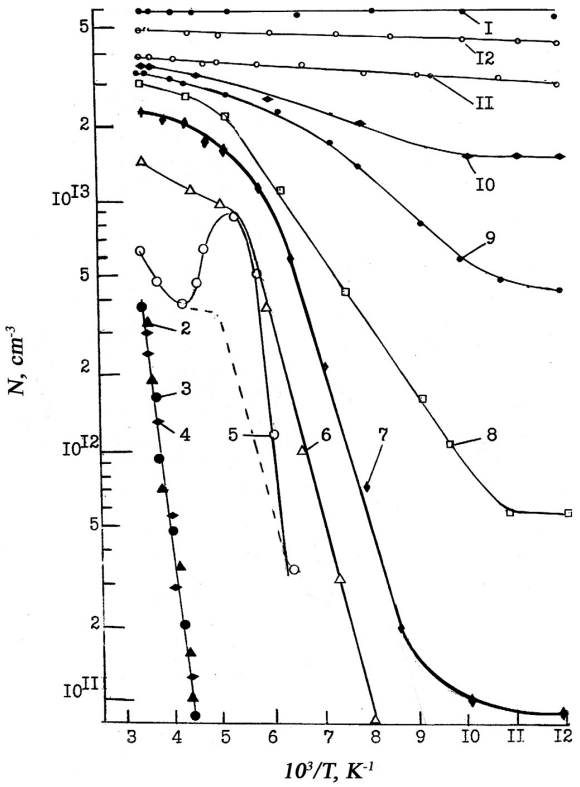

Рисунок 1. Зависимость концентраций электронов от температуры в облученных кристаллах n-Si: 1 – до облучения, 2 – после облучения, после отжигов при температуре 3 – 80, 4 – 90, 5 – 110, 6 – 120, 7 – 150, 8 – 290, 9 – 300, 10 – 350, 11 – 400, 12 – 600 °C.

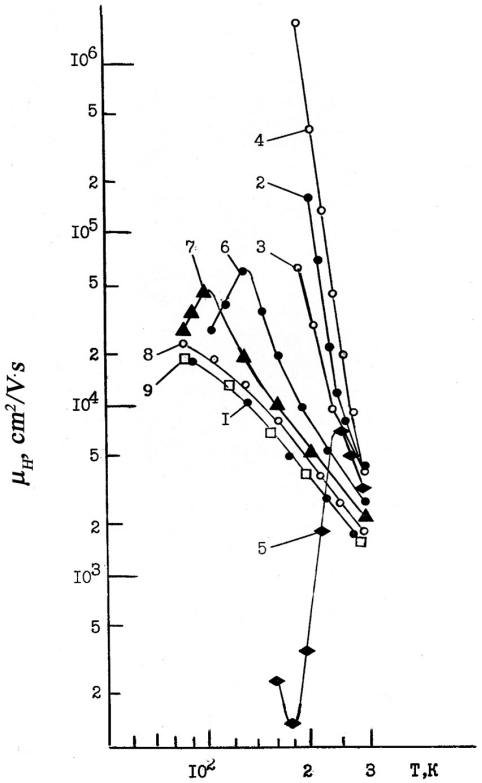

Рисунок 2. Зависимость холловской подвижности электронов от температуры в облученных кристаллах n-Si: 1 – до облучения, 2 – после облучения, после отжигов притемпературе 3 – 80, 4 – 90, 5 – 110, 6 – 120, 7 – 290, 8 – 350, 9 – 400 °C.

Увеличение μ_H сразу после облучения протонами с энергией 25 МэВ в работах [7, 8] объясняется образованием в объеме кристалла металлических включении с омическим переходом с матрицей. Такими включениями являются скопления межузельных атомов. Подобно дислокациям они в кристалле создают упругое напряжение и тем самим уменьшают T_{ann} вакансионных дефектов, например, тетравакансий – V_4 [3]. При T_{ann} = 110 °С отжигается значительная часть Е-центров.

Неравновесные вакансии, продукты распада V_4 и Е-центров устремляются к скоплениям междуузельных атомов и вступают квазихимическую реакцию с примесными атомами. На начальных стадиях ИО Е-центров вокруг скоплении межузельных атомов кроме РД с высокой термостабильностью (например, А-центров) образуются также сами Е-центры. В результате, вокруг включении образуется непрозрачная для электронов проводимости отрицательно заряженная оболочка из вторичных РД (А-, Е-центры, V_2 и т.д.), что вызывает наблюдаемое уменьшение μ_H после отжига при 110 °С (**рис. 2**, кривая 5).

Следует отметить, что А-центры, которые образуются вокруг скоплении межузельных атомов, в области минимума при 180 К не заряжены и не могут вызывать уменьшение подвижности. Образование дивакансий из одноименно заряженных моновакансии маловероятно. Таким образом, за уменьшением подвижности в области 180 К ответственны Е-центры, которые при этой температуре образуются эффективнее других РД по реакций: P + V = E – 2e.

Источником неравновесных вакансий в процессе ИО по-видимому являются также РО вакансионного типа, которые несомненно присутствуют в облученных протонами кристаллах кремния. Известно [7], что они играют большую роль в формировании непрозрачных для электронов проводимости оболочек вокруг металлических включений. Как известно [12], степень заполнения глубоких центров f в атмосфере вокруг скоплений межузельных атомов стремится к единице, причем энергия взаимодействия может достигать величины $E \sim fE_0$, где $E_0 = e^2 / \varepsilon d \sim 0.5$ эВ для кремния, e – заряд электрона, ε – диэлектрическая постоянная, d – расстояние между дефектами.

После термообработки при T_{ann} = 110 °С как уже отмечалось отжигается значительная часть Е-центров с концентрацией ΔN_E, а концентрация высвободившихся электронов и заряженных А-центров будет равно $2\Delta N_E$. Истощению А-центров соответствует немонотонная кривая 2 на **рис. 2**.

Электростатическое взаимодействие между отрицательно заряженными дефектами приводит к изменению энергий дейонизаций центров. По-видимому, когда $E \geq 0.17$ эВ, электроны с уровня, соответствующего А-центрам, в зону проводимости переходят при более низких температурах, чем обычно (**рис. 1**, кривая 5).

Полная концентрация А-центров $N_A = 2.5 \cdot 10^{13}$ см$^{-3}$ (**рис. 1**, кривая 7). Увеличение N_A до $3 \cdot 10^{13}$ см$^{-3}$ (**рис. 1**, кривая 8) после отжига облученных кристаллов n-Si при T_{ann} = 290 °С, связано дообразованием А-центров при отжиге дивакансий в интервале температур 225 – 290 °С. При T_{ann} = 300 °С начинается отжиг самих А-центров [13] и полностью отжигается при $T_{ann} \approx 400$ ° (**рис.** 1, кривая 11).

В силу электростатического взаимодействия в зону проводимости электроны переходят не только из А-центров, но из более глубоких уровней. В зону проводимости электроны переходят также из центров $C_i C_s$, с энергией ионизаций E_C – 0.16 эВ [14, 15]. В результате угол наклона кривой 5 на **рис. 2** увеличивается, а концентрация электронов при температуре 200 К достигает максимума – $N_H = 9 \cdot 10^{12}$ см$^{-3}$. После деионизаций

А-центров уменьшаются силы электростатического взаимодействия между радиационными дефектами. При 250 K электроны зоны проводимости захватываются глубокими центрами. В зоне проводимости остаются электроны с концентрацией $N_H = 4 \cdot 10^{12}$ см$^{-3}$, что соответствует заряженным А-центрам при отжиге Е-центров в области $T_{ann} = 110$ °C. При дальнейшем увеличении температуры измерения концентрация электронов монотонно возрастает. Концентрация электронов в отсутствии сил электростатического взаимодействия изменился бы так, как это проведено пунктирной линией на **рис. 2** (наклон кривой 2 соответствует истощению А-центров).

В процессе ИО при $T_{ann} = 120$ °C отжигается почти одна треть Е-центров, а концентрация вновь образовавшихся Е-центров ничтожно мала. Соответственно уменьшается энергия электростатического взаимодействия между отрицательно заряженными дефектами и кривая зависимости $N_H = f(1000 / T)$ монотонно возрастает от точки кипения азота вплоть до комнатной температуры. Характер изменения зависимости $N_H = f(1000 / T)$ не меняется после отжига при более высоких температурах (вплоть до $T_{ann} = 600$ °C).

При этом после отжига Е-центров в дефектно-примесной атмосфере вокруг металлических включений уменьшается степень экранирования скоплений межузельных атомов, что приводит к увеличению значения μ_H (**рис. 2**, кривая 6).

Наблюдаемая осцилляция величины холловской подвижности электронов можно объяснить изменением степени экранирования скоплений межузельных атомов в процессе ИО. При ИО изменяются концентрация и зарядовые состояния тех РД, которые способны воздействовать на степени экранирования металлических включений и соответственно на подвижность основных носителей тока в кремнии.

Отжиг Е-центров уменьшает сопротивление кристалла, что позволяет провести холловские измерения вплоть до точки кипения азота. При температуре ≤ 140 K полностью заряжаются А-центры, что несомненно приведет к увеличению степени экранирования скоплении межузельных атомов и соответственно к уменьшению μ_H, что и наблюдается в эксперименте (**рис. 2**, кривые 6, 7). После отжига А-центров (350 °C) уменьшение μ_H в области 77 K не наблюдается (рис. 2, кривые 8, 9).

После отжига при $T_{ann} = 400$ °C восстанавливается (и дальнейшем не изменяется) характерная для необлученного кристалла температурная зависимость холловской подвижности электронов. При этой температуре отжига скопления межузельных атомов по-видимому окончательно отжигаются (**рис. 2**, кривая 9).

По изменении подвижности электронов при 300 K нам удалось проследить за изменением радиуса атомных кластеров в процессе ИО в облученных кристаллах n-Si. Как известно [8], радиус атомных кластеров определяется по формуле $R = \sqrt{3 f / 4 \pi N_r}$, где N_r – концентрация атомных кластеров, которая по нашей оценке при облучении кристаллов n-Si протонами с энергией 25 МэВ дозой $8.1 \cdot 10^{12}$ см$^{-2}$, равняется $\sim 5 \cdot 10^{13}$ см$^{-3}$, f – объемная доля атомных кластеров, которая определяется по формуле $\mu_{eff} = \mu_H (1 + 3 f) / (1 - 6 f)$, где μ_{eff} – холловская подвижность электронов в облученных высокоэнергетическими протонами кристаллах, а μ_H – до облучения [9]. Зависимость $R(T_{ann})$ показана на **рис. 3**. Отметим, что концентрация электронов после ИО полностью не восстанавливается. По-видимому это связано образованием глубоких РД в процессе охлаждения кристаллов после отжига при 600 °C, как это происходит при термообработке деформированных образцов кремния с высокой плотностью дислокаций [12].

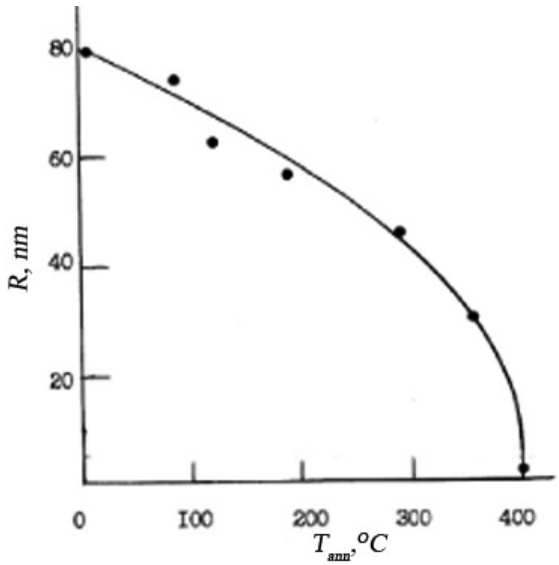

Рисунок 3. Зависимость радиуса наноразмерного атомного кластера от температуры отжига в облученных протонами кристаллах n-Si.

На основе проведенных исследований в данной и ранее опубликованных работах [7] и [8], можно предположить, что при облучении протонами с энергией 25 МэВ в кристаллах n-Si образуются наноразмерные атомные кластеры ($R \approx 80$ нм), которые отжигаются при T_{ann} = 400 °C. Радиусом атомных кластеров можно управлять изменением энергии облучения или температуры ИО, а концентрацией N_r – дозой облучения, т.к. $N_r = N_A \sigma_r$ Ф, где N_A – концентрация атомов Si, σ_r – сечение образования скоплении, Ф – доза облучения [5]. В кристаллах Si, полученных методом Чохральского, концентрация атомов кислорода в кластерах будет больше, чем в кристаллах, полученных зонной плавкой. К изменению примесного состава атомного кластера могут привести разные, в том числе легирующие примеси, определяющие тип проводимости образца, напримиер, атомы фосфора или бора.

С помощью термообработки можно управлять проводимостью атомных кластеров. Напримиер, в процессе ИО при T_{ann} = 110 °C металлические включения превращаются в квазидиэлектрические, и наоборот, после отжига при T_{ann} = 120 °C, квазидиэлектрические включения опять превращаются металлические (**рис. 2**, кривые 5, 6).

Как известно [16], если наноразмерные атомные кластеры составляют основную часть полупроводника, то изменения их размеров и концентраций приводят к изменению ширины запрещенной зоны, удельной проводимости, энергии фундаментальных оптических переходов и т.д. Это позволяет сконструировать новых полупроводниковых материалов, свойства которых отличаются от исходного материала.

Так как, кремний является базовым материалом для современной полупроводниковой электроники, реализация таких возможностей для него представляет большой интерес и требует дальнейшего исследования.

4. Заключение

В работе показано, что при облучении протонами с энергией 25 МэВ в кристаллах n-Si преимущественно образуются относительно высокопроводящие включения с

омическим переходом на границе раздела с матрицей полупроводника, чем объясняется наблюдаемое увеличение подвижности электронов μ_H. Такими включениями по-видимому являются скопления межузельных атомов, которые подобно дислокациям в кристалле создают упругие напряжения. В процессе ИО продукты диссоциации вакансионных РД – неравновесные вакансии – устремляются к этим включениям. Определенная часть вакансий рекомбинирует с межузельными атомами. Остальные вступая в квазихимическую реакцию с примесными атомами, вокруг скоплений межузельных атомов создают непрозрачную для электронов проводимости отрицательно заряженную оболочку из A-, E-центров и других акцепторов (образование дивакансий вокруг скоплений межузельных атомов по реакции $V_2 \rightarrow V + V$ в процессе ИО – в силу электростатического отталкивания между отрицательно заряженными вакансиями – маловероятно). Этими процессами объясняется уменьшение подвижности электронов μ_H. В процессе измерения в области высоких температур (200 – 300 K) за экранирование металлических включений ответственны E-центры; ниже 200 K кроме E-центров также заряженные A-центры; после отжига E-центров, только A-центры. Скопления межузельных атомов окончательно отжигаются при T_{ann} = 400 °C.

Как известно, все основные вторичные РД (E-центры, дикансии и A-центры) и РО вакансионного типа в n-Si отжигаются при T_{ann} < 400 °C. В образцах n-Si, облученных при T_{irr} < 400 °C, эти дефекты не образуются или образуются в очень малом количестве. В облученных этих условиях образцах n-Si, по-видимому, преимущественно образуются только наноразмерные атомные кластеры.

Ссылки

1. Ж. Бургуэн, М. Ланно. Точечные дефекты в полупроводниках. Экспериментальные аспекты. 1985, Москва: Мир.
2. В. С. Вавилов, В. Ф. Киселев, Б. Н. Мукашев. Дефекты в кремнии и на его поверхности. 1990, Москва: Наука.
3. В. В. Емцев, Т. В. Машовец. Примеси и точечные дефекты в полупроводниках. 1981, Москва: Радио и связь.
4. B. R. Gossik. J. Appl. Phys., 1959, 30, 1214.
5. Р. Ф. Коноплева, В. Л. Литвинов, Н. А. Ухин. Особенности радиационного повреждения полупроводников частицами высоких энергии. 1971, Москва: Атомиздат.
6. Отв. ред. Л. С. Смирнов. Физические процессы в облученных полупроводниках. 1977, Новосибирск: Наука.
7. Т. А. Пагава, Н. И. Майсурадзе. ФТП, 2010, 44, 160.
8. Т. А. Пагава, Н. И. Майсурадзе, М. Г. Беридзе. ФТП, 2011, 45, 582.
9. Е. В. Кучис. Гальваномагнитные эффекты и методы их исследования. 1990, Москва: Радио и связь.
10. А. А. Асеев, Л. Н. Федина, Д. Хоель, Х. Барч. Скопления межузельных атомов в кремнии и германии. 1991, Новосибирск: Наука.
11. И. В. Антонова, С. С. Шаймиев, С. А. Смагулова. ФТП, 2006, 40, 557.
12. Л. С. Милевский, Т. М. Ткачева, Т. А. Пагава. ЖЭТФ, 1975, 69, 2132.

13. Ю. В. Помозов, М. Г. Соснин, Л. И. Хируненко, В. И. Яшник, Н. В. Абрасимов, В. Шредер, М. Хене. ФТП, 2000, 34, 1030.
14. Н. И. Бояркина, С. А. Смагулова, А. А. Артемьев. ФТП, 2002, 36, 9007.
15. T. Pagava, L. Chkhartishvili, N. Maisuradze. Radiation Effects and Defects in Solids, 2006, 161, 709.
16. М. Г. Мильвидский, В. В. Чалдышев. ФТП, 1998, 32, 513.

РЕГУЛЯРНЫЕ РЕШЕТКИ И НИТИ НАНОЧАСТИЦ МЕТАЛЛОВ В ЦЕОЛИТНЫХ КАНАЛАХ

А. А. Капанадзе, Г. В. Ртвелиашвили, Г. Д. Табатадзе

Грузинский технический университет
Тбилиси, Грузия
skapanadze@gmail.com

Принята 1 мая 2012 года

В последнее время в связи с поисками новых материалов для твердотельной электроники была создана и исследована целая группа объектов, которые отличаются от свойств массивных тел за счет увеличения роли поверхности. Такими объектами, в частности, являются несмачивающие жидкие металлы, внедренные в полости цеолитов типа NaX, NaA и NaM. Цеолиты типа NaX и NaA представляют собой алюминосиликаты каркасной структуры, в которых в трех направлениях имеются строго одинаковые и регулярные полости, размеры которых 11.4 – 12.0 Å. Введение несмачивающих жидкостей в каналы столь малых размеров должно требовать энергии порядка теплот испарения, т.е. 10 – 100 ккал / гмоль. В пересчете на давление это величина порядка 5 – 50 кбар, т.е. практически весьма реальная.

Введение жидких металлов в каналы цеолита можно наблюдать как по скачку объема системы цеолит–металл, так и по скачку проводимости цеолитной прессовки, находящейся в контакте с жидким металлом [1 – 4]. При критическом давлении жидкие металлы проникают в полости цеолитов и образуют регулярные решетки, повторяющие конфигурацию каналов и полостей цеолитной матрицы – в случае цеолита NaA кубическую, а в случае цеолита NaX – структуру типа алмаза. Оценки скачка объема показывают, что в каждой полости находится 15 – 20 атомов. В результате заполнения жидким металлом полостей цеолитной матрицы кристаллы цеолита, каркас которого является хорошим диэлектриком типа кварца, приобретает металлическую проводимость, что указывает на достаточно сильное взаимодействие между кластерами. Изучение температурной зависимости галлия и ртути в цеолитах показала, что на 80 – 100 ° ниже точек плавления массивного металла под давлением наблюдаются скачки проводимости, которые можно приписать отвердеванию и плавлению цеолитного металла. Если снять внешнее давление, проводимость исчезает. При этом часть металла уходит из полостей. Данные по плотности свидетельствуют, что число атомов в полости сокращается до 10 – 15, что, по-видимому, приводит к ослаблению взаимодействия между кластерами и исчезновению металлического состояния. Рентгеновский анализ показал, что в каркасе цеолита возникают напряжения, которые исчезают, если металл из полости удалить. Структура цеолита сохраняется, но наблюдать капельные решетки не удалось. Однако и в такой диэлектрической системе кластеров, зафиксированной в пространстве полостями каркаса цеолитов, наблюдаются острые пики теплоемкости при температурах, соответствующих плавлению цеолитного металла. По мере уменьшения содержания металла этот пик закономерно уменьшается по величине и сдвигается в низкотемпературную область, что указывает на равномерность распределения металла в полостях цеолита. В точке плавления резко изменяется также магнитная проницаемость диэлектрической системы металлических кластеров [5]. В частности, в кластерах Hg_{13}, магнитным полем свыше 25 кЭ в

точке плавления возбуждается новое сильно намагниченное состояние, что указывает на то, что кластеры можно рассматривать как квазиатомы, заполнение уровней которых осуществляется в соответствии со спектроскопическими правилами.

Следует отметить, что расположение атомов металла в сферической полости цеолитов существенно отличается от их расположения в кристаллическом массиве. Однако, резкость переходов в точках плавления и отвердевания указывает на то, что во всех полостях число атомов в кластере, а также их конфигурация одинакова и определяется строгой одинаковостью полостей цеолита. Однако, не ясно, в чем состоит плавление таких капель – кластеров, фиксированных в полостях матрицы, и как это отражается на проводимости.

Известно, что фазовый переход в отдельном кластере, состоящем из 10 – 20 атомов металла, должен быть сильно размыт флуктуациями. Экспериментально обнаруженные фазовые переходы носят резкий характер, и можно утверждать, что флуктуационное уширение, естественное для малых частиц, в данном случае подавлено взаимодействием кластеров друг с другом либо непосредственно (кластерные металлы при $P > P_{кр}$), либо через диэлектрическую матрицу (кластерные диэлектрики при $P < P_{кр}$) и высокой степенью упорядочения системы. Проявление коллективных свойств в процессе фазового перехода указывает на то, что металл в цеолите можно рассматривать, как кристалл, образованный диэлектрической матрицей цеолита. Число кластеров в кристалле $5 \cdot 10^{20}$ см$^{-3}$, период и правильность его решетки определяются диэлектрической матрицей. Поэтому в зависимости от наполнителя и типа использованного цеолита, как диэлектрической матрицы, можно получить разные по свойству трехмерные сверхрешетки – кластерные металлы или диэлектрики на основе веществ в ультрамелкодисперсном состоянии.

Для создания одномерных металлических нитей путем вдавливания металла в диэлектрическую матрицу идеальным являются структуры типа морденита, в которых каналы имеют размеры, допускающие проникновение металла в виде одноатомных цепочек, располагающихся достаточно близко друг к другу так, чтобы между ними могло существовать взаимодействие. В таких системах взаимодействие атомов металла с диэлектрической матрицей будет, вероятно, достяточно слабым, обеспечивая требуемую квазиодномерность. Роль физического контакта с матрицей сводится лишь к стабилизации металлических нитей в пространстве. Синтетический цеолит Na–морденит (NaM) по своей структуре соответствует этим требованиям. В его каркасе отсутствуют пустоты «больших» диаметров, имеются лишь пересекающиеся каналы диаметром 6.6 и 2.8 Å. Поэтому этот цеолит можно считать обладающим практически одномерной системой каналов. Опыт показал, что критические давления, при которых происходит проникновение металлов ртути и висмута в каналы цеолита NaM, соответственно равны 29 и 20 кбар, величины скачка объема соответственно равны 3.6 и 6.0 %. После снятия внешнего давления ртуть, введенная в каналы цеолита NaM, по-видимому, полностью вытекает наружу, на что указывает измерение плотности данных материалов.

Ссылки

1. В. Н. Богомолов. ФТТ, 1971, 3, 815.
2. В. Н. Богомолов, Т. И. Волконская, А. И. Задорожний, А. А. Капанадзе. ФТТ, 1975, 3, 1707.
3. В. Н. Богомолов, А. И. Задорожний, А. А. Капанадзе, З. Л. Луценко. ФТТ, 1976, 18, 3050.
4. В. Н. Богомолов, А. А. Капанадзе. ФТТ, 1978, 20, 104.
5. В. Н. Богомолов, А. И. Задорожний, С. А. Панина. Письма в ЖЭТФ, 1980, 31, 371.

INVESTIGATION OF ACOUSTIC EMISSION ACCOMPANYING STICK-SLIP MOVEMENT OF ROCK SAMPLES AT DIFFERENT STIFFNESSES OF SPRING–BLOCK SYSTEM

T. Matcharashvili, T. Chelidze, N. Zhukova, A. Sborshchikovi

M. Nodia Institute of Geophysics
Tbilisi, Georgia
matcharashvili@gtu.ge
rossoneri08@yandrex.ru

Accepted May 31, 2012

1. Introduction

We observe the phenomenon of friction, or frictional resistance, in multitude of natural and mechanical systems, ranging, e.g. from earthquake faults to micro-electromechanical devices wherever two surfaces move against each other. Being always in the focus of scientific interest since the work of Amonton and Coulomb, significant advances have been made in the understanding of the mechanisms of friction especially in the last decades. It was established that friction could not be considered as an intrinsic material property and that depending on internal and external conditions (e.g. sliding rate, cumulative slip, roughness and other features of contact area, contact time, normal stress, spring stiffness, presence of gouge, fluids, environmental conditions, etc.) different static and dynamic regimes in frictional system may occur [1 – 8]. At the same time there are still many unanswered questions. These questions mostly are addressed to the statistical and dynamical aspects of behavior of frictional systems in general, as well as to its dependence on sliding conditions and properties of contacting materials.

From experimental studies of frictional movement between rock surfaces it is known that when the static friction resistance is overcome, two main modes of sliding regime can be observed. In the first mode, depending on system's conditions (such as velocity of movement, roughness, contact time of surfaces, stiffness, etc.) the two surfaces may slip steadily at a relative velocity equal to the load point velocity [9 – 11]. This sliding mode was referred as a stable sliding in the past [9, 12] or steady-state sliding [13 – 16] in more recent terminology, and it is considered as an analog of fault creep in geophysics. Change of one or several characteristics of system's conditions will result in the appearance of the second mode, when the frictional surfaces suddenly slip, lock and then slip again in a repetitive manner. This cyclic unstable transition from the static friction to kinetic one is known as a stick-slip. In geophysics this stick-slip movement mode is considered as a proxy of the earthquake occurrence along a preexisting crustal fault [17, 18 – 21].

In opposite to the stable sliding, at stick-slip movement the sliding velocity on the surface can be significantly higher or lower than the velocity of load point; in other words, the dynamics of load point and moving object is different. This means that stick-slip inherently comprises multitude of different dynamical regimes. Moreover, it is clear that the lower is the

velocity of load point (i.e. the force applied to a driving object increases slowly), the more complicated will be the observed movement regime(s). This is why the low velocity regime often is characterized as an "irregular" and "chaotic" stick-slip motion.

Thus being abundant in different systems ranging from seismology, basal ice flow and biology to microelectronic devices, the exact character of stick-slip movement may be qualitatively and quantitatively very different depending on the frictional system's conditions [1, 22 – 25].

In the past this problem of dynamical regimes of unstable stick-slip movement under different conditions of frictional system always has been the subject of intense scientific studies. Generally, this process is well described in the framework of large-scale molecular dynamics simulations [26 – 30], rate, and state models [10, 31 – 34] or the so-called minimalistic phenomenological models [7, 35 – 37]. At the same time, revelation of features of dynamical behavior of system at stick-slip movement, as well as the disclosure of the character of its dependence on sliding system's conditions, still remains a fundamental physical problem of prime practical importance [7, 8, 10, 11, 38].

Among others the influence of stiffness in frictional system on the movement regime during stick-slip process calls to be investigated in detail. Results of few studies known to us for tackling this problem convince that [1, 39] special attention should be paid to the analysis of statistical and dynamical characteristics of transitional regimes between stick-slip and sliding and vice versa.

Importance of such analysis is caused by the mentioned above ubiquity of irregular stick-slip behavior in nature and technique, as well as by the lack of knowledge of systems behavior at different conditions and contacting materials [5, 35, 40, 41].

The unique combination of advantages such as low cost, positioning flexibility, simple installation and processing, real time capability, and high sensitivity makes very popular the application of AE technique for different technical and scientific purposes [42, 43]. For example the distribution of noise amplitudes accompanying crack generation has been investigated for several materials such as concrete, paper, wood, glass, etc. [44 – 46]. Experiments also show that AE is much more efficient in revealing micro-scale fracture processes in real time than traditional strain measurements, which are only sensitive to large enough bulk deformations [47], namely, AE confirms nucleation of cracks in solids in the low stress (Hook) domain, where stress–strain dependence is practically linear.

Taking into consideration close cause-effect relationship between stick slip and AE, in the present research we aimed to investigate characteristics of acoustic emission at different movement conditions exactly, in this work we represent results of statistical and dynamical analysis of AE, accompanying stick slip of basalt samples, as well as the influence of spring stiffness on its characteristics.

2. Materials and methods

In this work AE, as a signature of elastic waves that appear during stick-slip experiments in a frictional pair composed of two basalt samples, has been registered and analyzed. AE was recorded by specially developed laboratory setup. Commonly, experimental base to investigate stick-slip process is presented by the physical model consisting of spring-slider systems (see, e.g. [8]). Use of such spring–block experimental devices is one of the most popular laboratory

approaches widely applied in different fields of science to investigate friction processes (e.g. [18, 38, 39, 48]). This is caused by the fact that the laboratory stick-slip experiments enable us to easily model different regimes of friction movements through variation of surface roughness, velocity of movement, spring stiffness, normal force, etc.

Description of main principles of our stick-slip AE experimental setup is presented in Chelidze et al. [49]. Our laboratory setup consists of supporting (fixed) and sliding plates of roughly finished basalt samples: the sliding and fixed blocks' length, width and thickness were accordingly sliding – 10, 10 and 2; fixed – 25, 10 and 2 cm. The load point or "free end" of the spring, attached by the other end to sliding block, is driven with a constant velocity V_d ¼ 2.9 mm / s. Numerous experiments have been carried out for eight different values of stiffness of pulling spring *Ks*.

Thus eight different regimes of stick-slip movement have been investigated. The resulting friction force *F* is proportional to the deflection of the spring.

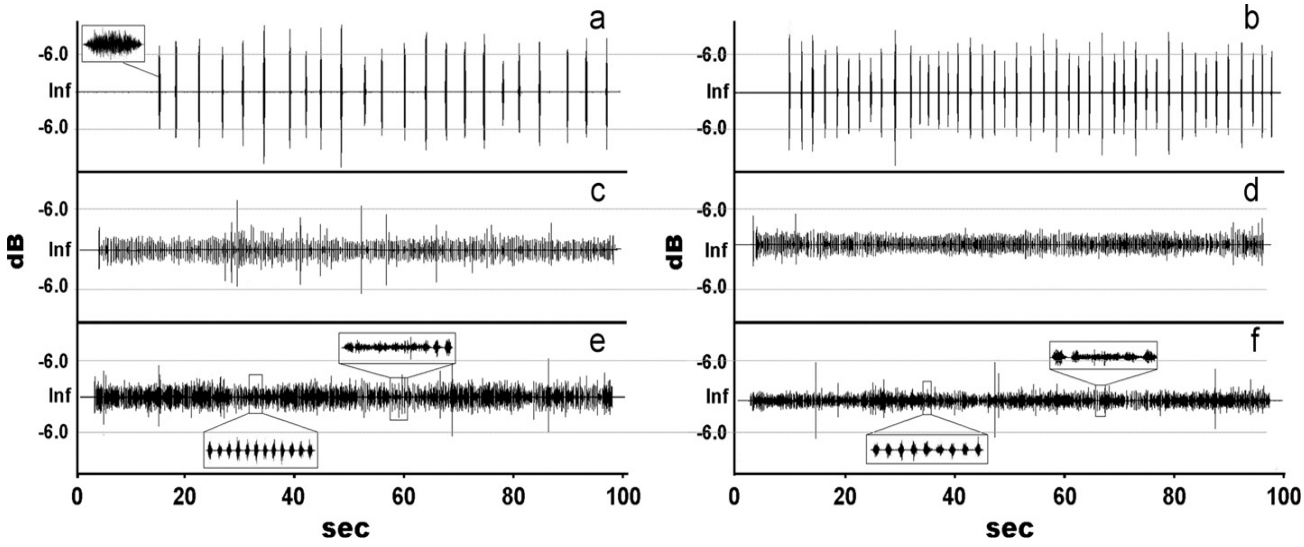

Figure 1. Typical examples of AE recordings at different values of dragging spring stiffness: (a) K ¼ 78.4, (b) K ¼ 143.1, (c) K ¼ 1068, (d) K ¼ 1705, (e) K ¼ 2000 and (f) K ¼ 2371.6 N / m. Insets show AE wave train on extended time scales.

First four of these regimes were named as soft, next one as medium and last three as stiff spring movement conditions. The AE accompanying the consecutive slip events of stick-slip process was amplified and then recorded on a PC sound card. The sensor for the AE was a lead circonate–titanate unit with a natural frequency of a piezoelectric crystal 100 KHz. At lower frequencies (from several Hz to 20 KHz) the response of crystal is much weaker, but still measurable and almost constant. This weak LF signal was amplified by a special standard broadband amplifier, with practically flat amplitude–frequency characteristic (deviation of the order of 0.1 db) in the range several Hz to 20 KHz. Thus, though the maximal sensitivity of sensor was at 100 KHz, amplification allows recording of AE signals at frequencies down to dozens of Hz without very strong distortion. Typical examples of AE recordings at different values of dragging spring stiffness are presented in **Fig. 1**. For each value of pulling spring stiffness (*Ks*), ten runs of AE experiments have been carried out. In order to ensure comparable standard roughness and avoid ageing effects of contacting surfaces [14], sliding surfaces were

carefully sanded up by sandpaper (with grade 150) before each experimental run. Grinding was carried out uniformly in all directions in order to ensure isotropic morphology of contacting surfaces and thus avoid appearance of privileged directions of sliding. After this in order to diminish influence of dust and gouge on the movement regime sliding surfaces of samples were cleaned by a vacuum cleaner. Though exact reproduction of surface characteristics in stick-slip experiments is practically impossible, these procedures help to maintain general reproducibility of experimental conditions and stationarity of measured data sets.

When recording of accompanying stick-slip acoustic emission has been accomplished we proceeded to the compilation of characteristic AE data series. This procedure consisted of several steps. The first step we have done was eliminating background noise in recorded wave trains. Knowing that in general filtering procedures may lead to distortion of dynamical structure of analyzed process [50, 51], we simply used background noise level between consecutive AE bursts as a threshold value. Exactly, by the step size equal to counting one, we moved different length sliding windows through our AE recording. When the standard deviation of data confined in the sliding window was less than the mean value of background noise, we equaled to zero just the first reading in the sliding window, etc. By moving the window through the whole wave train we separated consecutive AE waveforms ensuring that signal of interest will not be truncated or dynamically distorted. Then, for each AE burst, the start and end time of the waveform (wave packet) has been defined as the first and the last data above noise (zero) level.

Afterwards different AE characteristic data sets have been compiled from these wave train series, for example sequences of start and termination times of consecutive AE bursts, time intervals between consecutive AE bursts (waiting times), duration of consecutive waveforms and location of AE maximum in wave-forms, max amplitude of AE in a waveform (commonly named as amplitude of waveform), etc. We can mention here that the amplitude of AE is a very important characteristic of acoustic emission determining the detectability of the signal. Further data sets of energy of consecutive AE waveforms have been compiled by calculation of a sum of squared amplitudes in each waveform or acoustic burst. Time series of AE power also have been compiled by dividing calculated energy values to waveform's duration.

When compilation of AE characteristic data sets has been accomplished we proceeded to their statistical, linear, scaling, and nonlinear analyses. Exactly, besides common statistical and linear data analysis tests [51 – 53] we used modern data analysis tools such as detrended fluctuation analysis (DFA) and recurrence quantitative analysis (RQA) methods, which already have been many times used for different kinds of measured and model data sets [54 – 57]. Namely, in order to quantify the extent of intrinsic self-similarity embedded in an analyzed nonstationary time series we used DFA method. Nonlinear dynamical structure of AE data sets recorded at stick-slip process has been evaluated by RQA, which is sensitive and effective even for relatively short time series [56 – 60].

3. Results and discussion

Comprehensive awareness of the factors that influence friction (such as applied normal force, velocity, stiffness, surface roughness, etc.) and especially the analysis of the character of such influences is essential both from scientific and practical points of view.

Thus, in order to investigate influence of one of such factors, namely stiffness on the character of friction movement in this experimental research we have changed only spring stiffness, keeping constant other factors such as the load point velocity, weight of sample, normal force, surface roughness, environmental conditions, etc.

At the first glance, the increase of spring stiffness in our frictional laboratory system seems to lead to both qualitative and quantitative changes in the stick-slip movement (see **Fig. 1**). These are revealed in visible changes of features of AE waveforms and statistics of their appearance. Exactly, the number of AE bursts straightly increases (see also **Fig. 2**), while waveform amplitudes markedly decrease and consecutive wave trains become partly merged (see upper insets in **Fig. 1e** and **f**). This looks quite logical as far as according to previous results (e.g. [14]), increase of spring stiffness should lead to the transition from stick-slip to smooth movement (continuous sliding) regime, i.e. supposedly to the complete merging of waveforms constituting AE wave trains.

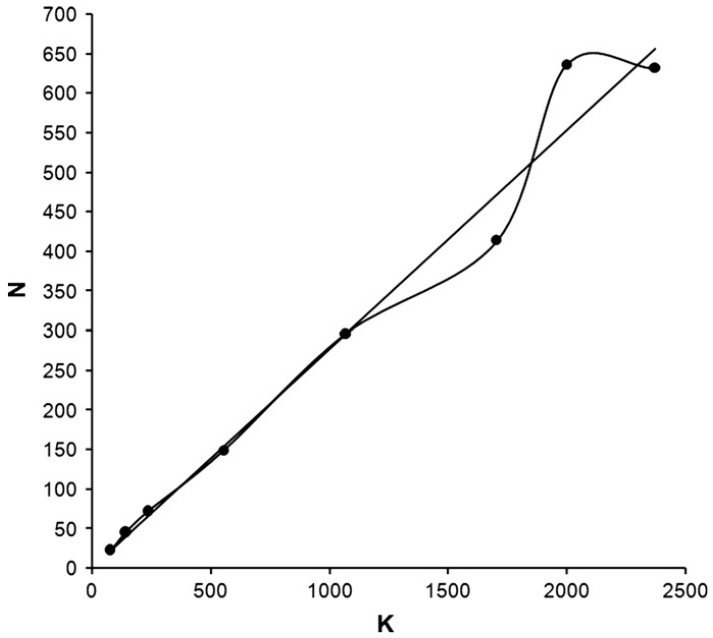

Figure 2. Mean number of stick-slip AE bursts in experimental runs vs. spring stiffness.

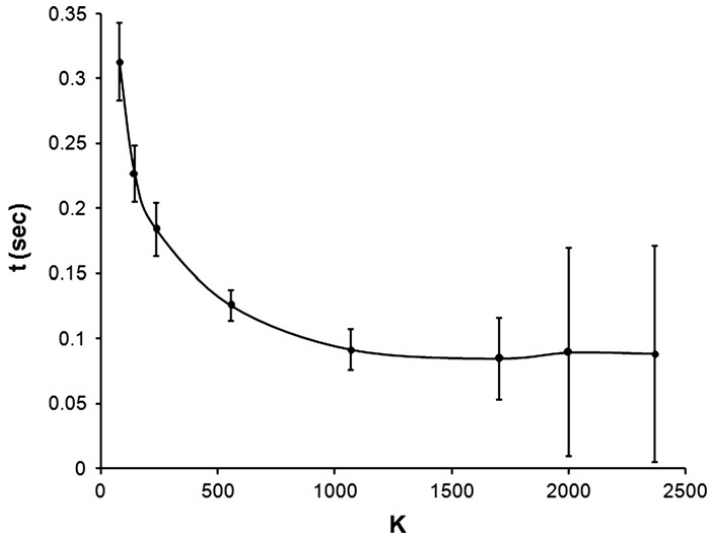

Figure 3. Duration of stick-slip AE bursts at different spring stiffness values.

At the same time, when the spring stiffness gradually rises (up to 30 times from K_1 ¼ 78 to K_8 ¼ 2370 N / m), together with overwhelming amount of merged ones, well separated individual AE waveforms in wave trains remain clearly visible. Also, though number of AE bursts increases almost linearly with stiffness (**Fig. 2**), the main statistical characteristics of acoustic emission process are subject to more complicated changes. Exactly, calcu- lated for each *Ks*, mean values of AE waveforms duration times (**Fig. 3**) tend to decrease, though for the stronger springs this decrease is hardly significant, statistically comparing to the softer ones. At the same time waiting time intervals between consecutive AE bursts (**Fig. 4**) clearly decrease exponentially when the driving spring stiffness increases. These differences in statistics of waveforms duration and waiting times could be caused by the mentioned coexistence of long (merged) and short single wave- forms in these regimes.

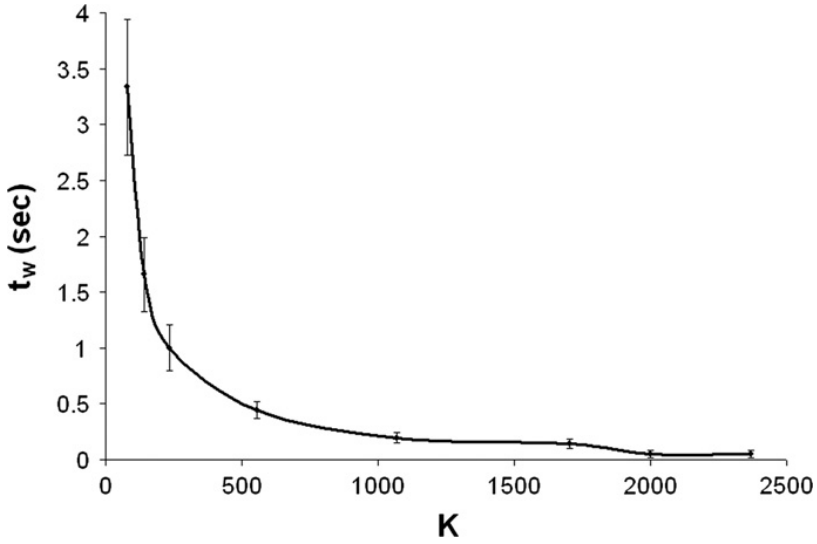

Figure 4. Variation of waiting times' sequences between stick-slip AE bursts with stiffness *K*.

This in turn will lead to the strongly increased deviation from the calculated mean waveforms duration times and will affect significance of the corresponding statistics. On the other hand, clear decrease in waiting times also indicates merging tendencies in waveform generation for stiffer springs. Strong exponential decrease was observed also for amplitudes of emitted AE waves for stiff springs, which causes exponential decay of the amount of emitted AE energy (not shown here).

Further, changes were observed for the cumulative amount of emitted acoustic energy, which for the stiffer springs decreases three times compared to soft ones, though the number of AE bursts increases with *Ks*. This result, which seems logically taking into account decreased amplitudes of AE at increased stiffness, may look not quite clear in the light of essential rise in the number of AE events at the stiffest springs (see **Figs. 1** and **2**). The only reliable explanation of this is the assumption that the smallest AE amplitudes prevail in movement regimes at the stiffest springs used in our experiments.

The frequency content was complicated and dependent on the waveforms location in the wave train. Seemingly, the wearing of contacting surfaces, changes in samples and ambient temperature, appearance of dust after breaking of contact asperities, etc. affect this process. Thus, thousands of AE waveforms in our experiments need to be carefully investigated in future

in relation to all or at least part of these mentioned factors. This work is in progress and not yet fulfilled. At the moment for preliminary consideration purposes we just assessed dominant frequencies registered in waveforms, which are located approximately in the middle of recorded AE time series. By that we keep more or less comparable conditions for different Ks values. This preliminary analysis shows the shift of prominent spectral peaks to higher frequencies (from about 1900 to 2400 Hz) at increased stiffness, which may point to quantitative changes in the frequency content of AE with the increase in spring stiffness. Unfortunately, at the moment we cannot further discuss AE waveform frequency content issue here and should resume that the considerable future work in this area is necessary for testing both frequency content and relation between characteristics of AE source and individual AE events (see, e.g. Mair et al. [61 – 62]). At the same time, though quantitative changes in AE frequency content remain still unclear, we can speak about clear qualitative changes in acoustic wave generation, mostly in the shape of waveforms. Indeed, in our experiments, for softer springs the shapes of detected AE waveforms were similar and almost identical, in good accordance with earlier results [63 – 65]. Contrary to this, for stronger springs, the shape of AE waveforms recorded in the same experimental run became noticeably dissimilar and significant merging of elastic waves of consecutive waveforms took place (see upper insets in **Fig. 1e** and **f**). First a sporadic merging of waveforms was observed for strong spring with a stiffness value K ¼ 1705 N / m, which is close to medium stiffness spring (see Section 2). At stiffer springs from several tens to hundreds of such prolonged (merged) waveforms were found among several hundreds of detected total AE bursts.

It should be stressed that in our experiments we have not observed complete merging of consecutive AE waveforms. Even for the stiffest used spring (K ¼ 2300 N / m) the discrete character of AE wave train is mostly preserved (see lower insets in **Fig. 1f**). Thus the complete transition to smooth sliding regime does not take place, and we observed sliding condition sometimes named as episodic stable sliding [14], comprising intermittent stick-slip and sliding movements during one experimental run.

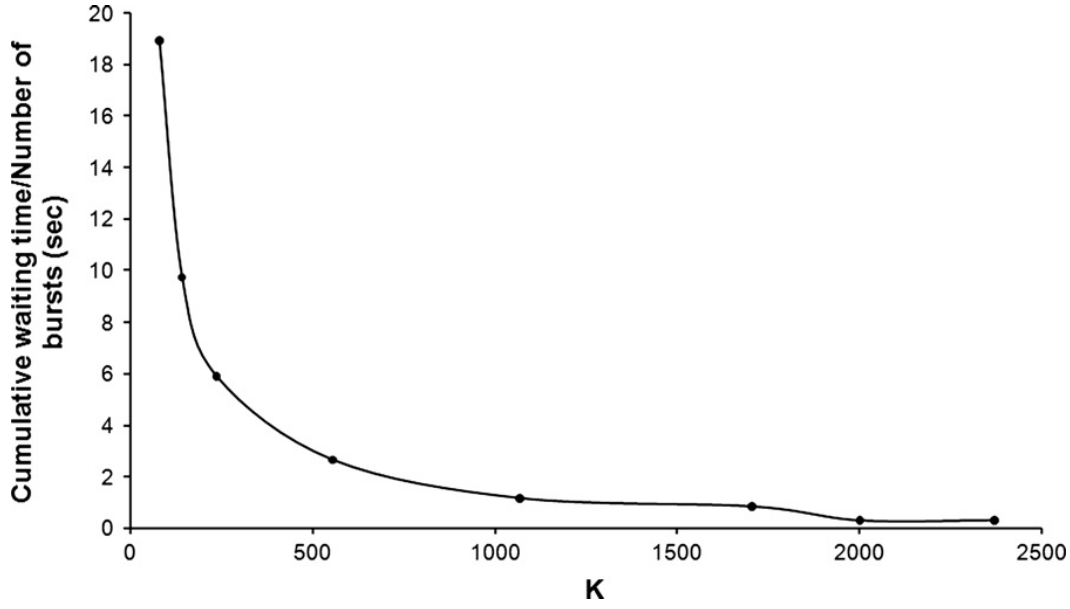

Figure 5. Normalized to the number of AE bursts integral waiting time vs. spring stiffness K.

It looks from the above stick-slip generated AE time domain statistics that at stiffer springs slip event time evolution is more irregular. To this points the increased scatter in data sets of duration times of observed AE waveforms (**Fig. 3**), coefficient of variation increases almost ten times with spring stiffness increase (not shown here). At the same time, the coefficient of variation of waiting times' sequences between consecutive AE bursts does not change much (see e.g. **Figs. 4** and **5**).

Because AE is associated with the failure of the asperities of contacting surfaces during stick-slip process, it is obvious that all described stiffness-related changes in AE, including ones in time domain, should be caused by inherent properties of stick-slip movement. Therefore, changes in the statistics of AE time evolution could be explained by increased instability of movement in case of stiff springs, which looks logical, because in this case sequences of similar (separate) waveforms are alternated by merged long AE bursts. So if we neglect possible appearance of qualitative transitions in the dynamics of stick-slip process with the rise in spring stiffness, the regimes closer to "stable sliding" should be considered as more "random like" from statistical point of view comparing to movement regimes at softer springs.

In order to elucidate dynamical aspects of transitional stick-slip movement regime we used data set of max amplitudes in consecutive waveforms of AE. As it was mentioned in Section 2, max amplitudes accompanying stick-slip motion are assumed as the most important characteristic of acoustic wave generation. Therefore, assessment of their distribution characteristics may provide valuable information on the stick-slip motion features. Indeed, the amplitude of the waves and thus the amount of energy released by acoustic emission are in turn closely related to the magnitude and velocity of the source event(s), as well as to the area of contacting surfaces and the amount of broken asperities. In this regard it should be mentioned that though the only phenomenon that is recognized as responsible for AE generation in stick-slip process is the slip (e.g. [15, 65]), the question about relation of separate AE waveforms, or its parts (e.g. AE maximums), to the different stages of stick-slip movement is not answered finally at present [65 – 67]. Among other causes hampering solution of this problem there are serious technical difficulties encountered when measuring real contac area, high sampling rates necessary for recording fast oscillatory movements, etc.

Logically, being dependent on many uncontrollable factors, the process of pre-sliding "wobbling" could bring uncertainty in the movement regime assessment. From the wave trains shown in **Fig. 1** and the results presented in **Fig. 6**, the distribution of AE maximums (which we assume marks the onset of slip) indeed looks more regular at softer springs than for stronger ones, when merging of bursts and episodic stable sliding occurs. Increase of coefficient of variation of measured values of max AE amplitudes also can be considered as a statistical signature of increased instability (or intermittency) of AE pattern at stiffer springs (**Fig. 6**).

As a next step in max AE amplitudes analysis we also examine their distribution features in two ways. Exactly, distribution of AE maximums was assessed in bins of duration time of each waveform, not with standing their different length. This enables to look whether distribution characteristics of max AE amplitudes in waveforms depend on stiffness of spring. As it follows from **Figs. 6** and **7**, the largest amplitudes of AE are closer to the onsets of waveforms at stiffer springs. We consider this as an indication that the sliding starts earlier for stiffer springs because in this case the time of "wobbling" is shorter due to the faster increase of imposed pulling force. Next, we see that the character of max AE amplitudes distribution is changed when stiffness increases. Generally in our AE experiments, we never observe clear

regularity in features of max AE amplitude appearance inside of waveforms. Character of observed distributions always is complicated and there is no clearly pronounced privileged location of AE maximums in waveforms. At the same time, distributions of max AE in waveforms differ by their shapes at different movement regimes, when dragging spring stiffness increases. These changes in shapes of distributions may point to the qualitative changes in the structure of acoustic waveforms. Revealed changes in AE values of Dt_{max}). Similar to features of distribution of max AE amplitudes in waveforms, temporal distribution of max AE amplitudes (Dt_{max} data) is also better described by normal distribution, when stiffness is small, but at stronger springs it is better fitted by long tailed distributions. Thus in case of the distribution of time intervals between AE maximums (or simply max AE temporal distribution) we also observe the shift to long tailed distributions. Hence, we may guess the increase of long range correlated features and appearance of nonlinear structure in the temporal evolution of stick-slip AE at increased stiffness. This can be interpreted as reflection of the increased extent of regularity in the dynamics of AE emission at stiffer springs. All these changes in distribution characteristics of max AE amplitudes, both in waveforms and time, signify the appearance of nonlinear intermittent effects in the stick-slip movement regimes at increased stiffness.

Thus, based on the above results and considerations we can't exclude appearance of qualitative changes not only in the shapes of waveforms and its amplitude contents but also in the temporal distribution of stick slip generated AE (or in the dynamics of AE generation), when the stiffness of frictional system increases.

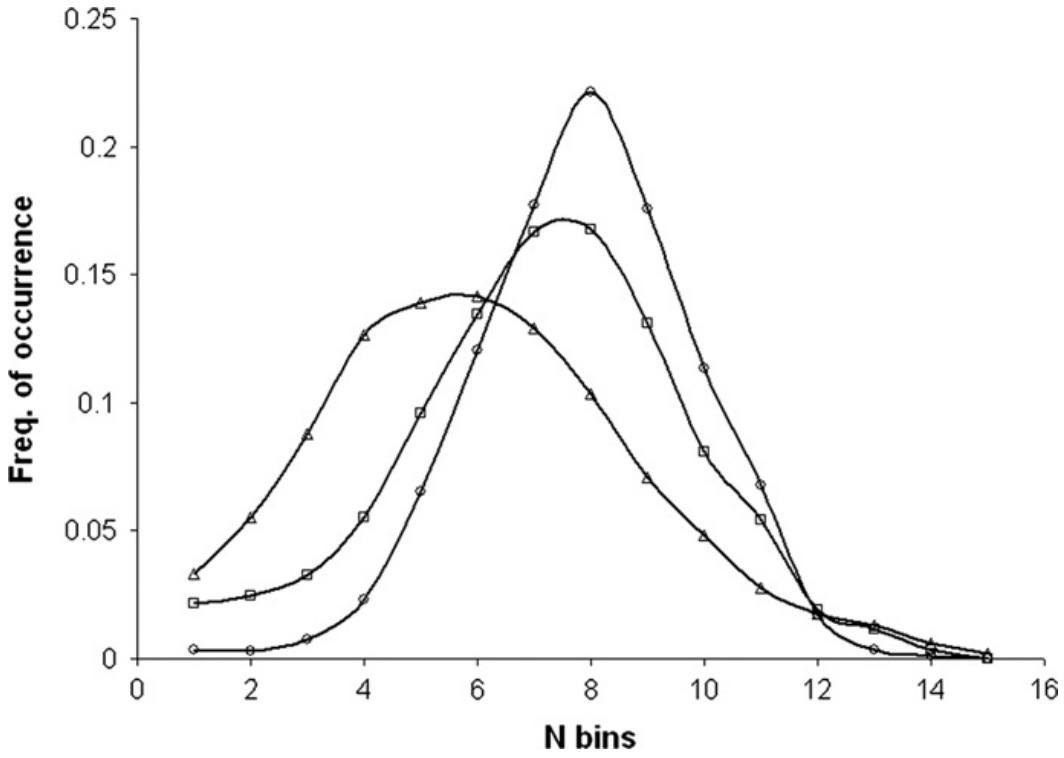

Figure 6. Location of max AE amplitudes in corresponding wave trains at different spring stiffnesses. Frequency of occurrence of max AE amplitudes in 15 bins of each train was calculated. Circles – avg. for soft springs (78.4, 143.1, 235.2, 555 N / m), squares – medium spring (1068 N / m), and triangles – avg. for stiff springs (1705, 1999.2, 2371.6 N / m).

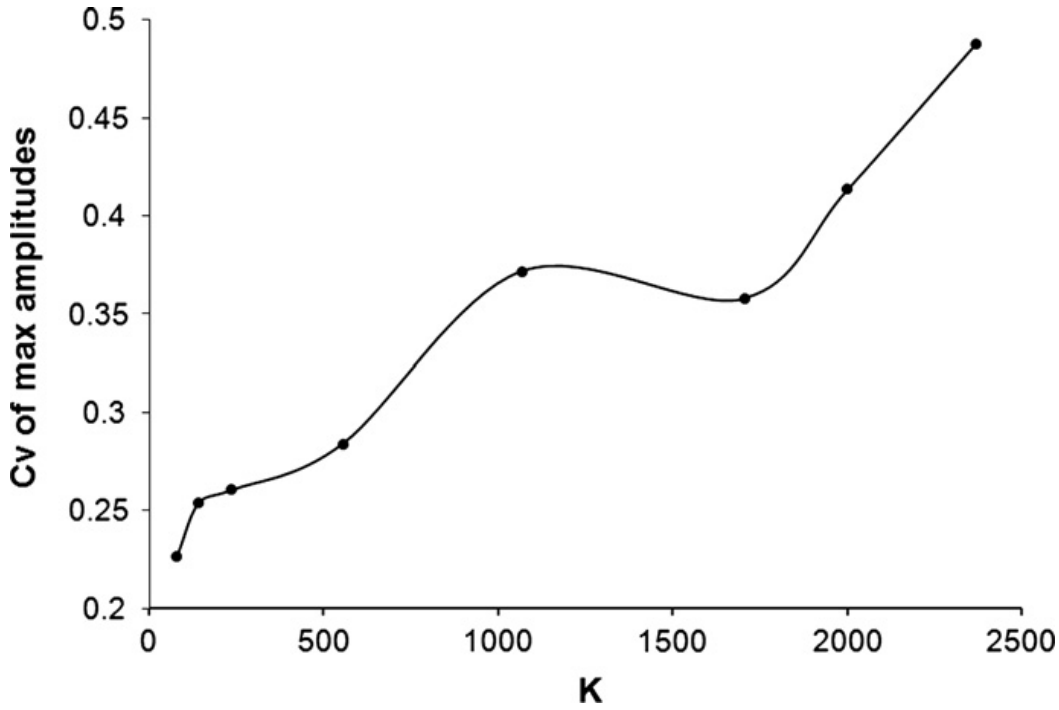

Figure 7. Coefficient of variation of mean max amplitudes of stick-slip AE bursts vs. stiffness of spring.

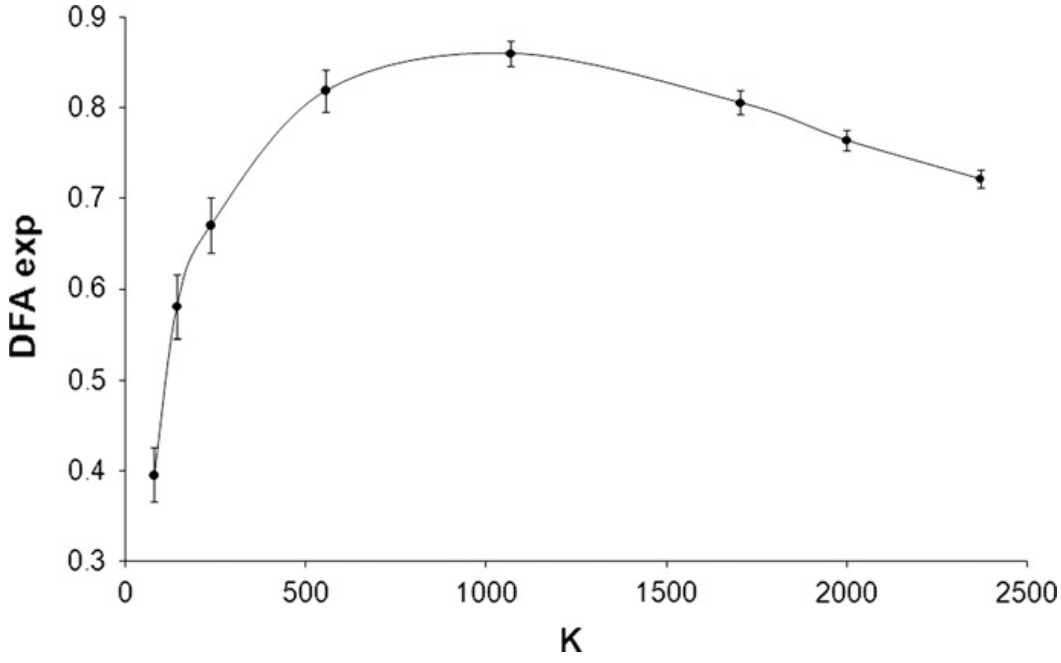

Figure 8. DFA exponent calculated for waiting times' sequences for different spring stiffness values *K*.

Further, in order to test our suggestions about dynamical changes in stick-slip process at different spring stiffnesses we proceeded to the self-similar and nonlinear properties analysis of temporal distribution of AE bursts. Exact sequences of waiting time intervals (Dt_w) between consecutive waveforms were analyzed. As we see in **Fig. 8** stick-slip process at different spring stiffness values indeed reveals different extent of self-similarity calculated by DFA. DFA exponent a varies in the range from about 0.4 up to 0.9. In other words, for softer spring we observe antipersistent, close to random walk process (antipersistent process exhibits negative long range correlations a 0 0.5), while for larger stiffness values the time distribution of AE bursts becomes increasingly persistent. Processes with such DFA exponents represent the long range correlated process close to $1/f$ type noise (a 4 0.5). Thus we conclude that scaling features of AE time distribution is changing depending on the spring stiffness. It is important to mention that in this case, we observe differences between temporal features of AE waveforms distribution for spring stiffness values, which we consider as belonged to the same movement regime groups (see Section 2). For instance for soft spring group, at Ks ¼ 78.4 N / m, the Dt_w variation looks antipersistent, at Ks ¼ 143.1 N / m it is close to persistence threshold, while at Ks ¼ 235.2 N / m and Ks ¼ 555 N / m time evolution becomes clearly persistent. Also it was observed that at the largest used stiffness values DFA exponents tend to decrease. Such result possibly points that stiffness related transition mechanism between different movement regimes may have specific fine structure that needs to be more carefully investigated in future. At this time, in the frame of present investigation, the most important result is that measurable quantitative differences have been detected in self-similar properties of stick-slip generated AE patterns depending on the spring stiffness variation. These changes point to changed internal nonlinear characteristics of stick-slip AE pattern at different movement regimes.

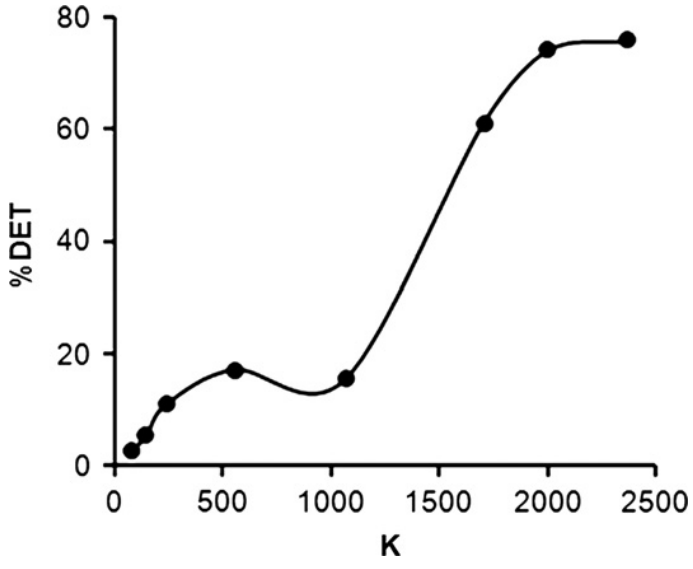

Figure 9. RQA % DET variable calculated for waiting times' sequences for different spring stiffness values K.

Lastly, to quantify changes in dynamics of AE time distribution we used RQA method aimed at testing of recurrence properties of investigated process based on analysis of line segments in symmetrical recurrence plots, which in turn are obtained from phase spaces reconstructed from the measured data sets [54, 56, 57]. RQA method provides valuable

information on the systems dynamical properties because recurrence in phase space is the hallmark of regular behavior. Analysis procedure is easy enough but needs careful selection of the number of parameters necessary for extracting reliable quantitative features from recurrence phase space plots [56, 57]. In practice quantifications of recurrence properties are provided through calculated recurrence variables [56, 57]. We present here results on one of such recurrence variable, namely, the percent of determinism (% DET), which measures the proportion of recurrent points forming diagonal line structures of recurrence plot. As it follows from the results presented in **Fig. 9**, % DET of our Dt_w data sets reveals quantitative changes in recurrence characteristics of waiting times evolution at different stiffnesses. This result together with similar results of other RQA variables (e.g. % REC and % LAM, not shown here) reveals quantitative changes in dynamics of temporal distribution of stick-slip generated AE according to movement regime variation. Here, as in the case of DFA analysis, we observe the fine structure of dynamical changes in stick-slip AE process at increased stiffness of dragging spring, which was not possible to detect by statistical analysis.

Thus, contrary to the visual inspection of AE wave trains and statistical observations presented above, we should conclude that at increased stiffness of springs both qualitative and quantitative changes in accompanying instable stick-slip process AE emission may occur. Finally these changes result in the clear increase of the extent of order in time distribution of AE bursts in ''stiff regime''. Thus dependence of extent of order in the dynamics of stick-slip process on system's conditions was experimentally confirmed.

4. Summary

Numerous experimental data on acoustic emission that appears during stick-slip experiments in a frictional pair composed of two basalt samples has been registered and analyzed. It follows from our analysis that change in the stiffness in frictional system invokes qualitative and quantitative differences both in AE waveforms and in statistics and dynamics of AE bursts distributions. Dynamical regime of stick-slip process is not unique and depends on stiffness of frictional system. The extent of order in time distribution of stick-slip AE bursts increases at stiffer springs. Thus, instable stick-slip process comprises multitude of patterns of behavior with different quantitative and qualitative characteristics.

Acknowledgements

The authors express their gratitude to the Georgian National Science Foundation (Grant No. GNSF / ST 06 / 5 – 028) and INTAS foundation (Ref. No. 05 – 100008 – 7889) for financial support.

References

1. F. Heslot, T. Baumberger, B. Perrin. Creep, stick-slip, and dry-friction dynamics: experiments and a heuristic model. Phys. Rev. E, 1994, 49, 4973-4988.
2. T. Baumberger, C. Caroli, B. Perrin, O. Ronsin. Nonlinear analysis of the stick-slip bifurcation in the creep-controlled regime of dry friction. Phys. Rev. E, 1995, 51 (5), 4005-4010.
3. B. N. J. Persson. Sliding friction. 1998, Springer.
4. A. L. Demirel, S. Granick. Phys. Rev. Lett., 1996, 77, 4330.
5. Y. Braiman, J. Barhen, V. Protopopescu. Phys. Rev. Lett., 2003, 90, 094301.
6. H. Czichos, T. Saito, L. Smith. Springer Handbook of Materials Measurement Methods. 2006, Springer.
7. M. Urbakh, J. Klafter, D. Gourdon, J. Israelachvili. Nature, 2004, 430, 525-528.
8. J. H. Dietrich. Applications of Rate and State Dependent Friction to Models of Fault Slip and Earthquake Occurrence. Earthquake Seismology, 4 (Ed. in Chief G. Schubert), 2009, Elsevier, 1124-1140.
9. Y. Gu, T. F. Wong. The transition from stable sliding to cyclic stick-slip: Effect of cumulative slip and load point velocity on the nonlinear dynamical behavior in three rock-gouge systems. Proc. 33th U.S. Symp. Rock Mechanics (USRMS), 1992, Santa Fe., 151-166.
10. B. N. J. Persson. Sliding Friction, Physical Properties and Applications. 2000, Berlin: Springer.
11. H. Matsukawa, T. Saito. Friction, Stick-Slip Motion and Earthquake. Lecture Notes in Physics, 705. 2007, Berlin: Springer–Verlag, 169-189.
12. J. D. Byerlee, R. Summers. Stable sliding preceding stick-slip on fault surfaces in granite at high pressure. Pure Appl. GeoPhys., 2002, 401, 1450-1466.
13. C. H. Scholz. The Mechanics of Earthquakes and Faulting, 471. 2002, Cambridge – New York – Melbourne: Cambridge Univ. Press.
14. C. Voisin, F. Renard, J. R. Grasso. Long term friction: From stick-slip to stable sliding. GeoPhys. Res. Lett., 2007, 34 (13), 5.
15. C. Voisin, J.-R. Grasso, E. Larose, F. Renard. Evolution of seismic signals and slip patterns along subduction zones: Insights from a friction lab scale experiment. GeoPhys. Res. Lett., 2008, 35, L08302.
16. A. Akay. Acoustics of friction. J. Acoust. Soc. Am., 2002, 111 (4), 1525-1548.
17. W. F. Brace, J. D. Byerlee. Stick-slip as a mechanism for earthquakes. Science (New Ser.), 1966, 153, 3739, 990-999.
18. H. Matsukawa, T. Saito. Friction, Stick-slip motion and earthquake. Lect. Notes Phys., 2007, 705, 169-189.
19. K. Popp, P. Stelter. Stick-slip vibrations and chaos. Phil. Trans. R. Soc. A, 1990, 332, 89-105.
20. M. G. Rozman, M. Urbakh, J. Klafter. The nonlinear nature of friction. EuroPhys. Lett., 1997, 39, 183.
21. A. Martini, Y. Dong, D. Perez, A. F. Voter. Low-speed atomistic simulation of stick-slip friction using parallel replica dynamics. Tribol. Lett., 2009, 36, 63-68.

22. D. B. Bahr, J. B. Rundle. Slip-stick statistical mechanics at the bed of a glacier. GeoPhys. Res. Lett., 1996, 23, 2073-2076.
23. Sh. N. Patek. Spiny lobsters stick and slip to make sound. Nature, 2001, 411,153-154.
24. J. Knight. Glacial sedimentary evidence supporting stick-slip basal ice flow. Quat. Sci. Rev. 2002, 21, 975-983.
25. E. A. Brener, S. V. Malinin, V. I. Marchenko. Fracture and friction: Stick-slip motion. EurPhys. J. E, 2005, 17, 101-113.
26. G. He, M. H. Muser, M. O. Robbins. Adsorbed layers and the origin of static friction. Science,1999, 284, 1650-1652.
27. U. Landman, W. D. Luedtke, E. M. Ringer. Nanotechnologies frictions wear and liubrications at the atomic scale. Fundamentals of Friction: Macroscopic and Microscopic Processes (Eds. I. L. Singer, H. M. Pollock). 1992, Dordrecht: Kluwer, 463-510.
28. M. O. Robbins, M. H. Muser. Conditions for static friction between flat crystalline surfaces. Modern Tribology Handbook (Ed. B. Bhushan), 2001, Boca Raton: CRC Press, 717-757.
29. M. H. Muser, M. Urbakh, M. O. Robbins. The basic of nanoscale friction and ways to control it. Adv. Chem. Phys., 2003, 126, 187-272.
30. J. P. Gao, W. D. Luendtke U. Landman. Friction control in thin-film lubrication. J. Phys. Chem B, 2004,108, 3410-3425.
31. A. Ruina. Rate- and state-dependent friction. J. GeoPhys. Res.,1983, 88, 10359-10370.
32. J. M. Carlson, A. A. Batista. Constitution relation for the friction between lubricated surfaces. Phys. Rev. E, 1996, 53, 4153-4165.
33. M. Urbakh, L. Daikhin, J. Klafter. Velocity profiles and brinkman equation in nanoscale confined liquids. Phys. Rev. E, 1995, 51, 2137-2141.
34. I. S. Aranson, L. S. Tsimring, V. M. Vinokur. Stick-slip friction and nucleation dynamics of ultrathin liquid films. Phys. Rev. B, 2002, 65, 125402.
35. M. G. Rozman, M. Urbakh, J. Klafter. The non-linear nature of friction. Phys. Rev. E, 1996, 54, 6485-6494.
36. M. G. Rozman, M. Urbakh, J. Klafter. Controlling chaotic frictional forces. Physica A, 1998, 249, 184-189.
37. M. H. Muser, L. Wenning, M. O. Robbins. Simple microscopic theory of Amontons's laws for static friction. Phys. Rev. Lett., 2001, 86, 1295-1298.
38. G. Ananthakrishna, R. De. Dynamics of Stick-slip: Some universal and not so universal features. Lect.Notes Phys., 2007, 705, 423-457.
39. T. Baumberger, P. Berthoud. Physical analysis of the state- and rate-dependent friction law. II. Dynamic friction. Phys. Rev. B, 1999, 60, 3928-3939.
40. M. G. Rozman, M. Urbakh, J. Klafter. Inverted stick-slip friction: What is the mechanism? Phys. Rev. Lett., 1996, 77, 683.
41. E. H. Yang, H. Fujita. Reshaping of single crystaline silicon microstrutures for 3D MEMS. Proc. 10th Ann. Int. Workshop Micro Electro Mech. Syst. 1997, New York: IEEE Robotics and Control Division, 67-70.
42. H. N. Bar, M. R. Bhat, C. R. L. Murthy. Parametric analysis of acoustic emission signals for evaluating damage in composites using a PVDF film sensor. J. Nondestr. Eval., 2005, 24 (4), 121-134.

43. C. L. Jiaa, D. A. Dornfeld. Experimental studies of sliding friction and wear via acoustic emission signal analysis. Wear, 1990, 139, 403-424.
44. A. Guarino, A. Garcimartın, S. Ciliberto. An experimental test of the critical behaviour of fracture precursors. EurPhys. J. B, 1998, 6, 13.
45. L. I. Salminen, A. I. Tolvanen, M. J. Alava. Acoustic emission from paper fracture. Phys. Rev. Lett., 2002, 89, 185503.
46. M. Minozzi, G. Caldarelli, L. Pietronero, S. Zapperi. Dynamic fracture model for acoustic emission. EurPhys. J. B, 2003, 36, 203-207.
47. S. Zhurkov, V. Kuksenko, V. Petrov. On prognosis of rock fracture. Izv. AN SSSR (Phys. Earth),1977, 36, 1-18.
48. S. Nasuno, A. Kudrolli, A. Bak, J. P. Gollub. Time-resolved studies of stick-slip friction in sheared granular layers. Phys. Rev. E, 1998, 58, 2161-2171.
49. T. Chelidze, O. Lursmanashvili, T. Matcharashvili, M. Devidze. Triggering and synchronization of stick slip: Waiting times and frequency-energy distribution. TectonoPhys., 2006, 424 (3-4), 139-155.
50. H. Kantz, T. Schreiber. Nonlinear Time Series Analysis. 1998, New York – Cambridge: Cambridge Univ. Press.
51. J. S. Sprott. Chaos and Time Series Analysis. 2006, Oxford: Oxford Univ. Press.
52. W. S. A. Teukolsky, W. T. Vetterling, B. P. Flannery. Numerical Recipes, 1996, New York – Cambridge: Cambridge Univ. Press.
53. F. James. Statistical Methods in Experimental Physics. 2006, World Scientific.
54. J. P. Zbilut, C. L. Webber. Embeddings and delays as derived from quantification of recurrence plots. Phys. Lett. A, 1992, 171, 199-203.
55. C. K. Peng, S. Havlin, H. E. Stanley, A. L. Goldberger. Chaos , 1995, 5 (1), 82-87.
56. M. Marwan, N. Wessel, U. Meyerfeldt, J. Kurths. Recurrence-plot-based measures of complexity and their application to heart-rate-variability data. Phys. Rev. E, 2002, 66, 026702.
57. C. L. Webber Jr., N. Marwan, A. Facchiani, A. Giuliani. Simpler methods do it better: Success of recurrence quantification analysis as a general purpose data analysis tool. Phys. Lett. A, 2009, 373, 3753-3756.
58. T. Matcharashvili, T. Chelidze, M. Janiashvili. Identification of complex processes based on analysis of phase space structures, imaging for detection and identification. NATO Security through Science Series (Ed. J. S. Byrnes). 2006, Dordrecht: Springer, 207-243.
59. J. H. Dietrich. Time-dependent friction and the mechanics of stick-slip. Pure Appl. GeoPhys., 1978, 116, 790-806.
60. B. Armstrong–Helouvry. Stick slip and control in low speed motion. IEEE Trans. Autom. Contr., 1993, 38 (10), 1483-1496.
61. H. Spetzler, G. Sobolev, A. Koltsov, A. Zang, I. Getting Some properties of unstable slip on rough surfaces. Pure Appl. GeoPhys., 1991, 137 (1-2), 95-112.
62. M. Shengli, M. Jin, L. Liqiang. Experimental evidence for seismic nucleation phase. Chin. Sci. Bull., 2002, 47, 769-773.
63. L. Burlini, G. di Toro, P. Meredith. Seismic tremor in subduction zones: Rock physics evidence. GeoPhys. Res. Lett., 2009, 36, L08305.
64. C. Ferrer, F. Salas, M. Pascual, J. Orozco. Discrete acoustic emission waves during stick-slip friction between steel samples. Tribol. Int., 2010, 43, 1-6.

65. K. Mair, C. Marone, P. Young. Rate dependence of acoustic emissions generated during shear of simulated fault gouge. BSSA, 2007, 97, 1841-1849.
66. B. D. Thompson, R. P. Young, D. A. Lockner. Observations of premonitory acoustic emission and slip nucleation during a stick slip experiment in smooth faulted Westerly granite. GeoPhys. Res. Lett., 2005, 32, L10304.
67. T. Chelidze, O. Lursmanashvili, T. Matcharashvili, N. Varamashvili, N. Zhukova, E. Mepharidze. High-order synchronization of stick-slip process: Experiments on spring-slider system. Nonlin. Dynam., 2010, 59 (1), 259-275.

ON THEORY OF DOPING IN NANOSIZED CRYSTALLOGRAPHIC VOIDS

L. Chkhartishvili

Georgian Technical University
Tbilisi, Georgia
chkharti2003@yahoo.com

Accepted June 10, 2012

1. Introduction

Doping is known to be the main method of tuning the electronic properties of semiconductors. In conventional crystalline semiconductors, like Ge, Si, GaAs, etc., the constituting atoms placed in regular lattice sites are substituted with dopant atoms. In beta-rhombohedral boron (β-B), which is a promising high-temperature material, an attempt to make the substitutional doping with some non-metallic elements, faces several obstacles.

Usually real β-B crystals contain very high concentrations of intrinsic structural defects which dominate in formation of electronic properties of undoped material. Consequently, β-B is characterized by a low sensitivity to doping: to achieve a desired effect in general it is necessary to introduce impurities with concentrations comparable with that of native defects. However, an attempt to replace such high number of boron atoms in regular sites by foreign atoms leads to lattice destruction and / or formation of phase inclusions.

On the other hand, in β-B it is possible to realize a fundamentally different mechanism of doping. The fact is that the crystalline structure of β-B is characterized by a variety of different crystallographic voids sufficiently large – they are nanosized – to accommodate metal atoms with very slight structural distortions. We should emphasize that here we are not discussing pores, 3D structural defects, but we mean large intersites existing in a perfect crystal. Such a mechanism of doping has several advantages compared with the standard, i.e. substitution, mechanism: (i) A number of metallic impurities in β-B boron crystallographic voids can be introduced to concentrations of several atomic percents; (ii) Because of a diversity of void types, which can accommodate atoms of the same chemical element, doping can simultaneously affect different physical properties of material; (iii) Since atoms of various chemical elements can be distributed in different ways between voids of different types, the same effect can be achieved by double, triple, etc. doping of boron combining two or more elements.

Nowadays many metallic elements have been experimentally introduced in different crystallographic voids of the β-B lattice. Some structural and ground-state parameters are

determined for β-B doped with $_{3}$Li, $_{12}$Mg, $_{13}$Al, $_{21}$Sc, $_{22}$Ti, $_{23}$V, $_{24}$Cr, $_{25}$Mn, $_{26}$Fe, $_{27}$Co, $_{28}$Ni, $_{29}$Cu, $_{40}$Zr, $_{41}$Nb, $_{72}$Hf, $_{73}$Ta, and $_{75}$Re. From these studies, one can identify types of voides in the β-B crystalline lattice preferentially filled by atoms of a metal M and make a conclusion that metal-doping in crystallographic voids usually leads to a slight increase in the β-B unit cell volume. The influence of same metallic elements introduced in different crystallographic voids of the lattice, on the electron energy spectrum of β-B is also studied experimentally. In addition, there are a number of papers in which some of electronic properties of metal-doped β-B are determined. The references of main part of these studies one can find in [1]. This problem has received a proper attention at the 17th International Symposium on Boron, Borides and Related Materials (e.g., see Refs. [2 – 5]). Recently, the 3*d*-metals doping impact on the β-B electronic properties has been analyzed in [6]. It was concluded that both gap and conduction band electron states of boron can be involved into the electron states formed by the metal dopants. However, none of the above studies report direct measurements of the discrete electron energy levels placed within the β-B band gap generated by the listed impurities.

At present, the dependences of the β-B conductivity and the Seebeck coefficient on the doping level and temperature are investigated. The sign of charge carriers was determined according to the Seebeck coefficient. In some cases (usually at sufficiently high doping levels) separate Hall measurements of the room temperature carrier concentration and mobility also have been carried out. As is known, most often β-B is characterized by the hopping mechanism of conductivity, which is unsuitable for the standard interpretation of Hall measurements: in such case even the sign of charge carriers is not determined by the sign of the Hall constant, to say nothing of the values of carriers' concentrations and their drift mobility. However, the smallness of the measured value of the Hall mobility can be regarded as an argument of the realization of the hopping conduction in the material.

For light and intermediate elements among the above listed ones – from $_{3}$Li to $_{29}$Cu inclusive – at first doping leads to the increased conductivity of p-type, which is inherent in the undoped β-B. And the hopping mechanism of conductivity is preserved as it is evidenced by the observation of the Mott's law for the temperature-dependence of conductivity in β-B samples doped with $_{3}$Li, $_{13}$Al, $_{23}$V, $_{26}$Fe and $_{29}$Cu. Therefore, it is believed that the doping with these elements leads to a multiplication of the same hopping carriers that are responsible for the electron transport in undoped material. As for the heavier dopant elements – from $_{40}$Zr to $_{75}$Re inclusive – their influence on the p-type conductivity in β-B is weaker. In addition, the super-linear growth of the Hall carriers' concentration with doping (with $_{75}$Re) level indicates that the effect of heavy impurities in p-type β-B, at least partly, may be indirect: introducing of a large impurity atom into a crystallographic void leads to the multiplication of the acceptor defect centers in the adjacent regions of the β-B crystal. For sufficiently heavy doping with a number of impurities ($_{3}$Li, $_{22}$Ti, $_{23}$V, $_{24}$Cr, $_{26}$Fe, $_{27}$Co, $_{28}$Ni, $_{29}$Cu and $_{72}$Hf) attenuation of the p-type conductivity is observed. For most of them the further increase in the doping level leads to the transition to the n-type conduction and the further growth in conductivity. Finally, at very high concentrations of some impurities ($_{23}$V, $_{24}$Cr, $_{26}$Fe and maybe $_{29}$Cu too) doping can lead even to the metallization of the β-B.

From the available experimental data one can make a general conclusion that metal impurities accommodated in crystallographic voids of the β-B lattice tend to behave as donor-centers. At relatively low concentrations, they can increase the p-type hopping conductivity intrinsically characteristic for undoped β-B. Such a specific effect has been explained by an

increase in the concentration of hopping sites (however, it cannot be ruled out that enhancement of the p-type hopping conductivity may simply be accounted for the formation of acceptor-centers as a result of doping). At higher dopant concentrations, the inversion of p-type conduction takes place and then the n-type conductivity increases. As it is, the donor-behavior of metal impurities introduced by interstitial doping is to be expected taking into account the electron-deficiency of a crystalline structure built up only from boron atoms, on the one hand, and the presence of relatively weakly bonded electrons on outer shells of the metal atoms, on the other hand. Therefore, it is important to analyze what kind of electronic energy levels the levels, created by metal impurities in the β-B, are and how deep they are.

However, the lack of theoretical studies both on the interstitial doping mechanism and the influence of interstitial doping on the β-B electron energy spectrum largely impede the purposeful design of the high-temperature semiconductor materials for various technical purposes based on the solid solutions of metals in β-B. This paper is an attempt to partially fill this gap. More precisely, it is a study, which is focused on the construction of the reliable model allowing the calculation of the binding energy of dopant atoms localized in crystallographic voids of a semiconductor lattice and their electron energy levels.

The key partemeters of such model are mean values of coordination numbers, N , and the bonds lengths (voids radii), d , of atoms located in voids of certain types. In case of β-B, these numbers of neighbors are defined by the Lundström criterion [7], according to which atoms in this lattice are considered as nearest neighbors if the corresponding bond length does not exceed 2.80 Å. Taking into account that different impurity atoms placed in voids of different types deform the host lattice structure, the values specified for the mean bonds lengths should be treated just as indicative values. In addition, the occupancy of the interstitial crystallographic voids depends on their size, shape and position in the unit cell.

The values of the binding energy of various interstitial dopants in a semiconductor crystal lattice and their electron energy levels, we intend to calculate by a quasi-classical-type method, which was developed earlier by us [8] and has been successfully used for calculating the ground-state parameters of boron nitride BN [9 – 17] and bare boron nanotubes [18, 19], as well as for examining of some of boron isotopic effects in solids [20 – 23]. The same method, was applied for determining the electron energy spectrum of modifications of boron nitride [9, 12, 24, 25].

2. Quasi-classical parameterization of the electron charge density and electrical field potential distributions in constituent atoms

Since the advent of the Bohr model for a hydrogen atom, semiclassical models of light atoms have been constructed to advantage. The effectiveness of this approach in describing the periodic motion of electrons in small-sized molecules has been demonstrated as well. For many-electron systems, a reasonable accuracy can be achieved in terms of the self-consistent-field (SCF) approximation within which an extreme of the total energy is sought in the class of quasi-classical wave functions. As is known, heavy atoms can be calculated in the framework of the density functional theory (DFT) using a quasi-classical expansion of the energy functional – local density approximation (LDA) is its initial approximation. A similar method appears to be

appropriate for atomic clusters and condensed phases. However, atomic, molecular, and crystal potentials do not satisfy the standard Wentzel–Kramers–Brillouin (WKB) quasi-classical condition due to singularities at nuclear sites and electron shell effects. The success of the above approaches can be explained on the basis of the quasi-classical expressions obtained by Maslov for the energies of bound electron states. It follows from these expressions that the exact and WKB spectra are similar to each other irrespective of the potential smoothness at $2\Phi_0 R_0^2 >> 1$, where Φ_0 and R_0 are the characteristic values of the potential and its effective range, respectively (hereafter all expressions and quantities will be given in atomic units (a.u.)).

Since atomic orbitals at long distances are characterized by an exponential decay, the use of the modified Thomas–Fermi models makes it possible to parameterize the electron density distribution in an atom by introducing a finite atomic radius $R < \infty$, which is however considerably larger than the Bohr radius, i.e., $R >> 1$, such that, at larger distances, the electron density is assumed to be zero. This is equivalent to the initial approximation in quasi-classical atomic models where the partial electron densities are ignored in classically forbidden regions. The radial potential $\Phi_i(r)$ of the effective field acting on the ith electron, $i = 1,2,3,...,Z$, in the atom with the number $Z \geq 1$ can be represented by Coulomb-like potentials $\Phi_i(r) = (Z_i / R)/(r / R)$, where $0 \leq r \leq R$ and $1 \leq Z_i = n_i\sqrt{-2E_i} \leq Z$ are the effective charges dependent on the principal quantum numbers $n_i = 1,2,3,...$ and eigenvalues $E_i < 0$ of the energy of the states, respectively. Consequently, we have $\Phi_0(r) \sim Z_i / R$ and $R_0 \sim R$, and the quasi-classicality condition for the electron energy spectrum of an atom takes the form $2Z_i R >> 1$. Therefore, atoms and the molecules and crystals formed by atoms are actually quasi-classical electronic systems in accordance with the Maslov criterion.

The potential energy of the ith electron with orbital quantum number $l_i = 0,1,2,...,n_i - 1$ is equal to $-\Phi_i(r)$. Therefore, the radii of classical turning points ($r_i' < r_i''$)

$$r_i' = \frac{n_i - \sqrt{n_i^2 - l_i(l_i+1)}}{\sqrt{-2E_i}}$$

and

$$r_i'' = \frac{n_i + \sqrt{n_i^2 - l_i(l_i+1)}}{\sqrt{-2E_i}}$$

can be found as the roots of the equation

$$E_i = -\frac{Z_i}{r} + \frac{l_i(l_i+1)}{2r^2}.$$

Let $\tilde{\Phi}_i(r)$ be the potential of the field induced by the ith electron. Then, the potential of the field induced by the electron cloud of the atom can be written as the sum of these potentials:

$$\tilde{\Phi}(r) = \sum_{i=1}^{i=Z} \tilde{\Phi}_i(r).$$

The potential of the effective field acting on an arbitrary ith electron of the atom is equal to the sum of the potentials of the Coulomb field of the nucleus and the field induced by all the electrons of the atom, except for the potential of the field of the electron under consideration:

$$\frac{Z_i}{r} = \frac{Z}{r} + \tilde{\Phi}(r) - \tilde{\Phi}_i(r).$$

Now we sum up these potentials over the electrons. As a result, the terms independent of the number of electrons on the right-hand sides are multiplied by the total number of electrons in the atom, Z, and the sum of the potentials $\tilde{\Phi}_i(r)$ gives $\tilde{\Phi}(r)$. The solution of the obtained equation has the form

$$\tilde{\Phi}(r) = -\frac{Z^2 - \sum_{i=1}^{i=Z} Z_i}{(Z-1)r}.$$

This relationship makes it possible to determine the potential energy $Z\tilde{\Phi}(r)$ of the interaction between the nucleus of the atom and the electron cloud. Since in the ground state their relative motion corresponds to a zero orbital quantum number, the radius of one classical turning point for this system is equal to zero and the radius $\tilde{r}$ of the other classical turning point is the root of the equation $\tilde{E} = Z\tilde{\Phi}(r)$, where $\tilde{E}$ is the eigenvalue of the energy associated with the relative motion of the electron cloud and the nucleus.

If the effective fields acting on electrons are represented by Coulomb-like potentials, the effective field of the interaction between the nucleus and the electron cloud also turns out to be a Coulomb-like field. Then, under the assumption that the nucleus has an infinite mass and, hence, is stationary (i.e., the reduced mass of the nucleus–electron cloud system is equal to the total mass of electrons in the atom, Z), the radius of the turning point for the motion of the electron cloud with respect to the nucleus is given by the formula

$$\tilde{r} = -\frac{2(Z-1)}{Z^2\left(Z^2 - \sum_{i=1}^{i=Z} Z_i\right)}.$$

The initial quasi-classical approximation implies that exponentially decaying partial electron densities are neglected in the classically forbidden regions and that oscillations of these densities are ignored in classically allowed regions $r_i' \le r \le r_i''$. As a result, the radial dependence of the direction-averaged partial charge density of the i th electron state in the atom is represented by a piecewise constant function, which is equal to zero in the classically forbidden regions. A similar averaging for the motion of the electron cloud as a whole with respect to the nucleus is equivalent to averaging the nuclear charge over a sphere of radius $\tilde{r}$. Summation of all the similar contributions gives the distribution of the total density of the electric charge in the atom in the form of a step radial function,

$$\rho(r) = \rho_k \qquad r_{k-1} \le r \le r_k \qquad k = 1,2,3,...,q,$$

where ρ_k are constants determined from the radii of the classical turning points and r_k coincide with these radii. Here, $0 \equiv r_0 < r_1 < r_2 < \cdots < r_q < \infty$ and q is the number of layers with uniform charge densities. The parameter r_q plays the role of the quasi-classical atomic radius: the charge density is equal to zero at $r > r_q$. This representation is equivalent to the volume averaging in radial layers $r_{k-1} \le r \le r_k$.

Next, we calculate the fields induced by the charged layers with densities ρ_k making use of the Gauss's theorem and sum these fields. Then the atomic potential can be written in the form of a continuously differentiable piecewise analytical function. However, since the energy of the electronic system is a single-valued functional of the electron density, it is reasonable to

approximate the obtained potential by a step function too. This can be adequately performed by averaging over the volume:

$$\varphi(r) = \varphi_k \qquad r_{k-1} \le r \le r_k \qquad k = 1,2,3,\ldots,q\,.$$

3. Quasi-classical calculation of the binding energies

The required binding energy $E_{Binding}(d)$ between a dopant atom (M) and N surrounding host lattice atoms (B) placed at average distance d can be written as $E_{Binding}(d) = -(E_{Static}(d) + E_{Vibrational}(d))$, where $E_{Static}(d)$ and $E_{Vibrational}(d)$ are the static energy of interaction of the cluster (except for the non-physical self-energy contribution) and the energy of the dopant atom vibration relative to the surrounding lattice atoms, respectively. In the initial quasi-classical approximation, these quantities are calculated from the following relations (we remind that all the expressions are given in a.u.):

$$E_{Static}(d) = \frac{N}{4}\sum_{i=1}^{i=q_{\mathrm{B}}}\sum_{j=1}^{j=q_{\mathrm{M}}}(\rho_{\mathrm{B}i}\varphi_{\mathrm{M}j} + \rho_{\mathrm{M}j}\varphi_{\mathrm{B}i})V_{ij}(d)\,,$$

$$E_{Vibrational}(d) = \frac{3}{2}\sqrt{\frac{N}{2M_{\mathrm{M}}}\sum_{i=1}^{i=q_{\mathrm{B}}}\sum_{j=1}^{j=q_{\mathrm{M}}}(\rho_{\mathrm{B}i}\varphi_{\mathrm{M}j} + \rho_{\mathrm{M}i}\varphi_{\mathrm{B}j})\frac{\partial V_{ij}(d)}{\partial d}}\,.$$

Here ($\rho_{\mathrm{B}i}$, $\varphi_{\mathrm{B}i}$) and ($\rho_{\mathrm{M}j}$, $\varphi_{\mathrm{M}j}$) are the volume averages of the electric charge density and the electric field potential in the ith and jth radial layers of B and M atoms, respectively, q_{B} and q_{M} are the numbers of layers of the quasi-classical averaging in these atoms, and M_{M} is the mass of the dopant atom. $V_{ij}(d)$ denotes the volume of the intersection of ith layer of the boron atom with the jth layer of the metal atom. It is calculated as a linear combination of intersection volumes of four pairs of spheres,

$$V_{ij}(d) = V(r_{\mathrm{B}i}, r_{\mathrm{M}j}, d) + V(r_{\mathrm{B}i-1}, r_{\mathrm{M}j-1}, d) - V(r_{\mathrm{B}i}, r_{\mathrm{M}j-1}, d) - V(r_{\mathrm{B}i-1}, r_{\mathrm{M}j}, d)\,.$$

As for the function $V(r_1, r_2, d_{12})$, it has a geometric meaning as the volume of an intersection of two spheres with radii r_1 and r_2 whose centers are at the distance d_{12} from each other. This is an analytic (algebraic) piece-wise continuous function. Its partial derivative $\partial V(r_1, r_2, d_{12})/\partial d_{12}$ is also continuous, but not continuously differentiable function. Explicit forms of $V(r_1, r_2, d_{12})$ and $\partial V(r_1, r_2, d_{12})/\partial d_{12}$ one can find in [8]. The expression under the square root in the vibrational energy term is the frequency of the mode localized at the dopant atom. When its value becomes negative, it is replaced by zero.

The parameters $r_{\mathrm{B}i}$ and $r_{\mathrm{M}j}$ are the external radii of the ith and jth layers of lattice and dopant atoms, respectively (the inner radii are $r_{\mathrm{B}i-1}$ and $r_{\mathrm{M}j-1}$, assuming $r_{\mathrm{B}0} = r_{\mathrm{M}0} \equiv 0$). The parameters ($q_{\mathrm{B}}$, $r_{\mathrm{B}i}$, $\rho_{\mathrm{B}i}$, $\varphi_{\mathrm{B}i}$) and (q_{M}, $r_{\mathrm{M}j}$, $\rho_{\mathrm{M}j}$, $\varphi_{\mathrm{M}j}$) are assumed to be given. Their numerical values have been calculated and tabulated in [26].

Intensity of binding between dopant and host atoms characterizes the binding energy per bond $E_{Binding}(d)/N$. By neglecting the vibrational energy correction $E_{Vibrational}(d)$, this quantity can be estimated from the expression for cluster static energy without factor N.

Under the equilibrium conditions, the resultant force acting on a dopant atom from surrounding lattice atoms has to be zero. This implies that in order to find the value of the binding energy of a dopant atom in different voids of the β-B crystal one should find extrema of the function $E_{Binding}(d)$. Note that one should consider both kinds of extrema, not only the binding energy maxima, which correspond to a stable equilibrium of the dopant atom surrounded by a cluster of lattice atoms, but also the minima, that define the interatomic distances in unstable equilibrium. This cluster is not a closed physical system: actually it is embedded into the crystalline lattice. Therefore, the dopant atom localized at an unstable equilibrium position with respect to the dopant atom surrounded by a subsystem of lattice atoms can be kinetically incapable to reach a stable equilibrium position. Obviously, one should take into account only the extrema, in which the binding energy is positive.

Furthermore, one should confine oneself to the extrema for which the deviations of the average distances between the voids' geometric centers (where the dopant atoms' nuclei are supposed to be located) and the surrounding lattice atoms are not too large compared with the predicted equilibrium lengths of B – M bonds.

One should not expect that the calculated B – M mean bonds length corresponding to an extremum must exactly coincide with the value actually realized in the crystal. It is likely to be an equilibrium bond length to which the subsystem tends. Based on its value one can estimate whether the crystal will expand or, on the contrary, contract due to doping. In the crystal, there is a specific B – M mean bond length for which the loss (gain) in the binding energy of a dopanty with the lattice associated with the deviation of the cluster, containing the dopant, from its stable (unstable) equilibrium is compensated by the gain (loss) in the deformation energy of the rest of the crystal due to doping. Therefore, the binding energy values at its extrema may be well used to estimate the binding energy of a dopant atom with the crystal as a whole. The fact is that by definition of the latter it is the difference between the total energies of a doped, and thus locally deformed crystal, and a pure ideal crystal.

4. Quasi-classical calculation of the electron energy spectra

Finding out the electron energy levels of various dopant elements accommodated in various types of crystallographic voids requires development of a special model of impurity centers. The situation when a dopant atom is embedded in a crystallographic void surrounded by already tightly bonded together atoms essentially differs from that when a constituent atom of the lattice tightly bonded with neighbors is substituted with a foreign atom. Therefore, standard models for impurity centers cannot be used for our purposes.

Taking into account that an impurity atom placed inside a crystallographic void should only slightly affect the crystalline structure, within the first approximation the donor energy level of the impurity atom can be found from the outer valence-shell ionization potential of the same chemical element in isolated state shifting the corresponding electron energy level in the cryatalline internal field. These shifts can be found assuming that changes in the electric field within a dopant atom introduced in a crystallographic void are determined mainly by lattice atoms directly surrounding the void.

Similarly, the acceptor energy level can be obtained from the dopant electron affinity unless the given chemical element exists in negatively charged ionic state. Then, based on the electron energy spectrum of an impurity atom determined in this way, one can find out whether the dopant creates a discrete energy level within the semicnductor band gap, and if so, determine its depth, or it is donor or acceptor, etc. In this way, one will be able to predict the character of influence of doping with a given element on the electrical conductance of the semicondictor.

Within the proposed model, the depth of the donor level E_D formed by a dopant atom embedded in a certain crystallographic void is determined from the relation $E_D = (E_{IP} + E'_{IP}) - E_C$, where E_{IP} is the known ionization potential of the dopant atom in the isolated state and E'_{IP} is its shift in the crystalline field, while E_C is the conduction band edge. If the valence band edge – electron work function $E_V = E_{WF}$ – and band gap E_G of the semiconductor are known, then $E_C = E_{WF} - E_G$, i.e. $E_D = (E_{IP} + E'_{IP}) - (E_{WF} - E_G)$. When the donor levels are too deep, $E_D > E_G$, they are placed inside the valence band and, consequently, virtually do not affect conductivity of the material. A detectible modification in semiconducting properties is available unless donor levels are placed inside the band gap, $0 < E_D < E_G$. If $E_D < 0$, i.e. donor levels are placed immediately inside the conduction band, the doping at sufficiently high concentrations yields semiconductor-to-n-type-semimetal transition.

Thus, to find the donor level location on the energy axis it is necessary to calculate only one quantity, E'_{IP} . It is possible to estimate its value as a quantum-mechanical mean of the electron potential energy in the crystalline field. In the initial quasi-classical approximation we obtain:

$$E'_{IP} = -\frac{3NE_{IP}}{4\pi(4n_{IP}^2 - l_{IP}(l_{IP}+1))}\sqrt{\frac{2E_{IP}}{n_{IP}^2 - l_{IP}(l_{IP}+1)}}\sum_{i=1}^{i=q_B}\varphi_{Bi}V_{IPi}(d) \ .$$

Here n_{IP} and l_{IP} represent, respectively, the principal and orbital quantum numbers of the outer valence shell electron in the dopant atom, N is the coordination number of the dopant atom, i.e., number of nearest neighboring lattice atoms, d is the length of corresponding bonds, φ_{Bi} is the volume-averaged electric field potential within the lattice atom's i th radial layer, and q_B is the number of such layers in atom.

In above expression, $V_{IPi}(d)$ denotes the intersection volume of the lattice atom radial i th (r_{Bi-1}, r_{Bi}) -layer with the dopant atom (r'_{IP}, r''_{IP}) -layer. r'_{IP} and r''_{IP} are the inner and outer classical turning points radii for the outer valence shell electron of the dopant atom, respectively:

$$r'_{IP} = \frac{n_{IP} - \sqrt{n_{IP}^2 - l_{IP}(l_{IP}+1)}}{\sqrt{2E_{IP}}},$$

$$r''_{IP} = \frac{n_{IP} + \sqrt{n_{IP}^2 - l_{IP}(l_{IP}+1)}}{\sqrt{2E_{IP}}}.$$

The quantity $V_{IPi}(d)$ is calculated as a linear combination of the intersection volumes of 4 pairs of spheres,

$$V_{IPi}(d) = V(r_{Bi}, r''_{IP}, d) + V(r_{Bi-1}, r'_{IP}, d) - V(r_{Bi}, r'_{IP}, d) - V(r_{Bi-1}, r''_{IP}, d).$$

As for the depth of the acceptor level E_A formed by a dopant atom embedded in a certain crystallographic void, it is determined from the relation $E_A = E_V - (E_{EA} + E'_{EA})$, i.e. $E_A = E_{WF} - (E_{EA} + E'_{EA})$. Here E_{EA} is the electron affinity of the atom in the isolated state (i.e. its value is known unless a chemical element possesses a negative ion) and E'_{EA} is the shift of the exited atomic level in the crystalline field. When acceptors are too deep, $E_A > E_G$, the corresponding unoccupied electron energy levels are placed inside the conduction band and, consequently, they practically do not affect conductivity of the material. A detectible modification in semiconducting properties is available unless acceptor levels are placed inside the band gap, $0 < E_A < E_G$. However, when $E_A < 0$, acceptor levels are placed immediately inside the valence band causing the semiconductor-to-p-type-semimetal transition if sufficiently high concentration of dopants is introduced in the semiconducting material. It is clear that to estimate the acceptor energy level it is necessary to calculate only one quantity, E'_{EA}. It can be done in the same way as it has been done above for E'_{IP}:

$$E'_{EA} = -\frac{3NE_{EA}}{4\pi(4n_{EA}^2 - l_{EA}(l_{EA}+1))}\sqrt{\frac{2E_{EA}}{n_{EA}^2 - l_{EA}(l_{EA}+1)}}\sum_{i=1}^{i=q_B}\varphi_{Bi}V_{EAi}(d) \ .$$

Here n_{EA} and l_{EA} represent, respectively, the principal and orbital quantum numbers of the first exited electron level in the dopant atom, N is the coordination number of the dopant atom, i.e., number of nearest neighboring lattice atoms, d is the length of corresponding bonds, φ_{Bi} is the volume-averaged electric field potential within the lattice atom's ith radial layer, and q_B is the number of such layers in atom. $V_{EAi}(d)$ denotes the intersection volume of the lattice atom radial ith (r_{Bi-1}, r_{Bi})-layer with the dopant atom (r'_{EA}, r''_{Ea})-layer. r'_{EA} and r''_{EA} are the inner and outer classical turning points radii for the first exited shell electron of the dopant atom, respectively:

$$r'_{EA} = \frac{n_{EA} - \sqrt{n_{EA}^2 - l_{EA}(l_{EA}+1)}}{\sqrt{2E_{EA}}},$$

$$r''_{EA} = \frac{n_{EA} + \sqrt{n_{EA}^2 - l_{EA}(l_{EA}+1)}}{\sqrt{2E_{EA}}}.$$

The quantity $V_{EAi}(d)$ is calculated as a linear combination of the intersection volumes of 4 pairs of spheres,

$$V_{EAi}(d) = V(r_{Bi}, r''_{EA}, d) + V(r_{Bi-1}, r'_{EA}, d) - V(r_{Bi}, r'_{EA}, d) - V(r_{Bi-1}, r''_{EA}, d).$$

In above relations, $V(r_1, r_2, d_{12})$ is the same function, which has already been introduced above. Parameters of lattice atoms φ_{Bi} are assumed to be given. As mentioned above, we have precalculated and tabulated their values together with other quasi-classical parameters for different chemical elements in [26].

5. Accuracy of the quasi-classical approach for the impurity center model used

The relative error of the quasi-classical method itself when determining values of energy does not exceed a few percent. However, the model describing a cluster of a dopant atom and

surrounding lattice atoms is based on a number of simplifications, which are necessary because of the complexity of a semiconductor lattice with large crystallographic voids. These simplifications act as additional sources of calculation errors.

The approximations of the model involve the determination of both the number of the nearest neighboring lattice atoms and the bonding lengths of the dopant atom with its neighbors: (i) even in a perfect crystal, different host lattice atoms surrounding a void are located in crystallographically non-equivalent positions and at different distances from the geometric center of the void; (ii) since real crystals with large unit cell are characterized by a high concentration (up to a few at. %) of intrinsic point defects in the form of partially occupied sites, some atomic sites, where neighboring lattice atoms are supposed to be found, actually may be unoccupied or vice versa; (iii) the nearest neighbors of the dopant atom are counted according to certain criterion (like the above mentioned Lundström criterion) and, therefore, their number is arbitrary to some extent.

Even more, the partial occupancies of lattice sites in the semiconductor may be correlated. Since dopant sites in form of crystallographic voids may be close to the partially occupied sites or even coincide with them, the interference between the occupancies of crystallographic voids by dopant atoms and the lattice sites seems plausible. Thus dopant atoms accommodated in crystallographic voids affect occupancies of the neighboring lattice atoms and may destabilise the structure. This is the reason why doping in semiconductor lattices containing large crystallographi voids is limited.

The binding energy of an impurity metal atom with neighboring lattice atoms is approximately proportional to their number N. Consequently, the maximal relative error in calculated value $E_{Binding}$ related with partial occupancies of the neighboring boron sites should be $\sim 1/N$. Since in case of β-B $N \geq 12$, for this material the error associated with the impurity center model used is expected to be < 10 %. The calculation error for the electron energy levels generated by the impurity atoms should be even smaller because the donor (acceptor) energy level E_D (E_A) is expressed by the sum, in which only one term – ionization potential (electron affinity) shift E'_{IP} (E'_{EA}) depends on N (is proportional to N). Thus, the approximations of the model used for impurity atoms doped in a semiconductor lattice do not significantly affect binding energies of such atoms and their electron energy levels calculated by the quasi-classical method.

For determining the position of an impurity level in the band gap within the frame of the proposed model, it is also necessary to know the positions of edges of both valence and conduction bands of the semiconductor or its electron work function and band gap width. The β-B band gap width E_G is well known: 1.56 eV [27].

As for the β-B work function E_{WF}, there are only old and to some extent contradictory measurements of this parameter. The values of the β-B work function measured by different (photoelectric, thermoelectric and high-energy electrons' surface-diffraction) methods show a fairly wide spread: 3.80 – 6.13 eV and there are suggestions explaining both under- and overestimated values. The reference book's value of 4.45 eV [28] is placed near the midpoint of this interval. However, we are inclined to accept the highest value proposed for the β-B work function, 6.13 eV [29]. Such choice of the zero reference point on the energy scale yields the location of the conduction band edge E_C at 6.13 eV – 1.56 eV = 4.57 eV giving quite a good estimate for the work function of contaminated and imperfect crystals, i.e. when electrons are

exciting in vacuum not from the valence band edge of an ideal crystal, but in the vicinity of the conduction band edge.

In any case, evaluating the calculated energy levels we should take into account the possible spread in values associated with the spread in input parameters, namely, the band edges' positions on the energy axis.

References

1. D. L. Gabunia, O. A. Tsagareishvili, L. S. Chkhartishvili, G. F. Tavadze. In: Proc. 8th Int. Cong. ETHTMA, Vol. 2: Nanostructural Functional Coatings. Perspective Materials and Nanomaterials (Eds. I. M. Neklyudov, V. M. Shulayev). 2007, Kharkov: NSC "KhPTI" – PPC "Contrast", 211-272.
2. K. Soga, H. Hyodo, H. Iseki, K. Kimura. In: 17th Int. Symp. Boron, Borides & Rel. Mater. (Abs.), 2011, Ankara: BKM, 68.
3. H. Werheit. In: 17th Int. Symp. Boron, Borides & Rel. Mater. (Abs.), 2011, Ankara: BKM, 80.
4. K. Kimura, H. Hyodo, Y. Takagiwa, K. Kirihara, K. Soga, K. Kato, M. Takata. In: 17th Int. Symp. Boron, Borides & Rel. Mater. (Abs.), 2011, Ankara: BKM, 102.
5. B. Albert. In: 17th Int. Symp. Boron, Borides & Rel. Mater. (Abs.), 2011, Ankara: BKM, 274.
6. H. Werheit. Solid State Sci., 2011, 139, 1786-1796.
7. T. Lundström. AIP Conf. Proc., 1986, 140, 19-30.
8. L. Chkhartishvili. Quasi-Classical Theory of Substance Ground-State, 2004, Tbilisi: Tech. Univ. Press.
9. L. Chkhartishvili, D. Lezhava, O. Tsagareishvili. J. Solid State Chem., 2000, 154, 148-152.
10. L. Chkhartishvili. In: Proc. 1st Int. Boron Symp. (Ed. K. Erarslan), 2002, Kütahya: Dumlupinar Univ. Press, 139-143.
11. L. Chkhartishvili. In: Proc. 2nd Int. Boron Symp. (Eds. H. Özdağ, H. Akdaş, V. Bozkurt, M. İphar), 2004, Eskişehir: Osmangazi Univ. Press, 165-171.
12. L. S. Chkhartishvili. Phys. Solid State, 2004, 46, 2126-2133.
13. L. S. Chkhartishvili. Phys. Solid State, 2006, 48, 846-853.
14. L. Chkhartishvili. GESJ Phys., 2006, 40, 130-138.
15. L. S. Chkhartishvili. Mater. Sci. Nanostr., 2009, 1, 33-44.
16. L. Chkhartishvili, I. Murusidze. Mater. Sci. Appl., 2010, 1, 223-246.
17. L. Chkhartishvili, T. Berberashvili, I. Murusidze. In: Phys., Chem. & Appl. Nanostr. (Eds. V. E. Borisenko, S. V. Gaponenko, V. S. Gurin), 2011, Singapore: World Scientific, 126-129.
18. L. Chkhartishvili. J. Phys. Conf. Ser., 2009, 176, 012013-9.
19. L. Chkhartishvili. In: Proc. 4th Int. Boron Symp. (Eds. A. Konuk, H. Kurama, H. Ak, M. İphar), 2009, Eskişehir: Osmangazi Univ. Press, 15-160.
20. L. S. Chkhartishvili, D. L. Gabunia, O. A. Tsagareishvili. Inorg. Mater., 2007, 43, 594-596.
21. L. S. Chkhartishvili, D. L. Gabunia, O. A. Tsagareishvili. Powd. Metall. Met. Ceram., 2008, 47, 616-621.

22. D. Gabunia, O. Tsagareishvili, L. Chkhartishvili, L. Gabunia. J. Phys. Conf. Ser., 2009, 176, 012022-10.
23. L. Chkhartishvili. Trends Inorg. Chem., 2009,11, 105-167.
24. L. Chkhartishvili. J. Solid State Chem., 2004, 177, 395-399.
25. L. Chkhartishvili. Mater. Sci. Ind. J., 2006, 2, 18-23.
26. L. Chkhartishvili, T. Berberashvili. J. Electromagn. Anal. Appl., 2010, 2, 205-243.
27. H. Werheit, F. Kummer. J. Phys. Conf. Ser., 2009, 176, 012020-4.
28. CRC Handbook of Chemistry and Physics (Ed. R. C. Weast), 1988, Boca Raton: CRC Press.
29. E. R. Kutelia, O. G. Dzimtseishvili, T. A. Dzigrashvili, D. M. Tsivtsivadze, P. D. Kervalishvili. J. Less-Comm. Met., 1986, 117, 283-286.

ПРИМЕНЕНИЕ ДИСПЕРСИОННОГО АНАЛИЗА ДЛЯ ОЦЕНКИ ФАКТОРОВ ДЕЙСТВУЮЩИХ НА МАГНИТООПТИЧЕСКИЕ СВОЙСТВА УЛЬТРАДИСПЕРСНЫХ СРЕД

Л. Г. Каландадзе

Государственный университет им. Шота Руставели
Батуми, Грузия
Lali62@mail.ru

Принята 13 июня 2012 года

Введение

Статистика при помощи статистических показателей характеризует размеры изучаемых явлений, их особенности, закономерности развития и их взаимосвязи. Так, аналитические показатели используются для характеристики особенностей развития явления, распространенности в пространстве, соотношения его частей, взаимосвязи с другими явлениями. В качестве аналитических показателей используются средние величины, показатели структуры, вариации, динамики и др.

Дисперсия и среднее квадратическое отклонение – наиболее широко применяемые показатели вариации. Объясняется это тем, что они входят в большинство теорем теории вероятностей, служащих фундаментом математической статистики. При этом, если статистическая совокупность разбита на группы по какому-либо признаку, то для оценки влияния различных факторов, определяющих колеблемость индивидуальных значений признака, можно воспользоваться разложением дисперсии на составляющие элементы: на межгрупповую и внутригрупповую дисперсии [1].

Если рассчитать дисперсию признака по всей изучаемой совокупности, т.е. общую дисперсию, то полученный показатель будет характеризовать вариацию признака как результат влияния всех факторов, определяющих индивидуальные различия единиц совокупности.

Если же поставить дальнейшую задачу – выделить в составе общей дисперсии ту ее часть, которая обусловлена влиянием какого-либо определенного фактора, то следует разбить изучаемую совокупность на группы, положив в основу группировки интересующий нас фактор. Затем нужно изучить раздельно вариацию признака внутри однородных в отношении данного фактора групп и изменения в величине признака от группы к группе. Выполнение такой группировки позволяет разложить общую дисперсию признака на две дисперсии, одна из которых будет характеризовать часть вариации, обусловленную влиянием фактора, положенного в основу группировки, а вторая – вариацию, происходящую под влиянием прочих факторов.

Теория

Элементы дисперсионного анализа успешно применяется в физике магнитных явлений для оценки влияния различных факторов, действующих на магнитооптические свойства ультрадисперсных сред [2, 3]. Следует отметить, что в настоящее время особое внимание уделяется изучению магнитооптических свойств ультрадисперсных сред. Это связано с тем, что ультрадисперсные среды, такие как, магнитные жидкости, гетерогенные стекла, островковые пленки, частицы магнитных металлов и окислов, широко применяются в различных областях науки и техники.

Интерес к исследованию магнитооптических эффектов на этих средах, размер структурных или магнитных неоднородностей в которых не превышает 1000 Å, обусловлен тем, что у них наблюдается ряд интересных свойств, отличающих ультрадисперсную среду от массивного материала. Так, при исследовании магнитооптических эффектов отражения на ультрадисперсных средах были обнаружены новые эффекты, такие как, рост экваториального эффекта Керра относительно его величины на массивных материалах, появление эффекта Керра на S-компоненте падающего света при экваториальном намагничивании т.д. [4].

В работе [3] применив метод дисперсионного анализа, показано, что влияние фактора q (коэффициента объемного заполнения магнитных жидкостей магнитными частицами) на вариацию дисперсионных зависимостей экваториального эффекта Керра, следовательно, на магнитооптические свойства магнетитовых магнитных жидкостей, составляет 53 %. Отсюда сделан вывод, что в рассмотренном случае q фактор имеет преобладающее влияние на вариацию эффекта и определяет магнитооптические свойства ультрадисперсных сред. Отмечено, что полученный результат будет справедливым для всех ультрадисперсных сред, оптические константы материала которых удовлетворяют соотношение $k_m^2 << n_m^2$.

Результаты и обсуждения

Второй главный фактор, действующий на магнитооптические свойства таких ультрадисперсных сред, является диэлектрическая проницаемость ε_0 окружающей среды жидкость – носитель. С целью оценки влияния фактора ε_0 на вариацию экваториального эффекта Керра относительно других факторов (размер магнитных частиц, их расположение, концентрация магнитных частиц и др.), мы решили применить правило сложения дисперсий. Этот метод описан в работе [2]. Количественная оценка влияния ε_0 фактора на магнитооптические свойства магнитных жидкостей докажет важность уже обоих факторов q и ε_0 на магнитооптические свойства ультрадисперсных сред.

Экспериментальные данные мы взяли из работ [5, 6], в которых исследованы дисперсионные зависимости экваториального эффекта Керра (угол падения света на образец $\varphi = 70°$) в магнетитовых магнитных жидкостях и их осадков на основе воды, керосина и разных кремнийорганических соединений с различными коэффициентами объемного заполнения q . Эти исследования дали возможность разложить экспериментальные данные на группы, положив в основу группировки интересующий

нас фактор – диэлектрическая проницаемость окружающей среды. Расчеты проводились для энергии квантов падающего света $\hbar\omega$ = 2 эВ. Экспериментальные данные, разложенные по ε_0 приведены в **Табл. 1**.

Таблица 1.

ε_0	$\delta_e(q)$		
Кремний органическое соединение	0.36	0.30	0.39
Вода	– 0.17	– 0.32	0.05
Керосин	0.20	0.25	0.15
Воздух	1.10	0.28	0.80

Расчеты, выполненные по этим данным, показали, что влияние фактора ε_0 на вариацию дисперсионных зависимостей экваториального эффекта Керра составляет 37 %.

Отсюда можно сделать вывод, что в рассмотренном случае факторы q и ε_0 оказывают главное влияние на вариацию эффекта и определяют магнитооптические свойства ультрадисперсных сред, так как влияние обеих факторов составляет 90% на вариацию дисперсионных зависимостей экваториального эффекта Керра.

Заключение

Магнитооптические свойства магнитных жидкостей в самом общем случае существенно отличаются от свойств массивных ферромагнетиков, что приводит к изменению дисперсионных и угловых зависимостей величины магнитооптических эффектов по сравнению с аналогичными зависимостями на массивных образцах. Отсюда следует, что затрудняется расшифровка экспериментально наблюдаемых магнитооптических спектров, дающих информацию, как о намагниченности тонкого приповерхностного слоя магнитных жидкостей, так и об электронной энергетической структуре малых магнитных частиц.

В связи с этим, в рассматриваемом примере для случая слабого поглощения $k_m^2 << n_m^2$ материала частиц найдены и количественно определены главные факторы действующие на магнитооптические свойства ультрадисперсных сред. При этом, настоящая работа также дает возможность прогнозировать магнитооптические свойства

таких ультрадисперсных магнитных структур и, следовательно, получить ультрадисперсные магнитные структуры нужных параметров.

Ссылки

1. М. П. Ефимова, Е. В. Петрова, В. Н. Румянцев Общая теории статистики. 1997, Москва: ИНФРАМ.
2. Л. Г. Каландадзе. Исследование влияния концентрации магнитных частиц на магнитооптические свойства ультрадисперсных сред методом дисперсионного анализа. Nano Studies, 2011, 3, 177-180.
3. L. G. Kalandadze. The influence of the magnetic particles concentration on the magneto-optical properties of the magnetite magnetic fluids. J. Sensor Lett., 2007, 5, 1, 13-14.
4. Л. В. Никитин, О. В. Касаткина. Аномалии оптических и магнитооптических свойств ультрадисперсных поверхностных структур. Тез. докл. XII Всесоюз. конф. по физике магн. явлений. 1983, Тула, 112-113.
5. Л. В. Никитин, А. А. Тулинов. Нечетные магнитооптические эффекты и исследование свойств тонкого приповерхностного слоя магнитной жидкости. Изв. АН СССР (Сер. физ.), 1991, 55, 1120-1126.
6. L. Kalandadze. Equatorial Kerr effect in ultrafine magnetic structures. New Develop. Mater. Sci., 2010, New York: Nova Sci. Publ., Ch. 16.

ОПТИЧЕСКИЕ И ПОВЕРХНОСТНЫЕ СВОЙСТВА НИТРИДБОРНЫХ СОЕДИНЕНИЙ, ПОЛУЧЕННЫХ В ОПТИЧЕСКОЙ ПЕЧИ БЕЗ КАТАЛИЗАТОРОВ

Л. Л. Сартинская [1], А. А. Фролов [1], А. Ф. Андреева [1], Е. В. Войнич [1], А. М. Касумов [1], Г. А. Фролов [1], В. А. Тиньков [2], В. В. Стонис [2]

[1] Институт проблем материаловедения им. И. Н. Францевича
Национальной академии наук Украины
Киев, Украина
sart@ipms.kiev.ua
[2] Институт металлофизики им. Г. В. Курдюмова
Национальной академии наук Украины
Киев, Украина
pepperland23@i.ua

Принята 13 июня 2012 года

Проведено исследование процессов, происходящих при нагреве в фокальной зоне оптической печи повышенной мощности в потоке азота. Показано, что преобразование графитоподобного h-BN инициирует формирование нанотрубок, вискерсов (нитей) вокруг кратера и капель на поверхности образца. Вискерсы (нити) в средней области имеют повышенное содержанке азота, а капли и вискерсы в начале и конце своей длины – повышенное содержание бора и кислорода. Подтверждено, что движение кислорода является главной движущей силой, которая способствует образованию нитевидных структур. Показано, что вдали от кратера на поверхности оседает порошковый материал с повышенным содержанием бора, состоящий из нитевидных образований – нанотрубок и вискерсов (нитей), равноосных наноразмерных кристаллитов, отдельных монокристаллов h-BN и тетрагональных фаз ($B_{25}N$) и ($B_{51}N_2$), а также аморфного нитрида бора. Для этого материала определены следующие ширины запрещенной зоны: 3.5, 3.8 и 4.8 эВ, отвечающие фазам: тетрагональным $B_{51}N_2$ и $B_{25}N$, а также гексагональной BN соответственно. Метод Оже-электронной спектроскопии может служить для предварительной оценки порошковых материалов, поскольку показывает различие в электронных структурах чистых элементов и их соединений.

Введение

Последнее десятилетие нитрид бора вызывает значительный интерес как технологически важный материал, который имеет интересное сочетание физических и химических свойств. Структуры BN можно наблюдать в виде нескольких модификаций, начиная от sp^2-связи гексагональной структуры BN (h-BN) или sp^3-связи кубической структуры BN (c-BN), до нанотрубок или фуллереноподобных структур [1, 2]. Созданные BN нанотрубки могут иметь структуру, подобную структуре углеродных нанотрубок, однако их свойства очень разные. Углеродные нанотрубки могут быть металлическими или полупроводниковыми в зависимости от направления хиральности и радиуса, BN

нанотрубки являются изоляторами с большой шириной запрещенной зоны, которая почти не зависит от хиральности трубки и ее морфологии. Как и в других формах нитрида бора, BN нанотрубки более термически и химически стабильны, чем углеродные нанотрубки, что способствует их широкому применению, и, поэтому, он также имеет большой потенциал в области нанотехнологий. Понимание механизма структурообразования нитрида бора имеет большое фундаментальное и технологическое значение, поскольку особенности полученной структуры играют важную роль в формировании электронного строения структуры и, таким образом, химических и физико-механических свойств BN [3].

В целом, нагрев поверхности BN мощным световым излучением может привести к существенным изменениям в объеме материала. Среди них местные уплотнения или плавления, сжимающие напряжения или создание точечных дефектов, которые могут играть доминирующую роль в свойствах конечного материала [4 – 7]. Молекулярный азот (N_2), например, может легко формировать N – N связи в BN во время ионной бомбардировки [8, 9]. Исследование поверхности нитрида бора также имеет важное значение для многих областей в электронике, для прямого преобразования тепловой, солнечной и химической энергии в электрическую, для катализа и других приложений, где чистота материалов и химическое состояние атомов в поверхностном слое имеет особое значение. Оже-электронная спектроскопия (ОЭС) поверхности очень мощный аналитический метод, который нашел применение во многих областях физики твердого тела и химии. Несколько таких явлений, как адсорбция, десорбция, поверхностная сегрегация в массивном теле, измерения коэффициентов диффузии и каталитическая активность поверхности были исследованы с помощью ОЭС [10, 11]. Основными преимуществами данного метода является его высокая чувствительность к химическому составу в пределах 5 – 20 Å вблизи поверхности, быстрый сбор данных, способность обнаруживать все элементы выше гелия, и его высокая пространственная разрешающая способность. Высокое разрешение достигается за счет того что образец возбуждается электронным пучком, который может быть сфокусирован в тонкий зонд [12]. Нитевидные структуры BN, полученные в оптической печи в атмосфере азота, благодаря их структурным особенностям, могут отличаться по химическому составу не только от поверхностного слоя атомов однородной плоской поверхности, но и от химического состава второго и последующих приповерхностных слоев, поскольку их химический состав определяется несовершенной и неоднородной структурой поликристаллической поверхности оболочки вискерса (нити) BN.

Нагрев чистого графитоподобного нитрида бора h-BN без катализаторов в потоке азота приводит к изменению его структуры, морфологии, фазового и элементного состава. Поверхностные и оптические свойства синтезированных нанотрубок, вискерсов (нитей) и других наноструктур дадут представление о происходящих процессах, что, в свою очередь, позволит получать материалы с наперед заданными свойствами. Таким образом, исследование особенностей нитридборных соединений, синтезированных в оптической печи большой мощности, является важной задачей.

Методика эксперимента

Испарение материала образца производилось при плотности потока энергии в фокальной зоне установки 7000 кВт / м^2. Камера продувалась осушенным и очищенным от

примесей кислорода азотом. Эксперимент продолжался 1 час. Давление азота в газовой магистрали поддерживалось на уровне чуть выше атмосферного [8, 9, 13]. Морфологию поверхности исходных порошков и полученных материалов исследовали на рентгеновском микроанализаторе Superprobe 733 (Япония, JEOL), фазовый состав – рентгенографически на дифрактометре Дрон – 3.0 в Kα – Cu излучении и на универсальном просвечивающей электронном микроскопе ПЭМ – В. Морфология поверхности полученных порошковых покрытий исследовалась также на сканирующем электронном микроскопе высокого разрешения с полевой эмиссией JEOL (Tokio – Boeki Ltd.). Для изучения спектральной зависимости оптического поглощения изучаемый материал в виде тонкой пленки был нанесен на подложку из аморфного кварца. Образцы для оптических исследований отличались высокой прозрачностью в видимой области спектра. Исследования проводились на спектрофотометре марки Specord UV – Vis в интервале длин волн 0.2 – 0.8 мкм.

ОЭС образцов структур BN, полученных в оптической печи, была проведена в высоком вакууме. До каждого образца, для лучшей оценки и для удаления наведенного поверхностного, статического заряда, который возникал на исследуемых диэлектрических объектах, добавляли чистый алюминий (Sigma–Aldrich, 99 %, размер частиц < 75 мкм). Для сравнения исследовались также мелкозернистые исходные порошки гексагонального графитоподобного h-BN (Chempur, CH070802). Оже-процесс был инициирован в образцах путем выбивания электронов из внутренних оболочек пучком электронов высокой энергии: 3 кэВ; ток пучка 120, 180, 200 мкА; модуляция 1 – 2 эВ, постоянная времени 3 с чувствительность 50 – 100 мкВ время сканирования 1000 с. Высокоэнергетические электроны имели достаточно энергии для ионизации необходимых энергетических состояний более легких элементов, и могли ионизировать более высокие уровни основных состояний более тяжелых элементов.

Результаты и обсуждение

Исследование показало, в результате нагрева в оптической печи при соответствующем градиенте температуры наблюдается газоперенос, способствующий формированию капель расплава и росту нитевидных структур вокруг кратера на поверхности компактированных образцов (**рис. 1**). Поскольку пары бора и азота повторно конденсируются и вновь испаряются, то такой процесс приводит к увеличению объема и размера нитевидных структур.

Полученные вискерсы (нити) не имели примесей в средней области, однако их состав отличался повышенным содержанием азота (**рис.** 2) при различном соотношении компонентов бора и азота (**рис. 2**), что можно объяснить повышенным давлением азота и турбулентностью его потока в центре кратера. Как правило, вискерсы (нити) не включали кислород в средней части длины.

Образованные капли имеют размеры до 100 мкм, содержат повышенное количество бора и некоторое количество кислорода (**рис. 3**), поскольку образуются при плавлении исходного h-BN, содержащего кислород в своем составе [14] и испарении азота. Создается впечатление, что присутствие кислорода настолько увеличивает поверхностное натяжение расплава, что образуются фуллереноподобные структуры, а повышенное содержание азота его уменьшает и способствует вытягиванию нитевидных структур.

Присутствие кислорода в расплаве объясняется его наличием в исходных порошках в виде оксидов и в качестве адсорбированного, а также его газопереносом из внутренних слоев компактированного образца порошка нитрида бора во время его дегазации при повышении температуры.

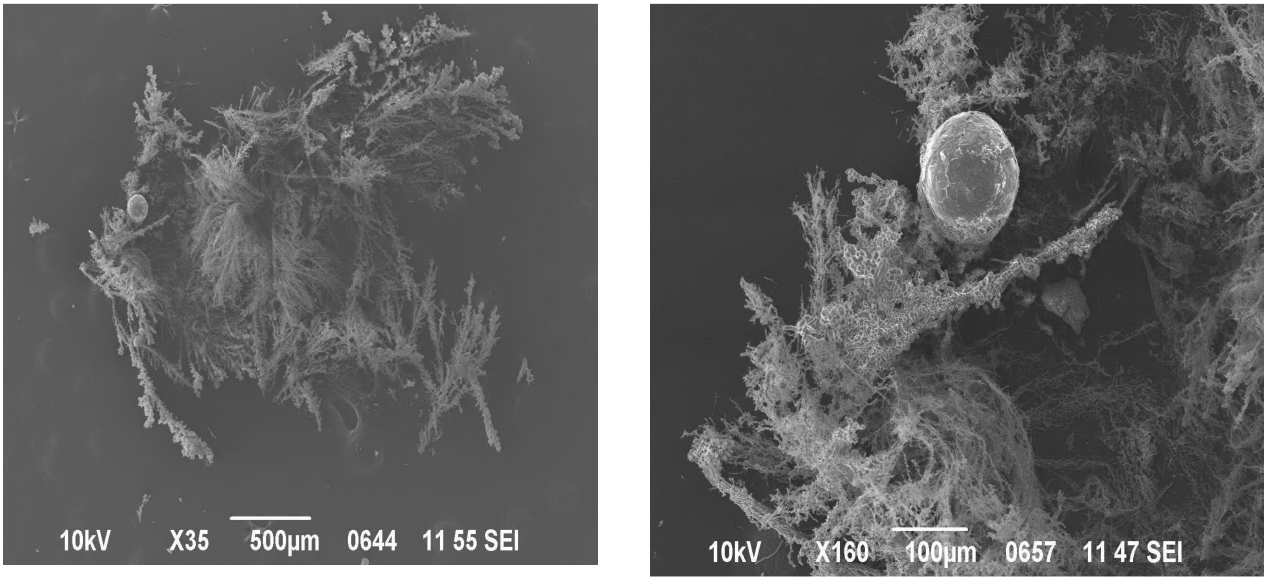

(а) (б)

Рисунок 1. Вискерсы (нити) и капли на поверхности исходного BN, полученные в результате нагрева в оптической печи большой мощности при различном увеличении: (а) × 35 и (б) × 160.

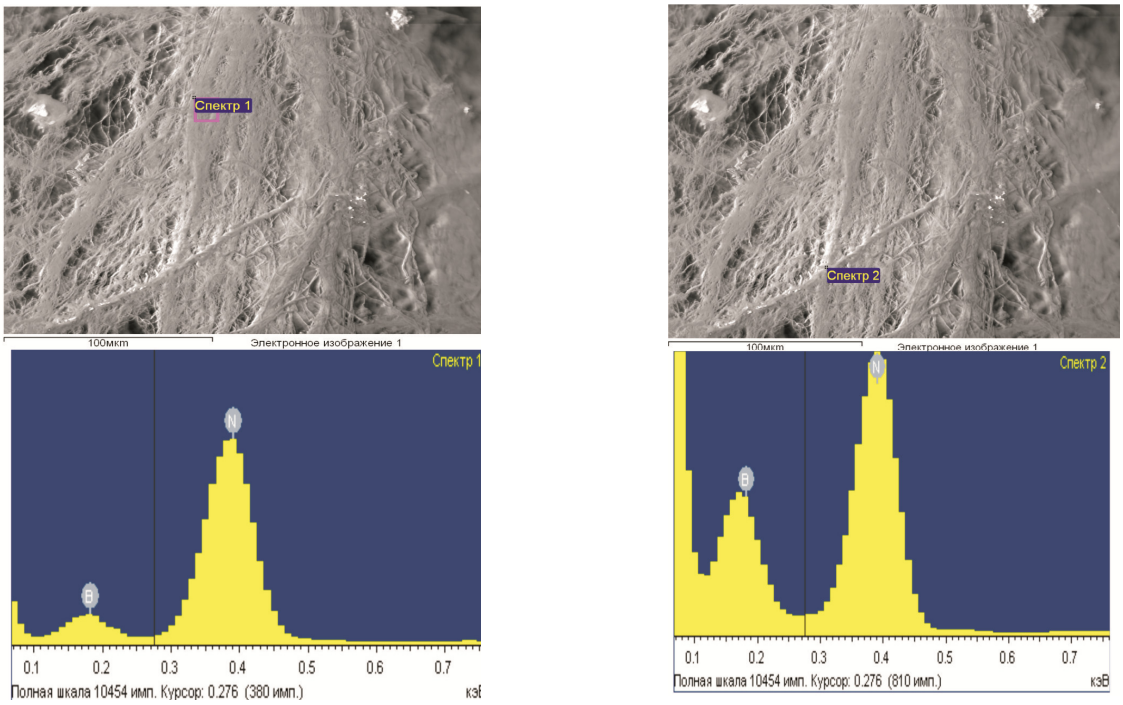

(а) (б)

Рисунок 2. Элементный состав вискерсов (нитей) с низкой (а) и высокой (б) концентрацией бора

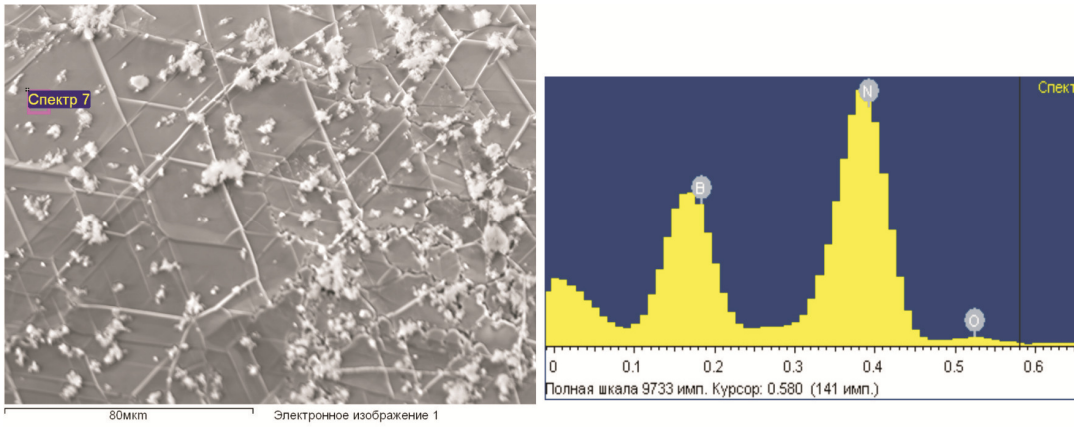

Рисунок 3. Поверхностная структура и элементный состав капли.

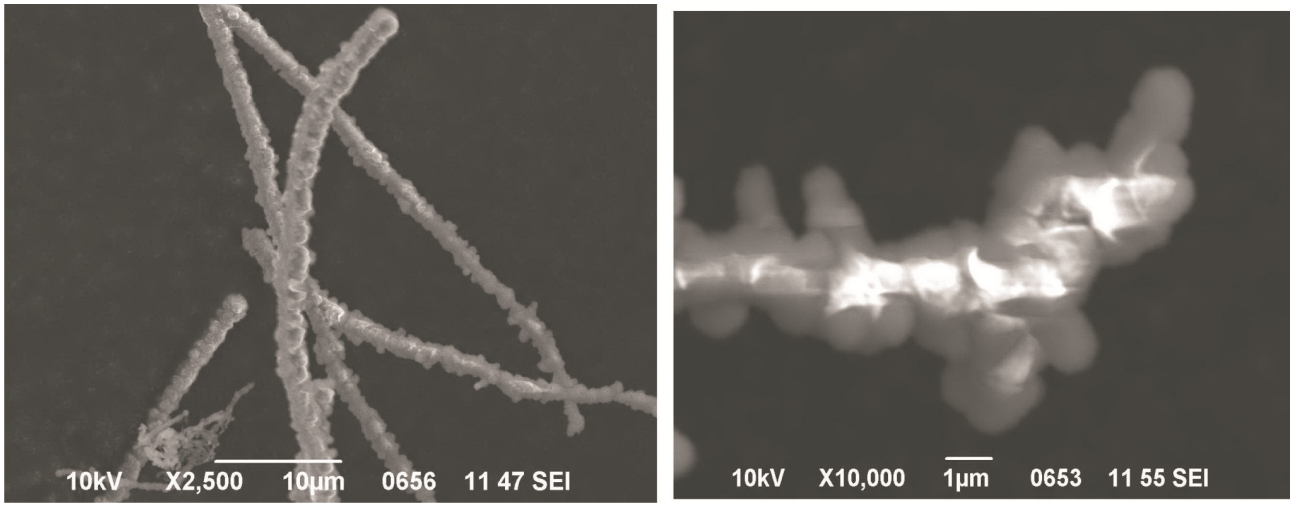

(а) **(б)**

Рисунок 4. Структура вершины вискерсов (нитей) при увеличениях (а) × 2500 и (б) × 10000.

Тщательное исследование вершин вискерсов показали, что они представляют собой отдельные переплетенные нити, полностью покрытые расплавленными капельками с вершиной, закрытой шляпкой (**рис. 4**). Интересно отметить, что элементный состав верхней и нижней частей вискерсов (нитей) имеет состав близкий по содержанию к элементному составу капли, поскольку включает кислород и повышенное содержание бора (**рис. 5**). Наличие кислорода в нижней части вискерсов (нитей) можно объяснить его присутствием в исходных порошках h-BN, а в верхней части – его движением вверх при нагреве и задержкой под шляпкой на своей вершине в связи с увеличением поверхностного натяжения при понижении температуры.Спектральная зависимость оптического поглощения исследовалась на порошках нитрида бора, образовавшихся при осаждении на кремниевую подложку вдали от кратера. Предыдущие исследования показали, что порошок состоит из равноосных, наноразмерных кристаллитов и нитевидных образований (**рис. 6**). По данным рентгенографического и электронно-микроскопического анализа, в осажденном материале присутствуют несколько модификаций нитрида бора – гексагональная фаза h-BN, две тетрагональные фазы с повышенным содержанием бора – $B_{25}N$ и $B_{51}N_2$, а также аморфная фаза [13, 15]. Такой состав существенно отличается от элементного состава вискерсов (нитей), что может свидетельствовать о том, что в процессе формирования покрытия структуры, уносимые потоком азота, не успевают доазотироваться из-за более низких температур на подложке.

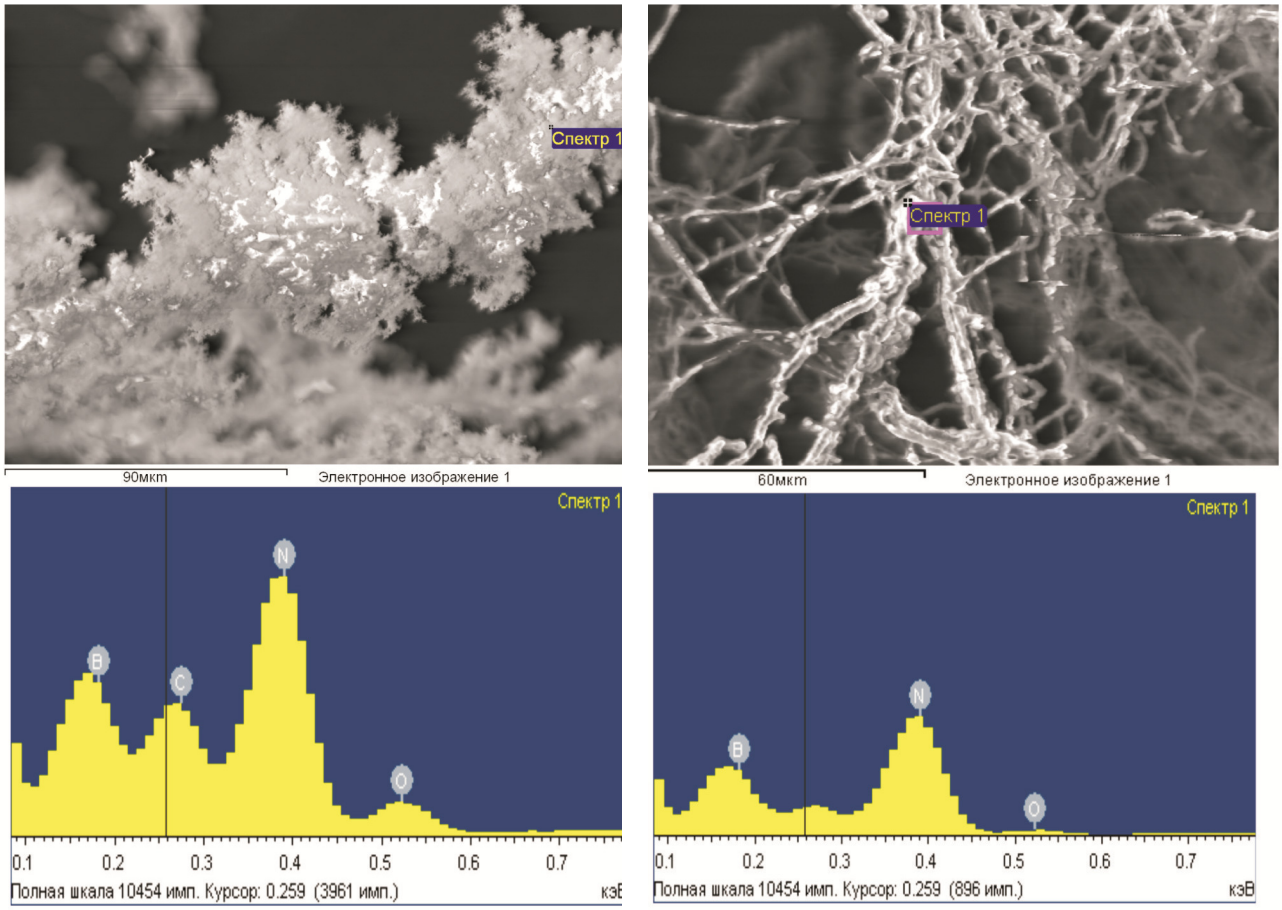

(а) (б)

Рисунок 5. Структура и элементный состав вискерсов (нитей) в верхней (а) и в нижней (б) частях.

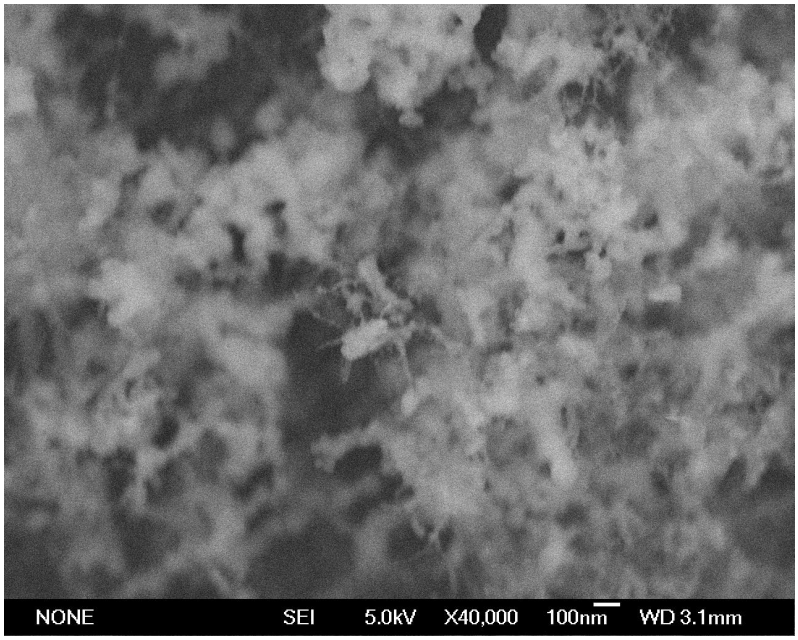

Рисунок 6. Структуры из нитрида бора, образуемые на поверхности кремниевой подложки.

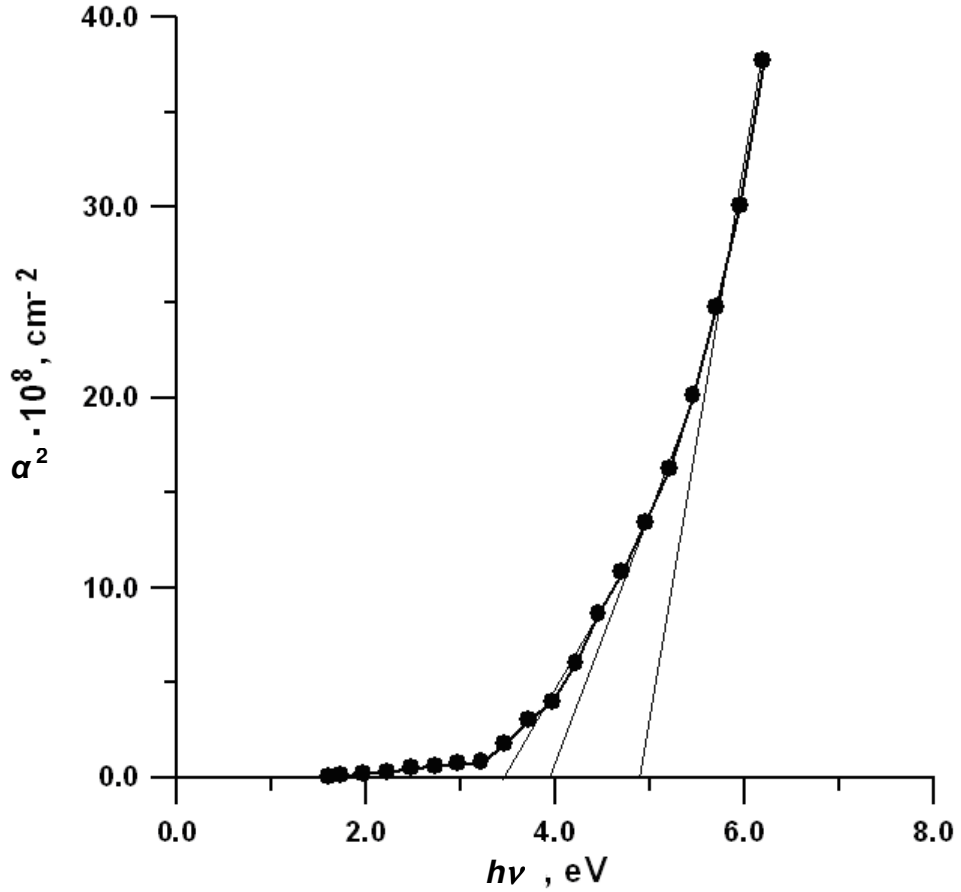

Рисунок 7. Зависимость квадрата коэффициента оптического поглощения покрытия с осажденного нитрида бора от энергии фотонов падающего света.

На графике зависимости квадрата коэффициента оптического поглощения α покрытия из осажденного порошка нитрида бора от энергии фотонов падающего света (**рис. 7**) можно выделить три прямолинейных участка. Они свидетельствуют о том, что в конденсате есть три фазы, в которых наблюдаются прямые разрешенные переходы между экстремумами валентной зоны и зоны проводимости, находящихся в одной точке ***k***-пространства. Ширина запрещенной зоны в соответствующих фазах, полученная экстраполяцией линейного участка на зависимости $\alpha^2 = f(h\nu)$ к оси абсцисс, где $h\nu$ – энергия фотонов падающего света, составила соответственно 3.5, 3.8 и 4.8 эВ. Величина 4.8 эВ попадает в интервал значений для ширины запрещенной зоны, которые приводятся в литературе как для массивного BN гексагональной модификации, так и BN нанотрубок. Линейный участок соответствующий 3.8 эВ, очевидно, можно объяснить присутствием тетрагональной фазы $B_{25}N$ с повышенным содержанием бора, а 3.5 эВ – тетрагональной фазой $B_{51}N_2$. Этот факт подтверждает экспериментально влияние собственных дефектов на электронную структуру нитридборных нанотрубок, которое исследовались методом линеаризованных присоединенных цилиндрических волн [16]. Рассматривались нанотрубки с протяженными дефектами замещения атома бора на атом азота и, наоборот, атома азота на атом бора с концентрацией примеси от 1.5 до 5 %. Было показано, что наличие таких дефектов существенно влияет на зонную структуру нитридборных нанотрубок и приводит к уменьшению ширины запрещенной зоны.

Таблица 1. Кинетическая энергия Оже-электронного спектроскопического перехода.

N	Элементы	ОЭС переход	Кинетическая энергия ОЭС перехода , эВ
1	Бор	KLL	179
2	Углерод	KLL	272
3	Азот	KLL	379
4	Кислород	KLL	508
5	Оксид алюминия	LMM	68

Известно, что метод Оже-электронной спектроскопии (ОЭС) основан на измерении кинетической энергии, испускаемой электронами, поэтому каждый элемент в образце, который изучается, представит характерный спектр пиков различных кинетических энергий. Количество выявленных Оже-электронов меняется в зависимости от рельефа. Топографические поправки могут быть сделаны только путем сравнения интенсивности различных элементов в одинаковых спектрах, так как влияние рельефа является одинаковым для всех элементов. Таким образом, интенсивность наших исследуемых элементов, входящих в состав порошков может отличаться от данных таблицы (**табл. 1**), которые были получены путем исследования плоских поверхностей материалов в твердом состоянии.

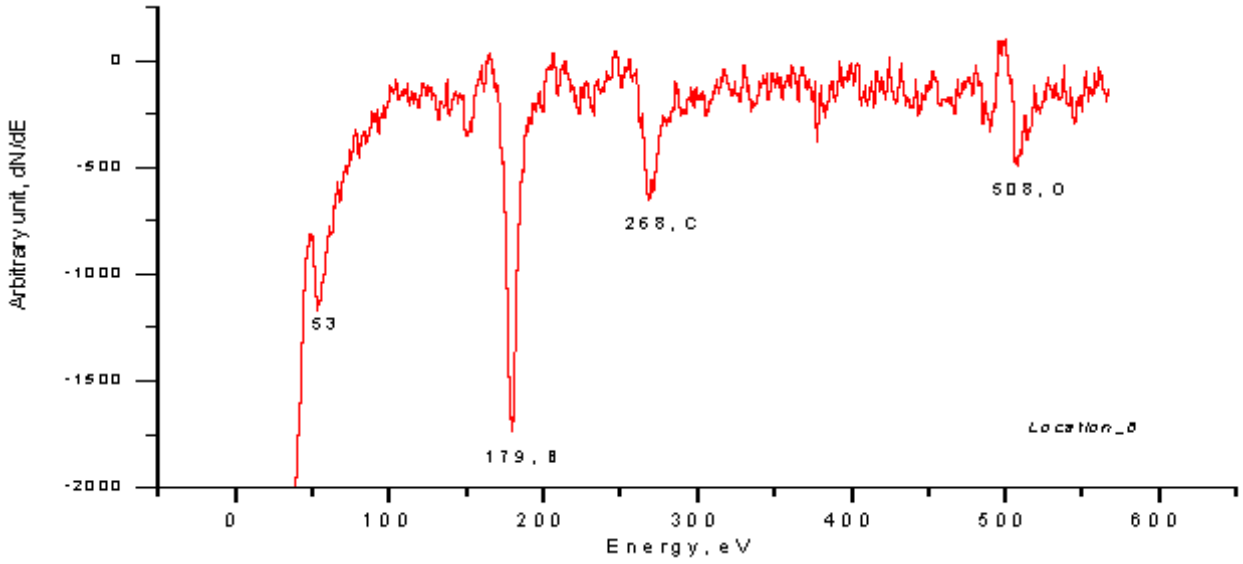

Рисунок 8. Дифференциальный Оже-спектр верхнего слоя поверхности порошка бора.

Предварительные расчеты дифференциальных Оже-спектров поверхности порошков бора (**рис. 8**) показали, что поверхность состоит из ~ 67 % бора, ~ 22 % углерода и ~ 11 % кислорода. ОЭС пики с участием валентных электронов несут значительную информацию о химическом состоянии поверхности. Химическое воздействие может проявиться как простым сдвигом пика, так и изменением формы пика, или и тем и другим. Поскольку бор исследуется в виде порошка, то такое состояние бора определяет смещение пика бора в сторону больших значений энергии по сравнению с данными **табл. 1** и сигналы дифференциальных Оже-спектров (**рис. 9**) из разных частей верхнего слоя

поверхности порошков бора имеют много шумов. Эти спектры ясно свидетельствуют о присутствии углерода и кислорода. Их пики смещены и имеются изменения в форме и интенсивности, поскольку способ получения порошка определяет его неоднородность. Если смещается пик углерода, то это означает наличие BC или Al_4C_3 на поверхности. Кислород обязательно присутствует в адсорбированном слое. Это свидетельствует о том, что порошки бора и алюминия имеют много кислорода и углерода на поверхности, которые могут быть компонентами таких соединений, таких как BC или Al_4C_3, CO, CO_2 и так далее.

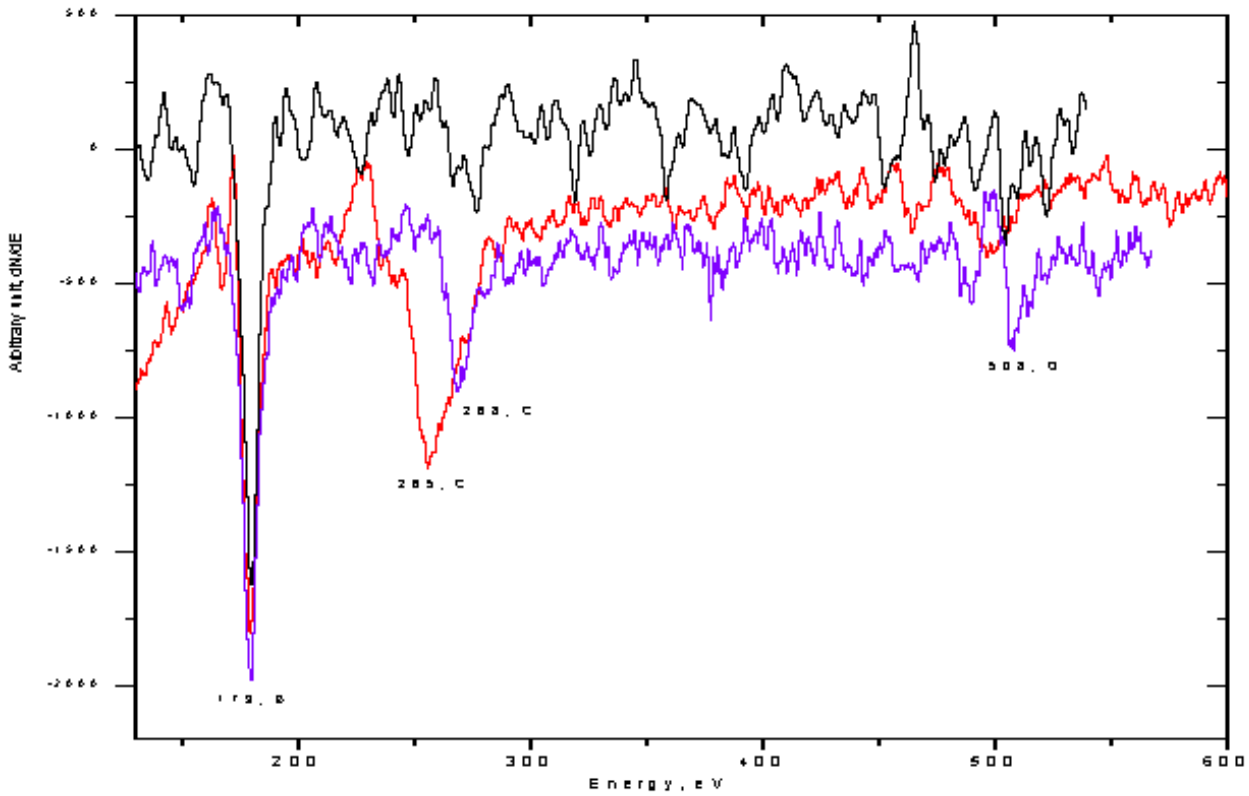

Рисунок 9. Дифференциальные Оже-спектры верхнего слоя поверхности порошка бора в различных точках.

Оже-спектроскопия исходных пластинчатых мелкозернистых порошков h-BN с примесями B_2O_3 подтвердила результаты рентгеноструктурного анализа [8, 13] о наличии достаточно большого количества кислорода на поверхности исходных порошков (**рис. 10**). Полуколичественные расчеты дифференциальных Оже-спектров поверхности порошков нитрида бора продемонстрировали, что их верхний слой состоит из ~ 13 % углерода, ~ 17 % кислорода, ~ 30 % бора, ~ 39 % азота. Содержание углерода на поверхности h-BN значительно меньше по сравнению с содержанием углерода на поверхности бора. Это может быть вызвано методом производства h-BN порошков. Расчеты дифференциальных Оже-спектров поверхности BN вискерсов (нитей) продемонстрировали, что их верхний слой состоит из ~ 23 % углерода, 4 % кислорода, 31 % бора, 42 % азота. В BN вискерсах (нитях) гораздо меньше кислорода (**рис. 11**). Наличие достаточно большого количества углерода на поверхности вискерсов (нитей), по сравнению с исходным нитридом бора можно объяснить с их более высокой активностью в адсорбции углеводородов и CO из

атмосферы. Появление расщепленного пика бора в исходных порошках h-BN и в BN вискерсах по сравнению с чистым нитридом бора указывает на влияние азота на изменение электронной структуры бора, т.е. на расщепление внутренней оболочки. Причем, изменение морфологии структуры нитрида бора приводит к более глубокому расщеплению (**рис. 11**). Оже-спектры поверхности BN вискерсов (нитей) также подтвердили их повышенное содержание азота.

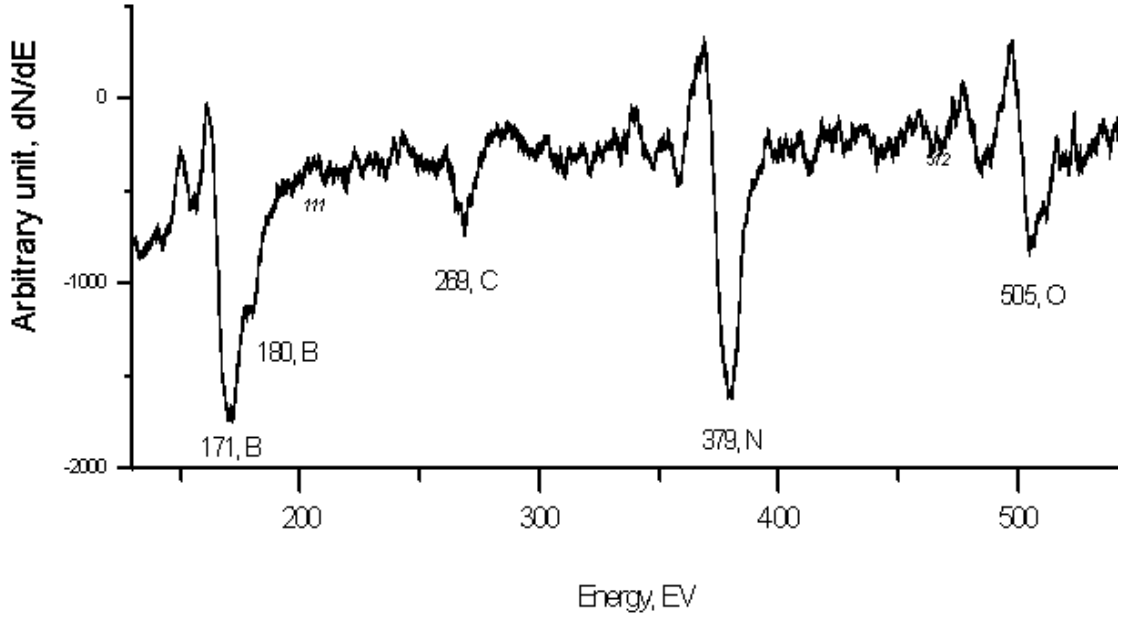

Рисунок 10. Дифференциальный Оже-спектр верхнего слоя поверхности исходных порошков мелкозернистого графитоподобного h-BN.

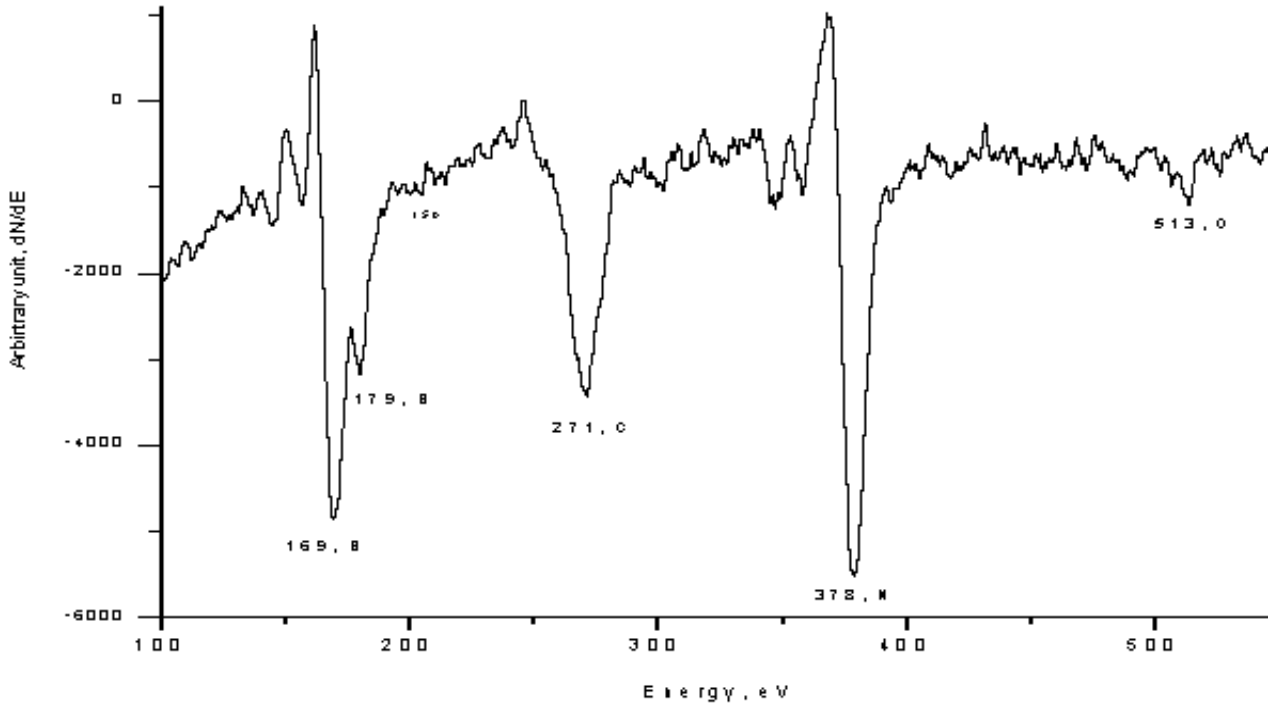

Рисунок 11. Дифференциальный Оже-спектр верхнего слоя поверхности вискерсов (нитей) из нитрида бора.

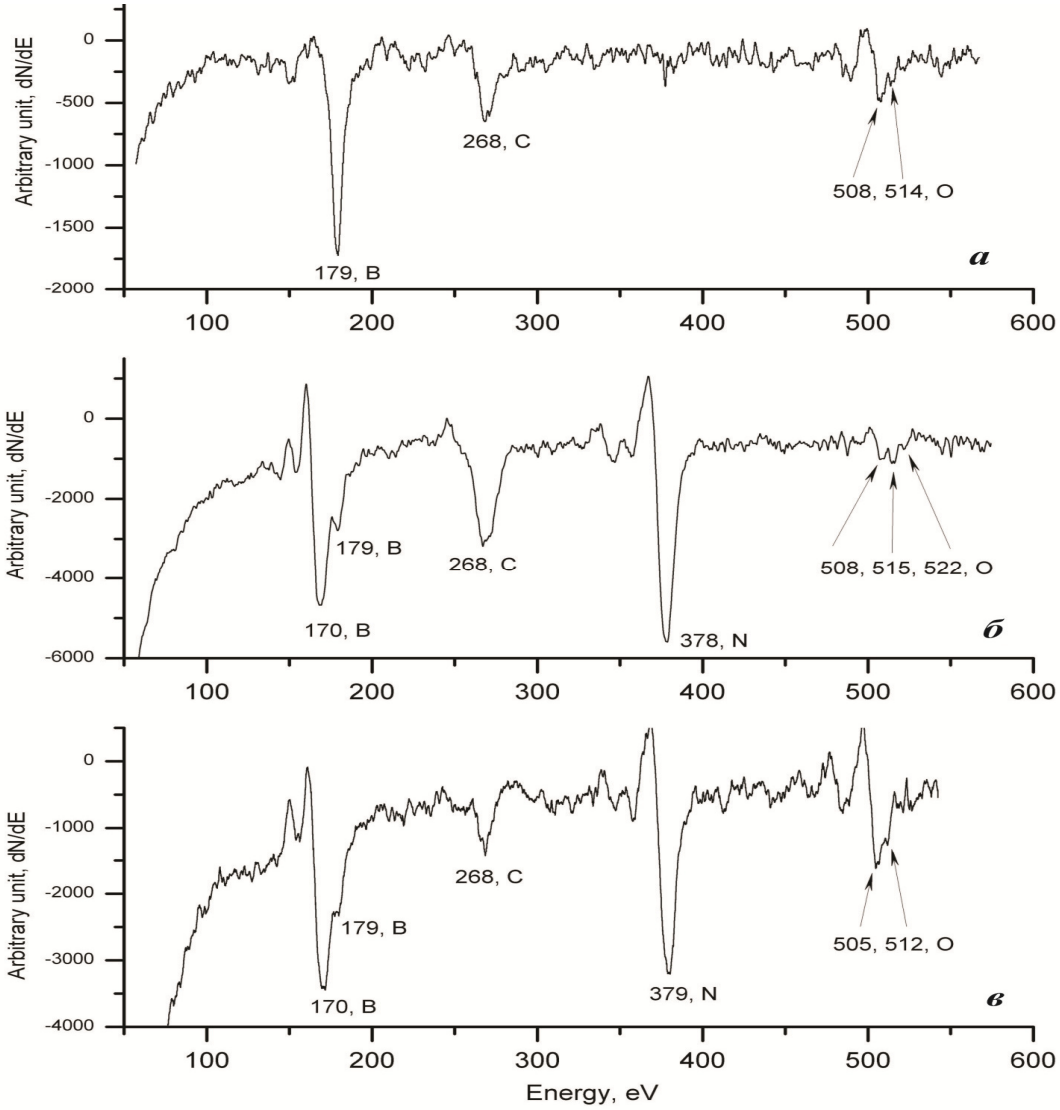

Рисунок 12. Оже-электронные спектры: бора (а), BN вискерсов (нитей) (б), исходного h-BN (в).

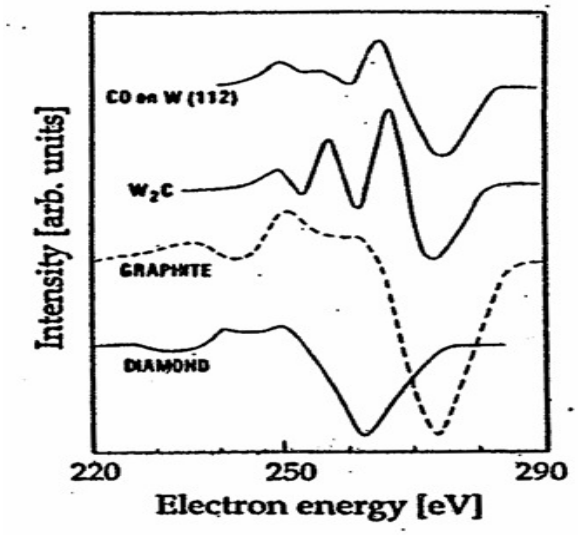

Рисунок 13. Оже-электронные спектры углерода в CO на W, W_2C, в графите и в алмазе [17].

Сравнение полученных дифференциальных Оже спектров бора, исходного порошка h-BN и BN вискерсов (нитей) (рис. 12) с электронными Оже-спектрами углерода в CO на W, W_2C, графите и алмазе [17] (**рис. 13**) позволяет объяснить сдвиг, изменение формы и интенсивности главных пиков бора, h-BN порошков и BN вискерсов (нитей). Смещение пиков бора в BN порошках и вискерсах демонстрирует наличие в них плотно упакованной структуры, что и приводит к снижению электронных уровней, как и в алмазе (**рис. 13**). Более того, плотно упакованная структура BN вискерсов (нитей) способствует появлению расщепленного пика бора через более глубокое расщепление электронных уровней (**рис. 12**). Сглаженный пик кислорода в BN вискерсах, подобный пикам CO на W (**рис. 13**), может свидетельствовать о том, что кислород адсорбирован.

Выводы

Таким образом, нагрев в фокальной зоне оптической печи повышенной мощности в потоке азота инициирует преобразование структуры графитоподобного h-BN в нанотрубки, вискерсы (нити) вокруг кратера и в капли на поверхности образца. Вискерсы (нити) в средней области имеют повышенное содержанке азота, а капли и вискерсы в начале и конце своей длины – повышенное содержание бора и кислорода. Различие в коэффициентах поверхностного натяжения, благодаря соответствующему элементному составу, и движение кислорода вверх в присутствии градиента температуры приводит к вытягиванию капли в трубку, поэтому движение кислорода является главной движущей силой, которая способствует образованию нитевидных структур.

Вдали от кратера, на поверхности кремниевой подложки, оседает порошковый материал с повышенным содержанием бора, состоящий из нитевидных образований - нанотрубок и вискерсов (нитей), равноосных наноразмерных кристаллитов, отдельных монокристаллов h-BN и тетрагональных фаз ($B_{25}N$) и ($B_{51}N_2$), а также аморфного нитрида бора. Для этого материала зависимость квадрата коэффициента поглощения от энергии фотонов падающего света в области собственного поглощения обнаружила 3 линейных участка, соответствующих ширин запрещенной зоны: 3.5, 3.8 и 4.8 эВ, отвечающих следующим фазам: тетрагональным $B_{51}N_2$ и $B_{25}N$, а также гексагональной BN, соответственно.

Метод Оже-электронной спектроскопии может служить для предварительной оценки, поскольку показывает различие в электронных структурах чистого бора и бора в h-BN и в BN вискерсах. Наличие азота приводит к снижению электронных уровней и к расщеплению пика бора благодаря более глубокому расщеплению электронных уровней, а преобразование h-BN в оптической печи без катализаторов снижает содержание кислорода в полученном материале.

Ссылки

1. E. Bengu, L. D. Marks. Single-walled BN nanostructures. Phys. Rev. Lett., 2001, 86, 11, 343- 347.
2. T. E. Mosuang, J. E. Lowther. Influence of defects on the h-BN to c-BN transformatio. Phys. Rev. B, 2002, 66, 14112-14119.
3. H. Hofsäss, H. Feldermann, S. Eyhusen, C. Ronning. Lattice location end annealing of ion implanted diamond. Phys. Rev. B, 2002, 65, 115410-115414.
4. I. Jiménez, A. F. Jankowski, L. J. Terminello, D. G. J. Sutherland, J. A. Carlisle, G. L. Doll, J. V. Mantese, W. M. Tong, D. K. Shuh, F. J. Himpsel. Core level photoabsorption study of defects and metastable bonding configurations in boron nitride. Phys. Rev. B, 1997, 55, 12, 25-31.
5. R. Gago, B. Abendroth, J. I. Cerdá, I. Jiménez, W. Möller. Detection of intrinsic stress in cubic boron nitride films by X-ray absorption near-edge structure: Stress relaxation mechanisms by simultaneous ion implantation during growth. Phys. Rev. B, 2007, 76, 174111-174116.
6. J.-D. Hecht, F. Frost, D. Hirsch, H. Neumann, A. Schindler, A. B. Preobrajenski, T. Chassé. Interstitial nitrogen induced by low-energy ion beam nitridation of A^{III}–B^{V} semiconductor surfaces. J. Appl. Phys, 2001, 90, 6066-6071.
7. M. Petravic, Q. Gao, D. Llewellyn, P. N. K. Deenapanray, D. Macdonald, C. Crotti. Broadening of vibrational levels in X-ray absorption spectroscopy of molecular nitrogen in compound semiconductors. Chem. Phys. Lett., 2006, 425, 262-266.
8. L. L. Sartinska, A. A. Frolov, A. Yu. Koval', N. A. Danilenko, I. I. Timofeeva, B. M. Rud'. Transformation of fine-grained graphite boron nitride induced by concentrated light energy. Mater. Chem. Phys., 2008, 109, 20-25.
9. A. A. Frolov, L. L. Sartinska, A. Yu. Koval'. Set-up for obtaining of nanostructure boron nitride by evaporation of concentrated solar radiation and condensation on the cooling surface. Proc. Int. Conf. Sci. Develop. Biosphere Process of the Arctic: Experience and Challenge of the Period, 2005, Apatity, 128-130.
10. J. Lander. Auger peaks in the energy spectra of secondary electrons from various materials. Phys. Rev., 1953, 91, 1382-1385.
11. K. Siegbahn. Electron spectroscopy for atoms, molecules and condensed matter. Nobel Lectures, 1, 1995, World Scientific, 63-70.
12. L. A. Harris. Analysis of materials by electron-excited. Auger electrons. J. Appl. Phys., 1968, 39, 1428-1434.
13. A. A. Frolov, L. L. Sartinska, A. Yu. Koval', N. A. Danilenko. Application of the optical furnace for nanosized boron nitride production. Nanomaterials, 2008, 2-4, 48-56.
14. L. A. Harris. Analysis of materials by electron-excited. Auger electrons. J. Appl. Phys., 1968, 39, 1428-1434.
15. L. L. Sartinska, V. A. Tinkov, A. A. Frolov. Oxygen and structure transformations of h-BN in focal zone of an optical furnace. Mod. Prob. Phys. Mater. Sci., 2009, Kiev: Digest NASU IPMS, 56-62.

16. A. Yu. Golovacheva, P. N. D'yachkov. Effect of intrinsic defects on the electronic structure of BN nanotubes. JETP Lett., 2005, 82, 11, 737-741.
17. A. W. Czanderna. Methods of Surface Analysis. 1975, Amsterdam: Elsevier Sci. Publ. Co.

ТОЧНЫЕ УРАВНЕНИЯ ДЛЯ КОРРЕЛЯЦИОННЫХ ФУНКЦИЙ ПОДСИСТЕМЫ ВЗАИМОДЕЙСТВУЮЩЕЙ С ТЕРМОСТАТОМ И ИХ ПРИМЕНЕНИЕ В ТЕОРИИ ЛИНЕЙНОГО ПЕРЕНОСА ПОЛЯРОНОВ

Б. Котия

Грузинский технический университет
Тбилиси, Грузия
bejankot@hotmail.com

Принята 1 июля 2012 года

1. Введение

Исследование кинетики малой подсистемы (частицы) взаимодействующей с квантованным полем (термостатом) представляет собой важную проблему квантовой теории поля и физики конденсированного состояния. Электрон в полярном (ионном) кристалле (полярон) представляет широко известный пример такой системы [1].

Удобным способом изучения релаксационных процессов и поведения частицы, взаимодействующей с термостатом под влиянием приложенного поля является метод корреляционных функций и функций Грина [2].

Двухвременные равновесные корреляционные функции являются основными величинами в теории линейного переноса Кубо [3]. Эта теория свободна от ограничений на процессы рассеяния (например, в случае взаимодействия электронов с примесями или с фононным полем в кристалле), в отличии от подхода, основанного на уравнении Больцмана, для которого процессы рассеяния должны быть хорошо разделены в пространстве и во времени [4]. Однако, при вычислении электропроводности $\sigma(\omega)$ (ω – частота приложенного электрического поля) согласно формуле Кубо (а также при вычислении корреляционной функции ток–ток) возникают трудности, обусловленные расходимостью членов разложения $\sigma(\omega)$ по взаимодействию электрона с рассеивателями при частоте $\omega \to 0$. Даже в случае слабого взаимодействия для получения правильного результата для проводимости на постоянном токе (dc) при $\omega \to 0$, необходимо просуммировать бесконечный ряд расходящихся членов (правилный порядок предельных переходов при таких вычислениях является переход $\lim_{\alpha\to 0}\lim_{\omega\to 0}$ [5], где α – это константа взаимодействия электронов с фононами). Существует большое количество работ по подвижности полярона, учитывающих различные апроксимации при вычислении корреляционной функции ток–ток (см. [6]). Однако, эти результаты для низкотемпературной подвижности полярона отличаются от результатов, найденных с помощью уравнения Больцмана [6].

Вышеуказанные трудности можно обойти, пользуясь вместо корреляционной функции эволюционным уравнением для корреляционной функции. Обобщенные уравнения эволюции для матрицы плотности и для корреляционных функций

подсистемы, взаимодействующей с квантованным бозонным полем (термостатом) были найдены в [7 – 11].

Уравнение Больцмана для статистического оператора, как и соответствующие приближенные уравнения для корреляционных функций подсистемы, следуют из точных уравнений, найденных в случае слабого электрон–фононного взаимодействия и слабого внешнего электрического поля. Приближенные уравнения эволюции были выведены также [10, 11] в случае сильного (произвольного) электрон–фононного взаимодействия в рамках модели Фейнмана для полярона [12].

Единственная апроксимация, которая используется при выводе обобщенных уравнений эволюции, является приближение случайных фаз (ПСФ) (в начальный момент времени t = 0 подсистема и термостат не взаимодействуют друг с другом или фактор Гибсса в двухвременной равновесной корреляционной функции апроксимируется произведением распределений Гибсса для подсистемы и термостата). Однако не очевидно, что результаты будут одинаковыми при различных начальных условиях.

В настоящей работе выведены новые, точные уравнения для корреляционных функций подсистемы, взаимодействующей с бозонным полем (с термостатом). Приближение случайных фаз (распределение в виде произведений) не используется при выводе этих уравнений. С помощью найденных уравнений рассмотрены корреляционные функции для электрон–фононной системы и развита теория электропроводности в рамках линейной теории переноса Кубо [3]. В частности построена последовательная теория подвижности полярона при низких температурах. Обсуждается также влияние начальных корреляций на процесс релаксации и на проводимость.

Работа организована следующим образом. Во второй части мы вводим корреляционные функции подсистемы, функций Грина, лиуввиллевский супероператорный формализм, технику проекционного оператора и выводим точные уравнения (не используя ПСФ) для корреляционных функций подсистемы, взаимодействующей с большой равновесной системой (с квантованным бозонным полем). Описывается процедура исключения операторов (амплитуд) бозонного поля и рассматривается переход к марковским уравнениям во втором приближении теории возмущений.

В третьей части рассматривается электрон–фононная система. Вводятся корреляционные функции ток–ток (скорость–скорость), которые определяют тензор электропроводности в теории линейнного переноса Кубо. На основе формализма развитой во 2-й части, в этой части мы выводим уравнения для корреляционных функций скорость–скорость для электрона слабо взаимодействующего с фононами и со слабым однородным внешним электрическим полем. В случае однозонной модели выведенные уровнения решаются в квадратурах в приближении времени релаксации (ПВР) и являются точными при низких температурах.

Соответственно, найденное выражение для тензора электропроводности пригодно для произвольного закона дисперсии электронов и фононов и при произвольных температурах. В этой части обсуждается также процесс релаксации и вклад начальных корреляций в этот процесс (в ПСФ начальные корреляции отсуствуют).

В четвертой части рассматривается проводимость медленно движущегося фрелиховского полярона (случай низких температур). Найден обобщенный результат Осака для проводимости (формула Друде), который содержит поправочный член от

начальных корреляций. Получено правильное выражение для низкотемпературной подвижности полярона.

В пятой части работы приводится дальнейшее обсуждение полученных результатов.

2. Уравнение для корреляционной функции

Рассмотрим динамическую подсистему S взаимодействующую с бозонным полем Σ. Гамильтониан всей системы (S+Σ) возьмем в виде:

$$H = H_s + H_\Sigma + H_i, \quad (1)$$

где H_s, H_Σ и H_i соответственно гамильтонианы подсистемы, бозонного поля и взаимодействия между ними.

$$H_\Sigma = \sum_k \hbar\omega(k) b_k^+ b_k,\ H_i = \sum_k [C_k(S) b_k + C_k^+(S) b_k^+]. \quad (2)$$

Здесь $\hbar\omega(\bar{k})$ энергия кванта бозонного поля, характеризующаяся квантовыми числами $\bar{k}$; b_k; b_k^+ – бозе-операторы уничтожения и рождения бозона в состоянии $\bar{k}$; $C_k(S)$ и $C_k^+(S)$ операторы принадлежащие подсистеме S. Бозонная система рассматривается как термостат.

Определим двухвременную корреляционную функцию F(t) и функции Грина $G^r(t)$, $G^a(t)$, $G^c(t)$ (запаздывающую, опережающую и причинную), от операторов A_s и B_s подсистемы в виде (см., например [2]):

$$F(t) = \langle A_S(t), B_S(0)\rangle,$$
$$G^r(t) = \theta(t)\langle [A_s(t), B_s(0)]_\eta\rangle,$$
$$G^a(t) = -\theta(-t)\langle [A_s(t), B_s(0)]_\eta\rangle,$$
$$G^c(t) = \frac{1}{i\hbar} \langle T\eta\{A_S(t)B_S(0)\}\rangle. \quad (3)$$

Здесь $A_s(t) = e^{\frac{i}{\hbar}Ht} A_s(0)\, e^{\frac{-i}{\hbar}Ht}$, $\langle \cdots \rangle$ – усреднение по равновесному ансамблю:

$$\langle \cdots \rangle = \mathrm{Tr}\{e^{-\beta H} \ldots\} Z^{-1},$$
$$Z = \mathrm{Tr}\, e^{-\beta H},\ \beta = \frac{1}{K_B T},$$
$$\theta(t) = 1 \text{ при } t > 0 \text{ и } \theta(t) = 0 \text{ при } t < 0,$$
$$[A_s(t), B_s(0)]_\eta = A_s(t)B_s(0) - \eta B_s(0)A_s(t),$$
$$T_\eta\{A_S(t)B_S(0)\} = \theta(t)A_s(t)B_s(0) + \eta\theta(-t)B_s(0)A_s(t),$$

$\eta=1$ если A_s и B_s бозе операторы и $\eta = -1$ для Ферми-операторов.

Запишем корреляционную функцию F(t) в следующем виде:

$$\langle A_s(t)B_s(0)\rangle = Z^{-1} Tr_{(S,\Sigma)}[B_s(0)\, e^{-\beta H} e^{iLt} A_S(0)]. \quad (4)$$

Здесь мы ввели лиувиллевский супероператор L, действующий на произвольный оператор D по правилу

$$LD = \frac{1}{\hbar}[H, D],$$
$$e^{\pm iLt} D\,(0) = e^{\pm\frac{i}{\hbar}Ht} D\,(0)\, e^{\mp\frac{i}{\hbar}Ht} \equiv D(\pm t)$$

($L = L_s + L_\Sigma + L_i$ – соответственно членам гамильтониана (1)), $Tr_{(S,\Sigma)}$ – след по состояниям всей системы $(S+\Sigma)$.

Из выражения (4) видно, что динамику корреляционной функций удобно рассматривать с помощью следующих супероператоров, действующих на оператор D, как:

$$R(t)D = Z^{-1} Tr_{(\Sigma)}[\, e^{-\beta H} e^{iLt} PD],$$

$$I(t)D = Z^{-1}Tr_{(\Sigma)}[\, e^{-\beta H}e^{iLt}QD], \quad (5)$$

где P – проекционный оператор ($P^2 = P$) усреднения по состояниям термостата (бозонного поля):

$$PD = Tr_{(\Sigma)}(\rho_\Sigma D) \equiv < D >_\Sigma,\ \rho_\Sigma = Z^{-1}_{(\Sigma)}e^{-\beta H_\Sigma},\ Z_{(\Sigma)} = Tr_{(\Sigma)}e^{-\beta H_\Sigma},\quad Q = 1 - P. \quad (6)$$

Выражение (3) для корреляционной функций F(t) можно записать в виде:

$$< A_s(t)B_s(0) > = < A_s(0)B_s(-t) > = Tr_{(S)}[B_s(0)R(t)A_s(0)]. \quad (7)$$

Нетрудно получить точные уравнения для супероператоров R(t) и I(t). Имеем:

$$\frac{\partial}{\partial t}R(t) = iR(t)\ PLP + iI(t)\ QLP, \quad (8)$$

$$\frac{\partial}{\partial t}I(t) = iI(t)\ QLQ + iR(t)PLQ.$$

Интегрируя уравнение (8) для супероператора I(t) мы находим следующее выражение:

$$I(t) = I(0)\ M_Q(t) + i\int_0^t d\tau R(\tau)PLQM_Q(t-\tau)\ , \quad (9)$$

где

$$I(0) = Z^{-1}Tr_{(\Sigma)}e^{-\beta H_\Sigma}Q \quad (10)$$

– начальное значение супероператора $\bar{I}(t)$ и

$$M_Q(t) = \exp(iQLQt)$$

– “массовый” супероператор.

Подставляя выражение (9) для супероператора I(t) в первое уравнение (8), мы находим точное неоднородное эволюционное уравнение для супероператора:

$$\frac{\partial}{\partial t}R(t) = iR(t)\ PLP + iI(0)M_Q(t)QLP - \int_0^t d\tau R(\tau)PLQM_Q(t-\tau)\ QLP \quad (11)$$

Полученное уравнение определяет уравнение для корреляционной функций (7). Используя определение (5) и возможность циклической перестановки операторов под знаком операций $Tr_{(S,\Sigma)}$ мы находим из выражений (7) и (11) следующее уравнение для корреляционной функции:

$$\frac{\partial}{\partial t} < A_s(0)B_s(-t) > = i < [PLPA_s(0)]B_s(-t) > +$$

$$QM_Q(t)QLPA_s(0)]B_s(0) > - \int_0^t d\tau < [PLQM_Q(t-\tau)\ QLPA_s(0)]B_s(-\tau) > . \quad (12)$$

Уравнения (11) и (12) являются точными немарковскими уравнениями эволюции для супероператора R(t) и корреляционной функций (3). Неоднородные члены в этих уровнениях (вторые члены в правых частях (11) и (12)) описывают влияние начальных (предсталкновительных) корреляций во времени, которые обусловлены взаимодействием между подсистемой S и термостатом Σ (бозонного поля) в начальный момент времени t = 0. Поэтому при решении начальной задачи (задачи Коши) для уравнения (11) (и, таким образом, для нахождения корреляционной функции) нам понадобится знание не только R(0), но и также I(0). Если память о начальных корреляциях со временем исчезает, то тогда в эволюции доминирует влияние столкновений. Однако, в принципе, присутствие предстолкновительного члена корреляции, связанного с I(0), влияет на релаксационный процесс, описываемый с помощью корреляционной функций F(t) даже при слабом взаимодействии подсистемы с термостатом. Как будет видно из дальнейшего изложения, начальные корреляции дают вклад в кинетический коэффициент переноса (в проводимость) подсистемы S' (электрона).

Удобно исходить из точного однородного уравнения эволюции, в котором начальные корреляции содержатся в неявном виде. Для нахождения такого уравнения воспользуемся известным интегральным операторным тождеством:

$$e^{-\beta H} = e^{-\beta H_0} - \int_0^\beta d\lambda e^{-\beta H}e^{\lambda H}H_1\ e^{-\lambda H_0}, \quad (13)$$

где $H = H_s + H_\Sigma$. Тогда нетрудно показать, что имеет место система уравнений для супероператоров I(t) и I(0), вытекающая из уравнения (9) и уравнения

$$I(0) = -R(t)L_Q(t,\beta) - I(t)L_Q(t,\beta), \quad (14)$$

которое следует из (13) и начального условия (10) для I(t). Здесь мы ввели интегральный супероператор, определяемый равенством

$$L_Q(t,\beta) = \int_0^\beta d\lambda e^{-iLt} e^{\lambda H} H_1 e^{-\lambda H_0} Q. \quad (15)$$

Решив уравнения (9) и (14) относительно I(0) и подставив в (11), мы найдем искомое точное однородное замкнутое уравнение для супероператора $R(t)$:

$$\frac{\partial}{\partial t} R(t) = iR(t)\,PLP - iR(t)PL_Q(t,\beta)\left[1 + M_Q(t)L_Q(t,\beta)\right]^{-1} M_Q(t)QLP +$$
$$+ \int_0^t d\tau R(\tau)PLQM_Q(t-\tau)\,L_Q(t,\beta)\left[1 + M_Q(t)L_Q(t,\beta)\right]^{-1} M_Q(t)QLP -$$
$$- \int_0^t d\tau R(\tau)PLQM_Q(t-\tau)QLP. \quad (16)$$

Заметим, что выведенные уравнения можно упростить, пользуясь нижеследующими общими соотношениями:

$$L_\Sigma P = 0,\ PL_sQ = QL_sP = 0,\ PL_iP = 0. \quad (17)$$

Наконец, используя (16) и (17), имеем вместо (12) следующее точное уравнение для корреляционной функций:

$$\frac{\partial}{\partial t} < A_s(0)B_s(-t) > = i < [PL_sPA_s(0)]B_s(-t) > -$$
$$-i\left\{PL_Q(t,\beta)\left[1 + M_Q(t)L_Q(t,\beta)\right]^{-1} M_Q(t)QL_iPA_s(0)\right\} B_s(-t) > +$$
$$+ \int_0^t d\tau < \left\{PL_iQM_Q(t-\tau)L_Q(t,\beta)\left[1 + M_Q(t)L_Q(t,\beta)\right]^{-1} M_Q(t)QL_iPA_s(0)\right\} B_s(-\tau) -$$
$$- \int_0^t d\tau < [PL_iQM_Q(t-\tau)QL_iPA_s(0)]B_s(-\tau) >. \quad (18)$$

Уравнения (16) и (18) являются достаточно сложными. Эволюция начальных корреляций описывается интегральным супероператором $L_Q(t,\beta)$ (15) и входит в уравнения как в марковской, так и в немарковской формах (второй и третий члены в правых частях (16) и (18)). В ПСФ, когда мы берем в корреляционной функций (4) $e^{-\beta H_0}$ вместо $e^{-\beta H}$, $\bar{I}(0)=0$, как это видно из (5) и (6) ($PQ = 0$), что ведет к раветству нулю $L_Q(t,\beta)$ и к исчезновению членов в (16) и (18), связанных с начальными корреляциями. Как следствие, мы получаем уравнение для корреляционной функции, найденное в [9, 11].

Уравнения для функций Грина (3) следуют из уравнениия (18). Так, для запаздывающей функции Грина мы имеем:

$$\frac{\partial}{\partial t} G^r(t) = \delta(t) < [A_s(t)B_s(0)]_\eta > + \theta(t)\frac{\partial}{\partial t} < A_s(0)\,B_s(-t) > - \eta\eta\theta(t)\frac{\partial}{\partial t} < B_s(0)A_s(t) >$$

и уравнение для корреляционной функций $< A_s(0)\,B_s(t) >$ можно наити из (18), используя подстановку $t \to -t$.

Супероператоры в уравнении (18) можно разложить в ряды по Li(Hi) с помощью следующих разложений:

$$\left[1 + M_Q(t)L_Q(t,\beta)\right]^{-1} = \sum_{k=o}^{\infty}(-1)^k\left[M_Q(t)L_Q(t,\beta)\right]^k, M_Q(t) = \sum_{n=o}^{\infty} M_Q{}^{(n)}(t),$$
$$M_Q{}^{(0)}(t) = e^{iL_0t},$$
$$M_Q{}^{(n)}(t) = \int_0^t dt_1 \int_0^{t_1} dt_2 \ldots \int_0^{t_{n-1}} dt_n\, e^{iL_0(t-t_1)}iQLi\, e^{iL_0(t_1-t_2)}iQLi \ldots e^{iL_0(t_{n-1}-t_n)}iQLie^{iL_0t_n},$$
$$n=1,2,3,\ldots,$$
$$e^{-iLt} = e^{-iL_0t}\,T\exp\left[-i\int_0^t Li(\xi)d\xi\right];\ e^{\lambda H} = e^{\lambda H_0}T'\exp\left[\int_0^\lambda Hi(\gamma)d\gamma\right],$$
$$Li(\xi) = e^{iL_0\xi}Lie^{-iL_0\xi}, H_i(\gamma) = e^{-iH_0}H_ie^{\gamma H_0}, L_0 = L_s + L_\Sigma, \quad (19)$$

где T и T′ означают упорядочивание операторов соответственно по переменным ξ и γ.

При слабом S – Σ взаимодействии разложения (19) можно рассматривать формально как ряды теории возмущений и вычислять члены в правых частях уравнений (16) и (18) с требуемой точностью. Нетрудно видеть, что при таком разложении по взаимодействию в случае H_Σ и H_i вида (2) в уравнении (18) отличными от нуля будут только средние $< \cdots >_\Sigma$, содержащие одинаковое количество операторов рождения и уничтожения бозонов и сводятся к величинам, пропорциональным произведениям средних чисел заполнения бозонов. Таким образом, бозонные (фононные) операторы полностью исключаются из уравнения (18).

Допустим, что из-за (вследствии) слабого взаимодействия между подсистемой S и термостатом Σ имеет место иэрархия времен:

$$\tau_{rel} \gg t_0 = \max(t_s, t_\Sigma), \qquad (20)$$

где τ_{rel} – характерное время релаксации подсистемы, t_s – время столкновений для подсистемы и t_Σ – время корреляции флуктуации в термостате.

Неравенство (20) позволяет нам совершить марковское приближение в уравнениях (16) и (18). Ограничиваясь вторым приближением теории возмущений по $H_i(L_i)$ и используя разложения (19), совершим следующие апроксимации:

$$\left[1 + M_Q(t)L_Q(t,\beta)\right]^{-1} => 1,$$
$$M_Q(t) => M_Q^{(0)}(t) = e^{iL_0 t},$$
$$L_Q(t,\beta) => L_Q^{(0)}(t,\beta) = \int_0^\beta d\lambda e^{iL_0 t} e^{\lambda H_0} H_i e^{-\lambda H_0} Q,$$
$$B_S(-\tau) => e^{iL_0(t-\tau)} B_S(-t).$$

Тогда (18) принимает следующий, более простой вид марковского уравнения:

$$\frac{\partial}{\partial t} < A_S(0)B_S(-t) >= i < [L_S A_S(0)]B_S(-t) > -i\int_0^\beta d\lambda < [P e^{iL_0 t} e^{\lambda H_0} H_i e^{-\lambda H_0} e^{iL_0 t} L_i A_S(0)]B_S(-t) > -$$
$$- \int_0^t d\tau < \left[P L_i e^{iL_0(t-\tau)} L_i A_S(0)\right] e^{iL_0(t-\tau)} B_S(-t) >. \qquad (21)$$

Используя явный вид (2) гамильтонианов H_Σ и H_i и исключая из (21) бозонные операторы с помощью процедуры описанной выше, находим уравнение для корреляционной функции в окончательном виде:

$$\frac{\partial}{\partial t} < A_S(0)B_S(-t) >= -\frac{i}{\hbar} < [A_S, H_S]_- B_S(-t) >$$
$$- \frac{i}{\hbar^2}\int_0^t d\xi \sum_k \{ e^{i\omega\omega(k)\xi} N_k < [[A_S C_k^+(S)]_- C_k(S,-\xi)]_- \omega\omega(k) B_S(-t) > + e^{-i\omega(k)\xi}(1+N_k) <$$
$$[[A_S, C_k(S)]_- C_k^+(S,-\xi)]_+ \omega(k) B_S(-t) > \} + \frac{i}{\hbar}\int_0^\beta d\lambda \sum_k \{ e^{i\omega\omega(k)(t+i\hbar\lambda)} N_k << C_k^+(S,-t-$$
$$i\hbar\lambda)[A_S, C_k(S)]_- B_S(-t) > + e^{i\omega\omega(k)(t+i\hbar\lambda)}(1+N_k) <$$
$$< C_k(S,-t-i\hbar\lambda)[A_S, C_k^+(S_i)]_- B_S(-t) > \}, \qquad (22)$$

где $N_k = \left[e^{\beta\hbar\omega\omega(k)} - 1\right]^{-1}$ – среднее число заполнения бозонов (фононов),

$$C_k(S, \pm Z) = e^{\pm L_s Z} C_k(S);\ C_k^+(S_i \pm Z) = e^{\pm L_s Z} C_k^+(S);$$

$[E, D]_{\pm\omega\omega(k)} = ED - e^{\mp\beta\hbar\omega(k)} DE$ – для произвольных операторов E и D. $A_S \equiv A_S(0)$.

При выводе уравнения (22) мы пользовались также сдедующими соотношениями:

$e^{\pm L_\Sigma t} b_k = e^{\mp i\omega\omega(k)t} b_k$, $e^{\pm L_\Sigma t} b_k^+ = e^{\pm i\omega\omega(k)t} b_k^+$, $P(b_k^+, b_{k'}) = N_{k'}\delta_{kk'}$, $P(b_k, b_{k'}^+) = (1+N_k)\delta_{kk'}$, $P(b_k b_{k'}) = P(b_k^+, b_{k'}^+) = 0$.

Легко найти также уравнение для корреляционной функции $< A_S(0)B_S(t) >$ с помощью подстановки $t \to -t$ в уравнение (22).

Уравнение (22) отличается от ранее полученного подобного уравнения в ПСФ [9, 11], третьим членом в правой части, который описывает влияние начальных корреляций.

3. Электрон–фонноная система

Рассмотрим следующий, более специфический случай взаимодействия частицы с квантованным полем, который описывается гамилтонианом (1 – 2) с

$$H_S = T(\vec{P}),\ C_{\vec{k}}(S) = V_{\vec{k}} e^{i\vec{k}\vec{r}}, \quad (23)$$

где $T(\vec{P})$ – кинетическая энергия частицы с импульсом $\vec{P}$, $\vec{r}$ – радиус-вектор частицы, $V_{\vec{k}}$ – энергия взаимодействия частицы с полем, соотвествующая кванту $\hbar\omega(\vec{k})$, характеризуемое волновым вектором $\vec{k}$ (в (2) k мы рассмотриваем как вектор).

Для полярона Фрелиха (электрон, движущийся в ионном кристалле и взаимодействующий с фононами) имеем:

$$T(\vec{P}) = \frac{\vec{P}^2}{2m^*},\ V_{\vec{k}} = i\frac{\hbar\omega(\vec{k})}{kU^{1/2}}\left(\frac{4\pi\alpha}{V}\right)^{1/2},\ U=\left(\frac{2m^*\omega\omega(\vec{k})}{\hbar}\right)^{1/2},\ \alpha = \frac{1}{2}\left(\frac{1}{\varepsilon_\infty}-\frac{1}{\varepsilon_0}\right)\frac{e^2U}{\hbar\omega(\vec{k})}, \quad (24)$$

где α – безразмерная константа связи электрон-фононного взаимодействия, m^* и e- эффективная масса электрона в кристалле и заряд электрона, V – обьем системы, $\omega\omega(\vec{k}) = \omega\omega_0$ – если рассматривается взаимодействие электрона только с оптической модой колебаний ионов.

Величина, представляющая интерес с точки зрения физики – это тензор проводимости. При слабом приложенном электрическом поле частоты ω тензор электропроводности можно выразить через корреляционную функцию ток-ток. Согласно формуле Кубо [3] диссипативную часть тензора проводимости можно представить в виде:

$$Re\sigma^S_{\mu\nu}(\omega) = \frac{1}{E_\beta(\omega\omega)}\int_0^\infty dt\cos(\omega\omega t)\psi^S_{\mu\nu}(t),\ E_\beta(\omega\omega) = \frac{\hbar\omega\omega}{2}cth\left(\frac{\beta\hbar\omega\omega}{2}\right), \quad (25)$$

где $\sigma^S_{\mu\nu}(\omega\omega)$ и $\psi^S_{\mu\nu}(t)$ – симметрические части тензора проводимости $\sigma_{\mu\nu}(\omega\omega)$ и корреляционной функции $\psi_{\mu\nu}(t)$ соответственно,

$$\sigma^S_{\mu\nu}(\omega\omega) = \frac{1}{2}\left[\sigma_{\mu\nu}(\omega\omega) + \sigma_{\nu\mu}(\omega\omega)\right],$$
$$\psi^S_{\mu\nu}(t) = \frac{1}{2}\left[\psi_{\mu\nu}(t) + \psi_{\nu\mu}(t)\right] = \frac{1}{2}\left[\psi_{\mu\nu}(t) + \psi_{\mu\nu}(-t)\right],$$
$$\psi_{\mu\nu}(t) = \frac{1}{2}\left[< \gamma_\nu(0)\gamma_\mu(t) > + < \gamma_\mu(t)\gamma_\nu(0) >\right] = \frac{1}{2}\left[< \gamma_\nu(0)\gamma_\mu(t) > + < \gamma_\mu(0)\gamma_\nu(-t) >\right]. \quad (26)$$

$\gamma_\mu(t) = e^{iLt}\gamma_\mu(0)$ – это представление Гайзенберга μ компоненты оператора электрического тока $\vec{\gamma}$.

Рассмотрим общий случай, когда электрон имеет кинетическую энергию $T(\vec{P})$ и взаимодействует с фононами. Таким образом, для нахождения проводимости (25) необходимо вычислить корреляционную функцию:

$$\psi_{\mu\nu}(t) = \frac{e^2}{2}\left[v_\nu(0)v_\mu(t) + v_\mu(0)v_\nu(-t)\right], \quad (27)$$

$\overrightarrow{v}$ – где оператор скорости электрона.

Для вычисления корреляционной функции (27), воспользуемся подходом, развитым по второй части. Используя уравнение (22) для рассматриваемой электрон–фононной системы и выражения (2) и (23) для H_S, H_Σ, H_i, находим следующее уравнение для корреляционной функции скорость – скорость ($A_S = v_\nu$, $B_S = v_\mu$).

$$\frac{\partial}{\partial t} < v_\nu(0)v_\mu(t) = \frac{i}{\hbar} < \left[v_\nu, T(\vec{P})\right]_- v_\mu(t) > \quad (28)$$

$$-\frac{1}{\hbar^2}\int_0^t d\xi \sum_{\vec{k}}\left|v_{\vec{k}}\right|^2 \left\{\left|e^{-i\omega\omega(\vec{k})\xi}N_{\vec{k}} + e^{i\omega\omega(\vec{k})\xi}\left(1+N_{\vec{k}}\right)\right| < \left|\mathrm{v}_\nu, e^{i\vec{k}\vec{r}}\right|_- e^{i\vec{k}\vec{r}(\xi)}\mathrm{v}_\mu(\mathrm{t}) >\right.$$
$$\left. -\left|e^{i\omega\omega(\vec{k})\xi}N_{\vec{k}} + e^{-i\omega\omega(\vec{k})\xi}\left(1+N_{\vec{k}}\right)\right| < e^{i\vec{k}\vec{r}(\xi)}\left|\mathrm{v}_\nu, e^{i\vec{k}\vec{r}}\right|_- \mathrm{v}_\mu(\mathrm{t}) >\right\} -$$
$$-\frac{i}{\hbar}\int_0^\beta d\lambda \sum_{\vec{k}}\left|v_{\vec{k}}\right|^2 \left|e^{i\omega\omega(\vec{k})(t-i\hbar\lambda)}N_{\vec{k}} + e^{-i\omega\omega(\vec{k})(t-i\hbar\lambda)}(1+N_{\vec{k}})\right| < e^{i\vec{k}\vec{r}(t-i\hbar\lambda)}\left|\mathrm{v}_\nu, e^{i\vec{k}\vec{r}}\right|_- \mathrm{v}_\mu(\mathrm{t}) >.$$

Здесь $\mathrm{v}_\mu(\mathrm{t}) = \mathrm{e}^{\frac{\mathrm{iHt}}{\hbar}}\mathrm{v}_\mu\mathrm{e}^{\frac{-\mathrm{iHt}}{\hbar}} \equiv \mathrm{e}^{\mathrm{iLt}}\mathrm{v}_\mu$, $\vec{r}(\xi) = \mathrm{e}^{\frac{\mathrm{iT}(\vec{\mathrm{P}})\xi}{\hbar}}\mathrm{e}^{\frac{-\mathrm{iT}(\vec{\mathrm{P}})\xi}{\hbar}} \equiv \mathrm{e}^{\mathrm{iL_S}\xi}$ – траектория свободного движения электрона.

При выводе (28) мы пользовались также соотношениями: $\omega(-\vec{\mathrm{k}}) = \omega(\vec{\mathrm{k}})$, $\mathrm{V}_{-\vec{\mathrm{k}}} = \mathrm{V}_{\vec{\mathrm{k}}}$. Уравнение для корреляционной функции $< \mathrm{v}_\mu(0)\mathrm{v}_\nu(-t) >$ можно получить из (28), используя следующие подстановки: $\mathrm{t} \to -\mathrm{t}, \mu \leftrightarrow \nu$.

В дальнейшем ограничимся случаем (приближением) одной зоны для электрона, когда оператор скорости электрона диагонален в импульсном представлении и

$$\mathrm{v}_\mu(\vec{\mathrm{P}}) = \frac{\partial}{\partial \mathrm{P_M}}(\vec{\mathrm{P}}),\ \left|\mathrm{v}_\mu(\vec{\mathrm{P}}), (\vec{\mathrm{P}})\right|_- = 0 \quad (\mu = \mathrm{x, y, z})$$

мы пользуемся обозначением $\mathrm{v}_\mu(\vec{\mathrm{P}})$ для матричного элемента от оператора скорости электрона $< \vec{\mathrm{P}}|\mathrm{v}_\mu|\vec{\mathrm{P}} >$ на собственных функциях оператора импульса электрона $|\vec{\mathrm{P}} >$.

Удобно ввести следующий вспомогательный оператор (ср. с (5)):

$$\mathrm{G}_\mu(\mathrm{t}, \beta) = \mathrm{Z}^{-1}\mathrm{Tr}_{(\Sigma)}\left[\mathrm{v}_\mu(\mathrm{t})\mathrm{e}^{-\beta\mathrm{H}}\right] \tag{29}$$

с начальным значением при $\mathrm{t} = 0$.

$$\mathrm{G}_\mu(\beta) = \mathrm{v}_\mu \frac{Z^S(\beta)}{Tr_{(S)}[Z^S(\beta)]}, \tag{30}$$

где $Z^S(\beta) = \mathrm{Tr}_{(\Sigma)}(\mathrm{e}^{-\beta\mathrm{H}})$ – приведенная (редуцированная) производящая функция для рассматриваемой электрон–фононной системы.

Введеный оператор (29) позволяет нам выразить корреляционные функции (27) и уравнения для них следующим образом:

$$< \mathrm{v}_\nu(0)\mathrm{v}_\mu(\pm t) > = Tr_{(S)}\left[\mathrm{v}_\nu(0)\mathrm{G}_\mu(\pm t, \beta)\right],$$
$$\frac{\partial}{\partial t} < \mathrm{v}_\nu(0)\mathrm{v}_\mu(\pm\mathrm{t}) > \equiv Tr_{(S)}\left[\mathrm{v}_\nu(0)\frac{\partial}{\partial t}\mathrm{G}_\mu(\pm t, \beta)\right] = \pm Tr_{(S)}\left[\mathrm{v}_\nu(0)\Gamma_\nu(\pm t, \beta)\mathrm{G}_\mu(\pm t, \beta)\right]. \tag{31}$$

Здесь оператор $\Gamma_\nu(\mathrm{t}, \beta)$ определен непосредственно из уровнения (28) и имеет вид:

$$\Gamma_\nu(\mathrm{t}, \beta) =$$
$$-\frac{1}{\hbar^2}\int_0^t d\xi \sum_{\vec{k}}\left|V_{\vec{k}}\right|^2 \left\{\left|e^{-i\omega\omega(\vec{k})\xi}N_{\vec{k}} + \right.\right.$$
$$e^{i\omega\omega(\vec{k})\xi}\left(1+N_{\vec{k}}\right)\left|\mathrm{v}_\nu^{-1}\left|\mathrm{v}_\nu, e^{i\vec{k}\vec{r}}\right|_- e^{i\vec{k}\vec{r}(\xi)} - \left[e^{-i\omega\omega(\vec{k})\xi}N_{\vec{k}} + \right.\right.$$
$$\left.\left. +e^{i\omega\omega(\vec{k})\xi}\left(1+N_{\vec{k}}\right)\right]\mathrm{v}_\nu^{-1}e^{-i\vec{k}\vec{r}(\xi)}\left|\mathrm{v}_\nu, e^{i\vec{k}\vec{r}}\right|_-\right\} - \frac{i}{\hbar}\int_0^\beta d\lambda \sum_{\vec{k}}|V|^2\left|e^{i\omega\omega(\vec{k})(t-i\hbar\lambda)}N_{\vec{k}} + \right.$$
$$\left. e^{-i\omega\omega(\vec{k})(t-i\hbar\lambda)}(1+N_{\vec{k}})\right|\mathrm{v}_\nu^{-1}e^{-i\vec{k}\vec{r}(t-i\hbar\lambda)}\left|\mathrm{v}_\nu, e^{i\vec{k}\vec{r}}\right|_-, \tag{32}$$

где $\mathrm{v}_\nu^{-1}\mathrm{v}_\nu = \mathrm{v}_\nu\mathrm{v}_\nu^{-1} = 1$. То есть эти операторы являются взаимно обратными.

След по состояниям электрона (подсистемы) в уравнениях (31) будем вычислять на собственных функциях $|\vec{\mathrm{P}}>$ оператора импульса электрона. Следовательно, эти уравнения можно записать в следующем виде:

$$< \mathrm{v}_\nu(0)\mathrm{v}_\mu(\pm\mathrm{t}) > = \int d\vec{\mathrm{P}}\,\mathrm{v}_\nu(\vec{\mathrm{P}})\mathrm{G}_\mu(\pm t, \beta, \vec{\mathrm{P}}),$$
$$\int d\vec{\mathrm{P}}\,\mathrm{v}_\nu(\vec{\mathrm{P}})\frac{\partial}{\partial t}\mathrm{G}_\mu(\pm t, \beta, \vec{\mathrm{P}}) = \pm\int d\vec{\mathrm{P}}\,\mathrm{v}_\nu(\vec{\mathrm{P}})\Gamma_\nu(\pm t, \beta, \vec{\mathrm{P}})\mathrm{G}_\mu(\pm t, \beta, \vec{\mathrm{P}}). \tag{33}$$

Здесь мы учли, что оператор скорости электрона диагонален в импульсном представлении и поэтому для случая пространственной однородности, рассматриваемой нами, только диагональные матричные элементы оператора $\Gamma_\nu(\mathrm{t}, \beta)$:

$$\Gamma_\nu(\pm t,\beta,\vec{P}) \equiv < \vec{P}|\Gamma_\nu(t,\beta)|\vec{P} >$$

отличны от нуля (смотри ниже). Используя соотношения:

$$< \vec{P}_1 \left| e^{\pm i\vec{k}\vec{r}} \right| \vec{P}_2 >= \delta(\vec{P}_2 \pm \hbar\vec{k} - \vec{P}_1),$$

$$e^{\pm i\vec{k}\vec{r}} f(\vec{P}) = f(\vec{P} \mp \hbar\vec{k}) e^{\pm i\vec{k}\vec{r}},$$

$$f(\vec{P}) e^{\pm i\vec{k}\vec{r}} = e^{\pm i\vec{k}\vec{r}} f(\vec{P} \pm \hbar\vec{k}),$$

где $f(\vec{P})$ – произвольная функция импульса $\vec{P}$, находим с помощью (32) для матричного элемента $\Gamma_\nu(t,\beta,\vec{P})$ оператора $\Gamma_\nu(t,\beta)$ выражение:

$$\Gamma_\nu(t,\beta,\vec{P}) =$$

$$\frac{2}{\hbar}\sum_{\vec{k}} |v_{\vec{k}}|^2 \frac{v_\nu(\vec{P}+\hbar\vec{k}) - v_\nu(\vec{P})}{v_\nu(\vec{P})} \left\{ N_{\vec{k}} \frac{sin\left[\frac{t}{\hbar}\Delta^-(\vec{k},\vec{P})\right]}{\Delta^-(\vec{k},\vec{P})} + (1+N_{\vec{k}}) \frac{sin\left[\frac{t}{\hbar}\Delta^+(\vec{k},\vec{P})\right]}{\Delta^+(\vec{k},\vec{P})} + \frac{i}{2}\left[N_{\vec{k}} e^{-\frac{i}{\hbar}t\Delta^-(\vec{k},\vec{P})} \frac{e^{-\beta\Delta^-(\vec{k},\vec{P})}-1}{\Delta^-(\vec{k},\vec{P})} + \right.\right.$$

$$\left.\left. + (1+N_{\vec{k}}) e^{-\frac{i}{\hbar}t\Delta^+(\vec{k},\vec{P})} \frac{e^{-\beta\Delta^+(\vec{k},\vec{P})}-1}{\Delta^+(\vec{k},\vec{P})} \right] \right\}. \qquad (34)$$

Здесь $\Delta^\pm(\vec{k},\vec{P}) = T(\vec{P} \pm \hbar\vec{k}) - T(\vec{P}) \pm \hbar\omega(\vec{k})$.

Для решения уравнения для корреляционной функции (33) рассмотрим изотропный случай, когда

$$\sigma^S_{\mu,\nu}(\omega\omega) = \sigma^S(\omega\omega)\delta_{\mu,\nu}; \quad \psi^S_{\mu,\nu}(t) = \psi^S(t)\delta_{\mu,\nu}$$

и будем пользоваться приближенным уравнением, которое следует из (33),

$$\frac{\partial}{\partial t} G_\mu(t,\beta,\vec{P}) = \pm\Gamma_\mu(\pm t,\beta,\vec{P}) G_\mu(\pm t,\beta,\vec{P}). \qquad (35)$$

Уравнение (35) представляет собой апроксимацию вида ПВР. Нетрудно видеть, что приближенное уравнение (35) становится точным, когда $\Gamma_\mu(\pm t,\beta,\vec{P})$ не зависит от импульса $\vec{P}$. Такой случай реализуется например, для фрелиховского полярона при низких температурах (см. четвертую часть).

Уравнение (35) сводится к следующему выражению:

$$G_\mu(\pm t,\beta,\vec{P}) = \exp\left[\widetilde{\Gamma}_\mu(\pm t,\beta,\vec{P}) G_\mu(\beta,\vec{P})\right], \qquad (36)$$

где

$$\widetilde{\Gamma}_\mu(\pm t,\beta,\vec{P}) = \int_0^t d\tau \Gamma_\mu(\tau,\beta,\vec{P}) \qquad (37)$$

и начальное условие

$$G_\mu(\beta,\vec{P}) \equiv < \vec{P}|G_\mu(\beta)|\vec{P} > = \frac{v_\mu(\vec{P}) Z^S(\beta,\vec{P})}{\int d\vec{P} Z^S(\beta,\vec{P})}, \qquad (38)$$

$$Z^S(\beta,\vec{P}) \equiv < \vec{P}|Z^S(\beta)|\vec{P} >$$

следует из условия (30).

Подставив выражен ие (34) для $\Gamma_\mu(t,\beta,\vec{P})$ в (37) находим в результате интеграции выражение:

$$\widetilde{\Gamma}_\mu(t,\beta,\vec{P}) = \mathrm{Re}\widetilde{\Gamma}_\mu(t,\beta,\vec{P}) + \mathrm{I_m}\widetilde{\Gamma}_\mu(t,\beta,\vec{P}),$$

$$\mathrm{Re}\widetilde{\Gamma}_\nu(t,\beta,\vec{P}) =$$

$$\sum_{\vec{k}} |v_{\vec{k}}|^2 \frac{v_\nu(\vec{P}+\hbar\vec{k}) - v_\nu(\vec{P})}{v_\nu(\vec{P})} \left\{ N_{\vec{k}} \left[1 + e^{\beta\Delta(\vec{k},\vec{P})}\right] \frac{1-cos\left[\frac{t}{\hbar}\Delta(\vec{k},\vec{P})\right]}{\left[\Delta^-(\vec{k},\vec{P})\right]^2} + (1+N_{\vec{k}}) \left[1 + e^{-\beta\Delta^+(\vec{k},\vec{P})}\right] \frac{1-cos\left[\frac{t}{\hbar}\Delta^+(\vec{k},\vec{P})\right]}{\left[\Delta^+(\vec{k},\vec{P})\right]^2} \right\},$$

$$\mathrm{I_m}\widetilde{\Gamma}_\mu(t,\beta,\vec{P}) = -\sum_{\vec{k}} |v_{\vec{k}}|^2 \frac{v_\nu(\vec{P}+\hbar\vec{k}) - v_\nu(\vec{P})}{v_\nu(\vec{P})} \times$$

$$\times \left\{ N_{\vec{k}} \frac{1-e^{-\beta\Delta^-(\vec{k},\vec{P})}}{\left[\Delta^-(\vec{k},\vec{P})\right]^2} sin\left[\frac{t}{\hbar}\Delta^-(\vec{k},\vec{P})\right] + (1+N_{\vec{k}}) \frac{1-e^{-\beta\Delta^+(\vec{k},\vec{P})}}{\left[\Delta^+(\vec{k},\vec{P})\right]^2} sin\left[\frac{t}{\hbar}\Delta^+(\vec{k},\vec{P})\right] \right\}. \qquad (39)$$

Заметим, что $\mathrm{Re}\widetilde{\Gamma_\nu}(t,\beta,\vec{\mathrm{P}})$ четная функция t, тогда как $\mathrm{I_m}\widetilde{\Gamma_\nu}(t,\beta,\vec{\mathrm{P}})$ нечетная функция t.

Выражения (36), (38) и (39) задают временную зависимость корреляционных функций (33) и позволяют в принципе вычислить тензор проводимости согласно формулам (25 – 27). Так как мы ограничиваемся вторым приближением по теории возмущений по Hi ($\mathrm{V}_{\vec{\mathrm{k}}}$) в уравнениях (22) и (28), то для последовательности совершим апроксимацию

$$e^{-\beta H} => e^{-\beta H_0} = e^{-\beta H_S} e^{-\beta H_{\Sigma\Sigma}}$$

в выражениях (30) и (38) для начальных значений корреляционных функций. Следовательно, мы полагаем:

$$\mathrm{G_\mu}(\beta) = \frac{e^{-\beta H_S}}{\mathrm{Tr_S} e^{-\beta H_S}} \mathrm{V_\mu}; \quad \mathrm{G_\mu}(\beta,\vec{\mathrm{P}}) = \frac{\mathrm{e}^{-\beta \mathrm{T}(\vec{\mathrm{P}})}}{\int \mathrm{d}\vec{\mathrm{P}} \mathrm{e}^{-\beta \mathrm{T}(\vec{\mathrm{P}})}} \mathrm{V_\mu}(\vec{\mathrm{P}}). \tag{40}$$

Далее, уровнения (33), (36) и (40) приводят к следующему выражению для корреляционной функции:

$$\psi_{\mu\nu}(t) = \frac{e^2}{2} \frac{\int \mathrm{d}\vec{\mathrm{P}} \mathrm{e}^{-\beta \mathrm{T}(\vec{\mathrm{P}})} \mathrm{V_\nu}(\vec{\mathrm{P}}) \mathrm{V_\mu}(\vec{\mathrm{P}}\{\exp[\widetilde{\Gamma_\nu}(t,\beta,\vec{\mathrm{P}})] + \exp[\widetilde{\Gamma_\mu}(-t,\beta,\vec{\mathrm{P}})]\}}{\int \mathrm{d}\vec{\mathrm{P}} \mathrm{e}^{-\beta \mathrm{T}(\vec{\mathrm{P}})}}, \tag{41}$$

где $\widetilde{\Gamma_\nu}(t,\beta,\vec{\mathrm{P}})$ и $\widetilde{\Gamma_\mu}(-t,\beta,\vec{\mathrm{P}})$ определены с помощью (39).

Согласно (41) и (39), корреляционные функции (подсистемы) электрона затухают с осцилляциями вследствии того, что фактор релаксации $\widetilde{\Gamma_\nu}(t,\beta,\vec{\mathrm{P}})$ является комплексной величиной и как будет видно в дальнейшем эти осцилляции выживают асимпточически при $\mathrm{t} \gg \mathrm{t}_0$ и дают вклад в кинетический коэффициент (в проводимость). Это утверждение следует из-за точного учета распределения Гибсса в определении корреляционной функций (4). В ПСФ мнимая часть $\widetilde{\Gamma_\nu}(t,\beta,\vec{\mathrm{P}})$, как и возможность вышеуказанных осцилляций отсутствуют [9, 11].

Надо отметить, что рассматриваемые рассуждения справедливы в случае соблюдения иерархии времен (20). Как видно из (39) в рассматриваемом случае взаимодействия электрона с фононами $\mathrm{t_S} \sim \hbar\beta$ и $t_{\Sigma_\Sigma} \sim \frac{1}{\bar{\omega}}$, где $\bar{\omega}$ характерная частота фононов. Более того, из выражения (39) следует что, закон сохранения энергии справедлив в процессе рассеяния электрона на фононах при больших временах

$\mathrm{t} \gg \mathrm{t}_0$, $\mathrm{t}_0 = \max(\mathrm{t_S}, \mathrm{t}_\Sigma)$.

Рассматривая времена $\mathrm{t} \gg t_0$, мы можем совершить в (39) предельный переход $\mathrm{t} \to \infty$ и найдем как результат:

$$\lim_{\mathrm{t}\to\infty} \mathrm{Re}\widetilde{\Gamma_\nu}(t,\beta,\vec{\mathrm{P}}) = -\Gamma_\nu^{\mathrm{rel}}(\beta,\vec{\mathrm{P}})\,|t| = -\frac{1}{\tau_\nu^{\mathrm{rel}}(\beta,\vec{\mathrm{P}})}|t|,$$

$$\Gamma_\nu^{\mathrm{rel}}(\beta,\vec{\mathrm{P}}) = -\frac{2\pi}{\hbar}\sum_{\vec{\mathrm{k}}}|\mathrm{V}_{\vec{\mathrm{k}}}|^2 \frac{\mathrm{v_\nu}(\vec{\mathrm{P}}+\hbar\vec{\mathrm{k}}) - \mathrm{v_\nu}(\vec{\mathrm{P}})}{\mathrm{v_\nu}(\vec{\mathrm{P}})} \{N_{\vec{k}}\delta[\Delta^-(\vec{\mathrm{k}},\vec{\mathrm{P}})] + (1+N_{\vec{k}})\delta[\Delta^+(\vec{\mathrm{k}},\vec{\mathrm{P}})]\},$$

$$\lim_{\mathrm{t}\to\infty} \mathrm{I_m}\,\widetilde{\Gamma_\nu}(t,\beta,\vec{\mathrm{P}}) = -\beta\pi\sum_{\vec{\mathrm{k}}}|\mathrm{V}_{\vec{\mathrm{k}}}|^2 \frac{\mathrm{v_\nu}(\vec{\mathrm{P}}+\hbar\vec{\mathrm{k}}) - \mathrm{v_\nu}(\vec{\mathrm{P}})}{\mathrm{v_\nu}(\vec{\mathrm{P}})} \{N_{\vec{k}}\delta[\Delta^-(\vec{\mathrm{k}},\vec{\mathrm{P}})] + (1+N_{\vec{k}})\delta[\Delta^+(\vec{\mathrm{k}},\vec{\mathrm{P}})]\}\mathrm{sign\ t}, \tag{42}$$

где были использованы следующие соотношения: $\lim_{\mathrm{t}\to\infty} \frac{1-\cos(\omega \mathrm{t})}{\omega^2} = \pi|t|\,\delta(\omega)$; $\lim_{\mathrm{t}\to\infty} \frac{\sin(\omega \mathrm{t})}{\omega} = \pi\,\delta(\omega)\mathrm{sign\ t}$. Отметим, что до вычисления предельного перехода $\lim\limits_{\mathrm{t}\to\infty}$, мы должны совершить в (39) термодинамический предельный переход

$$\sum_{\vec{\mathrm{k}}}(\cdots) = \frac{V}{(2\pi)^3}\int d\vec{\mathrm{k}}\,(\cdots).$$

Мы видим из (42), что на больших масштабах времени ($t \gg t_0, t \to \infty$) соотношение (42) принимает вид:

$$\lim_{t\to\infty} I_m \tilde{\Gamma}_\nu(t,\beta,\vec{P}) = \frac{\beta\hbar}{2}\Gamma_\nu^{rel}(\beta,\vec{P})\,\mathrm{sign}\, t\,. \qquad (43)$$

Согласно вышеизложенного, $\tilde{\Gamma}_\nu(t,\beta,\vec{P})$ можно интерпретировать как частоту релаксации ν-компоненты скорости $v_\nu(\vec{P})$ электрона, а ($\tau_\nu^{rel}(\beta,\vec{P})$ – как соответствующее время релаксации).

Пользуясь (25 – 27) и (41 – 42), наконец находим для диссипативной части проводимости при $\omega \ll t_0^{-1}$ выражение:

$$\sigma_{\mu\nu}^S(\omega) =$$

$$= \frac{he^2}{2E_\beta(\omega)} \int d\vec{P}\rho_S(\beta,\vec{P})v_\nu(\vec{P})v_\mu(\vec{P}) \left\{ cos\left[\frac{\beta\hbar}{2}\Gamma_\nu^{rel}(\beta,\vec{P})\right] + cos\left[\frac{\beta\hbar}{2}\Gamma_\mu^{rel}(\beta,\vec{P})\right] \frac{\Gamma_\nu^{rel}(\beta,\vec{P})}{\omega^2+[\Gamma_\mu^{rel}(\beta,\vec{P})]^2} \right\}$$

$$(\omega \ll t_0^{-1}), \qquad (44)$$

где $\rho_S(\beta,\vec{P}) = e^{-\beta T(\vec{P})}/\int d\vec{P} e^{-\beta T(\vec{P})}$ и была введена плотность (концентрация) электронов n как множитель в (44) для учета количества электронов существующего в системе.

Как видно из выражения для проводимости (44), начальные корреляции электронов с фононами присутствуют в виде множителей $cos\left[\frac{\beta\hbar}{2}\Gamma_\nu^{rel}(\beta,\vec{P})\right]$. Однако, ввиду условия (20), $\beta\hbar\Gamma_\nu^{rel}(\beta,\vec{P}) \ll 1$; ($\tau^{rel} \sim \frac{1}{\Gamma_\nu^{rel}(\beta,\vec{P})}, t_S \sim \beta\hbar$). Заметим, что эти корреляции не влияют асимптотически на время релаксации $\tau_\nu^{rel}(\beta,\vec{P})$.

В ПСФ для корреляционных функций (4) мы пренебрегаем взаимодействием H_i в факторе Гибсса $e^{-\beta H}$ (сохраняя их в факторах $e^{\pm\frac{i}{\hbar}Ht}$) [9, 11]. Это приближение сводит выражение (44) для $Re\sigma_{\mu\nu}^S(\omega)$ к виду, в котором совершены подстановки:

$$\cos\left[\frac{\beta\hbar}{2}\Gamma_\mu^{rel}(\beta,\vec{P})\right] => 1, \cos\left[\frac{\beta\hbar}{2}\Gamma_\nu^{rel}(\beta,\vec{P})\right] => 1$$

(см. также [11]).

Таким образом, найденные выражения для корреляционных функций скорость–скорость и проводимости являются наиболее общими в рамках рассматриваемой модели и совершенных приближений.

4. Подвижность полярона Фрелиха («Проблема $\frac{3}{2\beta\hbar\omega_0}$» в низкотемпературной подвижности полярона)

Рассмотрим теперь электрон, движущийся в ионном кристалле в рамках модели Фрелиха, описываемой с помощью гамильтонианов (1), (2), (23) и (24).

Кроме того, мы имеем в виду взаимодействие электронов только с оптическими бездисперсионными фононами для которых $\omega(\vec{k}) = \omega_0$. Действительно, рассмотрим изотропный случай, когда

$$T(\vec{P}) = \frac{\vec{P}^2}{2m^*}, \qquad v_\mu(\vec{P}) = \frac{P_\mu}{m^*}, \qquad (45)$$

Как видно из выражений (41), (42) и (44), проблема состоит в вычислении частоты релаксации $\Gamma_\mu^{rel}(\beta,\vec{P})$, в общем случае зависящей от импульса $\vec{P}$ электрона.

Для определенности рассмотрим $\Gamma_z^{rel}(\beta,\vec{P})$, так как считается, что электрическое поле приложено вдоль оси z. Совершая термодинамический предельный переход и интегрируя по переменной $|\vec{k}|$, из выражений (24) и (42) мы находим:

$$\Gamma_z^{rel}(\beta,\tilde{P}) = \frac{\alpha\omega_0}{2\pi}\frac{1}{\tilde{P}_z}\times$$
$$\times\left\{N_0(\gamma)\int_0^{2\pi}d\varphi\int_0^{\pi}d\theta\sin\theta\cos\theta\frac{\tilde{P}\cos\Phi}{\sqrt{\tilde{P}^2\cos^2\Phi+1}}+\right.$$
$$\left.[1+N_0(\gamma)]\int_0^{2\pi}d\varphi\int_0^{\pi}d\theta\sin\theta\cos\theta\frac{z\tilde{P}\cos\Phi}{\sqrt{\tilde{P}^2\cos^2\Phi-1}}\right\}$$
$$(\tilde{P}^2\cos^2\Phi \gg 1). \qquad (46)$$

Здесь мы ввели безразмерный импульс электрона:

$$\tilde{P}_i = \frac{P_i}{\sqrt{2\hbar\omega_0 m^*}} \quad (i = x, y, z), \quad N_0(\gamma) = (e^{\gamma}-1)^{-1},$$

$\gamma = \beta\hbar\omega_0$ и Φ – угол между векторами $\vec{k}$ и $\vec{P}$, связанный с углами θ и φ, определяющий направление $\vec{k}$, соотношением:

$$\tilde{P}\cos\Phi = \sin\theta\cos\varphi\tilde{P}_x + \sin\theta\sin\varphi\tilde{P}_y + \cos\theta\tilde{P}_z.$$

Для вычисления выражения (46), ограничимся случаем низких температур

$$\gamma \gg 1, \qquad (47)$$

когда корреляционные функции (41) определены областью малых значений импульса

$$\tilde{P}^2 \ll 1. \qquad (48)$$

В данном случае, медленно движущийся электрон не может излучать фононов, в виду того, что не будут выполнены законы сохранения энергии и импульса в таких процессах (см. (42) и (46)).

Таким образом, при соблюдении условий (47) и (48), второй член в правой части выражения (46) обращается в нуль. Учитывая, что $\tilde{P}^2\cos^2\Phi \ll 1$, выражение (46) можно привести к виду:

$$\Gamma_z^{rel}(\beta,\tilde{P}) \equiv \Gamma_0^{rel}(\gamma) = \frac{2}{3}\alpha\omega_0 N_0(\gamma), \quad (\tilde{P}^2 \ll 1). \qquad (49)$$

Следовательно, частота (время) релаксации скорости для медленно движущегося электрона не зависит от импульса электрона и обусловлена только процессами поглощения фононов электроном.

Используя (49), мы находим из (41):

$$< V_z(0)V_z(\pm t) > = \frac{\hbar\omega_0}{m^*\gamma}exp\left[-\Gamma_0^{rel}(\gamma)|t|\right]exp\left[\pm\frac{i\gamma}{2\omega_0}\Gamma_0^{rel}(\gamma)\right] \quad (\gamma \gg 1,\ t \gg \frac{\gamma}{\omega_0}), \qquad (50)$$

где использовали хорошо известные формулы:

$$\int d\,\tilde{P}e^{-\gamma\tilde{P}^2}\tilde{P}_z^{\,2} = \frac{1}{2\gamma}\left(\frac{\pi}{\gamma}\right)^{3/2},$$
$$\int d\,\tilde{P}e^{-\gamma\tilde{P}^2} = \left(\frac{\pi}{\gamma}\right)^{3/2}. \qquad (51)$$

Таким образом, как видно из (50), корреляционные функции скорость скорость для электрона затухают экспоненциально во времени в рассматриваемом случае низких температур. Согласно (50), для времени релаксации имеем выражение:

$$\tau^{rel}(\gamma) = \left[\Gamma_0^{rel}(\gamma)\right]^{-1}.$$

Полученный результат нами был найден без использования какой-либо апроксимации вида ПСФ. Выражение (50) отличается от результата, найденного при помощи ПСФ фактором $\exp\left[\pm\frac{i\gamma}{2\omega_0}\Gamma_0^{rel}(\gamma)\right]$ (см. [11]).

Вычислим теперь низкотемпературную проводимость и подвижность фрелиховского полярона, в рассматриваемом случае слабого электрон–фононного взаимодействия. Учитывая (45) и (49 – 51) из (44) для проводимости имеем:

$$\mathrm{Re}\sigma(\omega) = \frac{ne^2}{m^*\omega_0}\frac{2}{\gamma\tilde{\omega}}th(\frac{\gamma\tilde{\omega}}{2})\left[1-2sin^2(\frac{\gamma}{2}\Gamma_0(\gamma))\right]\frac{\Gamma_0(\gamma)}{\tilde{\omega}^2+\Gamma_0^2(\gamma)},\ (\alpha<1,\ \gamma\gg1,\ \tilde{\omega}\gamma\ll1), \quad (52)$$

где $\sigma(\omega)=\sigma_{xx}(\omega)=\sigma_{yy}(\omega)=\sigma_{zz}(\omega)$, $\tilde{\omega}=\omega/\omega_0$, $\Gamma_0(\gamma)=\omega_0^{-1}\Gamma_0^{\mathrm{rel}}(\gamma)=\frac{2}{3}\alpha\mathrm{N}_0(\gamma)$.

Выражение (52) можно рассматривать как обобщенный результат Осака [13] в случае слабого электрон–фононного взаимодействия, и представляет фактически формулу Друде для низкотемпературной проводимости, которая содержит поправку, обусловленную начальной корреляцией электронов с фононами (второй член в (52)). Первый член в (52) соответстует апроксимации ПСФ (см. [11]). Так как, $\tilde{\omega}\gamma\ll1$ (что следует из условия $t\gg t_0$) и $\gamma\Gamma_0(\gamma)\ll1$ (см. условие (20)), мы можем разложить $\frac{2}{\gamma\tilde{\omega}}th(\frac{\gamma\tilde{\omega}}{2})$ и $sin^2(\frac{\gamma}{2}\Gamma_0(\gamma))$ в выражении (52). Поэтому поправка, связанная с начальными корреляциями является малой величиной, для рассматриваемого случая ($\mathrm{N}_0(\gamma)=e^{-\gamma},\gamma\gg1$).

Из выражения (52) и (49) для низкотемпературной подвижности полярона $\mu=Re\sigma(0)/ne$ мы имеем:

$$\mu=\frac{3e}{2m^*\omega_0\alpha}e^{\gamma} \qquad (\gamma\gg1), \quad (53)$$

где мы пренебрегли поправкой от начальных корреляции.

Найденное выражение (53) представляет собой последовательный и правилный результат для низкотемпературной подвижности полярона в случае слабого взаимодействия ($\alpha<1$). Мы надеемся, что оно дает решение «$\frac{3}{2\beta\hbar\omega_0}$ проблемы» (см., например, [5]).

5. Заключение

В настоящей работе мы вывели точное замкнутое уравнение для соответствующего (вспомогательного) супероператора (см. уравнение (16)), который определяет точное уравнение для корреляционной функции подсистемы, взаимодействующей с бозонным полем, рассматриваемым как термостат (уравнение (18)). При этом нигде не использовался ПСФ.

Развиваемый подход был применен к электрон–фононной системе и последовательная теория проводимости была построена для случая однозонной модели электрона, слабо взаимодействующей с фононами и со слабым приложенным электрическим полем. В частности была развита последовательная теория низкотемпературной подвижности фрелиховского полярона. Отметим, что формула (50) описыват (демонстрирует) ергодические свойства рассматриваемой модели частицы, взаимодействующей с бозонным термостатом.

Предлагаемый формализм можно использовать для вычисления вкладов высоких порядков по взаимодействию подсистемы с термостатом в корреляционных функциях и, связанных с ними величин. С помощью этого метода можно также рассмотреть случай сильного (произвольного) электрон–фононного взаимодействия в рамках модели Фейнмана для полярона [12] или в обобщенной модели Фейнмана для полярона [14].

Очевидно, что предлагаемый подход можно применить для вывода уравнений матрицы плотности подсистемы, взаимодействующей с бозонным термостатом при смешанном (т.е. которое не представляется в виде произведений) начальном условии.

Ссылки

1. С. И. Пекар. Исследование по электронной теории кристалловю 1951, Москва – Ленинград: Гостехиздат.
2. Н. Н. Боголюбов, Н. Н. Боголюбов (мл.). Введение в квантовую статистическую механику. 1984, Москва: Наука.
3. R. Kubo. J. Phys. Soc. Jpn. 12, 1967, 570.
4. G. V. Chester, A. The IIung. Proc. Phys. Soc., 1959, 73, 745.
5. F. M. Peeters, J. T. Devreese. Phys. Status Solidi B, 1983, 115, 539.
6 F. M. Peeters, J. T. Devreese. Solid State Phys., 1984, 38, 81.
7. N. N. Bogolubov. Kinetic Equations for electron–phonon systems (Preprint E 17–11822), 1978, Dubna: IINR.
8. Н. Н. Боголюбов, Н. Н. Боголюбов (мл.). Элементарные частицы и атомное ядро, II. 1980.
9. В. Ф. Лось. ТМФ 39, 1979, 393.
10. V. F. Los', A. G. Martynenko. Physica A, 1986, 138, 518.
11. В. Ф. Лось. ТМФ, 1984, 60, 107.
12. R. P. Feynman. Phys. Rev., 1955, 97, 660.
13. Y. Osaka. Prog. Theo. Phys., 1961, 25, 517.
14. I. Luttinger, Ch.-Y. Lu. Phys. Rev., B, 1980, 21, 4251.

ELECTRO-PHYSICAL PROPERTIES OF DYSPROSIUM MONOANTIMONIDE

Z. U. Jabua, I. L. Kupreishvili, A. V. Gigineishvili,
G. N. Iluridze, I. G. Tabatadze

Georgian Technical University
Tbilisi, Georgia
Z.Jabua@hotmail.com

Accepted July 2, 2012

1. Introduction

Due to their interesting less studied and sometimes controversial properties, rare earth (RE) antimonides represent an interest as a group of electronic materials [1 – 4]. Within the framework of the given study, for the first time there has been developed the technology for preparation of DySb thin films, powders, ceramics and single-crystals. The X-ray and electronographical analysis of obtained samples were carried out.

For the DySb thin films and single-crystals, the temperature dependence of the specific resistivity and Hall constant in the temperature interval from 95 to 700 K were measured.

2. Experimental details

Single-phase DySb thin films were prepared by thermal vacuum evaporation from two independent sources Dy and Sb in the vacuum $1.3 \cdot 10^{-5}$ Pa on fused sapphire, polycrystalline pyroceramic and single-crystalline silicon substrates using the modernized device UN – 2. The components used in the compounds contained 99.9 % Dy and 99.999 % Sb of the basic materials. The films were prepared at the substrate temperature 1050 – 1110 K. The angles between the perpendicular to the substrate and evaporator were similar and made up 35 °. The distance of Dy and Sb evaporators from the substrate were 42 and 56 mm, respectively. The thickness of the films was from 1.2 to 2.1 μm, the rate of evaporation was ~ 68 Å / s.

The X-ray microanalysis revealed that the films contained 49/8 at. % Dy and 52.2 at. % Sb. Phase composition of the films was defined by X-ray method, roentgenograms were taken using Cu K_α irradiation and nickel filter, in conditions of the constant regime at the 0.5 – 1 degree / min rate. Identification of the roentgenograms was performed by comparing the obtained X-ray diffractogramm with the relevant diagram for the bulk DySb crystal built according to the reference data. The substrate material does not have any significant effect on the phase composition and crystallinity of the films. Keeping the samples in the open air for 4 – 6 days results in changes in their color, while on the roentgenogram occur additional maximums, which are no relation to DySb. All points to DySb thin films instability in the air.

It is known that, the DySb bulk crystal have NaCl type cubic lattice with parameters $a = 6.150$ Å [1]. The lattice parameter calculated from experimental roentgenogram for DySb thin films made up $a = 6.14$ Å which corresponds to the value for bulk crystals.

The powder of DySb was prepared by two methods: direct interaction of initial component and hydride method. For realization direction interaction method, initial components (Dy and Sb) was placed in tantalum ampoule and heated to 860 K with rate ~ 42 degree / min. Hydride method yields in reaction

$2\ DyH_3 + 2\ Sb = 2\ DySb + 3\ H_2$

at temperature 1045 K during 12 – 16 hours.

DySb ceramics were prepared by sintering powder pills at 2400 K in tantalum ampoule. Single-crystals were grown by Bridjmen method. X-ray investigation and microanalysis showed that single-crystals of PrSb were low quality containing 2 – 3 crystals which grew in parallel.

In the films and single-crystals of PrSb, the temperature dependence of the resistivity and the Hall constant were studied. The study interval was from 95 to 700 K. In order to measure the resistivity by means of compensation method, the Hall effect – using direct current and magnetic field (18 kOe). Two-layered islands were deposited on the samples. For the lower layer Cr (to improve adhesion) and for upper layer Cu was used.

3. Results and discussion

The temperature dependences of the obtained electro-physical parameters are shown in **Figs.1** and **2**.

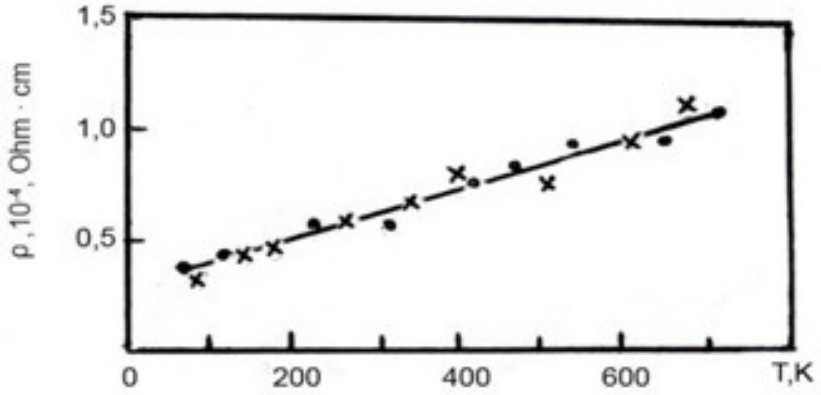

Figure 1. Resistivity of DySb single-crystals and thin films (× – single-crystal, • – thin film).

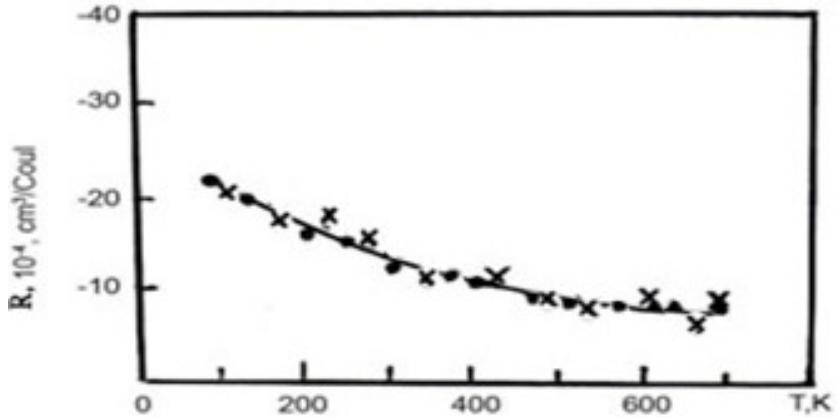

Figure 2. Temperature-dependence of the Hall constant of DySb single-crystals and thin films (× – single-crystal, • – thin film).

In the interval 95 – 700 K, the resistivity is linear with positive temperature coefficient. The dependence is week. The magnitude of the resistivity and the character of its temperature-dependence are similar to those observed in TmSb, $YbSb_2$, $SmSb_2$, SmSb and PrSb films [2, 3].

As shown in **Fig. 2**, in the whole temperature interval the Hall constant is negative. The absolute value of the Hall constant decreases non-linearly.

The measurement results were used for one-band-approximation evaluation the basic parameters such as the carriers' mobility and concentration (see **Figs.** 3 and **4**).

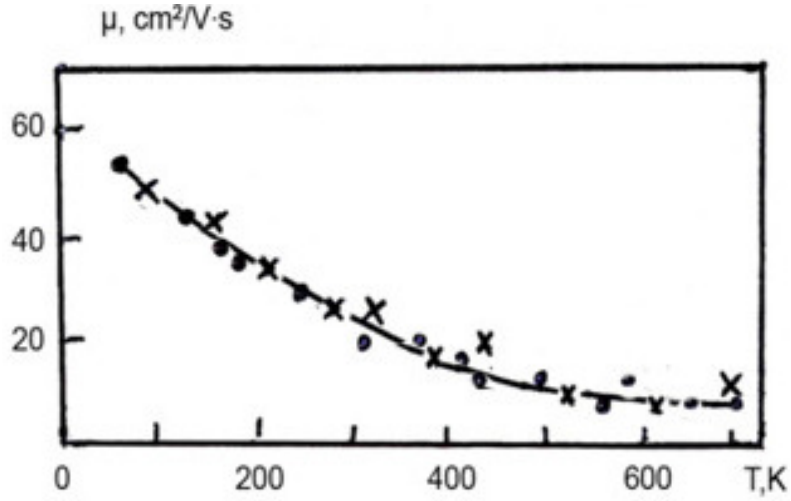

Figure 3. Temperature-dependence of the carriers' mobility of DySb single-crystals and thin films (× – single-crystal, • – thin film)

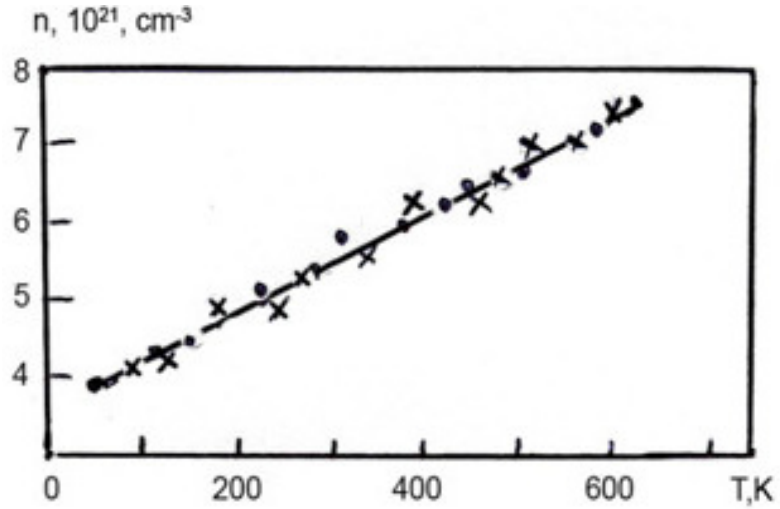

Figure 4. Temperature-dependence of the electron concentration of DySb single-crystals and thin films (× – single-crystal, • – thin film).

When the temperature increases the mobility decreases (**Fig. 3**), while the concentration increases too (**Fig. 4**). The character of the temperature-dependence of the electro-physical parameters and their absolute values enable us to assume that DySb is a semi-metal like other RE monoantimonides.

We should emphasize that in contrast to SmSb and TmSb [4] in the DySb samples no anomalies are observed in the temperature-dependence of the Hall constant related to the

intermediate valence phenomenon of Sm and Tm ions. It points to the fact that in DySb the Dy ion does not show the intermediate valence.

4. Conclusion

The technology for preparation DySb thin films, powders, ceramics and single-crystals was developed. For these samples, the temperature-dependences of the resistivity and Hall constant were measured in the temperature interval from 95 to 700 K. On the basis of measurements, in the one-band approximation there were assessed the basic electro-physical parameters: carriers' mobility and concentration.

References

1. M. N. Abdusalyamova. Physical and chemical properties of antimonides and bismutides of rare earth elements. J. Chem. Soc. D. I. Mendeleev, 1981, 26, 673-678.
2. Z. U. Jabua, T. O. Dadiani, A. V. Gigineishvili, M. I. Stamateli, T. S. Lochoshvili. Preparation of thin films of praseodymium monoantimonide and their electro-physical properties. Georg. Eng. News, 2004, 3, 36.
3. L. N. Glurjidze, M. I. Stamateli, T. S. Lochoshvili, E. V. Dokadze, Z. U. Jabua, T. O. Dadiani. Electro-physical properties of some antimonides of rare earth elements. Bull. Georg. Acad. Sci., 1990, 138, 533-536.
4. L. N. Glurjidze, T. O. Dadiani, Z. U. Jabua, E. V. Dokadze, M. S. Taktakishvili, V. V. Sanadze. Electro-physical properties of samarium monoantidomide thin film. Phys. Solid State, 1986, 28, 2860-2862.

IMAGINATION IN SCIENCE

F. Habashi

Laval University
Quebec City, Canada
Fathi.Habashi@arul.ulaval.ca

Accepted May 1, 2012

Introduction

"Imagination is more important than knowledge", is a statement attributed to Albert Einstein (1879 – 1955). This is certainly true. From ancient times imagination of researchers and scholars played an important role in the history of our civilizations.

The fantastic idea of measuring the size of our planet Earth was achieved by the ancient Greek mathematician Eratosthenes (**Fig. 1**) in the year 235 BC. He was able to calculate the radius of the Earth by an ingenious experiment. He measured the shadow of an obelisk in Alexandria at noon at the same time when there was no shadow in a well at Syene (present day Aswan). Knowing the height of the obelisk, it was possible to compute the angle that equalled that at the center of the Earth (**Fig. 2**). Knowing the distance between Alexandria and Syene (780 km), it was possible to compute the radius of the Earth (6320 km) hence its volume. The value he obtained was very near to the actual value.

Figure 1. Greek mathematician Eratosthenes.

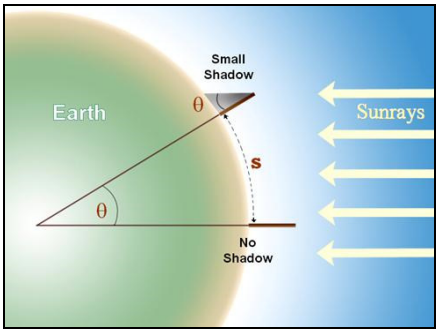

Figure 2. Eratosthenes calculation of the radius of the Earth.

In 1798, the British scientist Henry Cavendish (1731 – 1810) (**Fig. 3**) measured the mass of the Earth by another ingenious experiment (**Fig. 4**). He used a torsion balance to which two balls were attached and housed in a large wooden shed to prevent air currents. Once the system was stable, two large, known masses were positioned near the masses on the rod. The tiny gravitational attraction between the pairs of masses twists the wire slightly, and the force was calculated from the new equilibrium position. In practice, the deflection may be very small, but can be measured by mounting a mirror on the rod and measuring the deflection of a beam of light projected onto a distant screen.

Figure 3. British scientist Henry Cavendish (1731 – 1810).

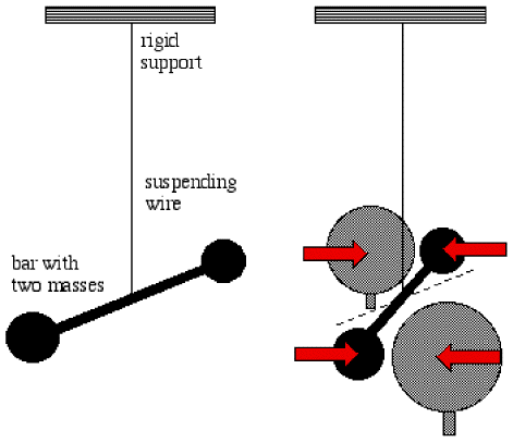

Figure 4. A sketch illustrating Cavendish experiment.

Cavendish then used the following equations to calculate the gravitation constant G: $F = G\,m\,M/R^2$, where F is the force of attraction between the two masses m and M placed at distance R apart. He found: $G = 6.67 \cdot 10^{-8}$ when the masses were expressed in grams, distance in centimetres, and the force in dynes. The weight of the Earth was then determined using the relation: $F = G\,m\,M/R^2 = m\,a$, where a is the acceleration imparted to a falling body m on the surface of the Earth of mass M, and R is the radius of the Earth (determined by Eratosthenes). Therefore: $M = R^2\,a\,/\,G$.

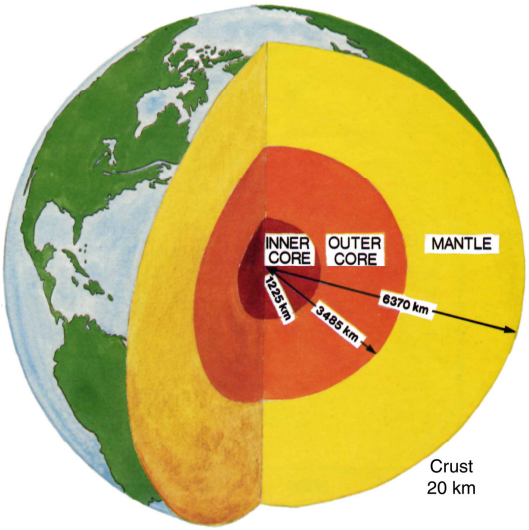

Figure 5. The layered structure of the Earth.

Scientists were able not only to estimate the weight of the Earth to be $6.6 \cdot 10^{21}$ tonnes but they also devoted some thought to its structure. Knowing the weight and the volume then the density was calculated as 5.5. Since the density of the crust is 2.8 while that of the Earth as a whole is 5.5. Therefore the Earth must contain a more dense part. The eruption of volcanoes is a reminder that the Earth has not completely cooled down. The Earth rotates around the Sun, once a year. It was thought that a molten mass separated from the Sun 4.9 billion years ago and formed the Earth on cooling. It must be composed of different layers surrounding an inner core (**Fig. 5**). The core must be a metal with a high abundance in the crust. This can be satisfied only by iron.

The fact that metallic meteorites which come from other planets are essentially iron is in favour of the iron core hypothesis.

The spectrum of the Sun is dominated by the lines of iron.

An analysis of the propagation of earthquakes shows that at three levels inside the Earth there is discontinuous changes in the density, the compressibility, and the solidity.

The composition of the crust was found to be mainly silicates. Hence, the formation of the Earth is similar to a metallurgical smelting process in which the metal is formed at the bottom of the furnace while the silicate slag forms at the top.

Alchemy

The alchemists of the 9th and 10th centuries (**Fig. 6**) found no reason why a base metal like iron cannot be transmuted into the noble metal gold. All observations did not negate this hypothesis. For example, when a piece of iron was immersed in a solution of copper vitriol (copper sulfate) the iron was transformed into copper. When a piece of lead was heated at high temperature it was reduced into a small piece of silver. When a copper ore was mixed with another ore obtained from a certain locality and smelted, a gold-like metal was obtained.

Figure 6. An alchemist in his laboratory.

Of course these arguments were fallacious because we know now that iron displaces copper from solution by an electrochemical reaction, that practically all lead ores contain silver and when these are smelted and the lead obtained is heated at high temperature, lead forms a molten oxide while silver remains intact. We also know that copper ore and zinc ores when reduced together they yield a copper-zinc alloy that has the appearance of gold and is known as brass. Although the imagination of the alchemists of this era did not yield the gold sought, yet many acids and alkalies were prepared for the first time and that helped the progress technology.

Figure 7. A 19th century painting by Joseph Nicolas Robert–Fleury (1797 – 1890) entitled Galileo before the Holy Office.

Galilio and Church

From antiquity, the majority of educated people subscribed to the Aristotelian view that the earth was the center of the universe and that all heavenly bodies revolved around the Earth which agreed with the Scripture. Further, since it was believed that in the incarnation the Son of God had descended to the earth and become man, it seemed fitting that the Earth be the center around which all other celestial bodies moved. The problem started around 1610, during which Galileo Galilei (1570 – 1612) came into conflict with the view of the universe supported by the Catholic Church. Galileo published his surprising observations that he had made with the new telescope, namely the phases of Venus and the moons of Jupiter. He went on to propose in 1616 that the tides were evidence for the motion of the Earth, and promoted the heliocentric theory of Copernicus published in 1543. These ideas created conflicts with other scientists and Catholic scholars. Galileo's part in the controversies over theology, astronomy, and philosophy culminated in his trial and sentencing by the Roman Inquisition in 1633 on a grave suspicion of heresy (**Fig. 7**).

Medicine

Ignaz Semmelweis (1818 – 1865) was a Hungarian physician a pioneer of antiseptic procedures. He discovered that the incidence of puerperal fever could be drastically cut by the use of hand disinfection in obstetrical clinics. Puerperal fever was common in mid-19th century hospitals and often fatal. Semmelweis postulated the theory of washing with chlorinated lime

solutions in 1847 while working in Vienna General Hospital's First Obstetrical Clinic, where high mortality was observed. He came to this conclusion in 1847, following the death of a person who had been accidentally poked with a student's scalpel while performing a postmortem examination. The autopsy showed a pathology similar to that of the women who were dying from puerperal fever. Semmelweis immediately proposed a connection between cadaveric contamination and puerperal fever. He concluded that he and the medical students carried "cadaverous particles" on their hands from the autopsy room to the patients they examined in the First Obstetrical Clinic. This explained why the student midwives in the Second Clinic, who were not engaged in autopsies and had no contact with corpses, saw a much lower mortality rate.

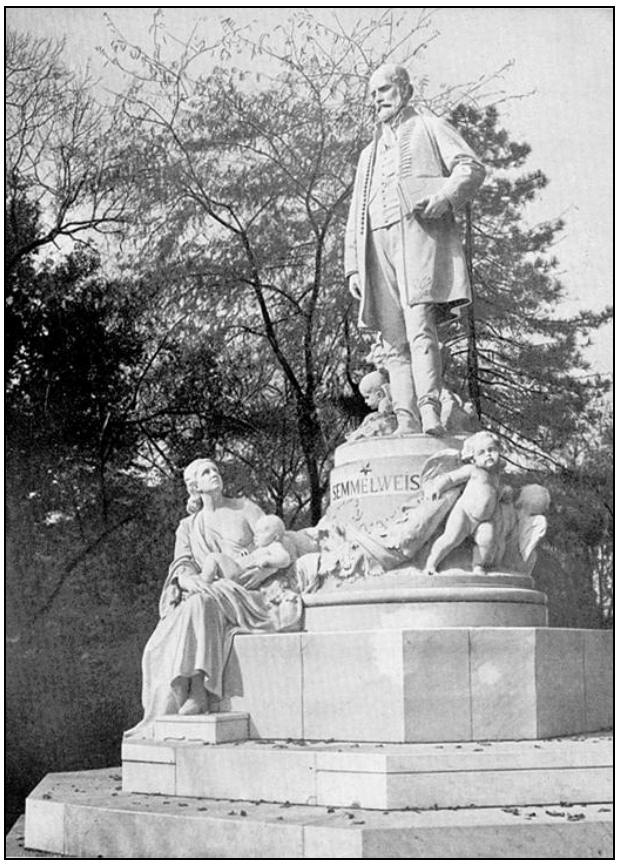

Figure 8. Monument to Ignaz Semmelweis in Budapest.

The germ theory of disease had not yet been developed. Thus, Semmelweis concluded some unknown "cadaverous material" caused childbed fever. He found that the chlorinated solution worked best to remove the putrid smell of infected autopsy tissue, and thus perhaps destroying the causal "poisonous" or contaminating "cadaveric" agent hypothetically being transmitted by this material. Despite various publications of results where hand-washing reduced mortality Semmelweis's ideas were rejected by the medical community. Semmelweis's practice earned widespread acceptance only years after his death, when Pasteur confirmed the germ theory. In 1865, Semmelweis was committed to a mental asylum, where he died two weeks later at the young age of 47. In 1904 a monument was erected in Budapest in his honor (**Fig. 8**).

Carbon atoms in space

In 1874 Jacobus Henricus van't Hoff (1852 – 1911) (**Fig. 9**) accounted for the phenomenon of optical activity by assuming that the chemical bonds between carbon atoms and their neighbors were directed towards the corners of a regular tetrahedron. This three-dimensional structure accounted for the isomers found in nature (He shares credit for this with the French chemist Joseph le Bel (1847 – 1930) in Paris, who independently came up with the same idea.). At that time van't Hoff was only 22 years old lecturing chemistry and physics at the Veterinary College in Utrecht. He published his work on stereochemistry in his book *La chimie dans l'espace* in 1874 (He published in French because he studied in Paris under Adolphe Wurtz (1817 – 1884) at the Faculty of Medicine in Paris.). His theory was considered revolutionary and was strongly rediculed by the scientific community. One such critic was the renowned editor of the German *Journal für praktische Chemie*, Adolph Kolbe (1818 – 1884).

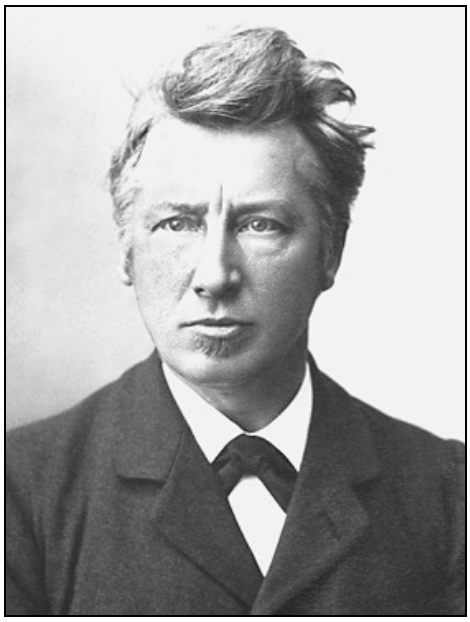

Figure 9. Jacobus Henricus van't Hoff (1852 – 1911).

Van't Hoff laid the foundation for physical chemistry through his discoveries in chemical kinetics, osmotic pressure, and other fields. He was awarded the first Nobel Prize in Chemistry in 1901. He died of tuberculosis at the early age of 58.

Predicting undiscovered elements

In 1869, the Russian chemist Dimitri Mendeleev (1834 – 1907) (**Fig. 10**) and in 1870 the German chemist Lothar Meyer (1830 – 1895) (**Fig. 11**) independently published data in which the elements were arranged in such a way to show certain regularities in most of the physical and chemical properties of the elements, e.g., specific gravity, melting point, hardness, thermal conductivity, etc. Both Mendeleev and Meyer considered it necessary to leave gaps in their Tables in order to keep certain related elements in the same vertical group.

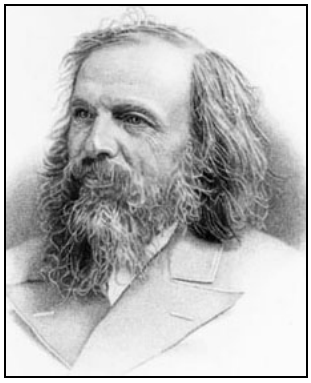

Figure 10. Russian chemist Dimitri Mendeleev (1834 – 1907).

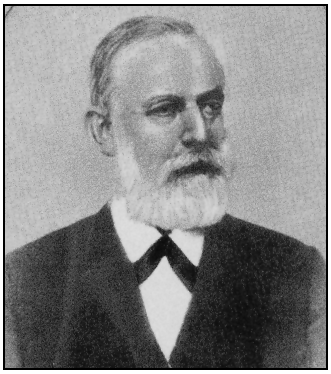

Figure 11. German chemist Lothar Meyer (1830 – 1895).

But Mendeleev went a step further by prophesying that the missing elements would be discovered later and in some cases even he predicted their properties in considerable detail. **Fig. 12** shows the 62 elements known to Mendeleev and the space left for undiscovered elements (Helium was discovered in 1868 in the Sun and was not included by Mendeleev.). When gallium, scandium, and germanium were discovered between 1875 and 1886 showing the exact fit for these elements as predicted by Mendeleev, the Periodic Table became an important tool for chemists and many started looking for the other missing elements.

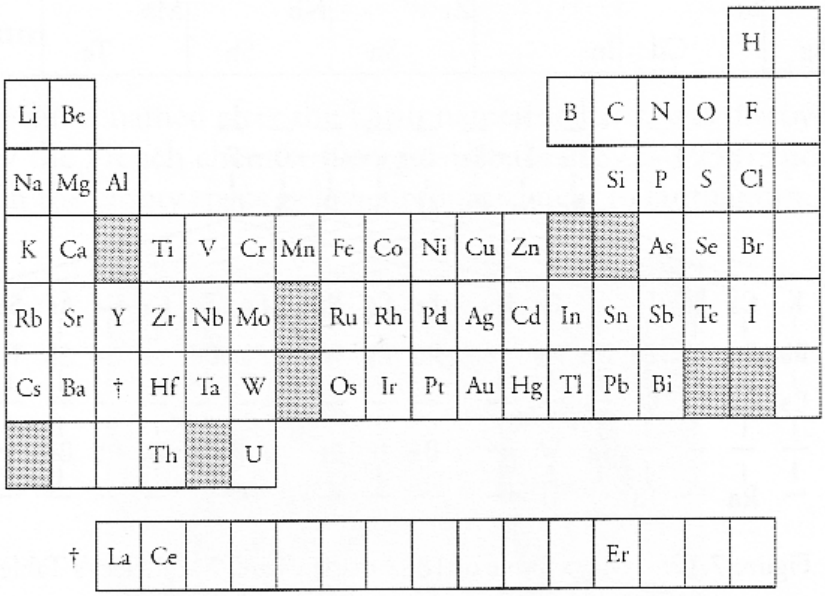

Figure 12. The 62 elements known to Mendeleev and the elements he predicted between 1869 and 1891 (shaded), shown here in a modern version.

In predicting the properties of the missing elements Mendeleev estimated the density, melting and boiling points to be somewhere between those of the neighbouring elements while the valency should be similar to the elements in the same vertical group. In the case of the elements below manganese he was unable to make prediction in chemical properties because he could not interpolate the properties. He called them eka- and dwi-manganese, respectively.

In 1921 Ida Tacke (1896 – 1978) (**Fig. 13**), a young chemistry graduate from the Technical University in Berlin, decided to investigate the mystery of these two missing elements with Walter Noddack, head of the chemical laboratory at the Physico-Technical Research Agency in Berlin. They made a systematic study of properties of the elements near these two gaps. They found that, although usually there was a gradual change in properties in the vertical groups, there were also sharp changes. From comparisons with other groups, they concluded that such sharp changes would occur between manganese and the two elements below it. For example, they believed that the sulfides of the missing elements would be insoluble in dilute acid in contrast to manganese disulfide which is acid-soluble.

Figure 13. Ida Tacke (became Ida Noddack after marriage with Walter Noddack).

They also predicted that the eka- and dwi-manganese should be relatively less abundant than ruthenium and osmium. Certainly, they would not be so abundant as manganese which is nearly of the same order of magnitude as iron, its horizontal neighbor. This explained why previous investigators failed to discover the missing elements – they were searching for them in manganese ores on the assumption that the missing elements would resemble manganese in chemical properties. Tacke and Noddack did not make this assumption.

Their search for the missing elements centered on ores containing minerals of the metals molybdenum, tungsten, ruthenium, and osmium – the horizontal neighbors of eka- and dwi-manganese. Tacke and Noddack prepared more than 400 enriched products from different ores according to the above criteria and examined their X-ray spectra. Then, in June 1925, with the help of Otto Berg, an X-ray specialist at Siemens-Halske in Berlin, they identified in a Norwegian columbite new spectral lines which they assigned to a new element they called rhenium in honor of the river Rhein. A year later, they prepared the first gram of rhenium from 660 kg molybdenite ore.

The fission of uranium atom

In 1934, Enrico Fermi in Rome discovered that neutrons may, be captured by atoms and was able to produce atoms of higher atomic weights than those bombarded. For example, on bombarding cobalt with neutrons he was able to produce nickel

$^{59}_{27}\mathrm{Co} + ^{1}_{0}\mathrm{n} \rightarrow ^{60}_{27}\mathrm{Co} \rightarrow ^{60}_{28}\mathrm{Ni} + \mathrm{e}^{-}$.

When, however, he and his co-workers bombarded uranium with neutrons, they obtained more than one radioactive product. Following the same line of thought as in their previous experiments they suggested that one of these products was formed by neutron capture, i.e., that it was a trans-uranium element or element number 93. Fermi put the new element under rhenium in the Periodic Table and called it eka-rhenium (**Fig. 14**).

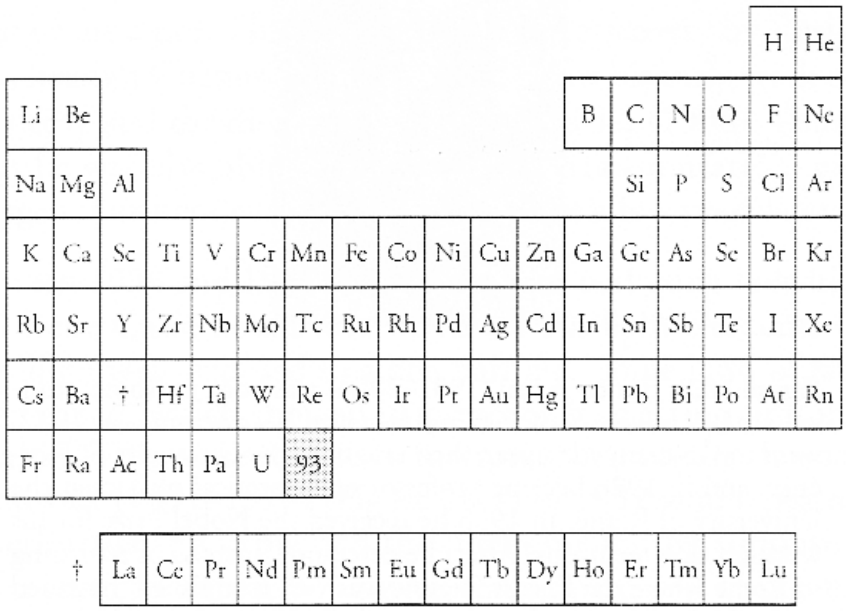

Figure 14. The Periodic Table in the 1930s.
Element 93 was referred to as eka-rhenium by Fermi.

The publication of Fermi's paper on eka-rhenium naturally attracted the attention of Ida Noddack one of the discoverers of rhenium. After reading Fermi's paper she published a comment criticising his conclusions. In this comment, entitled "The Periodic System of the Elements and its Gaps", she showed that Fermi's experimental evidence was incomplete and his conclusions were unjustified. She interpreted his results by saying that "When heavy nuclei are bombarded by neutrons, it would be reasonable to conceive that they break down into numerous large fragments which are isotopes of known elements but are not neighbours of the bombarded element (in the Periodic Table)" (Es wäre denkbar, daß bei der Beschießung schwerer Kerne mit Neutronen diese Kerne in mehrere größere Bruchstücke zerfallen, die zwar Isotope bekannter Elemente, aber nicht Nachbarn der bestrahlten Elemente sind – English translation by the writer). In this statement, Ida Noddack conceived, before anyone else, the idea of nuclear fission. Her argument was as follows: when atoms are bombarded by protons or alpha particles, the nuclear reactions that take place involve the emission of an electron, a proton, or a helium nucleus and the mass of the bombarded atom suffers little change. When, however, neutrons are used, new types of nuclear reaction should take place that are completely different from those previously known.

Nobody paid attention to this statement. Otto Hahn (in 1966) in his autobiography wrote a single phrase referring to Noddack's idea: "Her suggestion was so out-of-line with the then-accepted ideas about the atomic nucleus that it was never seriously discussed". Dieter Hahn, in his biography of his grandfather, wrote in 1979 that Lise Meitner rejected Noddack's

hypothesis describing it as a "free fantasy" – and there was no support for this hypothesis. Further, Meitner argued that there was nothing theoretically or experimentally wrong with the transuranium explanation.

Fermi's experiments were repeated by Otto Hahn (**Fig. 15**) and his co-workers in Berlin. They agreed with his conclusions and published a series of twenty papers on the complex radiochemical separations of the so-called trans-uranium elements. The results, however, became so conflicting that after four years of intensive research and extensive publication the concept of trans-uranium elements became doubtful. This doubt arose when experiments by Hahn's co-worker, Fritz Strassmann, showed that $BaCO_3$, which was added as a carrier in the radiochemical separation of the products of bombardment, could not be separated from these products by dissolution in HBr and fractional crystallization of the bromides.

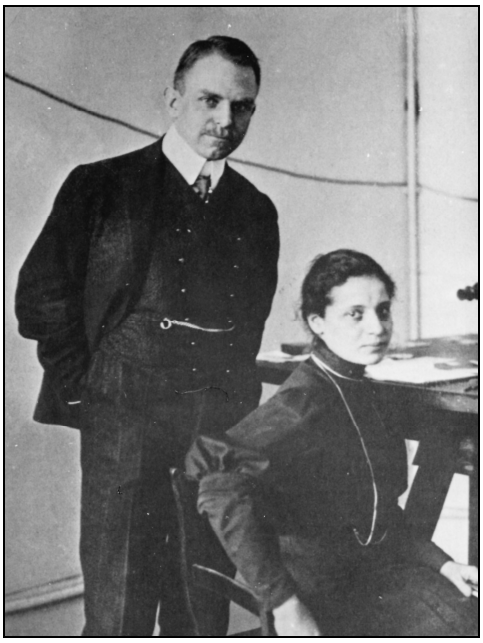

Figure 15. Otto Hahn (1879 – 1968) and his co-worker
Lise Meitner (1878 – 1968) in their laboratory in Berlin.

This observation eliminated the possibility that radium was present in the products and it became evident that barium itself must be one of the products. This conclusion could not be reconciled with the physics of the day because barium had an atomic weight of only 137 while that of uranium was 238. Hahn communicated these astonishing results to his former co-worker, Lise Meitner, in Stockholm.

In December 1938, physicist Otto Frisch was spending the Christmas holiday with his aunt, Lise Meitner in Sweden. She discussed with him the letter she had received from Otto Hahn in which he stated that the bombardment of uranium with neutrons had resulted in the production of isotopes of barium. They came to the conclusion that the uranium atom must have split into two nearly equal fragments – a process they called "fission" in analogy to the biological process of cell division. The process must have been accompanied by the release of a large amount of energy which Frisch calculated and verified experimentally. The results were so thrilling that Meitner sent a telegram in January 1939 to Niels Bohr who was in the USA attending a physics conference; he announced this news at the conference.

With the discovery of fission, the gap between chemistry and physics was closed. In their paper dated January 6, 1939, Hahn and Strassmann wrote in *Die Naturwissenschaften*, "As chemists we must actually say that the new particles do not behave like radium but in fact like barium; as nuclear physicists we cannot make this conclusion which is in conflict with all experience in nuclear physics" (Als Chemiker müssen wir tatsächlich sagen, daß die neuen Körper sich nicht wie Radium verhalten, sondern eher wie Barium; als Kern-Physiker können wir uns nicht dazu entschließen, diesen aller Erfahrung der Kern physikwiderspechenden Schritt zu tun – English translation by the writer).

After reading Hahn's article in *Die Naturwissenschaften*, Ida Noddack wrote a short article in the same journal in March 1939, in which she reminded Hahn of her suggestion five years earlier that the uranium atom might have undergone splitting, and ended by telling him regretfully that he never cited her paper on this matter although she had once explained her views to him personally. The editor of the journal apparently asked Hahn to comment, but he refused. As a result, the editor added a note to the article that read as follows.

Editor's remark: Otto Hahn and Fritz Strassmann informed us that they have neither the time nor the interest to answer the preceding note. They think that they would rather renounce commenting, as the possibility of breaking down a heavy atom into smaller fragments – an idea already expressed by many others – cannot be concluded without experimental evidence. They leave the judgment of the correctness of the views of Frau Ida Noddack and the way she expressed them to the peers.

The atomic bomb

It is remarkable that in 1913, the British writer H. G. Wells (1866 – 1946) wrote a novel entitled *The World Set Free,* in which he envisaged the possibility of quickening radioactive decay of uranium, thereby releasing its immense energy and starting a new chapter in the history of mankind. He even predicted that in 1933 a young scientist will succeed in inducing artificial radioactivity – the first step in the tapping of atomic energy, and in 1956 "atomic bombs", as Wells called them, will be dropped from airplanes in the world's full-scale atomic war. Strangely enough, these predictions were fulfilled. In 1934, Frédéric Joliot and his wife Irène Curie did exactly this by bombarding aluminum with beta particles, in the same year Enrico Fermi achieved similar results by bombarding fluorine and other elements by neutrons, and in 1945 bombs were dropped from airplanes on Japan.

In a similar but more mature vision, Oliver Lodge (1851 – 1940), Principal of the University of Birmingham and President of the British Association for the Advancement of Science, wrote in 1920: "The time will come when atomic energy will take the place of coal as a source of power… I hope that the human race will not discover how to use this energy until it has brains enough to use it properly…" Leo Szilard (1898 – 1964), the Hungarian physicist who went to Berlin to study under Albert Einstein and Max Planck but left to London in 1933 when the Nazis came to power, read Well's novel and was greatly impressed by it. In 1938 he immigrated to USA and was one of the first scientists to recognize the military consequences of the uranium fission discovered in the same year and was largely responsible for the letter which Einstein sent to President Roosevelt in 1939 advising him of the feasibility of the atomic bomb and the danger of Germany getting it first (**Fig. 16**).

Figure 16. Leo Szilard (1898 – 1964), was largely responsible for the letter which Einstein sent to President Roosevelt in October 1939, shown here with Einstein.

Suggested readings

1. F. Habashi. Metals from Ores. An Introduction to Extractive Metallurgy. 2003, Québec: Métallurgie Extractive Québec (distributed by Laval University Bookstore "Zone", www.zone.ul.ca).
2. F. Habashi. From Alchemy to Atomic Bombs. 2002, Québec: Métallurgie Extractive Québec (distributed by Laval University Bookstore "Zone", www.zone.ul.ca).
3. F. Habashi. Ida Noddack (1896 – 1978). Personal Recollections on the Occasion of 80th Anniversary of the Discovery of Rhenium. 2005, Québec: Métallurgie Extractive Québec (distributed by Laval University Bookstore "Zone", www.zone.ul.ca).

საერთაშორისო კონფერენცია “ფუნდამენტური და გამოყენებითი ნანოელექტრომაგნეტიკა” (ფგნემ’12)

უკანასკნელ წლებში მთელმა რიგმა ნანომასშატაბურმა სისტემებმა და ნანოატრუქტურებულმა მასალებმა ელექტრომაგნიტური ველებით მანიპულირებისა და მათი გარდაქმნის დიდი პოტენციალი გამოავლინეს. სწორედ ამ გარემოებამ წარმოშვა სრულიად ახალი ნანოტექნოლოგიური დისციპლინა – ნანოელექტრომაგნეტიკა. 2012 წლის 22 – 25 მაისს ბელარუსის დედაქალაქ მინსკში გაიმართა საერთაშორისო კონფერენცია “ფუნდამენტური და გამოყენებითი ნანოელექტრომაგნეტიკა” (ფგნემ’12), რომელიც მიზნად ისახავდა ეთამაშა იმ სამეცნიერო ფორუმის როლი, რომელიც ხელს შეუწყობდა, ერთის მხრივ, ნანონაწილაკებისა და ნანომასალების სინთეზისა და გამოყენების და, მეორეს მხრივ, თეორიული ელექტროდინამიკისა და გამოყენებითი ელექტრომაგნეტიკის სპეციალისტებს ურთიერთსასარგებლო თანამშრომლობის დამყარებაში.

კონფერენცია მიეძღვნა ბელარუსის სახელმწიფო უნივერსიტეტის ბირთვული პრობლემების კვლევითი ინსტიტუტის დაარსებიდან 25-ე წლისთავს. ესაა ინსტიტუტი, რომელიც ტრადიციულად მნიშვნელოვან როლს ასრულებს ზოგადად რადიაციული და, კერძოდ, ელექტრომაგნიტური დაცვისათვის განკუთვნილი ნანომასალების თეორიულ და ექსპერიმენტულ კვლევებში. ფგნემ’12 ჩატარდა ევროკავშირის კვლევისა და ინოვაციის მე-7 ჩარჩო-პროგრამის ფარგლებში და, აგრეთვე, მთელი რიგი სხვა სპონსორების ფინანსური მხარდჭერით.

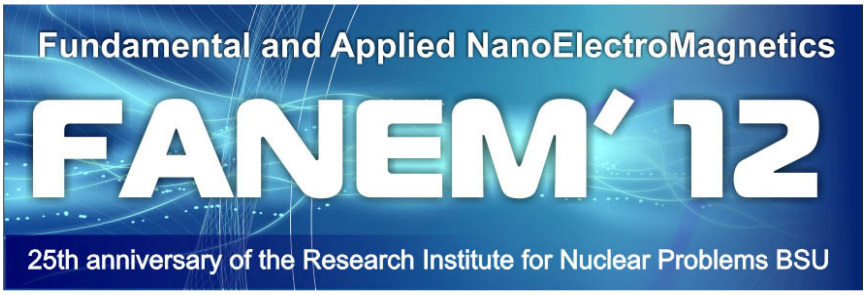

ფგნემ’12 მიეძღვნა ბელარუსის სახელმწიფო უნივერსიტეტის ბირთვული პრობლემების კვლევითი ინსტიტუტის დაარსებიდან 25-ე წლისთავს.

ფგნემ’12 გაიმართა ევროკავშირის კვლევისა და ინოვაციის მე-7 ჩარჩო-პროგრამის ფარგლებში და მთელი რიგი სპონსორების მხარდჭერით.

სავსებით გამართლდა ორგანიზატორთა მოლოდინი, რომ კონფერენციაზე გამართული დისკუსია ძლიერ ბიძგს მისცემდა ნანოელექტრომაგნეტიკის შემდგომ განვითარებას, დახვეწდა ამ ახალი დარგის ტერმინოლოგიას, ახლებურად დასვამდა ელექტროდინამიკის, ფოტონიკისა და ნანომასალათმცოდნეობის რიგ პრობლემებს. ფგნემ’12-ზე წარმოდგენილი მოხსენებები შეეხებოდა ნანოელექტრომაგნეტიკების ზოგადი თეორიის, მოდელირების, დიზაინის, სინთეზის, სტრუქტურული და ქიმიური დახასიათების, გამოყენების და ა.შ. სხვადასხვა ასპექტს. კერძოდ, განხილული იყო ისეთი მიმართულებები, როგორიცაა:

– ელექტრომაგნიტური ეფექტები ნანომასალებში: მოდელირება და ექსპერიმენტი;
– ნახშირბადის ნანომილაკები, გრაფენი და ნანონახშირბადის სხვა ფორმები ელექტრომაგნეტიკაში;
– ნანოფორები, ნანოანტენები და ნანოგადამცემი ხაზები;
– ოპტიკური არაწრფივობა ნანომასშტაბში;
– ნანოსტრუქტურებული კომპოზიტური მასალები და თხელი ფირები: სინთეზი და ფიზიკურ-ქიმიური თავისებურებანი;
– ნანოსტრუქტურებული კომპოზიტური მასალები ელექტრომაგნიტური ველის ეკრანირებისათვის და მაიონიზებელი რადიაციის ზემოქმედებისაგან დაცვისათვის;
– მოწესრიგებული ნანოსტრუქტურები და მეტამასალები ელექტრომაგნიტური ველებით მანიპულირებისა და მათი გარდაქმნისათვის;
– მეტალური ნანონაწილაკებისა და ნანონახშირბადის ბიოსამედიცინო გამოყენებები;
– ლაზერული გამოსხივების გარდაქმნა და ერთფოტონიანი ხელსაწყოები.

ფგნემ’12 გაიხსნა ე.წ. “წითელ სახლში”, სადაც არის განთავსებული ბელარუსის სახელმწიფო უნივერსიტეტის რექტორატი. იგი ერთ-ერთია მინსკის იმ იშვიათ ძველ შენობათაგან, რომლიც მეორე მსოფლიო ომის დროს დანგრევას გადაურჩა.

გარდა პლენარული სხდომებისა, მუშაობა მიმდინარეობდა რამდენიმე სპეციალიზებულ სექციაში:

- ნანომასალების კვანტურ-ქიმიური მოდელირება;
- ნანომასალები ელექტრომაგნიტური ველების ეკრანირებისათვის;
- ნანოსტრუქტურების სისტემატიზება და დახასიათება;
- ნანოსტრუქტურების ოპტიკური და ელექტრომაგნიტური თვისებები;
- ნანომასალების გამოყენების პერსპექტივები ბიოსამედიცინო სფეროში;
- ნანომასალების ელექტროდინამიკა და პლაზმონიკა.

შესაბამისად, ძალზე ფართო იყო კვლევის ობიექტების სფეროც – დაწყებული თხელფიროვანი კომერციული დანიშნულების ნანოდანაფარებით და დამთავრებული ინტეგრალური სქემების ელემენტებისა და ნანოხელსაწყოების დასამზადებლად განკუთვნილი მეტამასალებით. საერთაშორისო კონფერენციაზე "ფუნდამენტური და გამოყენებითი ნანოელექტრომაგნეტიკა" 19 ქვეყანა იყო წარმოდგენილი: ამერიკის შეერთებული შტატები, ბელარუსი, ბელგია, გერმანია, დანია, დიდი ბრიტანეთი, ინდოეთი, იტალია, ლატვია, ლიტვა, რუსეთი, საფრანგეთი, საქართველო, სინგაპური, სომხეთი, უკრაინა, უნგრეთი, ფინეთი და ყირგიზეთი.

საქართველოდან ფგნემ'12-ში მონაწილეობდა საქართველოს ტექნიკური უნივერსიტეტის ფიზიკის დეპარტამენტის პროფესორი ლევან ჩხარტიშვილი (მისი გამგზავრება დააფინანსა საორგანიზაციო კომიტეტმა საერთაშორისო სამეცნიერო-ტექნიკური ცენტრის გრანტით) მოხსენებით "ელემენტური ბორის ორგანზომილებიანი მეტალური კრისტალი, როგორც ელექტრომაგნიტური ეკრანირების მასალა".

პროფ. ლევან ჩხარტიშვილი ფგნემ'12-ზე გამოდის მოხსენებით "ელემენტური ბორის ორგანზომილებიანი მეტალური კრისტალი, როგორც ელექტრომაგნიტური ეკრანირების მასალა"

ფგნემ'12-ზე განიხილეს ევროკავშირის კვლევის და ინოვაციის მე-7 ჩარჩო-პროგრამის მიმდინარე პროექტები და მომავალი მე-8 ჩარჩო-პროგრამის პრიორიტეტული მიმართულებები.

კონფერენციის დამსწრეთა დიდი ინტერესი გამოიწვია ევროკავშირის კვლევისა და ინოვაციის ჩარჩო-პროგრამების წარმომადგენლების გამოსვლებმა. მათ დეტალურად ისაუბრეს მე-7 პროგრამის ფარგლებში მიმდინარე პროექტებზე და მომავალი მე-8 პროგრამის პრიორიტეტულ მიმართულებებზე.

საერთაშორისო კონფერენციის “ფუნდამენტური და გამოყენებითი ნანოელექტრომაგნეტიკა” (ფგნემ’12) მოხსენებების თეზისები ცალკე კრებულის სახით გამოიცა. წარმოდგენილი მოხსენებების ერთი ნაწილი სრული სტატიების სახით გამოქვეყნდება ჟურნალში Joiurnal of Nanophotonics.

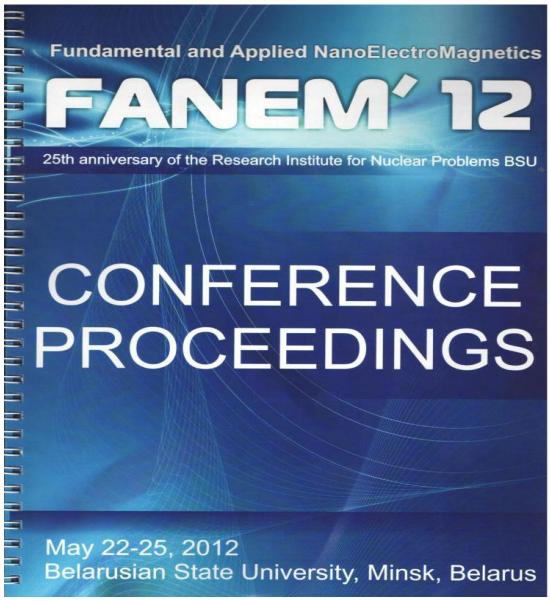

საერთაშორისო კონფერენციის “ფუნდამენტური და გამოყენებითი ნანოელექტრომაგნეტიკა” (ფგნემ’12) მასალების გარეკანი.

საორგანიზაციო კომიტეტმა საინტერესო სოციალური პროგრამა შესთავაზა კონფერენციის მონაწილეებს: ტური ბელარუსის დედაქალაქის ღირსშესანიშნაობების გასაცნობად, სახელმწიფო ოპერაში გამართული წარმოდგენა, მიღება ბელარუსის სახელმწიფო უნივერსიტეტის კაფეში “გაუდეამუსი” და სხვ.

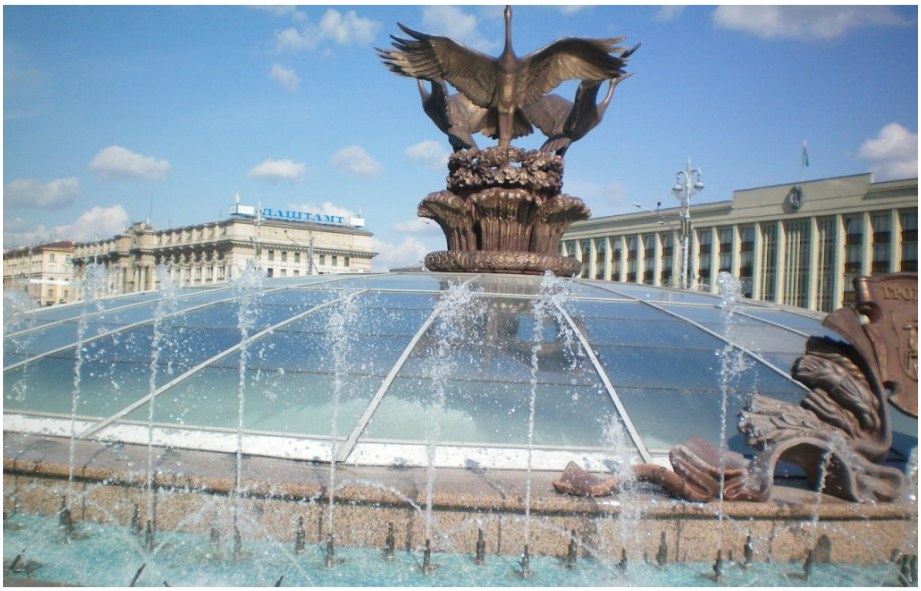

წეროების შადრევანი მინსკის ცენტრში.

ფოლკლორული ანსამბლი ბელარუსის
რესპუბლიკური საკონცერტო ცენტრის წინ.

მონაწილეებს მათთვის გამართულ მიღებაზე სიტყვით
მიმართა კონფერენციის საორგანიზაციო კომიტეტის
თანათავმჯდომარემ პროფ. სერგეი მაქსიმენკომ.

2012 წლის 22 – 25 მაისს ქალაქ მინსკში, ბელარუსში, გამართული საერთაშორისო კონფერენციის “ფუნდამენტური და გამოყენებითი ნანოელექტრომაგნეტიკა” (ფგნემ’12) მონაწილეთა საერთო აზრით, ეს იყო უაღრესად ნაყოფიერი სამეცნიერო ფორუმი, რომელმაც მნიშვნელოვანი როლი ითამაშა ნანოელექტრომაგნეტიკის, როგორც ახალი და პერსპექტიული დისციპლინის, განვითარებაში და კარგი იქნება, თუ ფგნემ’12-ით სათავე დაედება ნანოელექტრომაგნეტიკის პრობლემებისადმი მიძღვნილი კონფერენციების ჩატარების ტრადიციას.

ლევან ჩხარტიშვილი

2012 წლის 20 ოქტომბერი

NANOOZE

აშშ-ის ნაციონალური სამეცნიერო ფონდის (NSF) მხარდაჭერით 2007 წლიდან გამოდის სამეცნიერო ვებ-ჟურნალი “Nanooze” (info@nanooze.org და www.nanooze.org). ჟურნალი “Nanooze” გამოიცემა ინგლისურ, გერმანულ, ფრანგულ, იტალიურ, ესპანურ და პორტუგალიურ ენებზე. სულ 2012 წლისთვის გამოსულია 11 ნომერი.

ჟურნალი განკუთვნილია საშუალო სკოლის დონის ბავშვებისთვის. ჟურნალის სარედაქციო ხელმძღვანელია კორნელის უნივერსიტეტის (კოლუმბია, აშშ) პროფესორი Carl Batt. ჟურნალის ქაღალდის ვერსია უფასოდ ურიგდება სკოლის მასწავლებლებს.

“Nanooze”-ში გადმოცემულ სტატიებში, ფოტოგრაფიებში და თამაშებში ძალზედ ხატოვნად, მარტივად, ბავშვებისთვის გასაგები ენით არის მოთხრობილი ნანოტექნოლოგიის, ნანოქიმიის და, საზოგადოდ, მეცნიერების ურთულეს თანამედროვე პრობლემებზე, პერსპექტივებზე, უახლესი მიღწევების შესახებ, აღმოჩენებზე.

ჟურნალის გვერდებზე შეხვდებით ინტერვიუებს ნანოტექნოლოგიის ფუძემდებლებთან, დღეს მომუშავე მეცნიერებთან. “Nanooze”-ის ბლოგები მიძღვნილია ფიზიკის, ქიმიის, ბიოლოგიის და მედიცინის საკითხებისადმი.

ციური რამიშვილი

2012 წლის 28 ოქტომბერი

ISSN 1987-8826